






Universitat Autònoma de Barcelona

**ADVERTIMENT.** L'accés als continguts d'aquesta tesi queda condicionat a l'acceptació de les condicions d'ús establertes per la següent llicència Creative Commons:  [http://cat.creativecommons.org/?page\\_id=184](http://cat.creativecommons.org/?page_id=184)

**ADVERTENCIA.** El acceso a los contenidos de esta tesis queda condicionado a la aceptación de las condiciones de uso establecidas por la siguiente licencia Creative Commons:  <http://es.creativecommons.org/blog/licencias/>

**WARNING.** The access to the contents of this doctoral thesis it is limited to the acceptance of the use conditions set by the following Creative Commons license:  <https://creativecommons.org/licenses/?lang=en>



Universitat Autònoma  
de Barcelona

**ASSESSMENT, MODELLING AND  
MITIGATION OF GREENHOUSE GAS  
EMISSIONS FROM WATER RESOURCE  
RECOVERY FACILITIES**

— PhD Thesis —

**Borja Solís Duran**

Supervisors: Dr. Juan Antonio Baeza Labat

Dr. Albert Guisasola i Canudas

Academic tutor: Dr. Juan Antonio Baeza Labat

A thesis submitted in fulfilment of the requirements for the Doctoral degree in  
Environmental Science and Technology

GENOCOV research group

Departament d'Enginyeria Química, Biològica i Ambiental

Escola d'Enginyeria

Universitat Autònoma de Barcelona

Bellaterra, July 2021



**GENOCOV**  
Departament d'Enginyeria Química,  
Biològica i Ambiental  
Escola d'Enginyeria  
Universitat Autònoma de Barcelona  
Barcelona · Spain  
[info@genocov.com](mailto:info@genocov.com)



**UAB**  
Universitat Autònoma  
de Barcelona

**ALBERT GUIASOLA I CANUDAS**, Professor Agregat i **JUAN ANTONIO BAEZA LABAT**, Catedràtic Laboral del Departament d'Enginyeria Química, Biològica i Ambiental de la Universitat Autònoma de Barcelona,

**CERTIFIQUEM:**

Que l'enginyer **BORJA SOLÍS DURAN** ha realitzat sota la nostra direcció, el treball que amb títol "ASSESSMENT, MODELLING AND MITIGATION OF GREENHOUSE GAS EMISSIONS FROM WATER RESOURCE RECOVERY FACILITIES" es presenta en aquesta memòria, i que constitueix la seva Tesi per optar al Grau de Doctor per la Universitat Autònoma de Barcelona.

I per a què se'n prengui coneixement i consti als efectes oportuns, presentem a l'Escola d'Enginyeria de la Universitat Autònoma de Barcelona l'esmentada Tesi, signant el present certificat.

Bellaterra, 21 de juliol de 2021

Dr. Albert Guisasola i Canudas

Dr. Juan Antonio Baeza Labat



*A mis padres, Cele y Susana,*

*a Dani y Olalla*



## **Acknowledgements**

---

The author is grateful for the PIF PhD grant funded by Universitat Autònoma de Barcelona. The author is member of the GENOCOV research group (Grup de Recerca Consolidat de la Generalitat de Catalunya, 2017 SGR 1175). Chapter IV of this thesis reports results supported by the SMART-Plant project (Scale-up of low-carbon footprint Material Recovery Techniques, EUH2020, grant agreement 690323). The results reported in annex III of this thesis were developed with the support of the European Union's Horizon 2020 research and innovation program under the Marie Skłodowska-Curie C-FOOT-CTRL project (grant agreement No 645769).





## Summary

---

As global demand for water grows, the amount of wastewater produced and its overall pollution load are continuously increasing worldwide. Therefore, wastewater treatment is becoming a critical point in water management, as it prevents public health risks as well as environmental problems. In the face of ever-growing demand for water for different uses, wastewater has gained momentum as an alternative and reliable source of water, shifting the paradigm of wastewater management from treatment and disposal to reuse, recycle and resource recovery. In this sense, wastewater treatment plants (WWTPs) are being transformed into water resource recovery facilities (WRRFs). The main objective of these facilities is not only to achieve a good effluent quality, but also to recover resources (such as carbon (C), nitrogen (N) and phosphorus (P)), water and energy in a sustainable way.

In addition, over the past years, concerns regarding the sustainability of current WWTPs have increased, with a particular focus on the C footprint due to the impact of greenhouse gases (GHG) emissions on climate change. Therefore, many water utilities have become aware of the potential GHG emissions during the operation of WWTPs and there is a growing need to reduce these emissions and to identify the factors that control GHG emissions from WWTPs. Among the three major GHG that can be produced during wastewater treatment (carbon dioxide (CO<sub>2</sub>), methane (CH<sub>4</sub>) and nitrous oxide (N<sub>2</sub>O)), N<sub>2</sub>O is produced and emitted during the biological nitrogen removal (BNR) in WWTPs. Due to their high global warming potential, the C footprint of WWTPs is highly sensitive to N<sub>2</sub>O emissions. Currently, three biological pathways for N<sub>2</sub>O production during BNR have been identified. Measurement campaigns at full-scale WWTPs have shown a high variability in measured N<sub>2</sub>O emissions, with the percentage of influent N emitted as N<sub>2</sub>O-N ranging between 0.01 and 1.8% and in some cases even higher than 10%. Mathematical modelling of BNR processes has gained increased attention in view of a better understanding of N<sub>2</sub>O production, accumulation and emission. The ability to predict N<sub>2</sub>O emissions can serve for the design of potential mitigation control/operational strategies.

This thesis aims to advance the development, knowledge and application of novel operational and control strategies to mitigate N<sub>2</sub>O emissions during wastewater treatment. Most of the study has been approached from a modelling point of view, although GHG emissions have also been assessed in a novel pilot plant configuration. The thesis is divided into three parts.

In the first part, the ASM2d-N<sub>2</sub>O kinetic model, which accounts for the N<sub>2</sub>O production in C/N/P removal WWTPs, was used to study the associated emissions from a full-scale WWTP with two independent lines. Firstly, the hydraulics of the WWTP were characterized through a residence time distribution experiment. Results showed that the flow was equally divided into the two treatment lines, that each reactor worked as an ideal

continuous stirred tank reactor and secondary settler fluxes were similar to plug-flow reactor. After the hydraulic characterization, the ASM2d-N<sub>2</sub>O model was calibrated using experimental data obtained under dynamic conditions. The parameter subset to be calibrated was obtained by a global sensitivity analysis. The top ranked parameters (related to nitrifying organisms) were calibrated. A good model fit was obtained during the dynamic calibration, giving a good description of nutrients and N<sub>2</sub>O emissions. Finally, a simulation-based study was carried out to evaluate the effect on N<sub>2</sub>O emissions of different influent flow distributions between the treatment lines.

In the second part of the thesis, the performance and N<sub>2</sub>O and CH<sub>4</sub> emissions during long-term operation of a novel WRRF configuration, the mainstream SCEPPHAR, were monitored and assessed. The long-term N<sub>2</sub>O and CH<sub>4</sub> emission factors calculated were in the low range of the literature, 1% and 0.1%, respectively, even with high nitrite accumulation in the case of N<sub>2</sub>O. The dynamics and possible sources of production of these emissions were discussed. Finally, different aeration strategies were implemented to study the impact on N<sub>2</sub>O emissions in the nitrifying reactor. The results showed that operating the pilot-plant under different dissolved oxygen (between 1 and 3 g O<sub>2</sub> m<sup>-3</sup>) did not seem to have an effect on the N<sub>2</sub>O emission factor. The intermittent aeration was the aeration strategy that most mitigated the N<sub>2</sub>O emissions in the nitrifying reactor, obtaining a reduction of 40% compared to the normal operation of the pilot plant.

Finally, a plant-wide model describing the fate of chemical oxygen demand (COD), C, N and P compounds, upgraded to account for (on-site/off-site) GHG emissions, was implemented within the framework of the International Water Association (IWA) Benchmarking Simulation Model No. 2 (BSM2). The proposed approach (named BSM2-PSFe-GHG) included the main biological N<sub>2</sub>O production pathways and describes mechanistically the CO<sub>2</sub> emissions (biogenic/non-biogenic) in the activated sludge reactors as well as the biogas production (CO<sub>2</sub>/CH<sub>4</sub>) from the anaerobic digester. Indirect GHG emissions for power generation, chemical usage, effluent disposal and sludge storage and reuse were also included, using static factors for CO<sub>2</sub>, CH<sub>4</sub> and N<sub>2</sub>O. Global and individual mass balances were quantified to investigate the fluxes of the different components. Novel control strategies were proposed to obtain high plant performance as well as nutrient recovery and mitigation of GHG emissions in a plant-wide context. The implemented control strategies led to an overall more sustainable and efficient plant performance in terms of better effluent quality, reduced operational cost and lower GHG emissions. The maximum reduction obtained in N<sub>2</sub>O emissions from the biotreatment and total GHG emissions from the water resource recovery facility were 27% and 9%, respectively, compared to the default control strategy.

## Resumen

---

A medida que crece la demanda mundial de agua, la cantidad de aguas residuales producidas y su carga contaminante global aumentan continuamente en todo el mundo. Por ello, el tratamiento de las aguas residuales se está convirtiendo en un punto crítico en la gestión del agua, ya que previene los riesgos para la salud pública y los problemas medioambientales. Ante la creciente demanda de agua para diferentes usos, las aguas residuales han cobrado impulso como fuente alternativa y fiable de agua, cambiando el paradigma de la gestión de las aguas residuales, que ha pasado de ser tratamiento y eliminación a reutilización, reciclaje y recuperación de recursos. En este sentido, las estaciones depuradoras de aguas residuales (EDAR) se están transformando en estaciones de recuperación de recursos del agua (ERRA). El objetivo principal de estas instalaciones no es sólo conseguir una buena calidad de los efluentes, sino también recuperar de forma sostenible recursos como carbono (C), nitrógeno (N), fósforo (P), agua y energía.

Además, en los últimos años ha aumentado la preocupación por la sostenibilidad de las actuales EDAR, con especial atención a la huella de C debido al impacto de las emisiones de gases de efecto invernadero (GEI) en el cambio climático. Por ello, muchas empresas del sector del agua han tomado conciencia de las posibles emisiones de GEI durante el funcionamiento de las EDAR y existe una creciente necesidad de reducir estas emisiones y de identificar los factores que controlan las emisiones de GEI de las EDAR. Entre los tres principales GEI que pueden producirse durante el tratamiento de las aguas residuales (dióxido de carbono ( $\text{CO}_2$ ), metano ( $\text{CH}_4$ ) y óxido nitroso ( $\text{N}_2\text{O}$ )), el  $\text{N}_2\text{O}$  se produce y emite durante la eliminación biológica de nitrógeno (BNR) en las EDAR. Debido a su alto potencial de calentamiento global, la huella de C de las EDAR es muy sensible a las emisiones de  $\text{N}_2\text{O}$ . Actualmente, se han identificado tres vías biológicas de producción de  $\text{N}_2\text{O}$  durante la BNR. Las campañas de medición de las EDAR a escala real han mostrado una gran variabilidad en las emisiones de  $\text{N}_2\text{O}$  medidas, con un porcentaje del N del afluente emitido como  $\text{N}_2\text{O}$  que oscila entre el 0.01 y el 1.8% y, en algunos casos, incluso superior al 10%. La modelización matemática de los procesos de BNR ha cobrado mayor importancia en vistas a una mejor comprensión de la producción, acumulación y emisión de  $\text{N}_2\text{O}$ . La capacidad de predecir las emisiones de  $\text{N}_2\text{O}$  puede servir para el diseño de posibles estrategias de control/operación para mitigar las emisiones.

Esta tesis pretende avanzar en el desarrollo, conocimiento y aplicación de estrategias operativas y de control novedosas para mitigar las emisiones de  $\text{N}_2\text{O}$  durante el tratamiento de aguas residuales. La mayor parte del estudio se ha abordado desde el punto de vista de la modelización, aunque también se han evaluado las emisiones de GEI en una novedosa configuración de planta piloto. La tesis se divide en tres partes.

En la primera parte, se ha utilizado el modelo cinético ASM2d-N<sub>2</sub>O, que tiene en cuenta la producción de N<sub>2</sub>O en las EDAR con eliminación de C/N/P, para estudiar las emisiones asociadas a una EDAR a escala real con dos líneas independientes. En primer lugar, se caracterizó la hidráulica de la EDAR mediante un experimento de distribución del tiempo de residencia. Los resultados mostraron que el flujo se dividía por igual entre las dos líneas de tratamiento, que cada reactor funcionaba como un reactor de tanque agitado continuo ideal y que los flujos de los sedimentadores secundarios eran similares a los de un reactor de flujo pistón. Después de la caracterización hidráulica, se calibró el modelo ASM2d-N<sub>2</sub>O utilizando datos experimentales obtenidos en condiciones dinámicas. El subconjunto de parámetros a calibrar se obtuvo mediante un análisis de sensibilidad global. Se calibraron los parámetros mejor clasificados (relacionados con los organismos nitrificantes). Se obtuvo un buen ajuste del modelo durante la calibración dinámica, obteniendo una buena descripción de los nutrientes y de las emisiones de N<sub>2</sub>O. Por último, se llevó a cabo un estudio mediante simulación para evaluar el efecto sobre las emisiones de N<sub>2</sub>O de diferentes distribuciones de flujo de entrada entre las líneas de tratamiento.

En la segunda parte de la tesis, se ha monitorizado y evaluado el rendimiento y las emisiones de N<sub>2</sub>O y CH<sub>4</sub> durante el funcionamiento a largo plazo de una nueva configuración de ERRA, el SCEPPHAR de línea principal. Los factores de emisión de N<sub>2</sub>O y CH<sub>4</sub> a largo plazo se situaron en el rango bajo de la literatura, 1% y 0,1%, respectivamente. Las emisiones de N<sub>2</sub>O fueron bajas incluso operando con una elevada acumulación de nitrito. Se discutió la dinámica y las posibles fuentes de producción de estas emisiones. Finalmente, se implementaron diferentes estrategias de aireación para estudiar su impacto en las emisiones de N<sub>2</sub>O en el reactor de nitrificación. Los resultados mostraron que el funcionamiento de la planta piloto con diferentes niveles de oxígeno disuelto (entre 1 y 3 g de O<sub>2</sub> m<sup>-3</sup>) no parecía tener efecto sobre el factor de emisión de N<sub>2</sub>O. La aireación intermitente fue la estrategia de aireación que más mitigó las emisiones de N<sub>2</sub>O en el reactor de nitrificación, obteniendo una reducción del 40% respecto al funcionamiento normal de la planta piloto.

Por último, se desarrolló un modelo para una planta completa que describe la eliminación de C/N/P, actualizado para tener en cuenta las emisiones de GEI (in situ/extra situ), en el marco del modelo de simulación *benchmark* n° 2 (BSM2) de la Asociación Internacional del Agua (IWA). El modelo propuesto (denominado BSM2-PSFe-GHG) incluye las principales vías de producción biológica de N<sub>2</sub>O y describe mecánicamente las emisiones de CO<sub>2</sub> (biogénicas/no biogénicas) en los reactores de lodos activados, así como la producción de biogás (CO<sub>2</sub>/CH<sub>4</sub>) del digestor anaeróbico. También se incluyen las emisiones indirectas de GEI para la generación de energía, el uso de productos químicos, la eliminación de efluentes y el almacenamiento y la reutilización de lodos, utilizando factores estáticos para CO<sub>2</sub>, CH<sub>4</sub> y N<sub>2</sub>O. Una vez definido el modelo, se realizó un caso de estudio donde se cuantificaron los balances de masas globales e individuales

para investigar los flujos de los distintos componentes. Se propusieron estrategias de control novedosas para obtener un alto rendimiento de la planta, así como la recuperación de nutrientes y la mitigación de las emisiones de GEI en el contexto de toda la planta. Las estrategias de control aplicadas condujeron a un rendimiento global más sostenible y eficiente de la planta en términos de mejor calidad del efluente, reducción de los costes operativos y menores emisiones de GEI. La reducción máxima obtenida en las emisiones de N<sub>2</sub>O del biotratamiento y en las emisiones totales de GEI de la planta fue del 27% y del 9%, respectivamente, en comparación con la estrategia de control por defecto.



## Resum

---

A mesura que creix la demanda mundial d'aigua, la quantitat d'aigües residuals produïdes i la seva càrrega contaminant global augmenten contínuament a tot el món. Per això, el tractament de les aigües residuals s'està convertint en un punt crític en la gestió de l'aigua, ja que prevé els riscos per a la salut pública i els problemes mediambientals. Davant la creixent demanda d'aigua per a diferents usos, les aigües residuals han cobrat impuls com a font alternativa i fiable d'aigua, canviant el paradigma de la gestió de les aigües residuals, que ha passat de ser tractament i eliminació a ser reutilització, reciclatge i recuperació de recursos. En aquest sentit, les estacions depuradores d'aigües residuals (EDAR) s'estan transformant en estacions de recuperació de recursos de l'aigua (ERRA). L'objectiu principal d'aquestes instal·lacions no és només aconseguir una bona qualitat dels efluent, sinó també recuperar de forma sostenible recursos com carboni (C), nitrogen (N), fòsfor (P), aigua i energia.

A més a més, als últims anys ha augmentat la preocupació per la sostenibilitat de les actuals EDAR, amb especial atenció a la petjada de C a causa de l'impacte de les emissions de gasos d'efecte hivernacle (GEH) en el canvi climàtic. Per això, moltes empreses del sector de l'aigua han pres consciència de les possibles emissions de GEH durant el funcionament de les EDAR i hi ha una creixent necessitat de reduir aquestes emissions i d'identificar els factors que controlen les emissions de GEH de les EDAR. Entre els tres principals GEH que poden produir-se durant el tractament de les aigües residuals (diòxid de carboni ( $\text{CO}_2$ ), metà ( $\text{CH}_4$ ) i òxid nítrós ( $\text{N}_2\text{O}$ )), el  $\text{N}_2\text{O}$  es produeix i s'emet durant l'eliminació biològica de nitrogen (BNR) a les EDAR. A causa del seu alt potencial d'escalfament global, la petjada de C de les EDAR és molt sensible a les emissions de  $\text{N}_2\text{O}$ . Actualment, s'han identificat tres vies biològiques de producció de  $\text{N}_2\text{O}$  durant la BNR. Les campanyes de mesures a les EDAR a escala real han mostrat una gran variabilitat en les emissions de  $\text{N}_2\text{O}$  mesurades, amb un percentatge de N de l'afluent emès com  $\text{N}_2\text{O}$  que oscil·la entre el 0.01 i l'1.8% i, en alguns casos, fins i tot superior al 10%. La modelització matemàtica dels processos de BNR ha cobrat major importància en vista d'una millor comprensió de la producció, acumulació i emissió de  $\text{N}_2\text{O}$ . La capacitat de predir les emissions de  $\text{N}_2\text{O}$  pot servir per al disseny de possibles estratègies de control/operació per mitigar les emissions.

Aquesta tesi pretén avançar en el desenvolupament, coneixement i aplicació d'estratègies operatives i de control innovadores per a mitigar les emissions de  $\text{N}_2\text{O}$  durant el tractament d'aigües residuals. La major part de l'estudi s'ha abordat des del punt de vista de la modelització, encara que també s'han avaluat les emissions de GEH en una nova configuració de planta pilot. La tesi es divideix en tres parts.



A la primera part, s'ha utilitzat el model cinètic ASM2d-N<sub>2</sub>O, que té en compte la producció de N<sub>2</sub>O a les EDAR amb eliminació de C/N/P, per estudiar les emissions associades a una EDAR a escala real amb dues línies independents. En primer lloc, es va caracteritzar la hidràulica de l'EDAR mitjançant un experiment de distribució del temps de residència. Els resultats van mostrar que el flux es dividia per igual entre les dues línies de tractament, que cada reactor funcionava com un reactor de tanc agitat continu ideal i que els fluxos dels sedimentadors secundaris eren similars als d'un reactor de flux pistó. Després de la caracterització hidràulica, es va calibrar el model ASM2d-N<sub>2</sub>O utilitzant dades experimentals obtingudes en condicions dinàmiques. El subconjunt de paràmetres a calibrar es va obtenir mitjançant una anàlisi de sensibilitat global. Es van calibrar els paràmetres millor classificats (relacionats amb els organismes nitrificants). Es va obtenir un bon ajust del model durant el calibratge dinàmic, obtenint una bona descripció dels nutrients i de les emissions de N<sub>2</sub>O. Finalment, es va dur a terme un estudi mitjançant simulació per avaluar l'efecte sobre les emissions de N<sub>2</sub>O de diferents distribucions de flux d'entrada entre les línies de tractament.

A la segona part de la tesi, s'ha monitoritzat i avaluat el rendiment i les emissions de N<sub>2</sub>O i CH<sub>4</sub> durant el funcionament a llarg termini d'una nova configuració d'ERRA, el SCEPPHAR de línia principal. Els factors d'emissió de N<sub>2</sub>O i CH<sub>4</sub> a llarg termini calculats es van situar en el rang baix de la literatura, 1% i 0,1%, respectivament. Les emissions de N<sub>2</sub>O van ser baixes, fins i tot operant amb una elevada acumulació de nitrit. Es va discutir la dinàmica i les possibles fonts de producció d'aquestes emissions. Finalment, es van implementar diferents estratègies d'aireació per estudiar el seu impacte en les emissions de N<sub>2</sub>O en el reactor de nitrificació. Els resultats van mostrar que el funcionament de la planta pilot amb diferents nivells d'oxigen dissolt (entre 1 i 3 g de O<sub>2</sub> m<sup>-3</sup>) no semblava tenir efecte sobre el factor d'emissió de N<sub>2</sub>O. L'aireació intermitent va ser l'estratègia d'aireació que més va mitigar les emissions de N<sub>2</sub>O al reactor de nitrificació, obtenint una reducció del 40% respecte al funcionament normal de la planta pilot.

Finalment, es va desenvolupar un model per una planta completa que descriu l'eliminació de C/N/P, actualitzat per tenir en compte les emissions de GEH (in-situ/ex-situ), en el marc del model de simulació *benchmark* n° 2 (BSM2) de l'Associació Internacional de l'Aigua (IWA). El model proposat (denominat BSM2-PSFe-GHG) incloïa les principals vies de producció biològica de N<sub>2</sub>O i descriu mecanísticament les emissions de CO<sub>2</sub> (biogèniques/no biogèniques) en els reactors de fangs activats, així com la producció de biogàs (CO<sub>2</sub>/CH<sub>4</sub>) del digestor anaeròbic. També es van incloure les emissions indirectes de GEH per a la generació d'energia, l'ús de productes químics, l'eliminació d'efluents i l'emmagatzematge i reutilització de llocs, utilitzant factors estàtics per al CO<sub>2</sub>, CH<sub>4</sub> i N<sub>2</sub>O. Una vegada definit el model, es va realitzar un cas d'estudi on es van quantificar els balanços de masses globals i individuals per investigar els fluxos dels diferents components. Es van proposar estratègies de control innovadores per obtenir un alt

rendiment de la planta, així com la recuperació de nutrients i la mitigació de les emissions de GEH en el context de tota la planta. Les estratègies de control aplicades van conduir a un rendiment global més sostenible i eficient de la planta en termes de millor qualitat de l'efluent, reducció dels costos operatius i menors emissions de GEH. La reducció màxima obtinguda en les emissions de N<sub>2</sub>O del biotractament i en les emissions totals de GEH de la planta va ser del 27% i del 9%, respectivament, en comparació amb l'estratègia de control per defecte.



## List of publications and author's contributions

---

**I. Solís, B.,** Guisasola, A., Pijuan, M., Coromines, Ll. Baeza, J.A., 2021. **Systematic calibration of N<sub>2</sub>O emissions from a full-scale WWTP including a tracer test and a global sensitivity approach.** Chemical Engineering Journal, *Submitted*.

*Author's contribution:* Assistance in the experimental campaign, the development of the hydraulic and WWTP model, the implementation of global sensitivity analysis, the kinetic and hydraulic calibration and the exploitation of the model. Pijuan, M., contributed to the implementation of the N<sub>2</sub>O measurements, discussion of the results and editing. Coromines, Ll. contributed to the experimental campaign design and experimental work, the discussion of the results and editing. Guisasola, A., and Baeza, J.A. contributed to the research supervision, discussion of the results, writing and editing.

A preliminary version of this paper was presented as a poster presentation in the YWP IWA conference, 15-18 November 2017, Bilbao.

**II. Solís, B.,** Guisasola, A., Pijuan, M., Baeza, J.A., 2021. **Exploring GHG emissions in the mainstream SCEPPHAR configuration during wastewater resource recovery.** Water Research, *In preparation*.

*Author's contribution:* Experimental design, experimental work and writing research paper. Pijuan, M., contributed to the experimental N<sub>2</sub>O measurements, discussion of the results and editing. Guisasola, A., and Baeza, J.A., contributed to the research supervision, experimental design, discussion of the results, writing and editing.

Part of this paper was presented as an oral presentation in the IWA Digital World Water Congress, 24 May – 4 June 2021.

**III. Solís, B.,** Guisasola, A., Flores-Alsina, X., Jeppsson, U., Baeza, J.A., 2021. **A plant-wide model describing GHG emissions and energy/nutrient recovery options for water resource recovery facilities.** Water Research, *Submitted*.

*Author's contribution:* Plant-wide model development, implementation of the control strategies and evaluation criteria, discussion of the results and writing of the research paper. Flores-Alsina, X., and Jeppsson, U., provided the model code in which the developed model is based and contributed to the discussion of the results and editing. Guisasola, A., and Baeza, J.A., contributed to the research supervision, design of control strategies, discussion of the results, writing and editing.

A preliminary version of this paper was presented as an oral presentation in IWA Watermatex 2019 congress during 1-4 September 2019, Copenhagen, Denmark. Part of this paper was presented as a poster presentation in the IWA Digital World Water Congress, 24 May – 4 June 2021.

Other scientific publications not included in this thesis:

**IV.** Massara, T.M., Solís, B., Guisasola, A., Katsou, E., Baeza, J.A., 2018. **Development of an ASM2d-N<sub>2</sub>O model to describe nitrous oxide emissions in municipal WWTPs under dynamic conditions.** Chemical Engineering Journal, 335, 185-196.

*Author's contribution:* The development of the model to include N<sub>2</sub>O emissions in the ASM2d and the implementation of the different dynamic scenarios were carried out by Massara, T.M., as well as the paper preparation. My main contribution was related to the validation of the model stoichiometric matrix, the sensitivity analysis study, the results discussion and paper editing.

## Abbreviations

---

<b>A<sup>2</sup>/O</b>	Anaerobic-anoxic-aerobic (WWTP configuration)
<b>ABAC</b>	Aeration-based ammonium controller
<b>AD</b>	Anaerobic digester
<b>ADM1</b>	Anaerobic digestion model no. 1
<b>AER</b>	Aerobic reactor (Chapter IV and V)
<b>ANA</b>	Anaerobic reactor (Chapter IV)
<b>ANAER</b>	Anaerobic reactor (Chapter V)
<b>ANOX</b>	Anoxic reactor (Chapter V)
<b>ANX</b>	Anoxic reactor (Chapter IV)
<b>AOB</b>	Ammonia oxidizing bacteria
<b>AOR</b>	Ammonia oxidation rate
<b>AS</b>	Activated sludge
<b>ASM</b>	Activated sludge model
<b>ASM2</b>	Activated sludge model number 2
<b>ASM2d</b>	Activated sludge model number 2d
<b>ASMN</b>	Activated sludge model for nitrogen
<b>BNR</b>	Biological nitrogen removal
<b>BOD</b>	Biological oxygen demand
<b>Br<sup>-</sup></b>	Bromide
<b>BSM2</b>	Benchmark simulation model no. 2
<b>BSM2-PSFe</b>	BSM2 for phosphorus, sulphur and iron
<b>BSM2-PSFe-GHG</b>	BSM2 for phosphorus, sulphur and iron and greenhouse gases
<b>BSM2G</b>	BSM2 greenhouse gas
<b>C</b>	Carbon
<b>Ca<sub>3</sub>(PO<sub>4</sub>)<sub>2</sub></b>	Amorphous calcium phosphate
<b>Ca<sub>5</sub>(PO<sub>4</sub>)<sub>3</sub>OH</b>	Hydroxyapatite
<b>CaCO<sub>3</sub></b>	Calcite
<b>CBIM</b>	Continuity-based interfacing method
<b>CCF</b>	Calibration cost function (Chapter III)
<b>CCF<sub>N2O</sub></b>	Calibration cost function for nitrous oxide (Chapter III)
<b>CCF<sub>NH4</sub></b>	Calibration cost function for ammonium (Chapter III)
<b>CCF<sub>NO2</sub></b>	Calibration cost function for nitrite (Chapter III)
<b>CCF<sub>NO3</sub></b>	Calibration cost function for nitrate (Chapter III)
<b>CH<sub>4</sub></b>	Methane
<b>CH<sub>4</sub>-EF</b>	Methane emission factor
<b>CO<sub>2</sub></b>	Carbon dioxide
<b>CO<sub>2e</sub></b>	Carbon dioxide equivalents
<b>COD</b>	Chemical oxygen demand
<b>COD<sub>fil</sub></b>	Filtered COD

<b>COD<sub>fil,eff</sub></b>	Effluent filtered COD
<b>COD<sub>sol</sub></b>	Soluble COD
<b>COD<sub>tot</sub></b>	Total COD
<b>CONV<sub>AS-AD</sub></b>	Conversion ASM-ADM interface
<b>CSTR</b>	Continuous stirred tank reactor
<b>DEN pathway</b>	Denitrification pathway
<b>DEW</b>	Dewatering unit
<b>D<sub>i</sub></b>	Diffusivity of component <i>i</i> in liquid phase (m <sup>2</sup> d <sup>-1</sup> )
<b>DO</b>	Dissolved oxygen
<b>D<sub>O2</sub></b>	Diffusivity of oxygen in liquid phase (m <sup>2</sup> d <sup>-1</sup> )
<b>DO<sub>SP</sub></b>	Dissolved oxygen set point
<b>DPAO</b>	Denitrifying polyphosphate accumulating organisms
<b>EBPR</b>	Enhanced biological phosphorus removal
<b>E<sub>production</sub></b>	Electricity production (Chapter V)
<b>EQI</b>	Effluent quality index (Chapter V)
<b>FA</b>	Free ammonia
<b>Fe</b>	Iron
<b>FeCl<sub>3</sub></b>	Ferric chloride
<b>FeS</b>	Iron sulphide
<b>FNA</b>	Free nitrous acid
<b>GHG</b>	Greenhouse gas
<b>GSA</b>	Global sensitivity analysis
<b>GWP</b>	Global warming potential
<b>H<sub>2</sub></b>	Hydrogen gas
<b>H<sub>2</sub>O</b>	Water
<b>H<sub>2</sub>S</b>	Hydrogen sulphide
<b>HCCF</b>	Hydraulic calibration cost function (Chapter III)
<b>HCO<sub>3</sub><sup>-</sup></b>	Bicarbonate
<b>HD pathway</b>	Heterotrophic denitrification pathway
<b>HFO</b>	Hydrous ferric oxides
<b>IC</b>	Inorganic carbon
<b>IR</b>	Internal recirculation
<b>IWA</b>	International water association
<b>KBr</b>	Potassium bromide
<b>K<sub>H,i</sub></b>	Henry's constant for the specie <i>i</i>
<b>k<sub>L,a<sub>i</sub></sub></b>	Mass transfer coefficient for component <i>i</i> (d <sup>-1</sup> )
<b>k<sub>L,a<sub>O2</sub></sub></b>	Mass transfer coefficient for oxygen (d <sup>-1</sup> )
<b>KNH<sub>4</sub>PO<sub>4</sub></b>	k-Struvite
<b>MC</b>	Monte carlo
<b>Mg(OH)<sub>2</sub></b>	Magnesium hydroxide
<b>Mg<sup>2+</sup></b>	Magnesium ion

<b>MgCl<sub>2</sub></b>	Magnesium chloride
<b>MgCO<sub>3</sub></b>	Magnesite
<b>MgHPO<sub>4</sub></b>	Newberyite
<b>MgNH<sub>4</sub>PO<sub>4</sub></b>	Struvite
<b>MLSS</b>	Mixed liquor suspended solids
<b>MMP</b>	Multiple mineral precipitation
<b>N</b>	Nitrogen
<b>N<sub>2</sub></b>	Nitrogen gas
<b>N<sub>2</sub>O</b>	Nitrous oxide
<b>N<sub>2</sub>O-EF</b>	Nitrous oxide emission factor (%)
<b>N<sub>2</sub>O-N</b>	Nitrous oxide nitrogen
<b>NaOH</b>	Sodium hydroxide
<b>ND pathway</b>	Nitrifier denitrification pathway
<b>NH<sub>2</sub>OH</b>	Hydroxylamine
<b>NH<sub>4</sub><sup>+</sup></b>	Ammonium
<b>NN pathway</b>	Nitrifier nitrification pathway
<b>NO</b>	Nitric oxide
<b>NO<sub>2</sub><sup>-</sup></b>	Nitrite
<b>NO<sub>3</sub><sup>-</sup></b>	Nitrate
<b>NOB</b>	Nitrite oxidizing bacteria
<b>NO<sub>x</sub></b>	Oxidized forms of nitrogen
<b>O<sub>2</sub></b>	Oxygen gas
<b>OCI</b>	Operational cost index (Chapter V)
<b>OHO</b>	Ordinary heterotrophic organism
<b>ORP</b>	Oxidation-reduction potential
<b>P</b>	Phosphorus
<b>PAO</b>	Phosphorus accumulating organism
<b>PCCF</b>	Preliminary calibration cost function (Chapter III)
<b>PCM</b>	Physico-chemical models (Chapter V)
<b>PHA</b>	Poly-hydroxyalkanoate
<b>P<sub>i</sub></b>	Partial pressure of the gas specie <i>i</i>
<b>PI</b>	Proportional integral controller
<b>PO<sub>4</sub><sup>3-</sup></b>	Phosphate
<b>PRIM</b>	Primary clarifier
<b>PROCESS<sub>AS-AD</sub></b>	Process ASM-ADM interface (Chapter V)
<b>Q<sub>w</sub></b>	Purge flow rate
<b>R1-HET</b>	Heterotrophic reactor of mainstream SCEPPHAR configuration
<b>R2-AUT</b>	Autotrophic reactor of mainstream SCEPPHAR configuration
<b>R3-PRE</b>	Precipitation reactor of mainstream SCEPPHAR configuration
<b>R4-INT</b>	Interchange reactor of mainstream SCEPPHAR configuration
<b>REC</b>	Recovery unit



<b>RSA</b>	Regional sensitivity analysis
<b>RTD</b>	Residence time distribution
<b>S</b>	Sulphur
<b>S<sub>A</sub></b>	Acetate (ASM state variable) (g m <sup>-3</sup> ) (Chapter V)
<b>S<sub>aa</sub></b>	Amino acids (ADM state variable) (kg m <sup>-3</sup> ) (Chapter V)
<b>S<sub>ac</sub></b>	Acetate (ADM state variable) (kg m <sup>-3</sup> ) (Chapter V)
<b>SBR</b>	Sequential batch reactor
<b>SCEPPHAR</b>	Short-cut enhanced phosphorus and PHA recovery
<b>SEC</b>	Secondary settler
<b>S<sub>F</sub></b>	Soluble fermentable (ASM) (g m <sup>-3</sup> ) (Chapter V)
<b>S<sub>fa</sub></b>	Fatty acids (ADM) (kg m <sup>-3</sup> ) (Chapter V)
<b>S<sub>i</sub></b>	Sensitivity index
<b>S<sub>I</sub></b>	Unbiodegradable soluble organics (ASM) (g m <sup>-3</sup> ) (Chapter V)
<b>S<sub>IC</sub></b>	Inorganic carbon (ASM, ADM) (g m <sup>-3</sup> ) (kmol m <sup>-3</sup> ) (Chapter V)
<b>S<sub>N2O</sub></b>	Nitrous oxide (ASM) (g m <sup>-3</sup> ) (Chapter V)
<b>S<sub>NH2OH</sub></b>	Hydroxylamine (ASM) (g m <sup>-3</sup> ) (Chapter V)
<b>S<sub>NH4</sub></b>	Ammonium plus ammonia nitrogen (ASM) (g m <sup>-3</sup> ) (Chapter V)
<b>S<sub>NO</sub></b>	Nitric oxide (ASM) (g m <sup>-3</sup> ) (Chapter V)
<b>S<sub>NO2</sub></b>	Nitrite (ASM) (g m <sup>-3</sup> ) (Chapter V)
<b>S<sub>O2</sub></b>	Dissolved oxygen (ASM) (g m <sup>-3</sup> ) (Chapter V)
<b>SP</b>	Set point
<b>S<sub>PO4</sub></b>	Phosphate (ASM) (g m <sup>-3</sup> ) (Chapter V)
<b>SRT</b>	Sludge retention time
<b>SS</b>	Steady-state
<b>S<sub>su</sub></b>	Sugars (ADM) (kg m <sup>-3</sup> ) (Chapter V)
<b>ST</b>	Storage tank
<b>T</b>	Temperature
<b>THK</b>	Thickener
<b>TIV</b>	Time in violation
<b>TKN</b>	Total kjeldahl nitrogen
<b>TN</b>	Total nitrogen
<b>TP</b>	Total phosphorus
<b>TSS</b>	Total suspended solid
<b>V</b>	Volume
<b>VFA</b>	Volatile fatty acid
<b>VS</b>	Volatile solids
<b>VSS</b>	Volatile suspended solid
<b>WRRF</b>	Water resource recovery facility
<b>WWTP</b>	Wastewater treatment plant
<b>X<sub>AOB</sub></b>	Ammonia oxidizing bacteria (ASM) (g m <sup>-3</sup> ) (Chapter V)
<b>X<sub>ch</sub></b>	Carbohydrates (ADM) (kg m <sup>-3</sup> ) (Chapter V)

$X_i$	Mineral concentration in solid phase (PCM) ( $\text{kmol m}^{-3}$ ) (Chapter V)
$X_I$	Inert particulates organics (ASM, ADM) ( $\text{g m}^{-3}$ ) ( $\text{kg m}^{-3}$ ) (Chapter V)
$X_{li}$	Lipids (ADM) ( $\text{kg m}^{-3}$ ) (Chapter V)
$X_{MeOH}$	Ferric hydroxide state variable (Chapter III)
$X_{NOB}$	Nitrite oxidizing bacteria (ASM) ( $\text{g m}^{-3}$ ) (Chapter V)
$X_{PP}$	Polyphosphates (ASM, ADM) ( $\text{g m}^{-3}$ ) ( $\text{kmol m}^{-3}$ ) (Chapter V)
$X_{pr}$	Proteins (ADM) ( $\text{kg m}^{-3}$ ) (Chapter V)
$X_S$	Biodegradable particulate organics (ASM) ( $\text{g m}^{-3}$ ) (Chapter V)
$X_{TSS}$	Total suspended solids (ASM) ( $\text{g m}^{-3}$ ) (Chapter V)



## Contents

---

Acknowledgements .....	vii
Summary .....	ix
Resumen .....	xi
Resum .....	xv
List of publications and author's contributions .....	xix
Abbreviations .....	xxi
Contents .....	xxvii
<b>Chapter I: General Introduction.....</b>	<b>1</b>
<b>1.1. Wastewater treatment.....</b>	<b>3</b>
1.1.1. The importance of wastewater treatment .....	3
1.1.2. Wastewater treatment plants .....	3
1.1.2.1. Activated sludge process for biological nutrient removal .....	4
1.1.2.1.1. Biological nitrogen removal (BNR) .....	5
1.1.2.1.2. Enhanced biological phosphorus removal (EBPR) .....	7
1.1.2.1.3. AS configurations for biological nutrient removal.....	8
<b>1.2. Energy and nutrient recovery from wastewater.....</b>	<b>8</b>
1.2.1. Mainstream SCEPPHAR configuration .....	9
<b>1.3. GHG emissions during wastewater treatment.....</b>	<b>10</b>
1.3.1. Biological pathways of N <sub>2</sub> O production .....	11
<b>1.4. Modelling of wastewater treatment processes .....</b>	<b>13</b>
1.4.1. Modelling of N <sub>2</sub> O production in ASM.....	14
<b>1.5. Benchmark Simulation Model platform.....</b>	<b>15</b>
<b>1.6. Research motivations and thesis overview .....</b>	<b>17</b>
1.6.1. Research motivations .....	17
1.6.2. Thesis overview.....	18
<b>Chapter II: Objectives.....</b>	<b>19</b>
<b>Chapter III: Systematic calibration of N<sub>2</sub>O emissions from a full-scale WWTP including a tracer test and a global sensitivity approach.....</b>	<b>23</b>
<b>Abstract .....</b>	<b>25</b>
<b>3.1. Motivations.....</b>	<b>25</b>
<b>3.2. Materials and methods.....</b>	<b>25</b>
3.2.1. Girona WWTP description.....	25
3.2.2. Hydraulic characterization procedure .....	26

3.2.3.	Experimental data campaign .....	28
3.2.4.	ASM2d-N <sub>2</sub> O structure .....	29
3.2.5.	Influent characterization.....	29
3.2.6.	Global Sensitivity Analysis (GSA) .....	31
3.2.7.	Calibration procedure .....	33
<b>3.3.</b>	<b>Results and Discussion .....</b>	<b>34</b>
3.3.1.	Experimental data and plant performance.....	34
3.3.2.	Hydraulic characterization .....	42
3.3.3.	Preliminary calibration.....	45
3.3.4.	Development of the Calibration Cost Function (CCF) .....	46
3.3.5.	Global Sensitivity Analysis .....	46
3.3.6.	Dynamic calibration .....	47
3.3.7.	Model exploitation .....	52
<b>3.4.</b>	<b>Conclusions.....</b>	<b>54</b>
<b>Chapter IV: Exploring GHG emissions in the mainstream SCEPPHAR</b>		
<b>configuration during wastewater resource recovery.....</b>		
		<b>55</b>
<b>Abstract .....</b>		<b>57</b>
<b>4.1. Motivations.....</b>		<b>57</b>
<b>4.2. Materials and Methods .....</b>		<b>57</b>
4.2.1.	Pilot plant configuration and influent.....	57
4.2.2.	Pilot plant monitoring and control architecture.....	60
4.2.3.	Chemical Analysis.....	61
4.2.4.	GHG emissions and Emission Factor calculations.....	61
<b>4.3. Results.....</b>		<b>62</b>
4.3.1.	Long term operation of the pilot plant.....	62
4.3.2.	Process performance of the pilot plant .....	63
4.3.3.	Overall GHG emissions of the pilot plant .....	70
4.3.4.	Effect of the aeration strategy on the N <sub>2</sub> O emissions.....	72
4.3.4.1.	Different DO <sub>SP</sub> .....	72
4.3.4.2.	Intermittent aeration.....	75
4.3.4.3.	Steps on the DO <sub>SP</sub> .....	77
<b>4.4. Overall assessment of GHG emissions.....</b>		<b>79</b>
4.4.1.	Comparison of GHG emissions with other WRRFs .....	79
4.4.2.	Factors affecting N <sub>2</sub> O emissions .....	80
<b>4.5. Conclusions.....</b>		<b>82</b>
<b>Chapter V: A plant-wide model describing GHG emissions and energy/nutrient</b>		
<b>recovery options for water resource recovery facilities .....</b>		
		<b>85</b>
<b>Abstract .....</b>		<b>87</b>

<b>5.1. Motivations</b> .....	<b>87</b>
<b>5.2. Materials and Methods</b> .....	<b>88</b>
5.2.1. BSM2-PSFe-GHG description .....	88
5.2.1.1. Biological models .....	88
5.2.1.2. Physico-Chemical Models (PCMs).....	89
5.2.1.2.1. pH and ion speciation/pairing.....	89
5.2.1.2.2. Multiple Mineral Precipitation (MMP) .....	89
5.2.1.2.3. Gas-liquid transfer .....	89
5.2.2. Model integration .....	90
5.2.3. Plant layout and ancillary processes.....	90
5.2.4. Estimation of GHG emissions.....	91
5.2.5. Evaluation criteria .....	93
5.2.6. Control strategies and sensors characteristics .....	93
<b>5.3. Results</b> .....	<b>94</b>
5.3.1. Steady State Simulations .....	94
5.3.2. Dynamic Simulations .....	98
5.3.2.1. Control strategy A <sub>1</sub> : Ammonium cascade & waste controller.....	99
5.3.2.2. Control strategy A <sub>2</sub> : Fe chemical precipitation of PO <sub>4</sub> <sup>3-</sup> .....	104
5.3.2.3. Control strategy A <sub>3</sub> : Struvite recovery.....	107
5.3.2.4. Control strategy A <sub>4</sub> : Ammonium & nitrite cascade controllers and struvite recovery .....	110
5.3.2.5. Control strategy A <sub>5</sub> : Ammonium & nitrous oxide cascade controllers and struvite recovery .....	114
5.3.2.6. Comparison of the evaluation criteria for the control strategies implemented .....	117
<b>5.4. Comparison with other works and limitations of the proposed methodology</b> .....	<b>118</b>
<b>5.5. Conclusions</b> .....	<b>120</b>
<b>Chapter VI: General Conclusions and Future Work</b> .....	<b>123</b>
<b>6.1. General Conclusions</b> .....	<b>125</b>
<b>6.2. Future Work</b> .....	<b>127</b>
<b>Chapter VII: References</b> .....	<b>129</b>
<b>Annex</b> .....	<b>141</b>
<b>Annex I: ASM2d-N<sub>2</sub>O model description</b> .....	<b>143</b>
<b>Annex II: ASM2d-PSFe-N<sub>2</sub>O stoichiometric matrix</b> .....	<b>157</b>
<b>Annex III: Evaluation of potential operational and control strategies in a plant- wide WWTP model to mitigate GHG emissions</b> .....	<b>165</b>
<b>Abstract</b> .....	<b>165</b>

<b>A3.1. Motivations</b> .....	165
<b>A3.2. Materials and Methods</b> .....	166
<b>A3.3. Results</b> .....	175
<b>A3.4. Conclusions</b> .....	194
<b>A3.5. References</b> .....	194

# **Chapter I:**

---

## **General Introduction**





## 1. General Introduction

### 1.1. Wastewater treatment

#### 1.1.1. *The importance of wastewater treatment*

Most of the human activities that use water produce wastewater. Wastewater can be defined as the combination of the water-carried wastes removed from residences, institutions and industrial establishments, together with groundwater, surface water and storm water (Metcalf & Eddy, 2003). As the overall demand for water grows, the quantity of wastewater produced and its overall pollution load are continuously increasing worldwide (WWAP, 2017). Therefore, wastewater treatment is becoming a critical point on water management.

Wastewater contains significant amounts of pollutants and the composition largely varies depending on the area where is collected. The main pollutants of wastewater are biodegradable and non-biodegradable compounds, nutrients (mostly nitrogen (N) and phosphorus (P)), toxic substances, pathogens and inorganic suspended solids. Therefore, wastewater should be treated before its discharge to surface waters to prevent both public health risks due to spreading pathogenic diseases and environmental problems to natural waters, such as the eutrophication, and environmental problems to air by greenhouse gas (GHG) emissions. Eutrophication occurs on water bodies due to the fact that unbalanced N and P concentrations lead to oxygen depletion and a significant ecological degradation (Metcalf & Eddy, 2014).

Therefore, the main objective of wastewater treatment is to allow treated urban wastewater discharge into surface waters ensuring protection of public health and environment. In the last decades, wastewater discharges in sensitive areas are regulated by legislation (Urban Wastewater Treatment Directive, Council Directive 91/271/EEC) in order to control nutrient pollution in water ecosystems. The directive sets emission limit values and, therefore, wastewater should be treated to a certain degree before disposal to receiving waters or before reuse.

#### 1.1.2. *Wastewater treatment plants*

The process of wastewater treatment takes place in wastewater treatment plants (WWTPs). An example of conventional WWTP treating urban wastewater is shown in Figure 1.1. Due to the different nature of contaminants present in the wastewater, WWTP constitutes several stages wherein a certain type of contaminant is targeted to be removed in each stage in different ways of treatment: physical, chemical or biological.

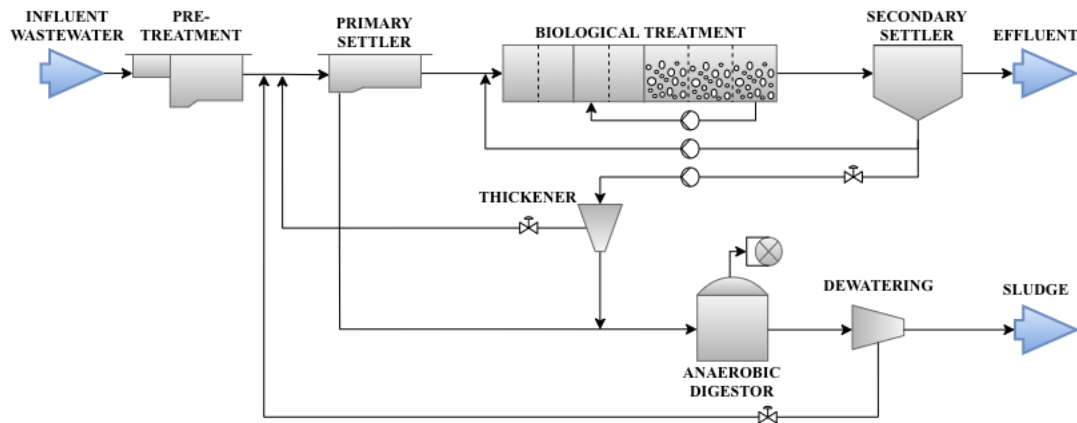


Figure 1.1. Example of a wastewater treatment plant configuration.

Traditionally, the first stage of a WWTP is the pre-treatment. The main objective of the pre-treatment is to remove the coarse materials and large solids, such as sand, present in the influent wastewater. The pre-treatment usually consists of bar screens, sieves and grit chambers. The next stage is the primary sedimentation of undissolved particles. Particle settling may be boosted with the addition of chemicals for its flocculation or by biological mechanisms. The next stage of a WWTP is the biological treatment. The most commonly used technology is the activated sludge (AS) process (Ardern and Lockett, 1914; Van Loosdrecht and Brdjanovic, 2014). Microorganisms are used to consume and degrade pollutants in the biological treatment. Usually, aerobic microorganisms grow using oxygen as electron acceptor. This oxygen is supplied through different aeration strategies and equipment. A secondary settler separates the effluent treated wastewater from the sludge containing the microorganisms. The settled sludge is recycled again to the biological treatment. The excess sludge is sent to the sludge line. The main objective of the sludge line of WWTPs is to reduce the volume of the sludge and stabilize it. Therefore, the excess sludge is first sent to a thickener or flotation unit to remove part of wastewater from the sludge. This extracted liquid is fed again to the primary sedimentation tank. Then, the concentrated sludge is either valorised externally or sent to an anaerobic digester where different types of anaerobic bacteria degrade it in view of its energetic valorisation as biogas. Finally, the stabilized sludge is sent to a dewatering unit to further reduce its volume. The effluent sludge is chemically stable and contains a reduced number of pathogens. Thus, the sludge can be disposed and reused.

#### *1.1.2.1. Activated sludge process for biological nutrient removal*

The AS process is currently the most widely used process for biological wastewater treatment due to its high versatility to treat different influent compositions (organic matter, N and P) ensuring stringent effluent criteria (Ardern and Lockett, 1914; Metcalf & Eddy, 2003; Van Loosdrecht and Brdjanovic, 2014).

Initially, the AS process was designed to remove organic matter by means of an aerobic reactor for biological organic matter oxidation followed by a sedimentation tank where the sludge is separated from the treated wastewater. The AS process is a suspended growth process that maintains a high concentration of biomass by recycling the sludge from the sedimentation tank to the biological reactor. This system allows the conversion of approximately half of the chemical oxygen demand (COD) to sludge and the other half to carbon dioxide ( $\text{CO}_2$ ). During the last decades, many improvements were made to upgrade the AS process by implementing biological nutrient removal processes such as the biological nitrogen removal (BNR) and the enhanced biological phosphorus removal (EBPR).

#### 1.1.2.1.1. Biological nitrogen removal (BNR)

Conventional BNR in AS systems takes place through two main bioprocesses called nitrification and denitrification, whereby most of the N entering the WWTP is finally emitted as nitrogen gas ( $\text{N}_2$ ) and released into the atmosphere (Bernhard, 2010; Massara et al., 2017). Figure 1.2 shows a simplified N cycle and relevant biological transformations during wastewater treatment.

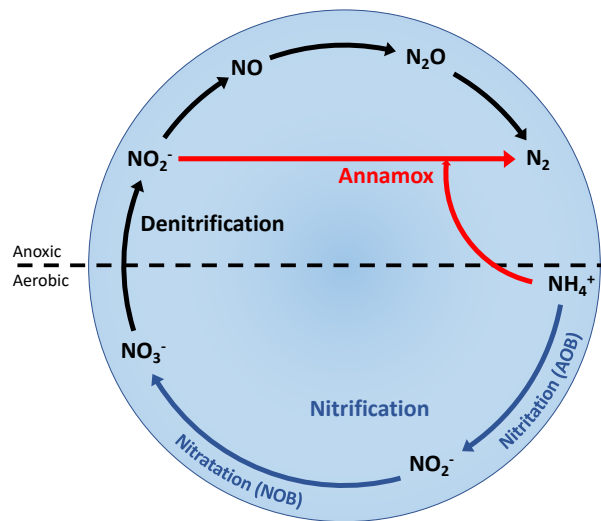
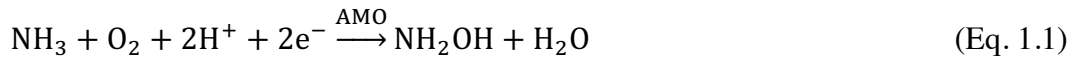


Figure 1.2. Biological transformations in the N cycle during wastewater treatment. Blue and black arrows represent the conventional nitrification and denitrification processes, respectively. In red arrows are represented the Anammox process (adapted from Bernhard, (2010)).

Nitrification is the first step of conventional BNR, in which ammonium ( $\text{NH}_4^+$ ) is converted in aerobic conditions to nitrate ( $\text{NO}_3^-$ ) with nitrite ( $\text{NO}_2^-$ ) as intermediate. Two different microbial populations are responsible for the nitrification process: the ammonia oxidation bacteria (AOB) and the nitrite oxidizing bacteria (NOB). In WWTPs, nitrification is assumed to be predominantly performed by autotrophic AOB and NOB

that use  $\text{CO}_2$  as their C source and the substrate ( $\text{NH}_4^+$  and  $\text{NO}_2^-$ , respectively) as their energy source (Kampschreur et al., 2009b). In a first step, AOB convert ammonia ( $\text{NH}_3$ ) to  $\text{NO}_2^-$  with hydroxylamine ( $\text{NH}_2\text{OH}$ ) as an intermediate and with oxygen ( $\text{O}_2$ ) as electron acceptor. This process is known as nitrification, and it is a two-step process that requires two enzymes, the first reaction is catalysed by ammonia monooxygenase (AMO) and the second one by hydroxylamine oxidoreductase (HAO) (Equation 1.1 and Equation 1.2) (Bernhard, 2010). The majority of AOB belong to *Nitrosomonas*, *Nitrosospira* and *Nitrosococcus* genera (Bernhard, 2010; Purkhold et al., 2000).



The second step of nitrification is known as nitratation, in which NOB further oxidize nitrite to nitrate using oxygen as electron acceptor (Equation 1.3). This reaction is catalysed by the nitrite oxidoreductase (NXR) enzyme of NOB. Some of the genera involved in NOB includes *Nitrospira*, *Nitrobacter*, *Nitrococcus* and *Nitrospina* (Bernhard, 2010).



Denitrification is the second step of conventional BNR (Figure 1.2). In this process, nitrate is reduced to nitrogen gas under anoxic conditions mostly by facultative heterotrophic bacteria using organic carbon as electron donor (organic matter oxidation). Denitrification consists of four sequential reduction reactions: first, nitrate is reduced to nitrite, then to nitric oxide (NO), nitrous oxide ( $\text{N}_2\text{O}$ ) and finally to nitrogen gas. The enzymes involved in the process are nitrate reductase (NaR), nitrite reductase (NiR), nitric oxide reductase (NoR) and nitrous oxide reductase (NoS) (Equation 1.4) (Zumft, 1997).



Both nitrification and denitrification processes are highly affected by different environmental parameters such as: temperature, pH, dissolved oxygen (DO) concentration, free nitrous acid and free ammonia concentrations, and the lack of inorganic carbon for nitrification and of organic matter (low COD/N ratio) for denitrification (Kampschreur et al., 2009b; Metcalf & Eddy, 2003).

Novel BNR solutions have been developed in the past years in view of reducing the costs due to aeration and the organic carbon requirements for the denitrification process. Nitritation/denitritation process is an alternative BNR process, also known as N-removal shortcut or nitrite pathway. Nitritation/denitritation process is the conversion of ammonium to nitrite (nitritation) followed by nitrite reduction (denitritation) (Henze et

al., 2008; Mavinic and Turk, 1987). Autotrophic N-removal is other cost-effective BNR solution known as anaerobic ammonium oxidation (Anammox), in which Anammox microorganisms oxidize ammonium to nitrogen gas under anoxic conditions using nitrite (produced by AOB during nitrification) as electron acceptor (Figure 1.2) (Bernhard, 2010; Sliemers et al., 2002).

#### 1.1.2.1.2. Enhanced biological phosphorus removal (EBPR)

The removal of phosphorus by biological means during wastewater treatment is known as enhanced biological phosphorus removal (EBPR) process. P removal during wastewater treatment is done to control eutrophication in freshwater systems. EBPR process is considered the most efficient, cost-effective and sustainable ways to remove P from wastewater, because it reduces chemical costs and less sludge production as compared to P removal via chemical precipitation, as traditionally done (Metcalf & Eddy, 2003; Oehmen et al., 2007).

EBPR is based on the enrichment of polyphosphate accumulating organisms (PAO) in the AS system, by alternating anaerobic and aerobic(anoxic) conditions (Figure 1.3). PAO, under anaerobic conditions, are capable of accumulating poly-hydroxyalkanoates (PHA) intracellularly from the volatile fatty acids (VFA) taken up. The required energy for this process is obtained from the hydrolysis of the intracellular poly-phosphate reserves, releasing thereby phosphate ( $\text{PO}_4^{3-}$ ) into the medium. In the subsequent aerobic phase, PAO use oxygen as electron acceptor to oxidize the accumulated PHA and to uptake the released  $\text{PO}_4^{3-}$ . PAO are able to accumulate more poly-phosphate than the phosphate previously released under anaerobic conditions. Therefore, the net removal of P is based on wasting the excess sludge after the aerobic step. Part of the PAO, the denitrifying PAO (DPAO), are capable of using nitrite or nitrate as electron acceptors (anoxic conditions) to oxidize PHA while uptaking  $\text{PO}_4^{3-}$ . A more detailed description of the PAO metabolism can be found in Oehmen et al. (2007).

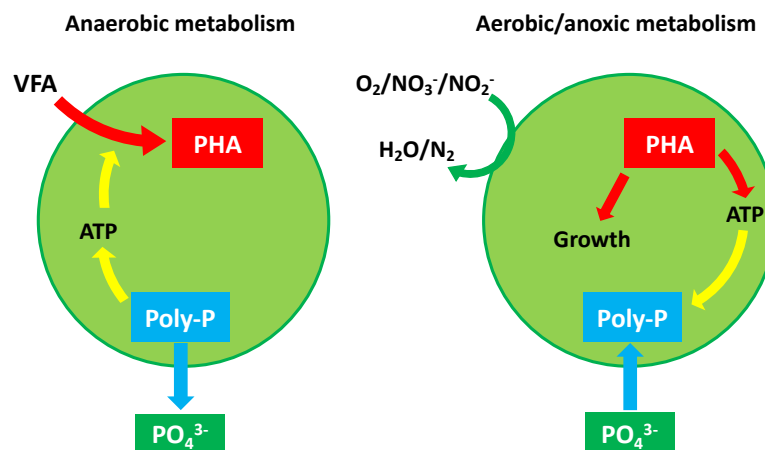


Figure 1.3. Simplified schematic representation of PAO metabolism.

### 1.1.2.1.3. AS configurations for biological nutrient removal

Organic matter oxidation, BNR and EBPR have to coexist with each other. Therefore, simultaneous carbon (C), N and P removal implies an anaerobic reactor for promoting PAO growth, an anoxic reactor to promote denitrification and an aerobic reactor for nitrification, PAO growth and removal of the excess of COD. The anaerobic-anoxic-aerobic (A<sup>2</sup>/O) configuration of AS has been widely used (Figure 1.4). Despite the high versatility of A<sup>2</sup>/O configuration, the main disadvantages are the detrimental effects that appear due to the incomplete denitrification of nitrate and nitrite (NO<sub>x</sub>), since nitrification occurs in the last reactor (aerobic), and some nitrate is recirculated to the anaerobic reactor leading to possible EBPR failure (Henze et al., 2008). In this sense, alternative configurations have been designed to reduce the NO<sub>x</sub> concentration recycled to the anaerobic reactor such as the 5-stage Bardenpho, the University of Cape Town (UCT) configuration and modified UCT configuration, the Johannesburg process or sequential batch reactor (SBR) configurations (Barnard, 1976; Bunce et al., 2018; Henze et al., 2008; Metcalf & Eddy, 2003).

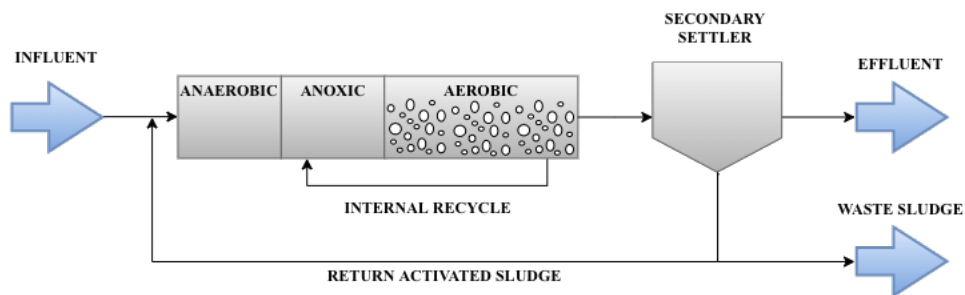


Figure 1.4. Anaerobic-anoxic-aerobic (A<sup>2</sup>/O) configuration of AS.

## 1.2. Energy and nutrient recovery from wastewater

During the last decade, in the face of ever-growing demand, wastewater had gained momentum as a reliable alternative source of water, shifting the paradigm of wastewater management from treatment and disposal to reuse, recycle and resource recovery (WWAP, 2017). In this sense, WWTP are being transformed into water resource recovery facilities (WRRF). The objective of these facilities is not only to achieve a good effluent quality under constraints of technical feasibility and cost, but also to recover resources (bioplastics, cellulose or N and P into fertilizers such as struvite), water and energy (in energy carriers such as biogas or hydrogen) in a sustainable way. Novel WRRFs configurations as well as innovative operational and control strategies have been arisen recently to promote this new paradigm shift.

Energy can be recovered in the form of biogas for heating/cooling and electricity generation. Technologies exist for on-site energy recovery through sludge treatment processes integrated in WWTPs, allowing them to transition from energy consumers to

energy neutrality, or even to net energy producers (WWAP, 2017). In conventional WWTPs (Figure 1.1), the biogas that is produced in the anaerobic digester can be combusted in a cogeneration unit to obtain heat and power.

Regarding resource recovery, P arises as a perfect candidate for its recovery from wastewater. P is essential for our society in the production of fertilizers. However, the main source of P is the phosphate rock, which is estimated to be depleted in the next 50-300 years (Cieřlik and Konieczka, 2017; Cordell et al., 2011). During wastewater treatment, it is estimated that 3 million tons of P are removed yearly, showing that the implementation of P-recovery strategies would mitigate the current dependency on the phosphate rocks (Mayer et al., 2016). Among others, struvite precipitation (Equation 1.5) has been shown as a feasible and cost-effective process for P and N recovery because it can be directly applied as a substitute for conventional agricultural fertilizers (Shu et al., 2006).



Different studies have shown that P-recovery based on EBPR activity seems to be a good option to undertake P-recovery strategies (Baeza et al., 2017; Guisasola et al., 2019; Larriba et al., 2020; Lizarralde et al., 2019; Valverde-Pérez et al., 2015).

### 1.2.1. Mainstream SCEPPHAR configuration

The novel mainstream SCEPPHAR (Short Cut Enhanced Phosphorus and PHA recovery) configuration of WRRF has demonstrated at demo scale and under real influent conditions the feasibility of implementing resource recovery in the mainstream line (struvite and PHA-rich sludge) (Larriba et al., 2020). The mainstream SCEPPHAR is one of the novel technologies involved in the SMART-Plant project ([www.smart-plant.eu](http://www.smart-plant.eu)). The whole project aimed to prove the feasibility of novel wastewater treatment technologies at pilot-scale towards a circular economy scenario. The mainstream SCEPPHAR pilot plant is based on two sequenced batch reactors (SBR), the first mainly heterotrophic (R1-HET), designed to promote EBPR, and the second reactor mainly autotrophic (R2-AUT) (Larriba et al., 2020). During the first long term operation of the mainstream SCEPPHAR, the pilot plant achieved successful removal efficiencies for C, P and N under nitrite shortcut N-removal, i.e. the N-removal via nitritation and denitrification. The advantages of nitrite pathway approach are the lower oxygen requirements for N oxidation, the lower COD requirements for denitrification processes and faster denitrification rate (Mavinic and Turk, 1987). However, the nitrite accumulation could have a negative effect on the N<sub>2</sub>O emissions (Law et al., 2012b). Regarding nutrient recovery results, up to 45-63% of the influent P load could be recovered as struvite in a separate reactor in the mainstream line (Larriba et al., 2020), which is higher than the 12% of influent P reported within side-stream P-recovery (Remy



and Jossa, 2015). In addition, the implementation of the R1-HET purge at the end of the anaerobic phase enabled purging a sludge with a concentration of 6.9-9.2% of PHA (Larriba et al., 2020). Although this concentration is not economically feasible for a potential recovery of PHA as bioplastic, it increased the CH<sub>4</sub> production in the anaerobic digester (Chan et al., 2020). However, the GHG emissions associated to this novel operation strategy were not assessed. A detailed description of the mainstream SCEPPHAR configuration and operation is presented in section 4.2.1.

### 1.3. GHG emissions during wastewater treatment

Over the past years, concerns regarding the sustainability of WWTPs have increased, with particular attention on the C footprint from the impact of greenhouse gases (GHG) emissions on the climate change. Therefore, many water utilities have become aware of the potential GHG emissions during the operation of WWTPs and there is an increasing need to reduce these emissions and to identify the factors that control the GHG emissions from WWTPs. Three major GHGs can be produced and emitted during wastewater treatment: carbon dioxide (CO<sub>2</sub>), methane (CH<sub>4</sub>) and nitrous oxide (N<sub>2</sub>O) (Kampschreur et al., 2009b; Lijó et al., 2017).

The GHG emitted from WWTPs are divided into two groups: direct or indirect emissions, referring to whether the emissions happen at the WWTP or externally as a consequence of its operation. Usually, the total GHG emissions from the operation of WWTP are given in unit of CO<sub>2</sub> equivalents (CO<sub>2e</sub>) according to the Intergovernmental Panel on Climate Change (IPCC). Each GHG has defined a global warming potential (GWP) reported by the IPCC that compares the global warming effect of each GHG by the GWP of CO<sub>2</sub> (defined as 1) (IPCC, 2014).

Regarding CO<sub>2</sub> emissions, indirect emissions are estimated based upon the energy requirements and the use of external chemicals of the plant, while direct emissions are calculated based on the processes occurring during the different stages of the WWTP (Massara et al., 2017). The CO<sub>2</sub> emissions from oxidation of COD from the influent are considered biogenic and usually are not accounted on the total emissions of the WWTP because is not originated from fossil fuels (Kampschreur et al., 2009b).

CH<sub>4</sub> is also emitted during wastewater treatment. CH<sub>4</sub> has a GWP 21 times higher than that of CO<sub>2</sub> (IPCC, 2014). Previous studies have demonstrated that the CH<sub>4</sub> emitted during wastewater treatment can be present in the influent of the plant, produced under the anaerobic environments in the sewer network (Guisasola et al., 2008; Gutierrez et al., 2014), or present in the reject water recirculated from the anaerobic digester, which is usually recirculated to the inlet of the plant (Ribera-Guardia et al., 2019; Rodriguez-Caballero et al., 2014). This dissolved CH<sub>4</sub> is usually emitted after it is stripped in the aerobic reactors of the WWTP (Daelman et al., 2012).

Finally,  $N_2O$  is a GHG that is produced and emitted during BNR in WWTPs. Due to its high GWP, 265 times higher than that of  $CO_2$  (IPCC, 2014), the C footprint of WWTPs are highly sensitive to  $N_2O$  emissions (Gustavsson and Tumlin, 2013). In addition,  $N_2O$  is an ozone layer depletion substance (Ravishankara et al., 2009). Measurement campaigns on full scale WWTPs have shown high variability on the measured  $N_2O$  emissions, with a  $N_2O$  emission factor ( $N_2O$ -EF, defined as the fraction of influent nitrogen load emitted as  $N_2O$ ) ranging between 0.01% and 1.8%, and in some cases even higher than 10% (Foley et al., 2010; Kampschreur et al., 2009b; Peng et al., 2015). The large variation in  $N_2O$  emissions reported by different studies was probably due to the different configurations and operational conditions applied, in addition that different monitoring and quantification methods used could had a contribution factor (Ribera-Guardia et al., 2019). The large variation also implies that  $N_2O$  emissions can be reduced through proper design and operation. In the next section the biological mechanisms for  $N_2O$  production/emission and the parameters that affect these mechanisms are discussed.

### 1.3.1. Biological pathways of $N_2O$ production

Based on the current knowledge, both autotrophic and heterotrophic bacteria can produce  $N_2O$  during nitrification and denitrification processes. The biological pathways leading to  $N_2O$  production are three: i)  $NH_2OH$  oxidation, ii) nitrifier denitrification and iii) heterotrophic denitrification (Law et al., 2012b; Massara et al., 2017; Ni and Yuan, 2015; Wunderlin et al., 2013, 2012). These processes are schematically shown in Figure 1.5. AOB can produce  $N_2O$  in the first step of nitrification (Equation 1.1) through the  $NH_2OH$  oxidation and through the nitrifier denitrification as a side process of nitrification. It is generally accepted that NOB and anammox bacteria do not contribute to  $N_2O$  production (Kampschreur et al., 2009a; Law et al., 2012b).

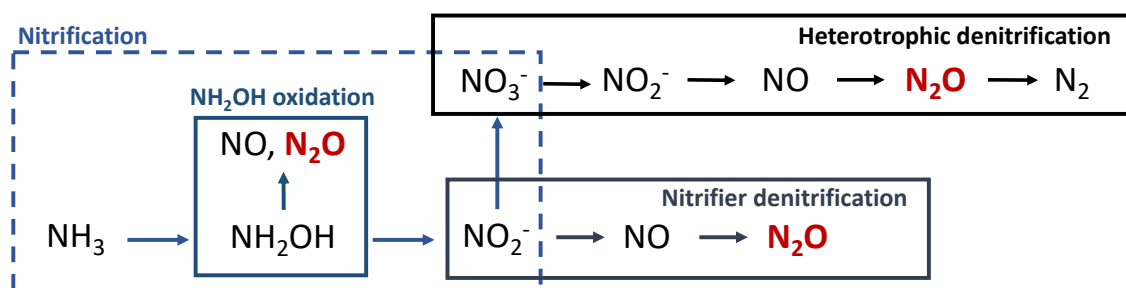


Figure 1.5. Simplified representation of the three biological  $N_2O$  production pathways during conventional nitrification and denitrification processes (adapted from Arnell, (2016)).

The  $N_2O$  production through  $NH_2OH$  oxidation pathway, also known as nitrifier nitrification pathway, denoted as NN pathway, occurs as an incomplete oxidation of  $NH_2OH$  to  $NO_2^-$  by AOB during the second step of nitrification (Equation 1.2). In fact, the oxidation of  $NH_2OH$  to  $NO_2^-$  is a two-step process with a nitrosyl radical (NOH) as an

intermediate. Being a radical, NOH is very unstable and it can be degraded to NO and N<sub>2</sub>O if accumulated (Law et al., 2012b). Process disturbances leading to increased ammonium oxidation rates can cause unbalanced AOB activity and can lead to incomplete NH<sub>2</sub>O oxidation with N<sub>2</sub>O as a final product rather than NO<sub>2</sub><sup>-</sup>, leading to significant N<sub>2</sub>O production via this pathway (Law et al., 2012b; Massara et al., 2017; Ni and Yuan, 2015; Peng et al., 2014). The two conditions suggested to increase the N<sub>2</sub>O production via the NN pathway are elevated NH<sub>4</sub><sup>+</sup> levels and transient conditions, such as increasing levels of dissolved oxygen (DO) (Law et al., 2012b; Peng et al., 2014).

AOB can also produce N<sub>2</sub>O via the nitrifier denitrification pathway (Figure 1.5), denoted as ND pathway. AOB have the capability to reduce NO<sub>2</sub><sup>-</sup> to NO catalysed with the nitrite reductase (NirK) enzyme, and further to N<sub>2</sub>O catalysed with the nitric oxide reductase (Nor) enzyme. Although, nitrifier denitrification is not an important bioprocess in terms of N removal, it can be critical in terms of N<sub>2</sub>O emissions (Law et al., 2012b; Massara et al., 2017; Ni and Yuan, 2015). In addition, the ND pathway has been shown to be the most contributor pathway to total N<sub>2</sub>O production. One condition shown to trigger the N<sub>2</sub>O production through the ND pathway is the NO<sub>2</sub><sup>-</sup> accumulation, which is promoted under anoxic conditions and aerobic conditions with low DO levels (Kampschreur et al., 2009b; Peng et al., 2014; Tallec et al., 2006). The second parameter that most affect the N<sub>2</sub>O emission via the ND pathway is the DO concentration, with lower oxygen concentration leading to higher N<sub>2</sub>O emissions (Kampschreur et al., 2009b; Tallec et al., 2006). In oxygen limiting conditions, AOB use NO<sub>2</sub><sup>-</sup> as the terminal electron acceptor to save oxygen for the oxidation of NH<sub>4</sub><sup>+</sup> to NH<sub>2</sub>OH (Kampschreur et al., 2009b).

The last biological production pathway is during the heterotrophic denitrification (Figure 1.5 and Equation 1.3) and is usually denoted as HD pathway. N<sub>2</sub>O is formed as an obligate intermediate of the four-step reduction of NO<sub>3</sub><sup>-</sup> to N<sub>2</sub>. Therefore, the heterotrophic denitrification serves as a mechanism of N<sub>2</sub>O consumption if not disturbed (Massara et al., 2017). However, some operation conditions such as DO, pH and organic matter availability, have shown to disturb the reduction reactions, leading to accumulation of intermediate compounds. Furthermore, low COD to N ratio in the influent leads to electron competition, triggering the accumulation of N<sub>2</sub>O (Kampschreur et al., 2009b; Pan et al., 2013a).

Chemical N<sub>2</sub>O production is also possible (Domingo-Félez and Smets, 2016; Heil et al., 2014; Soler-Jofra et al., 2016). However, the percentage of N<sub>2</sub>O emitted in full-scale WWTPs due to chemical processes is still under research. In any case, the current research suggests that most of the N<sub>2</sub>O emitted in WWTPs is generated during biological processes (Massara et al., 2017).

It is important to note that N<sub>2</sub>O has a relatively high solubility in water and accumulation of N<sub>2</sub>O in the liquid phase does not imply an instant emission to the atmosphere. If the

subsequent reactor is not aerated, the denitrifying bacteria can reduce the  $N_2O$  to  $N_2$ . However, if the subsequent reactor is aerated,  $N_2O$  will be stripped to the atmosphere.

#### 1.4. Modelling of wastewater treatment processes

In WWTP operation, the main objective is to remove pollutants from the wastewater, obtaining an effluent below the legal discharge limits at the lowest possible cost. However, due to complex interactions between the different variables relating to the operation of the WWTP, it is challenging to control the plant operation in such a way as to treat wastewater at the lowest possible cost. In this sense, mathematical models for wastewater treatment plant processes become useful in predicting their behaviour and in exploring different approaches to improve the WWTP performance (Henze et al., 2008; Jeppsson et al., 2013). In the field of wastewater, the three main models applications are for learning, design and process optimization (Gernaey et al., 2004).

In addition, the new challenges of wastewater treatment, i.e. the resource recovery and the mitigation of the C-footprint, has promoted both the chemical and environmental engineering community and the water industry to open the scope of the new WRRFs. To better understand and design these facilities, plant-wide modelling tools have become essential (Jeppsson et al., 2013; Seco et al., 2020). Wastewater treatment modelling researchers have integrated the main unit operations of a WWTP (primary clarifier, biological reactor, secondary settler, thickener, anaerobic digester, dewatering unit, etc.) to account for all the interactions among processes (Barat et al., 2013; Gernaey et al., 2014; Grau et al., 2007; Hauduc et al., 2019; Solon et al., 2017; Vaneeckhaute et al., 2018) in view of simulating plant yields under different scenarios and of designing novel control strategies for a better performance.

Traditionally, the unit process that has received more attention in the wastewater treatment modelling community is the activated sludge system. The activated sludge models (ASM), developed by the International Water Association (IWA) (Henze et al., 2000), are mathematical models describing biological and chemical transformations occurring in activated sludge systems. The ASMs are a set of ordinary differential equations. Each differential equation describes the rate of change of a state variable due to consumption and production of this variable for all the processes where it is involved. The process rate is described by model components and kinetic parameters. The mass balances of the model components are coupled through stoichiometry. The first ASM published was the ASM1 (Henze et al., 1987). The objective of the ASM1 was to create a standard framework of a model with the lowest complexity as possible but still able to accurately predict biological processes. The ASM2d is able simulate the fate of organic matter, N and P transformations (Henze et al., 2000) and it is widely-used when accounting for EBPR processes. The ASMs have been accepted by wastewater treatment

researchers and practitioners over the last two decades and several ASM-extensions models have been published.

Aside from the ASM family, the standard Anaerobic Digestion Model No. 1 (ADM1) (Batstone et al., 2002) was developed as a consensus model for the anaerobic digester processes (Figure 1.1). To date, several extensions to the ADM1 have been proposed by the wastewater treatment community to explain different processes such as the P transformation (Flores-Alsina et al., 2016) or the anaerobic co-digestion (Arnell et al., 2016). Another unit process at WWTPs that gained a lot of attention in modelling are settlers, mainly secondary settling, in order to improve the simulation of a complete activated sludge unit. Traditionally, the most used secondary settler model was the ten-layer 1-dimension settling model of Takács et al., (1991). However, new settler models have been published (Bürger et al., 2013) allowing for a more realistic effluent total suspended solids (TSS) prediction.

#### *1.4.1. Modelling of N<sub>2</sub>O production in ASM*

Over the past years, modelling BNR has gained more attention in view of a better understanding of N<sub>2</sub>O production, accumulation and emission. The ability to predict N<sub>2</sub>O emissions serves as a method for verifying hypothesis related to fundamental mechanisms for N<sub>2</sub>O production, and it can be used to anticipate N<sub>2</sub>O emissions in the design and operation of WWTPs as well as in the design of potential mitigation strategies (Massara et al., 2017; Ni and Yuan, 2015).

Different ASM-based models have been developed aiming at predicting different lab-scale or full-scale N<sub>2</sub>O emissions (Domingo-Félez and Smets, 2016; Massara et al., 2018; Ni et al., 2013b; Ni and Yuan, 2015; Pocquet et al., 2016) These models vary on the biological description and the number of N<sub>2</sub>O pathways that incorporate, accounting for one, two or three of the biological pathways for N<sub>2</sub>O production (ND, NN and/or HD, Figure 1.5).

Regarding nitrification-based N<sub>2</sub>O emissions, single-pathway models were initially proposed, describing either the ND or NN pathway (Massara et al., 2017; Ni and Yuan, 2015). The inclusion of NH<sub>2</sub>OH as state variable allowed the modelling of the NN pathway as a fraction of NH<sub>2</sub>OH oxidation to NO<sub>2</sub><sup>-</sup> and also allowed the description of NH<sub>2</sub>OH as electron donor for the reduction of NO<sub>2</sub><sup>-</sup> to N<sub>2</sub>O (ND pathway) (Law et al., 2012b; Ni et al., 2013a). However, it was seen that the models only including a single N<sub>2</sub>O production pathway could not explain all the experimental data in the literature. Therefore, it was formulated that two-pathway AOB models are adequate in predicting the shift in ND and NN pathways contribution to total N<sub>2</sub>O production under different DO and NO<sub>2</sub><sup>-</sup> levels (Pocquet et al., 2016).

On the other hand, the extension of ASM for N removal processes (ASM<sub>N</sub>) (W. C. Hiatt and Grady, 2008) is widely used to describe the heterotrophic denitrification processes and, therefore, the production of N<sub>2</sub>O as an intermediate (HD pathway). This approach is based on the four consecutive reduction reactions (Equation 1.3) and considers every reduction rate independent from each other. The ASM<sub>N</sub> can predict COD and N removal for systems with low intermediates levels (NO<sub>2</sub><sup>-</sup>, NO and N<sub>2</sub>O) but might be inadequate for systems with high accumulation of intermediates (Ni and Yuan, 2015). Other models have been developed to describe the competitive electron distribution during the denitrification processes (Pan et al., 2013b; Richardson et al., 2009).

ASM-based models that account for N<sub>2</sub>O production for both nitrification and denitrification processes consist usually in a single- or two-pathway AOB model and an heterotrophic denitrification model (Domingo-Félez and Smets, 2016; Guo and Vanrolleghem, 2014; Massara et al., 2018). Among the different published N<sub>2</sub>O models, the ASM2d-N<sub>2</sub>O model developed by Massara et al., (2018) is an ASM type model that includes N, P and organic matter removal; integrates all the microbial pathways for N<sub>2</sub>O production and consumption: the NN and ND pathway of AOB and the HD pathway of heterotrophic organisms; contains N<sub>2</sub>O stripping modelling and estimates the N<sub>2</sub>O-EF under a wide range of operating conditions. Therefore, the ASM2d-N<sub>2</sub>O model is a promising tool for developing N<sub>2</sub>O mitigation strategies during full-scale WWTP. However, although the different sub-models of the whole ASM2d-N<sub>2</sub>O were calibrated separately, the prediction capability of the ASM2d-N<sub>2</sub>O model has not been proved during full-scale treatment. A description of the ASM2d-N<sub>2</sub>O model is presented in section 3.2.4 and in Massara et al., (2018). The stoichiometric matrix, the kinetic rates and the parameters involved in the ASM2d-N<sub>2</sub>O are shown in the annex I section.

### **1.5. Benchmark Simulation Model platform**

In process modelling and control, a benchmark is defined as a process model and the associated control strategy that can be used as a reference point for simulation-based comparison of control strategies (Downs and Vogel, 1993). As discussed in previous chapters, the operation of a WWTP has to be controlled to ensure good effluent quality, at minimum operational cost. Many control strategies have been proposed in the literature, however, the performance of the different control strategies is difficult to compare due to varying conditions such as plant designs, loads and disturbances, in addition with the lack of standard evaluation criteria. Simulations provide a cost-effective method for the evaluation and comparison of different control strategies, but the unlimited number of simulation permutations makes the need for a standardised protocol. In this sense, each control strategy must be simulated under the same conditions to ensure unbiased comparisons (Gernaey et al., 2014).

The Benchmark Simulation Model (BSM) platform was developed with the purpose of making simulation-based comparison of WWTP control strategies. Consequently, the main products of the BSM Task Group are WWTP simulation models, a simulation protocol for these WWTP simulation models and a set of benchmarking evaluation criteria for objective evaluation (Gernaey et al., 2014). All these items together form the BSM platform. Specifically, the WWTP simulation models comprise a standardised treatment plant layout with fixed reactor volumes; set of process models for each unit operation of the WWTP; predefined influent flow and loads and sensors and actuators models for monitoring the WWTP processes and implement control strategies realistically. The standardised evaluation criteria comprise an effluent quality index, an operational cost index and risk index (Comas et al., 2008; Flores-Alsina et al., 2009; Jeppsson et al., 2007). The first BSM platform was officially called Benchmark Simulation Model No. 1 (BSM1), which comprised a stand-alone activated sludge unit and was assessed for a period of seven days. Later, the Benchmark Simulation Model No. 1 Long Term (BSM1\_LT) was proposed and aimed for long term assessment of control strategies, since the evaluated period was extended from 7 days to a whole year. Finally, the Benchmark Simulation Model No. 2 was developed for use in plant-wide and long-term evaluation of control strategies considering both water and sludge lines of the WWTP. Detailed description of the BSM1, BSM1\_LT and BSM2 platforms are provided in Gernaey et al., (2014).

Since the publication of the IWA Task Group BSM platforms (BSM1, BSM1\_LT and BSM2) (Gernaey et al., 2014), the BSM platform has been continuously expanded to allow for evaluation of operation and control strategies in emerging areas, such as nutrient recovery strategies or mitigation of GHG emissions control strategies.

Recently, Solon and co-workers (Solon et al., 2017) proposed a novel plant-wide model capable of predicting the fate of P in both water and sludge lines as well as the interactions with sulphur (S) and iron (Fe) thanks to the implementation of comprehensive physico-chemical process models. This work combined a modified ASM2d with a speciation model routine to predict pH at each time step (Flores-Alsina et al., 2015). This model evaluated and compared several energy and nutrient recovery strategies, but without accounting for GHG emissions.

Indeed, GHG emissions should be included when evaluating the overall sustainability of control/operational strategies for water resource recovery to add another important criterion in the multivariable space of performance assessment; otherwise, a good a priori control structure providing excellent effluent quality and lower costs could obtain this at the expense of high GHG emissions that are not being considered. Previous modelling studies have already included GHG emissions as a potential performance criterion when evaluating the sustainability of WWTPs. As discussed in previous section, several

extensions based on ASM models have been proposed in the literature to better describe  $\text{N}_2\text{O}$  emissions during biological nitrogen removal (Domingo-Félez et al., 2017; Mannina et al., 2016; Massara et al., 2018; Ni and Yuan, 2015). However, although some parameters of the models are pH-dependent, the evolution of pH in the different reactors is not predicted since the effect on pH of the processes taking place are not considered. Specifically the growth rate of nitrifiers depends on pH, and consequently the  $\text{N}_2\text{O}$  emissions produced by nitrifiers cannot be described accurately for several operational conditions (Su et al., 2019). In addition,  $\text{CO}_2$  emissions are typically not accounted for, since the evolution of inorganic carbon (IC) is not modelled. However, nitrifiers growth depend on IC availability (Guisasola et al., 2007; Torà et al., 2010; Wett and Rauch, 2003; Zhang et al., 2018) and its limitation could be significant in some scenarios.

One of the most used plant-wide model that takes into account the GHG emissions is the BSM2G (Flores-Alsina et al., 2011). Several works in the literature have applied this model to study the effect on GHG emissions when implementing different control/operational strategies (Barbu et al., 2017; Flores-Alsina et al., 2014, 2011; Santín et al., 2018, 2017; Sweetapple et al., 2015). However, BSM2G cannot describe the transformations and fate of P in the plant and, moreover, not all the known  $\text{N}_2\text{O}$  biological production pathways are included in this model. Hence, a new model extension is needed to enable the evaluation of all the potential GHG emission sources when integrating the potential resource recovery mechanisms in WRRFs.

## **1.6. Research motivations and thesis overview**

### *1.6.1. Research motivations*

In recent years, both the scarcity of natural resources and the concern about climate change have shifted the wastewater management sector paradigm from treatment and disposal to wastewater reuse, recycle and recovery in a sustainable way. Therefore, WWTPs are required to become WRRFs and, for this aim, novel configurations and control/operational strategies have arisen. Regarding the sustainability of the operation,  $\text{N}_2\text{O}$  is a deleterious GHG that is emitted during BNR in WWTPs. Due to its high GWP, the C-footprint of WWTPs is highly sensitive to  $\text{N}_2\text{O}$  emissions and therefore, there is an increase need to understand and mitigate these GHG emissions through novel operational and control strategies.

Mathematical modelling becomes useful to predict the behaviour of WWTPs and to explore these novel operational and control approaches to improve its performance, study the impact of nutrient recovery strategies, verify hypothesis related to fundamental mechanisms and to anticipate  $\text{N}_2\text{O}$  emissions in the design and operation of WWTPs, as well as in the design of potential mitigation strategies for  $\text{N}_2\text{O}$  emissions.

In this sense, the research motivations of this thesis are:



- i) Validate a novel mathematical model that accounts for N<sub>2</sub>O emissions to real full-scale WWTP data, in order to verify the ability to predict overall N<sub>2</sub>O emissions and nutrients removal.
- ii) Elucidate the effect that different operational strategies have on the N<sub>2</sub>O emissions through a simulation-based study.
- iii) Study the interactions and trade-offs between nutrient recovery strategies and GHG emissions in both a novel pilot-plant WRRFs configuration and in a plant-wide model.
- iv) Study the implementation of potential novel control strategies for mitigation of N<sub>2</sub>O emissions in a real pilot-plant scenario and through a Benchmark Simulation Model platform.

### 1.6.2. Thesis overview

This document is divided into seven chapters. Chapter I, in which this section is included, presents a general introduction to the topic, focused on nutrient removal and modelling GHG emissions during wastewater treatment, with a brief literature review of the state of the art. In Chapter II the main objectives of the thesis are presented. Chapter III to Chapter V present the results obtained during the development of the thesis. Chapter III describes a systematic calibration study of the ASM2d-N<sub>2</sub>O for a full-scale WWTP, including hydraulics, nutrient removal and N<sub>2</sub>O emissions. In Chapter IV, the GHG emissions of a novel WRRF pilot-plant configuration, the mainstream SCEPPHAR, are assessed while recovering nutrients from the wastewater. In addition, possible mitigation strategies for N<sub>2</sub>O emissions are implemented and evaluated. Chapter V comprises the benchmark simulation results. A new plant-wide model is developed which accounts for nutrient recovery options and GHG emissions. Five novel control strategies are evaluated by means of sustainability and cost of the operation. Chapter VI outlines the main conclusions extracted from this thesis. Finally, Chapter VII shows all the literature references used including the references of the annex. Additionally, Annex I includes the ASM2d-N<sub>2</sub>O model description used in Chapter III. Annex II includes the stoichiometric matrix of the modified ASM2d model of the BSM developed in Chapter V. Finally, Annex III includes a preliminary study to that one included in Chapter V, named “Evaluation of potential operational and control strategies in a plant-wide WWTP model to mitigate GHG emissions” in which a first version of the plant-wide model able to predict the carbon footprint of WWTP operation is developed and operational and control strategies for the mitigation of N<sub>2</sub>O emissions are implemented and evaluated. This model was integrated into the online tool developed in the EU-Rise project C-FOOT-CTRL, which aimed to monitor, control and mitigate GHG emissions in WWTPs.

## **Chapter II:**

---

## **Objectives**



## 2. Objectives

The main objective of this thesis is to advance in the development, knowledge and application of novel operational and control strategies to mitigate N<sub>2</sub>O emissions during wastewater treatment. Most of the study has been approached from a modelling point of view, however, GHGs emissions have also been assessed in a novel pilot-plant.

Following the main objective, the specific goals for this thesis are:

- To comprehensively calibrate the novel ASM2d-N<sub>2</sub>O model with dynamic data from a full-scale WWTP to verify the ability of the proposed model approach to describe N<sub>2</sub>O emissions and nutrient removal (Chapter III).
- To understand the possible effect of plant hydraulics on N<sub>2</sub>O emissions in a real continuous full-scale WWTP, by modelling the effect of different influent flowrate distribution between two parallel treatment lines (Chapter III).
- To assess the overall GHG emissions and the dynamics of these emissions during the long-term operation of a WRRF configuration with P-recovery at pilot-plant scale (Chapter IV).
- To experimentally assess the effect of different aeration control strategies on the N<sub>2</sub>O liquid concentration and emissions (Chapter IV).
- To define a new extended benchmarking scenario (BSM2-PSFe-GHG) for WRRFs, including C/N/P removal, GHG emissions and chemical and physico-chemical models to describe resource recovery (Chapter V).
- To develop a novel BSM-based study on the proposed plant-wide model (BSM2-PSFe-GHG) to study the effect of nutrient recovery control strategies on GHG emissions and to design and implement novel control strategies to optimise plant performance while reducing GHG emissions (Chapter V).



# **Chapter III:**

---

## **Systematic calibration of N<sub>2</sub>O emissions from a full-scale WWTP including a tracer test and a global sensitivity approach**

**A modified version of this chapter has been submitted to Chemical Engineering Journal for its publication as:**

Borja Solís, Albert Guisasola, Maite Pijuan, Lluís Coromines, Juan Antonio Baeza, 2021. Systematic calibration of N<sub>2</sub>O emissions from a full-scale WWTP including a tracer test and a global sensitivity approach.



### 3. Systematic calibration of N<sub>2</sub>O emissions from a full-scale WWTP including a tracer test and a global sensitivity approach

#### Abstract

Nitrous oxide (N<sub>2</sub>O) is a greenhouse gas (GHG) and ozone depleting substance emitted during biological nitrogen removal from wastewater treatment plants (WWTP). Mathematical modelling of N<sub>2</sub>O production and emissions has emerged to simulate the fundamental mechanisms of N<sub>2</sub>O production and can be used to anticipate N<sub>2</sub>O emissions during the design and operation of WWTP. In this study, the novel ASM2d-N<sub>2</sub>O model, which accounts for the production of N<sub>2</sub>O in C/N/P removal WWTPs, was used to study the associated emissions from a full-scale WWTP with two independent lines. Firstly, the hydraulics of the WWTP were characterized by introducing a KBr pulse at the influent and sampling at different zones of the secondary treatment. Results showed that the flow was equally divided into the two treatment lines, that each reactor worked as an ideal continuous stirred tank reactor and secondary settlers model flux was similar to the plug-flow reactor. After the hydraulic characterization, the ASM2d-N<sub>2</sub>O model was calibrated using experimental data obtained under dynamic conditions. The parameter subset to be calibrated was obtained by a global sensitivity analysis. The top ranked parameters (related to nitrifying organisms) were calibrated. A good model fit was obtained during the dynamic calibration, giving a good description of nutrients and N<sub>2</sub>O emissions. Finally, a simulation-based study was carried out to evaluate the effect on N<sub>2</sub>O emissions of different influent flow distributions between the treatment lines.

#### 3.1. Motivations

The main objective of this study was to comprehensively calibrate the ASM2d-N<sub>2</sub>O model with full-scale WWTP dynamic data. For this purpose, calibrating WWTP hydraulics is an essential first step to obtain posterior accurate predictions for nutrient removal and N<sub>2</sub>O emissions. An experimental campaign was carried out during three days in different zones of a full-scale municipal WWTP to measure the N<sub>2</sub>O emission dynamics. The parameter subset selection to calibrate the ASM2d-N<sub>2</sub>O model was obtained through a Global Sensitivity Analysis (GSA) to select the best parameter subset independently from the initial parameter value. Finally, a simulation-based study was carried out to identify the effect of varying the influent flowrate between both treatment lines on the N<sub>2</sub>O emissions of the WWTP.

#### 3.2. Materials and methods

##### 3.2.1. Girona WWTP description

The full-scale urban WWTP is located in Girona (Catalonia, Spain) with a design capacity of 275000 person equivalent and 55000 m<sup>3</sup> d<sup>-1</sup>. A schematic overview of the WWTP



process layout is shown in Figure 3.1. After the pre-treatment (grit and gross removal), the influent is distributed in three rectangular lamella-plate primary clarifiers. The biological section has a 5-stage Bardenpho configuration. It consists of two main treatment lines with seven separated reactors in each line. The wastewater flows through an anaerobic reactor (ANA1, 1335 m<sup>3</sup>), an anoxic reactor (ANX1, 4554 m<sup>3</sup>), three aerobic reactors with the same volume (AER1 to AER3, 1929 m<sup>3</sup>), a second anoxic reactor (ANX2, 1276 m<sup>3</sup>) and finally a fourth aerobic reactor (AER4, 1409 m<sup>3</sup>). The internal recycle (IR) flows from the third aerobic reactor (AER3) to the first anoxic reactor (ANX1) and it is independent in each line (Figure 3.1). In addition, sodium aluminate is injected into each IR stream to favour chemical P precipitation. The flow is mixed again at the outlet of the last aerobic zone and divided into three parallel secondary clarifiers (5332 m<sup>3</sup> each settler) where the biomass is separated from the treated effluent. The concentrated outflows from each secondary clarifier are mixed and, after extracting the purge flow, recycled to the influent of the biological reactors. Aeration is supplied by blowers in the aerobic zones. Each line has a blower whose air is sparged through diffusers.

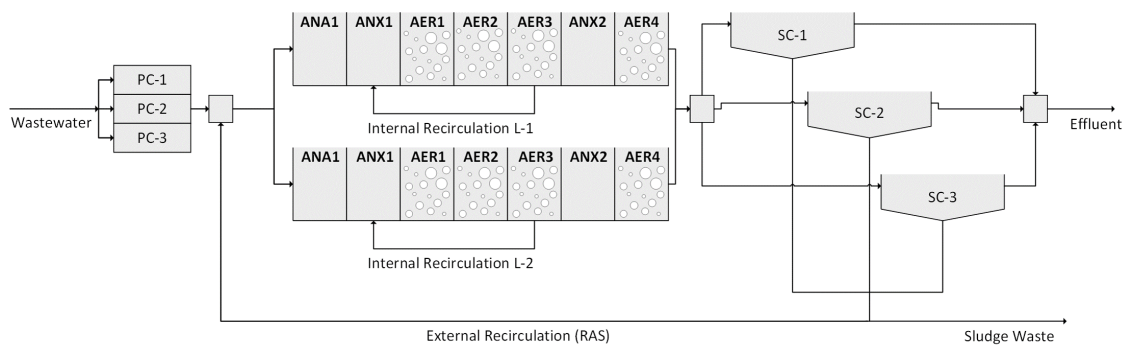


Figure 3.1. Plant layout of the Girona WWTP (PC = Primary Clarifier, SC = Secondary Clarifier, ANA = Anaerobic reactor, ANX = Anoxic reactor and AER = Aerobic reactor).

### 3.2.2. Hydraulic characterization procedure

Tracer experiments to characterize the hydraulics of the secondary treatment of the WWTP (i.e. biological reactors and secondary clarifiers) were carried out with potassium bromide (KBr). The objectives of the hydraulic characterization were: 1) to determine the flow distribution between both treatment lines in the biological reactor, as the plant operators suspected that it was not equally distributed in each treatment line and 2) to understand the hydraulics of each reactor to identify possible dead-zones. An amount of 24.9 kg of KBr (16.7 kg of Br<sup>-</sup>) was added to the influent of the primary clarifiers. During the experiment, liquor samples were taken from different zones of the two treatment lines of the biological reactor and in the effluent. The locations of the tracer pulse and the different tracer samples zones are indicated in Figure 3.2.

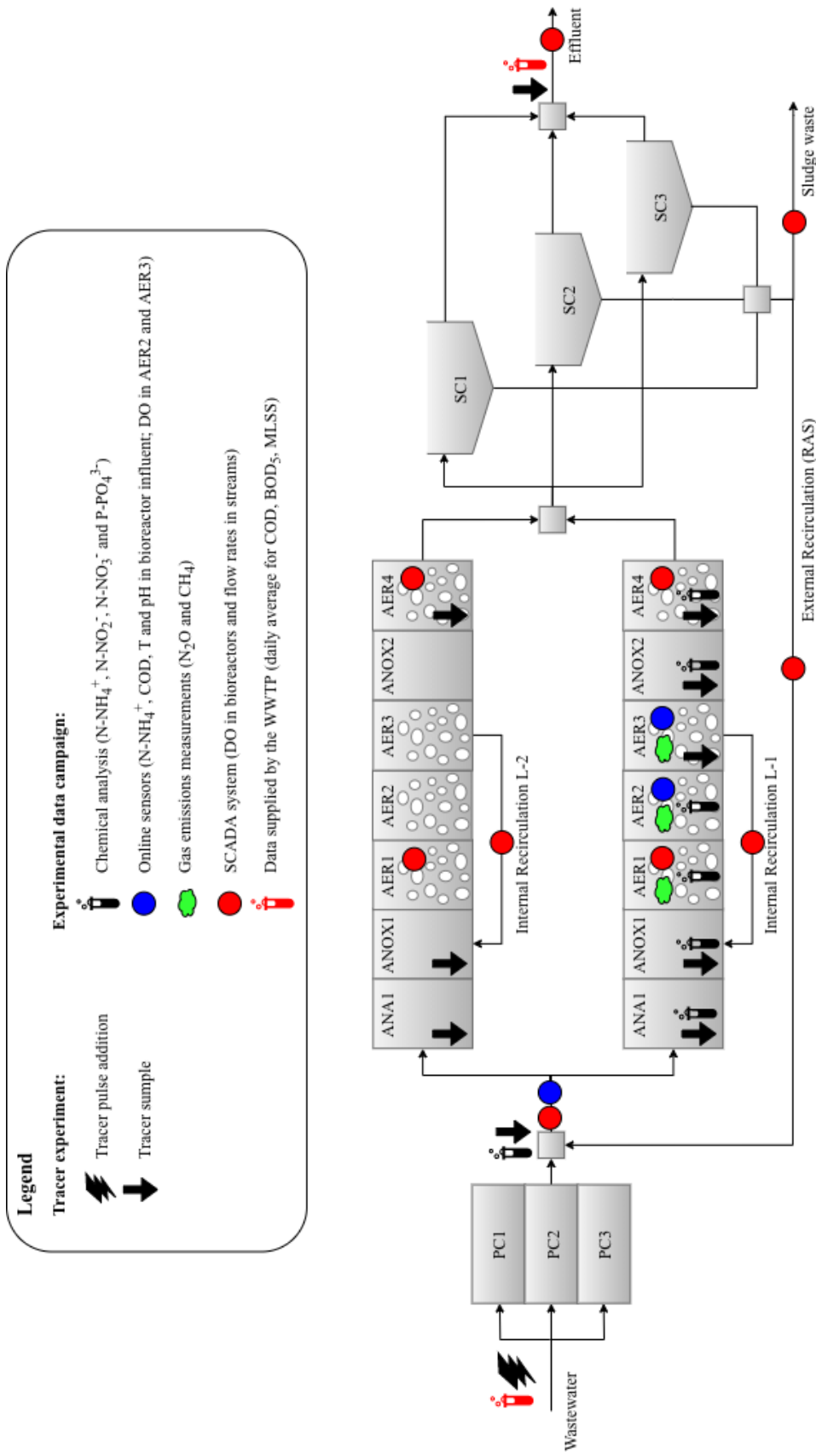


Figure 3.2. Scheme of the Girona WWTP showing the locations and data of the samples collected during tracer experiments and experimental data campaign.

The model structure used to determine the residence time distribution (RTD) of the activated sludge (AS) system of the Girona WWTP was the n-tanks in series (Metcalf & Eddy, 2003), a widely used method in the calibration of full-scale WWTPs (Coen et al., 1998; Olivet et al., 2005; Vanrolleghem et al., 2003). The pulse was added in the influent of the primary clarifiers but, for simulation purposes, the data at the effluent of the primary clarifiers were used as the input simulation because modelling of the complex hydraulic lamella-plates clarifiers of the primary settler was out of the scope of this work and was not needed for the WWTP calibration. As an initial approach, each vessel was considered to be an ideal Continuous Stirred Tank Reactor (CSTR) and the influent flow was equally divided into each treatment line. Hence, each treatment line of the biological reactors of the WWTP was initially simulated as 7 tanks in series plus the secondary settler. The latter was also simulated as a single tank (8 total tanks-in-series for the secondary treatment). The mass balance of the tracer concentration in each tank is described by Equation 3.1:

$$V_i \cdot \frac{dC_i}{dt} = Q_i \cdot (C_{in,i} - C_i) \quad (\text{Eq. 3.1})$$

Where:  $V_i$  is the volume of reactor “i”;  $Q_i$  is the volumetric flowrate in reactor “i”,  $C_{in,i}$  is the inlet tracer concentration and  $C_i$  the tracer concentration in reactor “i”.

The calibration cost function of the hydraulic experiment to be minimized was named HCCF (Equation 3.2):

$$\text{HCCF} = \sum_{i=1}^N \frac{\max|C_{ANA1-L1}|}{\max|C_i|} \cdot \sqrt{(C_{i,\text{exp}} - C_{i,\text{model}})^2} \quad (\text{Eq. 3.2})$$

Where: “i” refers to each reactor;  $C_{i,\text{exp}}$  is the experimental concentration;  $C_{i,\text{model}}$  is the model prediction and  $\max|C_{ANA1-L1}|/\max|C_i|$  is a weight factor to normalize the concentrations of each reactor to those of ANA1 from biological treatment line one. Thus, each of the experimental inputs has the same influence on the HCCF.

### 3.2.3. Experimental data campaign

A three-day data sampling campaign was carried out from 18 to 20 July 2017 to calibrate the ASM2d-N<sub>2</sub>O model at the Girona WWTP under dynamic conditions. Figure 3.2 shows a scheme of the Girona WWTP with the locations and data collected during the experimental data campaign. Only one biological treatment line was sampled (Line 1, Figure 3.1). The data collected are summarized below:

- *Chemical analysis:* Grab samples were collected to analyse NH<sub>4</sub><sup>+</sup>, NO<sub>2</sub><sup>-</sup>, NO<sub>3</sub><sup>-</sup> and PO<sub>4</sub><sup>3-</sup> by ion chromatography (ICS5000, DIONEX) at different locations and intervals. Grab samples were taken 5 times a day at 3h intervals (from 9:00 to 18:00) plus midnight for 3 days at reactors ANX1, AER1, AER3 and AER4. At

reactors ANA1 and ANX2, the grab samples were taken less frequently, only 3 times a day. In addition, two refrigerated automatic samplers also took samples every 3 hours during the 3 days of the data campaign (8 times per day) at the influent of the biological reactors and in AER2 reactor.

- *Online sensors:*  $\text{NH}_4^+$ , COD, pH and temperature at the bioreactor inlet were continuously monitored utilizing two on-line ion-selective electrodes (ammo::lyser™) coupled to a monitoring station (S::CAN Messtechnik GmbH, Austria). In addition, three Dissolved Oxygen (DO) probes (oxi::lyser™) were installed in AER1, AER2 and AER3 coupled to the same S::CAN monitoring station.
- *Gas emission measurements:*  $\text{N}_2\text{O}$  emissions were measured in reactors AER1, AER2 and AER3 using a system with three gas collection hoods. The gas collected in the hoods was coupled with an online analyser (Horiba VA3000).  $\text{N}_2\text{O}$  concentration (in ppmv), pressure, gas flowrate and temperature were logged at 15 seconds intervals. The analyser measured only one hood at a time in 20-minute intervals between each reactor. A detailed methodology for the gas emission measurement system can be found in Ribera-Guardia et al., (2019).
- *Data from the WWTP SCADA system:* data of the hydraulics (biological influent, internal and external recirculation and wastage flowrates) and aeration (DO of AER4 reactor) were collected from the SCADA system of the WWTP.

#### 3.2.4. ASM2d- $\text{N}_2\text{O}$ structure

The ASM2d- $\text{N}_2\text{O}$  kinetic model (Massara et al., 2018) was calibrated to describe the Girona WWTP. The ASM2d- $\text{N}_2\text{O}$  model is able to predict COD, N and P removal and  $\text{N}_2\text{O}$  production. The model structure is based on the ASM2d model developed by Henze et al., (2000), and extended to account for  $\text{N}_2\text{O}$  production with the 2-pathway model for  $\text{N}_2\text{O}$  emissions by AOB, developed by Pocquet et al., (2016) and the denitrification processes with the Activated Sludge Model for Nitrogen (ASMN) developed by Hiatt and Grady (2008). The temperature dependence of the biological reactions was implemented following the guidelines of the Activated Sludge Model No. 2 (ASM2) (Henze et al., 2000) to describe the different seasonal patterns. The subset of all parameters involved in ASM2d- $\text{N}_2\text{O}$ , with updated values, stoichiometric matrix and kinetics rates can be found in Annex I section.

#### 3.2.5. Influent characterization

The influent characterization, i.e. the step from the measured variables to the model state variables was performed following the methodology detailed in this section.

The influent-related COD characterization was performed by standard calculations from three different influent COD measures: total COD ( $\text{COD}_{\text{tot}}$ ), filtered COD at  $1.2 \mu\text{m}$

(COD<sub>fil</sub>) and flocculated-filtered COD at 0.45 μm (COD<sub>sol</sub>) and the measure of filtered COD in the effluent (COD<sub>fil,eff</sub>). Total COD is divided into particulate and filtered COD (Equation 3.3) and filtered COD is divided into soluble and colloidal (COD<sub>col</sub>) (Equation 3.4).

$$\text{COD}_{\text{part}} = \text{COD}_{\text{tot}} - \text{COD}_{\text{fil}} \quad (\text{Eq. 3.3})$$

$$\text{COD}_{\text{col}} = \text{COD}_{\text{fil}} - \text{COD}_{\text{sol}} \quad (\text{Eq. 3.4})$$

The soluble unbiodegradable COD (COD<sub>sol,unbio</sub> equivalent to S<sub>I</sub>) was assumed to be equal to the measured filtered COD in the effluent. Then, the soluble biodegradable COD (COD<sub>sol,bio</sub>) was calculated with Equation 3.5.

$$\text{COD}_{\text{sol,bio}} = \text{COD}_{\text{sol}} - \text{COD}_{\text{fil,eff}} \quad (\text{Eq. 3.5})$$

The state variable soluble fermentable COD was calculated with Equation 3.6. In this case, the volatile fatty acids concentration (S<sub>A</sub>) in the influent was assumed to be zero.

$$S_{\text{F}} = \text{COD}_{\text{sol,bio}} - S_{\text{A}} \quad (\text{Eq. 3.6})$$

The calculation of colloidal unbiodegradable and biodegradable COD (COD<sub>col,unbio</sub> and COD<sub>col,bio</sub>, respectively) was performed with Equation 3.7 and Equation 3.8, respectively.

$$\text{COD}_{\text{col,unbio}} = \text{COD}_{\text{col}} \cdot \frac{\text{COD}_{\text{sol,unbio}}}{\text{COD}_{\text{sol}}} \quad (\text{Eq. 3.7})$$

$$\text{COD}_{\text{col,bio}} = \text{COD}_{\text{col}} - \text{COD}_{\text{col,unbio}} \quad (\text{Eq. 3.8})$$

All biomass-related model state variables (X<sub>H</sub>, X<sub>AOB</sub>, X<sub>NOB</sub> and X<sub>PAO</sub>) were assumed to be the 0.1% of the total COD, except for ordinary heterotrophs organisms (X<sub>H</sub>) which were assumed to be 5% of the total influent COD. Polyphosphate and poly-hydroxyalkanoate concentrations (X<sub>PP</sub> and X<sub>PHA</sub>) were assumed to be 1% of the total X<sub>PAO</sub> concentration.

The particulate biodegradable COD (COD<sub>part,bio</sub>) was estimated a 40% of the total influent COD and the calculation of the slowly biodegradable COD (particulate and colloidal) X<sub>S</sub>, was performed with Equation 3.9:

$$X_{\text{S}} = \text{COD}_{\text{col,bio}} + \text{COD}_{\text{part,bio}} \quad (\text{Eq. 3.9})$$

The particulate unbiodegradable COD (X<sub>I</sub>) was calculated as the remaining fraction of the total COD (Equation 3.10):

$$X_{\text{I}} = \text{COD}_{\text{tot}} - (S_{\text{F}} + S_{\text{A}} + S_{\text{I}} + X_{\text{S}} + X_{\text{H}} + X_{\text{AOB}} + X_{\text{NOB}} + X_{\text{PAO}} + X_{\text{PHA}}) \quad (\text{Eq. 3.10})$$

The N related influent model states were kept at the same values for those measured in the influent of the biological reactors, which were N-NH<sub>4</sub><sup>+</sup>, N-NO<sub>2</sub><sup>-</sup> and N-NO<sub>3</sub><sup>-</sup>. The rest

of the N-species were not measured and were assumed to be zero ( $S_{\text{NH}_2\text{OH}}$ ,  $S_{\text{N}_2\text{O}}$ ,  $S_{\text{NO}}$ ,  $S_{\text{N}_2}$ ). The  $S_{\text{PO}_4}$  model state variable was also kept at the same value as measured. Finally, the influent alkalinity ( $S_{\text{ALK}}$ ) was assumed to be 6 mole  $\text{HCO}_3^-/\text{m}^3$ .

### 3.2.6. Global Sensitivity Analysis (GSA)

A GSA was performed to identify the input factors (i.e. parameters) that most affected the model outputs and, therefore, the parameters that should be calibrated preferentially. The selected model output was the Calibration Cost Function (CCF), which is the sum of the squared differences between experimental data and dynamic model output (see section 3.3.4).

Among the different GSA methods, the Monte Carlo (MC) filtering or Regional Sensitivity Analysis (RSA) was a suitable method to select the parameters that were not only more sensitive to CCF but also reduced it (Saltelli et al., 2005, 2004). RSA is based on mapping the input factors space according to whether the associated output, i.e. the CCF, is below (i.e. “behavioural” samples) or above (i.e. “non-behavioural” samples) a predefined threshold (Pianosi et al., 2016; Saltelli et al., 2008). The workflow used to apply the RSA method was (Saltelli et al., 2004): 1) a range was defined for the input factor space and a MC experiment was performed. 2) The model outputs were classified as behavioural (B) or non-behavioural ( $\bar{B}$ ) according to the specified threshold of the CCF and associated to the input factors values. 3) A set of binary elements was defined, distinguishing between two subsets for each parameter ( $X_i$ ): the behavioural subset ( $X_i|B$ ) and the non-behavioural subset ( $X_i|\bar{B}$ ). 4) The Smirnov test (Equation 3.11) was performed for each input factor and used as a measure of the Sensitivity index ( $S_i$ ) (Saltelli et al., 2004); The parameters were ranked in order of influential on CCF reduction by  $S_i$ .

$$S_i = \max |F(X_i|B) - F(X_i|\bar{B})| \quad (\text{Eq. 3.11})$$

Where  $F(X_i|B)$  and  $F(X_i|\bar{B})$  are the empirical cumulative distribution functions of the parameter ( $X_i$ ) when considering the input samples associated with the behavioural and non-behavioural outputs, respectively.

A total of 59 parameters were included in the GSA study. The included parameters and their uncertainty ranges are shown in Table 3.1. The parameters were assumed to be uniformly distributed and the uncertainty ranges were set according as proposed by Brun et al., (2002). All parameters included in the GSA study were kinetic parameters of ASM2d-N<sub>2</sub>O. The hydraulic WWTP parameters were not considered because they were calculated during the hydraulic characterization. Moreover, the influent characterization parameters were neither included, as they were measured during the experimental data campaign. Finally, the stoichiometric parameters of ASM2d-N<sub>2</sub>O were assumed to be accurately known parameters and were not included in the GSA. Moreover, as the Girona

WWTP removes P by chemical precipitation with sodium aluminate dosage, the parameters related to Polyphosphate Accumulating Organisms (PAO) were not included.

Table 3.1. Symbols, description, default values at 20°C, units and variation range of the ASM2d-N<sub>2</sub>O parameters included in the GSA.

Parameter	Description	Default value at 20°C	Units	Min/max range
K <sub>H</sub>	Hydrolysis rate constant	3	d <sup>-1</sup>	1.5 / 4.5
K <sub>O<sub>2</sub>_H</sub>	Saturation/inhibition coefficient for O <sub>2</sub>	0.2	g O <sub>2</sub> m <sup>-3</sup>	0.1 / 0.3
K <sub>x_H</sub>	Saturation coefficient for particulate COD	0.1	g X <sub>S</sub> (g X <sub>H</sub> ) <sup>-1</sup>	0.05 / 0.15
n <sub>NO<sub>3</sub>_H</sub>	Anoxic hydrolysis reduction factor	0.6	-	0.3 / 0.9
n <sub>NO<sub>2</sub>_H</sub>	Anoxic hydrolysis reduction factor	0.6	-	0.3 / 0.9
K <sub>NO<sub>3</sub>_H</sub>	Saturation/inhibition coefficient for NO <sub>3</sub> <sup>-</sup>	0.5	g N m <sup>-3</sup>	0.25 / 0.75
K <sub>NO<sub>2</sub>_H</sub>	Saturation/inhibition coefficient for NO <sub>2</sub> <sup>-</sup>	0.5	g N m <sup>-3</sup>	0.25 / 0.75
n <sub>fe_H</sub>	Anaerobic hydrolysis reduction factor	0.4	-	0.2 / 0.6
μ <sub>H</sub>	Maximum growth rate on substrate	6	g X <sub>S</sub> (g X <sub>H</sub> ) <sup>-1</sup> d <sup>-1</sup>	3 / 9
K <sub>O<sub>2</sub></sub>	Saturation/inhibition coefficient for O <sub>2</sub>	0.1	g O <sub>2</sub> m <sup>-3</sup>	0.05 / 0.15
K <sub>F</sub>	Saturation coefficient for growth on S <sub>F</sub>	20	g COD m <sup>-3</sup>	10 / 30
K <sub>NH<sub>4</sub></sub>	Saturation coefficient for NH <sub>4</sub> <sup>+</sup> (nutrient)	0.05	g N m <sup>-3</sup>	0.025 / 0.075
K <sub>P</sub>	Saturation coefficient for PO <sub>4</sub> <sup>3-</sup> (nutrient)	0.01	g P m <sup>-3</sup>	0.005 / 0.015
K <sub>ALK</sub>	Saturation coefficient for alkalinity (HCO <sub>3</sub> <sup>-</sup> )	0.1	mole HCO <sub>3</sub> <sup>-</sup> m <sup>-3</sup>	0.05 / 0.15
K <sub>A</sub>	Saturation coefficient for growth on acetate S <sub>A</sub>	20	g COD m <sup>-3</sup>	10 / 30
K <sub>NO<sub>3</sub></sub>	Saturation/inhibition coefficient for NO <sub>3</sub> <sup>-</sup>	0.5	g N m <sup>-3</sup>	0.25 / 0.75
K <sub>NO<sub>2</sub></sub>	Saturation/inhibition coefficient for NO <sub>2</sub> <sup>-</sup>	0.5	g N m <sup>-3</sup>	0.25 / 0.75
n <sub>NO<sub>3</sub>_D</sub>	Reduction factor for denitrification	0.28	-	0.14 / 0.42
q <sub>fe</sub>	Maximum rate for fermentation	3	g S <sub>F</sub> (g X <sub>H</sub> ) <sup>-1</sup> d <sup>-1</sup>	1.5 / 4.5
K <sub>fe_H</sub>	Saturation coefficient for fermentation of S <sub>F</sub>	4	g COD m <sup>-3</sup>	2 / 6
b <sub>H</sub>	Rate constant for lysis and decay	0.4	d <sup>-1</sup>	0.2 / 0.6
n <sub>G3</sub>	Anoxic growth factor (NO <sub>2</sub> <sup>-</sup> →NO)	0.16	-	0.08 / 0.24
n <sub>G4</sub>	Anoxic growth factor (NO→N <sub>2</sub> O)	0.35	-	0.175 / 0.525
n <sub>G5</sub>	Anoxic growth factor (N <sub>2</sub> O→N <sub>2</sub> )	0.35	-	0.175 / 0.525
K <sub>S3</sub>	Half-saturation coefficient for substrate	20	g COD m <sup>-3</sup>	10 / 30
K <sub>S4</sub>	Half-saturation coefficient for substrate	20	g COD m <sup>-3</sup>	10 / 30
K <sub>S5</sub>	Half-saturation coefficient for substrate	40	g COD m <sup>-3</sup>	20 / 60
K <sub>NO<sub>2</sub>_Den</sub>	Half-saturation coefficient for NO <sub>2</sub> <sup>-</sup>	0.2	g N m <sup>-3</sup>	0.1 / 0.3
K <sub>OH4</sub>	Half-saturation coefficient for O <sub>2</sub>	0.1	g O <sub>2</sub> m <sup>-3</sup>	0.05 / 0.15
K <sub>N<sub>2</sub>O_Den</sub>	Half-saturation coefficient for N <sub>2</sub> O	0.05	g N m <sup>-3</sup>	0.025 / 0.075
K <sub>OH3</sub>	Half-saturation coefficient for O <sub>2</sub>	0.1	g O <sub>2</sub> m <sup>-3</sup>	0.05 / 0.15
K <sub>NO_Den</sub>	Half-saturation coefficient for NO	0.05	g N m <sup>-3</sup>	0.025 / 0.075
K <sub>OH5</sub>	Half-saturation coefficient for O <sub>2</sub>	0.1	g O <sub>2</sub> m <sup>-3</sup>	0.05 / 0.15
K <sub>I3NO</sub>	NO inhibition coefficient (NO <sub>2</sub> <sup>-</sup> →NO)	0.5	g N m <sup>-3</sup>	0.25 / 0.75
K <sub>I4NO</sub>	NO inhibition coefficient (NO→N <sub>2</sub> O)	0.3	g N m <sup>-3</sup>	0.15 / 0.45

Parameter	Description	Default value at 20°C	Units	Min/max range
K <sub>I5NO</sub>	NO inhibition coefficient (N <sub>2</sub> O→N <sub>2</sub> )	0.075	g N m <sup>-3</sup>	0.038 / 0.112
μ <sub>AOB_HAO</sub>	Maximum AOB growth rate	0.78	d <sup>-1</sup>	0.39 / 1.17
q <sub>AOB_AMO</sub>	Maximum rate for the AMO reaction	5.2	g N (g COD) <sup>-1</sup> d <sup>-1</sup>	2.6 / 7.8
K <sub>O2_AOB1</sub>	AOB affinity constant for O <sub>2</sub> (AMO reaction)	1	g O <sub>2</sub> m <sup>-3</sup>	0.5 / 1.5
K <sub>NH4_AOB</sub>	AOB affinity constant for NH <sub>4</sub> <sup>+</sup>	0.2	g N m <sup>-3</sup>	0.1 / 0.3
K <sub>O2_AOB2</sub>	AOB affinity constant for O <sub>2</sub> (HAO reaction)	0.6	g O <sub>2</sub> m <sup>-3</sup>	0.3 / 0.9
K <sub>NH2OH_AOB</sub>	AOB affinity constant for NH <sub>2</sub> OH	0.3	g N m <sup>-3</sup>	0.15 / 0.45
q <sub>AOB_HAO</sub>	Maximum rate for HAO reaction	5.2	g N (g COD) <sup>-1</sup> d <sup>-1</sup>	2.6 / 7.8
K <sub>NO_AOB_HAO</sub>	AOB affinity constant for NO (from HAO)	0.0003	g N m <sup>-3</sup>	0.00015 / 0.00045
q <sub>AOB_N2O_NN</sub>	Maximum N <sub>2</sub> O production rate by NN pathway	0.0078	g N (g COD) <sup>-1</sup> d <sup>-1</sup>	0.004 / 0.012
K <sub>NO_AOB_NN</sub>	AOB affinity constant for NO (from NirK)	0.008	g N m <sup>-3</sup>	0.004 / 0.012
K <sub>O2_AOB_ND</sub>	AOB constant for O <sub>2</sub> effect on the ND pathway	0.5	g O <sub>2</sub> m <sup>-3</sup>	0.25 / 0.75
K <sub>I_O2_AOB</sub>	N <sub>2</sub> O constant for production inhibition by O <sub>2</sub>	0.8	g O <sub>2</sub> m <sup>-3</sup>	0.4 / 1.2
K <sub>HNO2_AOB</sub>	AOB affinity constant for HNO <sub>2</sub>	0.004	g N m <sup>-3</sup>	0.002 / 0.006
q <sub>AOB_N2O_ND</sub>	Maximum N <sub>2</sub> O production rate by the ND pathway	1.3	g N (g COD) <sup>-1</sup> d <sup>-1</sup>	0.65 / 1.95
K <sub>ALK_AOB</sub>	Saturation coefficient for alkalinity (HCO <sub>3</sub> <sup>-</sup> )	0.1	mole HCO <sub>3</sub> <sup>-</sup> m <sup>-3</sup>	0.05 / 0.15
K <sub>P_AOB</sub>	Saturation coefficient for PO <sub>4</sub> <sup>3-</sup> (nutrient)	0.01	g P m <sup>-3</sup>	0.005 / 0.015
μ <sub>NOB</sub>	Maximum NOB growth rate	0.78	d <sup>-1</sup>	0.39 / 1.17
K <sub>O2_NOB</sub>	Half-saturation coefficient for O <sub>2</sub>	1.2	g O <sub>2</sub> m <sup>-3</sup>	0.6 / 1.8
K <sub>ALK_NOB</sub>	Saturation coefficient for alkalinity (HCO <sub>3</sub> <sup>-</sup> )	0.1	mole HCO <sub>3</sub> <sup>-</sup> m <sup>-3</sup>	0.05 / 0.15
K <sub>NO2_NOB</sub>	Saturation coefficient for NO <sub>2</sub> <sup>-</sup>	0.5	g N m <sup>-3</sup>	0.25 / 0.75
K <sub>P_NOB</sub>	Saturation coefficient for PO <sub>4</sub> <sup>3-</sup> (nutrient)	0.01	g P m <sup>-3</sup>	0.005 / 0.015
b <sub>AOB</sub>	Decay rate of AOB	0.096	d <sup>-1</sup>	0.048 / 0.144
b <sub>NOB</sub>	Decay rate of NOB	0.096	d <sup>-1</sup>	0.048 / 0.144

### 3.2.7. Calibration procedure

The ASM2d-N<sub>2</sub>O model was calibrated once the hydraulics of the Girona WWTP had been identified and the influent of the experimental data campaign had been characterized. The overall procedure followed to calibrate the model is summarized below:

1) a preliminary calibration was performed, aiming to fit the P chemical removal by sodium aluminate addition. This calibration was performed under pseudo-steady state conditions to decrease the computational cost. Thus, the experimental values collected during the experimental campaign were averaged. 2) The CCF was built with the dynamic data of nutrients and GHG emissions collected during the experimental data campaign.



3) The RSA was performed with the kinetic parameters of the ASM2d-N<sub>2</sub>O model as input factors and the CCF as output. The combinations of the parameters that most influenced the CCF, i.e. the five top ranked parameters of the GSA, were calibrated in dynamic conditions. 4) The subset of the optimized parameters that most reduced the CCF was selected.

The aim of the preliminary calibration was to fit the sodium aluminate addition to describe the phosphate concentration in the biological reactors. During the preliminary calibration, the influent and operational dynamic data from the experimental campaign were averaged and used as model inputs (constants inputs). The phosphate concentration in the reactors were also averaged and used as output variables. The sodium aluminate addition to the IR stream was calibrated using the X<sub>MeOH</sub> state variable of ASM2d-N<sub>2</sub>O, which stands for ferric-hydroxide. Equation 3.12 was used as the preliminary calibration cost function (PCCF):

$$\text{PCCF} = \sqrt{\sum_{i=1}^7 (y_{\text{exp},i} - y_{\text{model},i})^2} \quad (\text{Eq. 3.12})$$

Where: “i” is related to each sample in the biological reactor,  $y_{\text{exp}}$  is the averaged experimental phosphate concentration and  $y_{\text{model}}$  is the steady state phosphate concentration obtained after a simulation of 300 days.

Each dynamic simulation started with a 300-day steady-state (SS) simulation (constant inputs). Then, a 3-day dynamic simulation was performed using the SS simulation results as the initial point and the CCF was calculated using the operational data sampled during the experimental campaign. Each parameter subset was calibrated by minimising the CCF through a global searching minimization method using the Matlab function *patternsearch*.

The experimental campaign lasted three days. In addition, the gas collection system could only analyse one aerobic zone at a time and unfortunately the system failed during one day. Therefore, in the absence of a large dynamic data set, all available data were used for the calibration process and no data were available for validation. This could lead to model overfitting, but to minimise this potential problem the parameter subset size to be calibrated was set to a maximum of five parameters to minimize the number of parameters to be modified compared to the default values that are selected to predict most situations during municipal wastewater treatment.

### 3.3. Results and Discussion

#### 3.3.1. Experimental data and plant performance

The NH<sub>4</sub><sup>+</sup>, NO<sub>2</sub><sup>-</sup>, NO<sub>3</sub><sup>-</sup> and PO<sub>4</sub><sup>3-</sup> profiles in the influent and in each compartment are shown in Figure 3.3 to Figure 3.6. The influent temperature and pH were approximately

constant during the experimental campaign at  $24.4 \pm 0.5$  °C and  $7.44 \pm 0.09$ , respectively. Good plant performance was achieved, obtaining a COD removal of 96% and higher than 99% for total Kjeldahl nitrogen (TKN) and P. Mean DO values were 1.8, 1.5, 1.2 and 2.0 g O<sub>2</sub> m<sup>-3</sup> in AER1 to AER4 compartments, respectively. Nitrite concentrations were below 0.25 g N m<sup>-3</sup> in all compartments, showing high NOB activity. Figure 3.6 shows that the PO<sub>4</sub><sup>3-</sup> concentration only increased on average by 2.5 g P m<sup>-3</sup> in the anaerobic reactor (ANA1), compared to the PO<sub>4</sub><sup>3-</sup> concentration in the influent, showing a low PAO activity. Hence, the addition of chemical P precipitant limited the PAO activity.

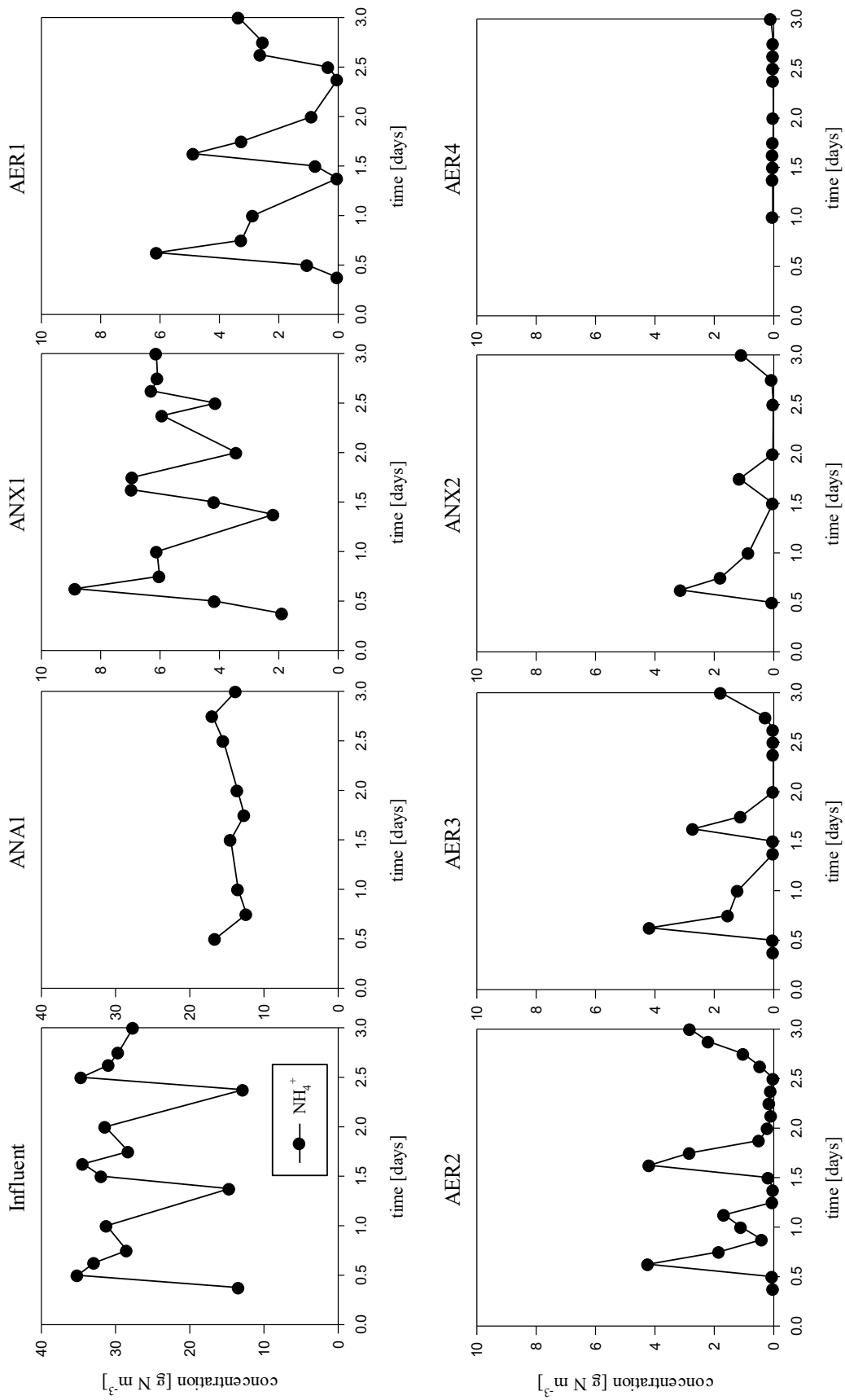


Figure 3.3. Ammonium concentration profiles measured in the influent and in each compartment of the biological reactor during the experimental data campaign.

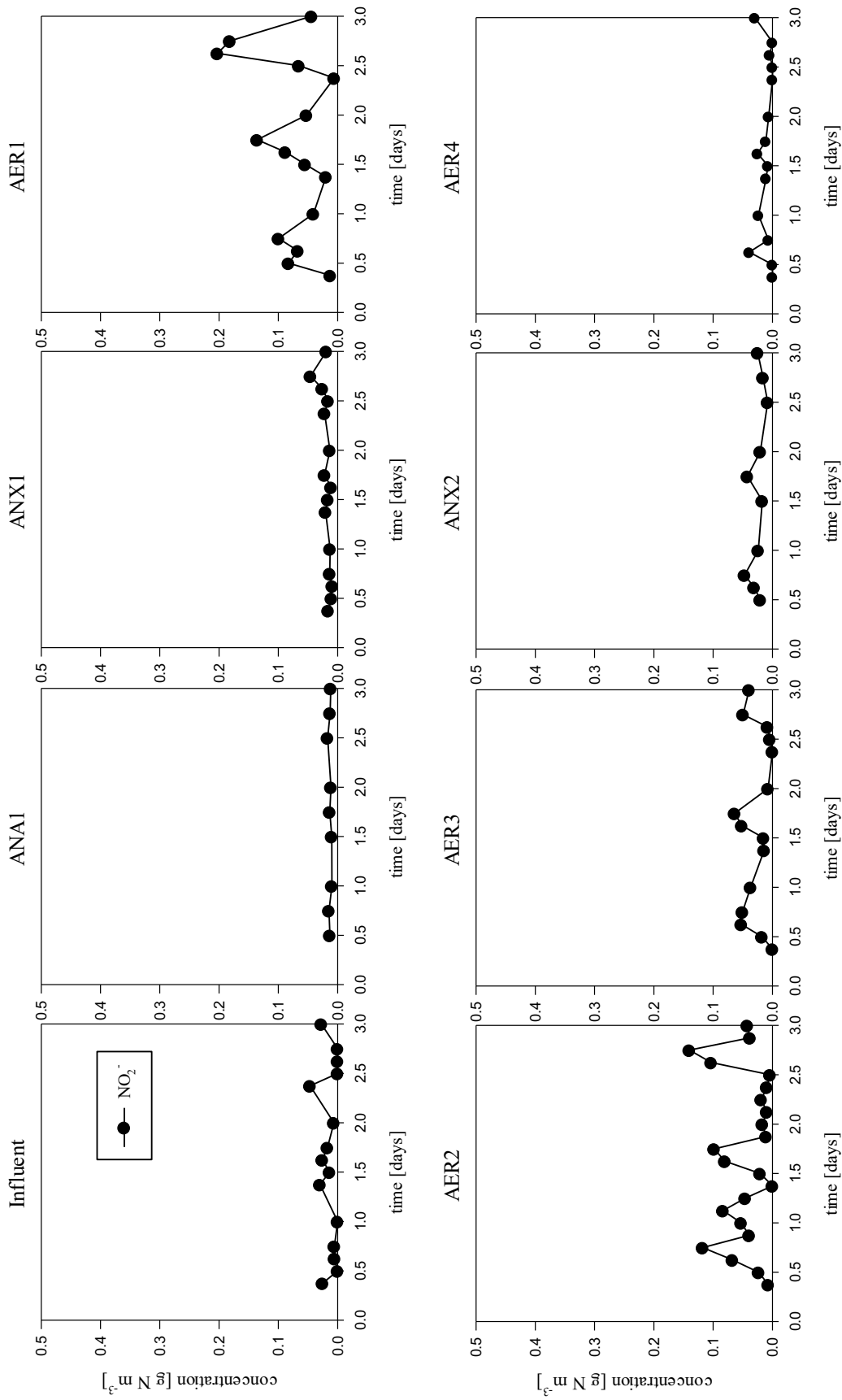


Figure 3.4. Nitrite concentration profiles measured in the influent and in each compartment of the biological reactor during the experimental data campaign.

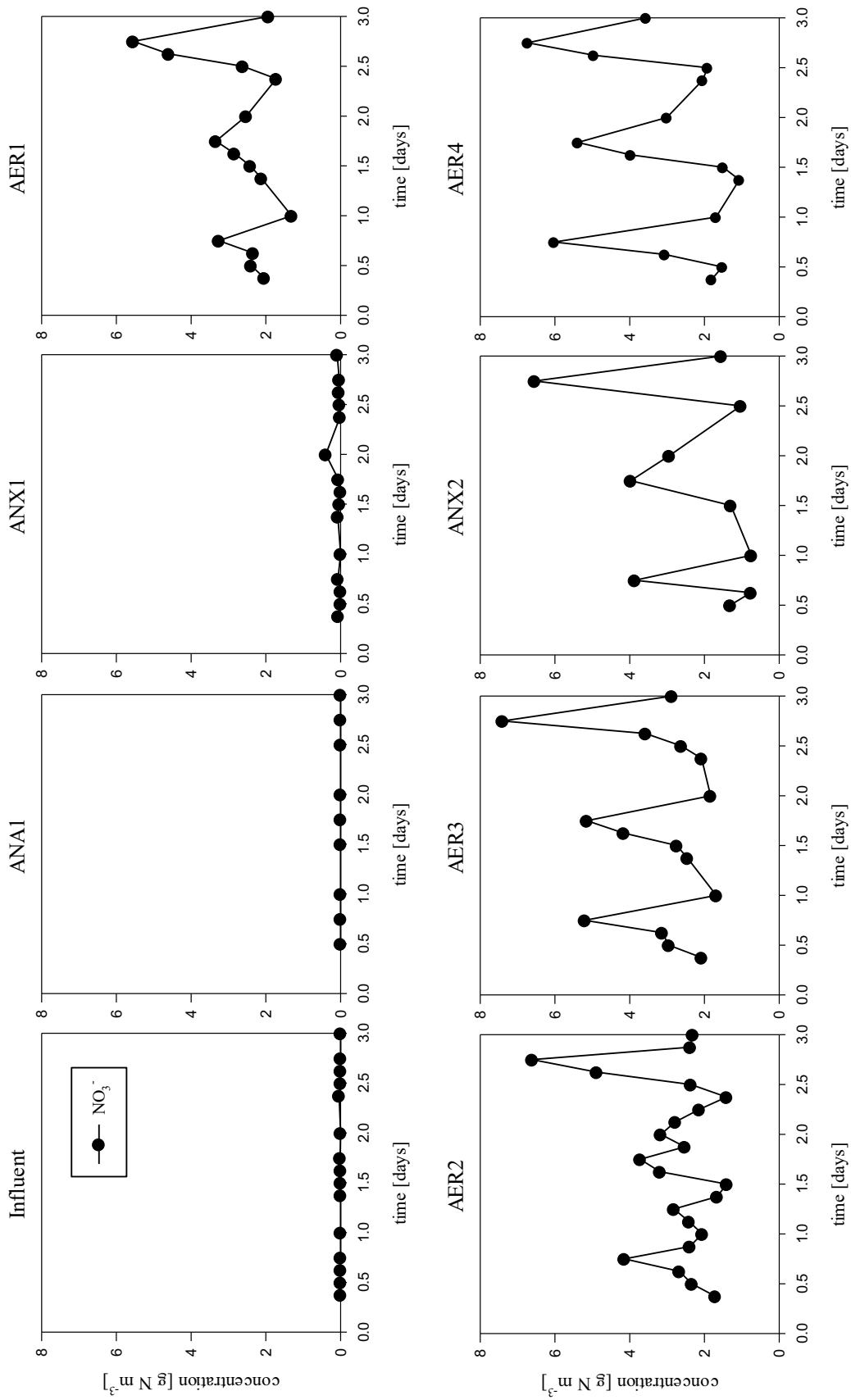


Figure 3.5. Nitrate concentration profiles measured in the influent and in each compartment of the biological reactor during the experimental data campaign.

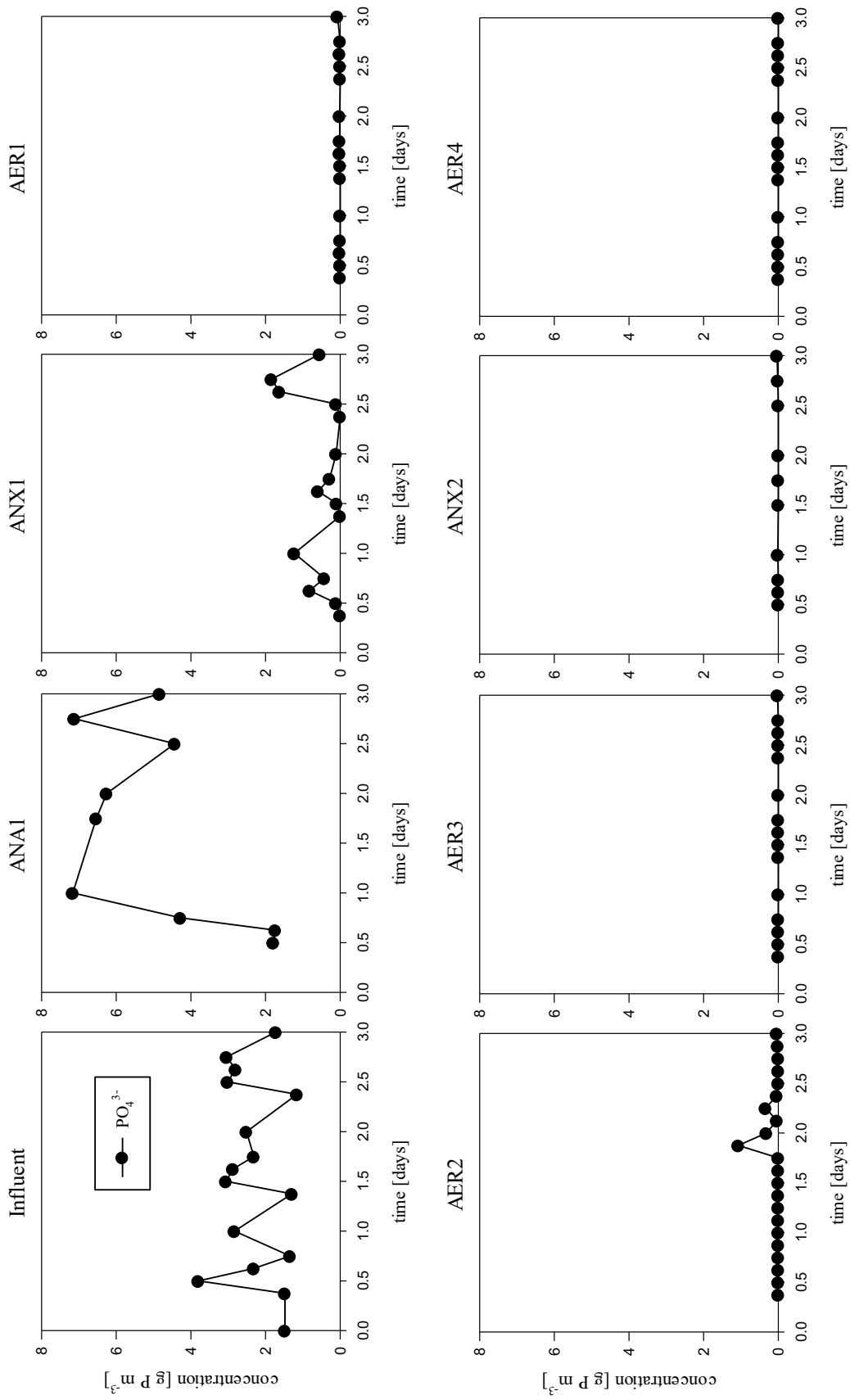


Figure 3.6. Phosphate concentration profiles measured in the influent and in each compartment of the biological reactor during the experimental data campaign.

Figure 3.7 shows the influent COD and flowrate profiles measured during the experimental data campaign. Table 3.2 shows all the determined model influent state variable. The influent characterization was kept constant during the dynamic calibration.

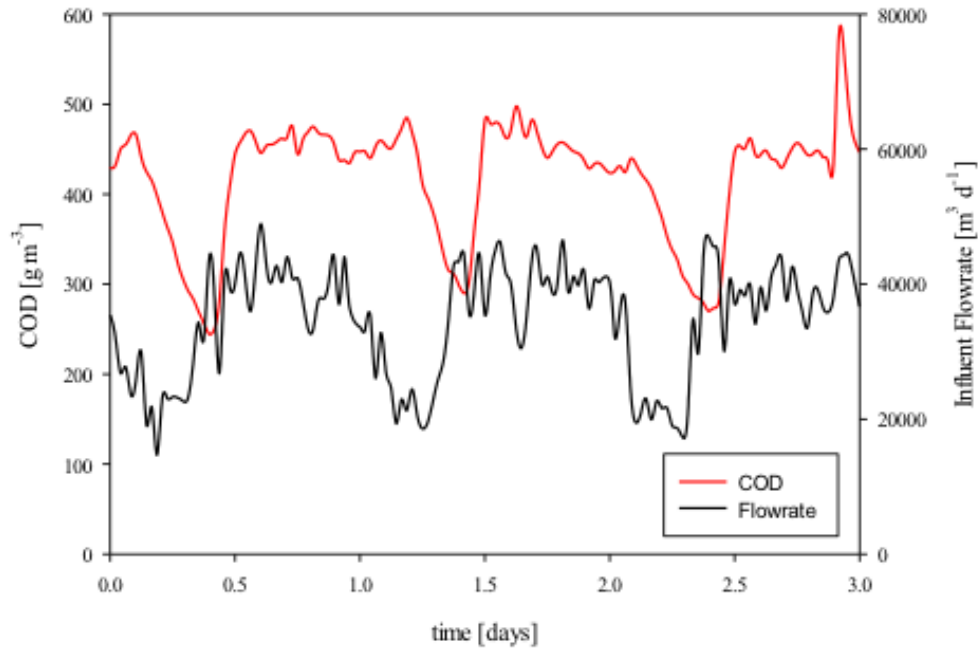


Figure 3.7. Influent COD and flowrate profiles during the experimental data campaign.

Table 3.2. Calculated COD fractions of the ASM2d-N<sub>2</sub>O model state variables in the influent.

Variable	Value
$f_{SI}$	0.035
$f_{SA}$	0
$f_{SF}$	0.415
$f_{XS}$	0.43
$f_{XH}$	0.05
$f_{XPAO}$	0.001
$f_{XAOB}$	0.001
$f_{XNOB}$	0.001
$f_{XPHA}$	0.0001
$f_{XI}$	0.0668

Figure 3.8 shows the N<sub>2</sub>O emissions from the first three aerated zones (AER1 to AER3) together with the ammonium concentration profile obtained from analytical tests and from an online sensor in AER2. The grey area in Figure 3.8 indicates that N<sub>2</sub>O data was

not available due to a technical failure. Similar peak profiles of  $N_2O$  emissions were observed for the other three aerobic reactors monitored. However, the amount of gas emitted was different, with AER1 being the compartment with highest  $N_2O$  emissions and AER3 with the lowest. This could be related to the fact that more ammonium was nitrified in AER1. Furthermore, Figure 3.8 shows that  $N_2O$  emissions were related to ammonium concentration and thus emissions decreased to negligible levels when ammonium was depleted. The same pattern of  $N_2O$  peak emissions were reported in other studies in full-scale WWTPs or in lab experiments with nitrifying-enriched sludge. The peak is attributed to the sudden increase of ammonium, which produce a transient between low-activity to high-activity of nitrifying biomass (Kampschreur et al., 2009b; Law et al., 2012b; Ribera-Guardia et al., 2019). During the experimental campaign, the averaged  $N_2O$  Emission Factor ( $N_2O$ -EF) (calculated as the percentage of the influent TKN load emitted as  $N_2O$ -N), of AER1 to AER3 reactors was 0.41%, which is in the low range of the  $N_2O$ -EF reported for full-scale WWTPs (Kampschreur et al., 2009b; Law et al., 2012b; Massara et al., 2017; Ribera-Guardia et al., 2019). However,  $N_2O$ -EF slightly increased compared to  $N_2O$ -EF measured during a large monitoring campaign at the same WWTP,  $N_2O$ -EF of 0-0.13% (Ribera-Guardia et al., 2019). The increase observed in the current monitoring campaign could be related to the wastewater temperature, which was higher than that of (Ribera-Guardia et al., 2019) and could lead to increased  $N_2O$  emissions due to increased nitrification rates (Bao et al., 2018; Law et al., 2012a).



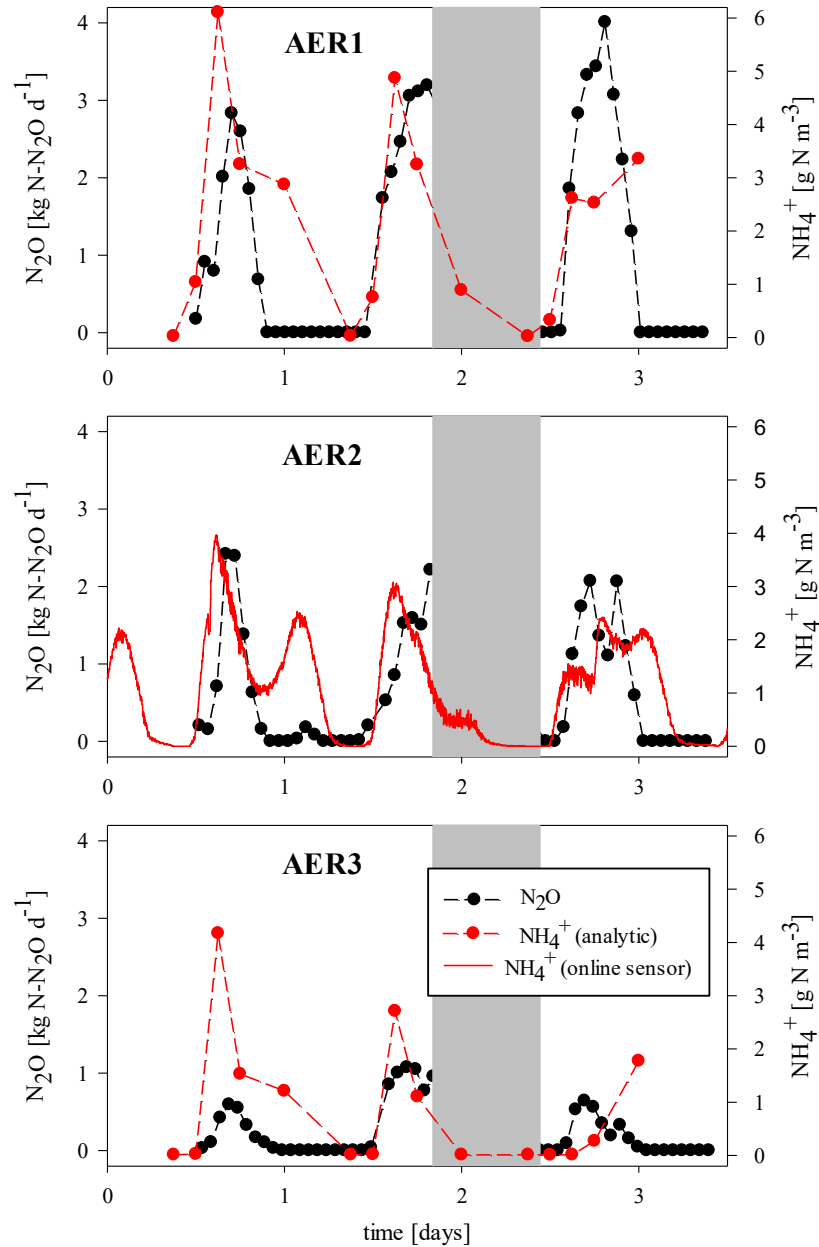


Figure 3.8. Measured N<sub>2</sub>O emissions and NH<sub>4</sub><sup>+</sup> concentration in compartments AER1, AER2 and AER3. The grey area represents a technical failure in the N<sub>2</sub>O gas measurement system. The dashed line at the N<sub>2</sub>O and NH<sub>4</sub><sup>+</sup> analytical data points is an aid for better visualization of the experimental profiles.

### 3.3.2. Hydraulic characterization

The pulse response at the influent of biological reactors and the flowrates measured during the RTD experiment are shown in Figure 3.9. The influent tracer concentration, the flowrates and the dimensional data of the Girona WWTP were used as model inputs to characterize the hydraulics of the plant.

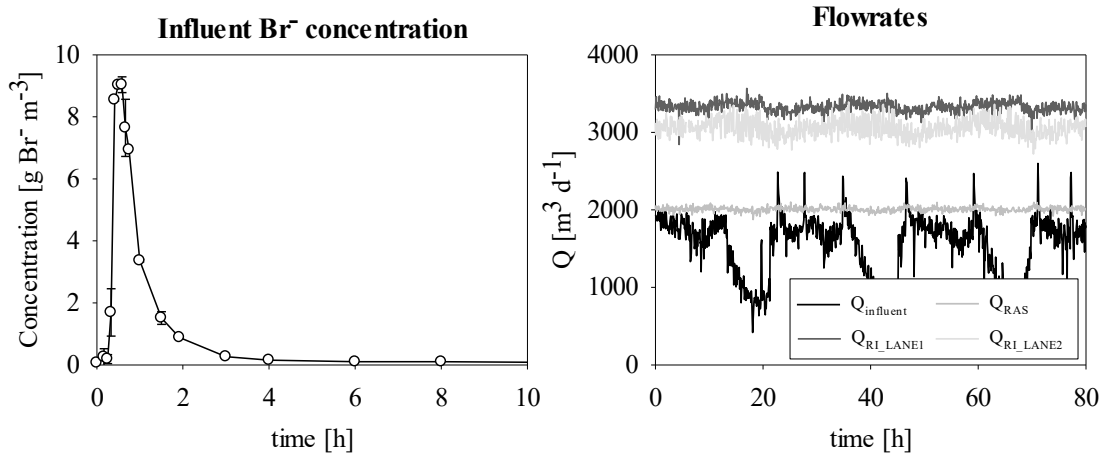


Figure 3.9. Pulse response concentration measured in the effluent of the primary clarifier (influent of the biological reactors) and flowrates measured during the tracer experiment.

Figure 3.10 shows the experimental bromide concentrations measured during the tracer test. The concentration of  $\text{Br}^-$  before the  $\text{KBr}$  pulse was not negligible. Therefore, a constant inlet bromide concentration of  $0.0627 \text{ g m}^{-3}$  was considered during the experiment. A tracer mass balance over the secondary treatment after 78 hours shows that a 79% of the total tracer introduced was detected at the output and that 3.5 kg of the injected  $\text{Br}^-$  remained in the reactor when the experiment was stopped.

The initial assumption that each reactor operated as an ideal CSTR was correct, as the model predictions fitted well with the experimental values. However, the assumption that the secondary settler flow pattern was ideally mixed was false and the model needed to be revised. The parameters to be estimated were the number of  $N$  tanks-in-series of the secondary settler and the percentage distribution of the influent flow between each biological line (i.e.  $f_{Q1}$  and  $f_{Q2}$ , where  $f_{Q1}$  and  $f_{Q2}$  are the percentage of the influent flow going to the first and second biological treatment lines, respectively, and  $f_{Q1}+f_{Q2}=1$ ).

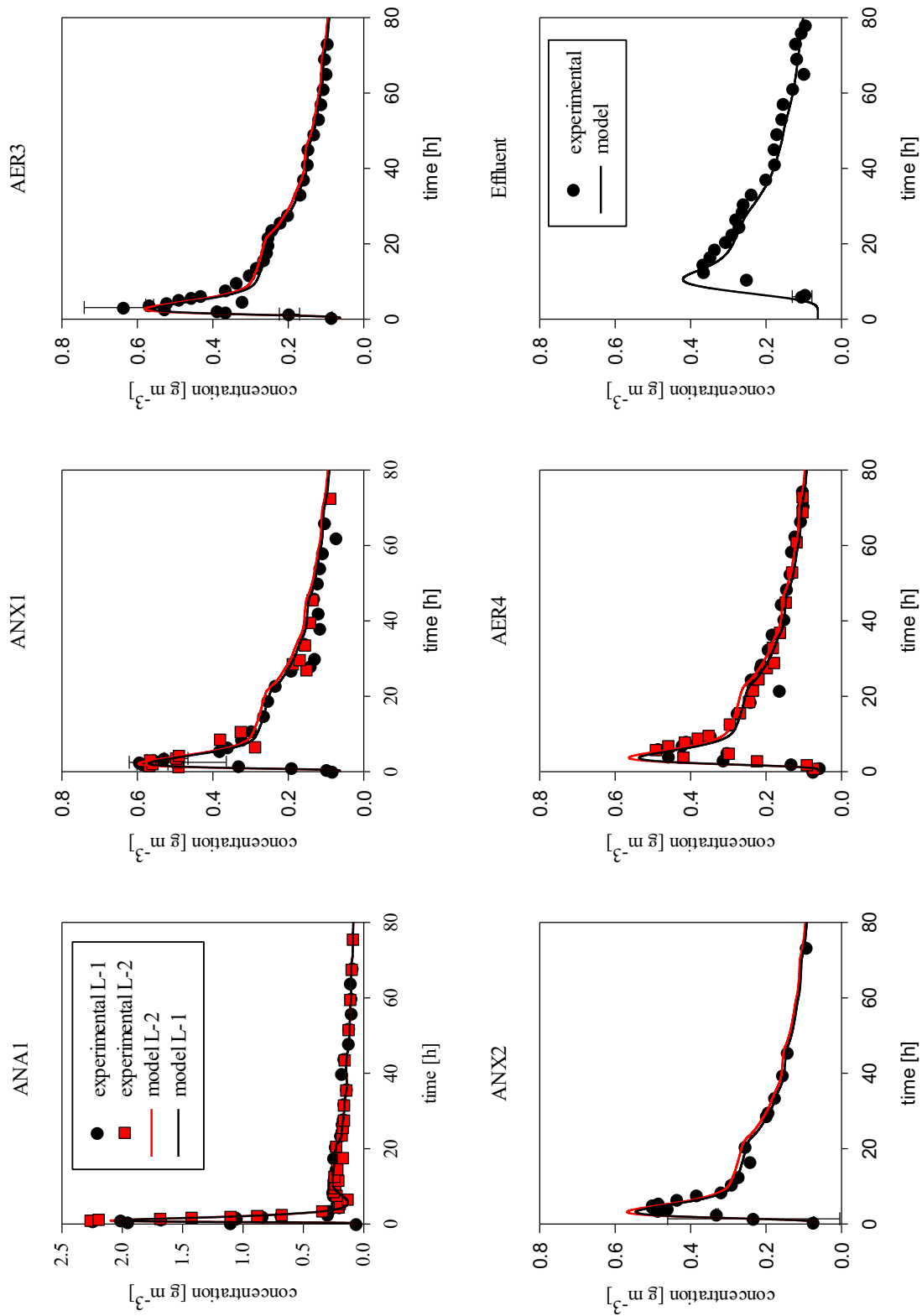


Figure 3.10. Tracer experiment results and model results in each measured compartment and in the effluent.

Figure 3.10 shows the results obtained during the hydraulic calibration. The model accurately described the experimental data. The optimized parameters for the secondary settler flow pattern were  $N=5$  tanks and hence the secondary settler flow pattern was closer to a plug flow reactor flux model than to a CSTR. The flowrate was distributed approximately equally between the two lines, with 49.33% of the influent flowrate going to the first biological treatment line and 50.67% to the second treatment line. These results contradict the initial thinking of the plant operators.

### 3.3.3. Preliminary calibration

The next step after the identification of the WWTP hydraulics was the calibration of the kinetic model ASM2d-N<sub>2</sub>O. As the flow distribution between both biological treatment lines was approximately the same, only one biological treatment line was considered in the kinetic calibration and in the GSA studies. The preliminary calibration (see section 3.2.7) aimed to reduce structural discrepancies between the model and the experimental variables (Machado et al., 2013), particularly for those related to P, before performing the GSA and the subsequent dynamic calibration.

The  $X_{\text{MeOH}}$  addition that minimized the PCCF was 184 kg Fe(OH)<sub>3</sub> d<sup>-1</sup>. The PCCF obtained was 2.7, achieving a reduction of 74% compared to the PCCF before the preliminary calibration. The fits obtained on the average phosphate concentration are shown in Figure 3.11. The calibrated  $X_{\text{MeOH}}$  addition value was maintained constant during all dynamic simulations. Moreover, as phosphate concentrations were calibrated by chemical precipitation, PAO-related parameters were not considered during the ASM2d-N<sub>2</sub>O calibration and phosphate concentrations were not considered in the CCF.

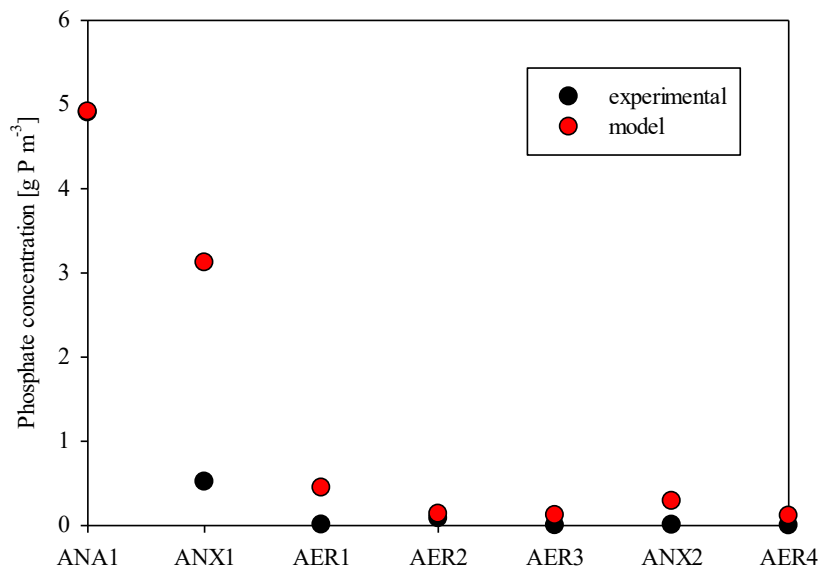


Figure 3.11. Fit obtained in the average phosphate concentrations during preliminary calibration.

### 3.3.4. Development of the Calibration Cost Function (CCF)

The data obtained during the experimental campaign were used to dynamically calibrate the ASM2d-N<sub>2</sub>O model to the Girona WWTP. In total, four variables were included in the cost function and considered as the output variables of interest: ammonium, nitrite and nitrate in the biological reactors and N<sub>2</sub>O emissions from AER1 to AER3. Therefore, the CCF was divided into four different cost functions (named CCF<sub>i</sub>) for each output variable of interest (i.e. CCF<sub>NH<sub>4</sub><sup>+</sup></sub>, CCF<sub>NO<sub>2</sub><sup>-</sup></sub>, CCF<sub>NO<sub>3</sub><sup>-</sup></sub>, CCF<sub>N<sub>2</sub>O</sub>). The overall CCF was calculated as the sum of each individual output variable CCF<sub>i</sub>. As all the CCF<sub>i</sub> were of the same order of magnitude, no weighting factors were included in the CCF calculation. Equation 3.13 was used to calculate each CCF<sub>i</sub> and Equation 3.14 was used to calculate the overall CCF:

$$CCF_i = \sum_{r=1}^m \sqrt{\sum_{j=1}^n (y_{\text{exp } i,j} - y_{\text{model } i,j})^2} \quad (\text{Eq. 3.13})$$

$$CCF = \sum_{i=1}^4 CCF_i = CCF_{\text{NH}_4^+} + CCF_{\text{NO}_2^-} + CCF_{\text{NO}_3^-} + CCF_{\text{N}_2\text{O}} \quad (\text{Eq. 3.14})$$

Where: “i” is related to the output variable of interest (NH<sub>4</sub><sup>+</sup>, NO<sub>2</sub><sup>-</sup>, NO<sub>3</sub><sup>-</sup> or N<sub>2</sub>O); “j” is related to each experimental data point (n measures); “r” is related to each sample zone and y<sub>exp</sub> and y<sub>model</sub> are related to experimental data and model output, respectively. The phosphorus related variables were not added in the CCF for the reasons discussed in the above section.

### 3.3.5. Global Sensitivity Analysis

A number of N=2000 simulations was selected for the MC experiment. The CCF and each CCF<sub>i</sub> for each simulation were then evaluated and discretized into two populations, B and  $\bar{B}$  (see section 3.2.6). The threshold fixed to discretize the CCF (and the associated input parameters) was the maximum reduction on the CCF that can be achieved with a number of simulations of the behavioural group of at least N<sub>B</sub>=100, representing 5% of all simulations. The maximum reduction in CCF that satisfied the requirement of N<sub>B</sub> = 100, and therefore, the threshold selected for RSA evaluation was 40%, compared to the CCF calculated with the default parameter values of ASM2d-N<sub>2</sub>O. For this selected threshold, the top ranked RSA indices are shown in Table 3.3.

Among the CCF<sub>i</sub>-related results, a high reduction threshold of around 80% was found for nitrite and nitrous oxide CCFs. On the other hand, the thresholds found for the ammonium and nitrate CCFs were around 10%. These results showed that the maximum reduction in the overall CCF that could be achieved was related to the reduction in the nitrite and nitrous oxide CCFs. The initial simulations were in agreement with this observation, as the predicted ammonium and nitrate concentrations were in good agreement with the experimental values. In addition, Table 3.3 shows that the five top ranked parameters

were related to nitrification processes, more specifically to the nitrification process, as four of the five top ranked parameters were related to NOB ( $\mu_{\text{NOB}}$ ,  $b_{\text{NOB}}$ ,  $K_{\text{NO}_2\text{-NOB}}$  and  $K_{\text{O}_2\text{-NOB}}$ ) and the other parameter was related to AOB bacteria ( $q_{\text{AOB\_AMO}}$ ). Therefore, the GSA results showed that the ASM2d-N<sub>2</sub>O model calibration for the Girona WWTP should focus on the calibration of the nitrifying bacteria parameters.

Table 3.3. Ranking of the first twenty parameters obtained in the GSA.

Position	Parameter	Description
1	$\mu_{\text{NOB}}$	Maximum NOB growth rate
2	$b_{\text{NOB}}$	Decay rate of NOB
3	$K_{\text{NO}_2\text{-NOB}}$	Saturation coefficient for $\text{NO}_2^-$
4	$q_{\text{AOB\_AMO}}$	Maximum rate for the AMO reaction
5	$K_{\text{O}_2\text{-NOB}}$	Half-saturation coefficient for $\text{O}_2$
6	$n_{\text{G5}}$	Anoxic growth factor ( $\text{N}_2\text{O} \rightarrow \text{N}_2$ )
7	$K_{\text{OH5}}$	Half-saturation coefficient for $\text{O}_2$
8	$q_{\text{AOB\_HAO}}$	Maximum rate for HAO reaction
9	$q_{\text{AOB\_N}_2\text{O\_ND}}$	Maximum $\text{N}_2\text{O}$ production rate by the ND pathway
10	$K_{\text{NO}_2}$	Saturation/inhibition coefficient for $\text{NO}_2^-$
11	$K_{\text{I5NO}}$	NO inhibition coefficient ( $\text{N}_2\text{O} \rightarrow \text{N}_2$ )
12	$K_{\text{I\_O}_2\text{-AOB}}$	$\text{N}_2\text{O}$ constant for production inhibition by $\text{O}_2$
13	$K_{\text{O}_2\text{-AOB1}}$	AOB affinity constant for $\text{O}_2$ (AMO reaction)
14	$n_{\text{G3}}$	Anoxic growth factor ( $\text{NO}_2^- \rightarrow \text{NO}$ )
15	$K_{\text{S5}}$	Half-saturation coefficient for substrate
16	$K_{\text{NO}_2\text{-Den}}$	Half-saturation coefficient for $\text{NO}_2^-$
17	$K_{\text{I4NO}}$	NO inhibition coefficient ( $\text{NO} \rightarrow \text{N}_2\text{O}$ )
18	$K_{\text{ALK}}$	Saturation coefficient for alkalinity ( $\text{HCO}_3^-$ )
19	$K_{\text{HNO}_2\text{-AOB}}$	AOB affinity constant for $\text{HNO}_2$
20	$K_{\text{NO}_3\text{-H}}$	Saturation/inhibition coefficient for $\text{NO}_3^-$

### 3.3.6. Dynamic calibration

The dynamic calibration was conducted after identifying the ASM2d-N<sub>2</sub>O parameters most likely to reduce the CCF. Different parameter subsets were defined with all the possible combinations of the five top ranked parameters from the RSA (Table 3.3). The size of parameter subsets ranged from one to four parameters, resulting in a total of 30 parameter subsets to be calibrated. The parameter subset and calibrated values that most reduced the CCF were for  $\mu_{\text{NOB}} = 0.67 \text{ d}^{-1}$ ,  $q_{\text{AOB\_AMO}} = 5.52 \text{ d}^{-1}$ ,  $K_{\text{O}_2\text{-NOB}} = 0.126 \text{ g O}_2 \text{ m}^{-3}$  and  $K_{\text{NO}_2\text{-NOB}} = 0.126 \text{ g N m}^{-3}$ . The CCF was reduced by 53.3% with this parameter subset, compared to the CCF after preliminary calibration, mainly due to the reduction of the CCF of  $\text{NO}_2^-$  and  $\text{N}_2\text{O}$  (87.7 and 86.5%, respectively). The calibration results for each parameter subset can be found in Table 3.4. The fit between experimental data and model

predictions for N-species is shown in Figure 3.12 and those for N<sub>2</sub>O emissions are shown in Figure 3.13.

Table 3.4. Dynamic calibration results for each subset of parameters tested.

Parameter subset	Optimized values	CCF
[ $\mu_{\text{NOB}}$ ]	[3.580]	80.0
[ $b_{\text{NOB}}$ ]	[0.000]	79.7
[ $q_{\text{AOB\_AMO}}$ ]	[4.680]	165.3
[ $K_{\text{O}_2\_ \text{NOB}}$ ]	[0.003]	83.4
[ $K_{\text{NO}_2\_ \text{NOB}}$ ]	[0.002]	90.4
[ $\mu_{\text{NOB}}$ , $b_{\text{NOB}}$ ]	[0.8707, 0.0000]	79.6
[ $\mu_{\text{NOB}}$ , $q_{\text{AOB\_AMO}}$ ]	[3.6140, 5.5387]	79.2
[ $\mu_{\text{NOB}}$ , $K_{\text{O}_2\_ \text{NOB}}$ ]	[1.4537, 0.1328]	78.4
[ $\mu_{\text{NOB}}$ , $K_{\text{NO}_2\_ \text{NOB}}$ ]	[7.7996, 1.3848]	79.6
[ $b_{\text{NOB}}$ , $q_{\text{AOB\_AMO}}$ ]	[0.0003, 5.5270]	79.0
[ $b_{\text{NOB}}$ , $K_{\text{O}_2\_ \text{NOB}}$ ]	[0.0360, 0.1395]	78.3
[ $b_{\text{NOB}}$ , $K_{\text{NO}_2\_ \text{NOB}}$ ]	[0.0003, 0.4766]	79.7
[ $q_{\text{AOB\_AMO}}$ , $K_{\text{O}_2\_ \text{NOB}}$ ]	[5.4508, 0.0008]	83.0
[ $q_{\text{AOB\_AMO}}$ , $K_{\text{NO}_2\_ \text{NOB}}$ ]	[5.1622, 0.0025]	90.4
[ $K_{\text{O}_2\_ \text{NOB}}$ , $K_{\text{NO}_2\_ \text{NOB}}$ ]	[0.1290, 0.1802]	78.3
[ $\mu_{\text{NOB}}$ , $b_{\text{NOB}}$ , $q_{\text{AOB\_AMO}}$ ]	[0.8933, 0.0003, 5.5446]	78.9
[ $\mu_{\text{NOB}}$ , $b_{\text{NOB}}$ , $K_{\text{O}_2\_ \text{NOB}}$ ]	[0.3698, 0.0003, 0.1531]	78.0
[ $\mu_{\text{NOB}}$ , $b_{\text{NOB}}$ , $K_{\text{NO}_2\_ \text{NOB}}$ ]	[7.5730, 0.0062, 5.0000]	79.2
[ $\mu_{\text{NOB}}$ , $q_{\text{AOB\_AMO}}$ , $K_{\text{O}_2\_ \text{NOB}}$ ]	[1.4802, 5.5226, 0.1312]	77.7
[ $\mu_{\text{NOB}}$ , $q_{\text{AOB\_AMO}}$ , $K_{\text{NO}_2\_ \text{NOB}}$ ]	[7.7995, 5.5289, 1.3594]	78.9
[ $\mu_{\text{NOB}}$ , $K_{\text{O}_2\_ \text{NOB}}$ , $K_{\text{NO}_2\_ \text{NOB}}$ ]	[6.6980, 0.1424, 2.9475]	78.4
[ $b_{\text{NOB}}$ , $q_{\text{AOB\_AMO}}$ , $K_{\text{O}_2\_ \text{NOB}}$ ]	[0.0347, 5.5221, 0.1387]	77.6
[ $b_{\text{NOB}}$ , $q_{\text{AOB\_AMO}}$ , $K_{\text{NO}_2\_ \text{NOB}}$ ]	[0.0003, 5.5367, 0.4648]	79.0
[ $b_{\text{NOB}}$ , $K_{\text{O}_2\_ \text{NOB}}$ , $K_{\text{NO}_2\_ \text{NOB}}$ ]	[0.0008, 0.1453, 1.2529]	78.1
[ $q_{\text{AOB\_AMO}}$ , $K_{\text{O}_2\_ \text{NOB}}$ , $K_{\text{NO}_2\_ \text{NOB}}$ ]	[5.5192, 0.1282, 0.1740]	77.6
[ $\mu_{\text{NOB}}$ , $b_{\text{NOB}}$ , $q_{\text{AOB\_AMO}}$ , $K_{\text{O}_2\_ \text{NOB}}$ ]	[0.3825, 0.0008, 5.5211, 0.1492]	77.3
[ $\mu_{\text{NOB}}$ , $b_{\text{NOB}}$ , $q_{\text{AOB\_AMO}}$ , $K_{\text{NO}_2\_ \text{NOB}}$ ]	[1.5525, 0.0023, 5.5289, 1.0000]	78.7
[ $\mu_{\text{NOB}}$ , $b_{\text{NOB}}$ , $K_{\text{O}_2\_ \text{NOB}}$ , $K_{\text{NO}_2\_ \text{NOB}}$ ]	[0.5945, 0.0594, 0.1258, 0.2070]	78.3
[ $\mu_{\text{NOB}}$ , $q_{\text{AOB\_AMO}}$ , $K_{\text{O}_2\_ \text{NOB}}$ , $K_{\text{NO}_2\_ \text{NOB}}$ ]	[0.6736, 5.5172, 0.1258, 0.1260]	77.6
[ $b_{\text{NOB}}$ , $q_{\text{AOB\_AMO}}$ , $K_{\text{O}_2\_ \text{NOB}}$ , $K_{\text{NO}_2\_ \text{NOB}}$ ]	[0.0071, 5.5211, 0.1395, 1.0000]	77.4

As can be seen, the model predicts reasonably well the concentration of the different N-species in the reactor. The ASM2d-N<sub>2</sub>O was able to explain the low nitrite concentrations measured during the experimental campaign, by reducing the NOB oxygen and nitrite affinity constants with respect to the default values (Massara et al., 2018). Experimental nitrate data and model fits showed a discrepancy in nitrification capacity, as measured

nitrate showed smaller increases among aerobic reactors (AER1 to AER3) compared to model predictions. The model could not predict such a high degree of simultaneous nitrification and denitrification occurring in AER2 and AER3. This was due to the low DO levels in AER2 and AER3 (1.5 and 1.2 g O<sub>2</sub> m<sup>-3</sup>, respectively) in addition to the inherent instability of the DO control system in the plant, which caused significant noise in the DO concentration and favoured denitrification processes when the DO concentration was low.



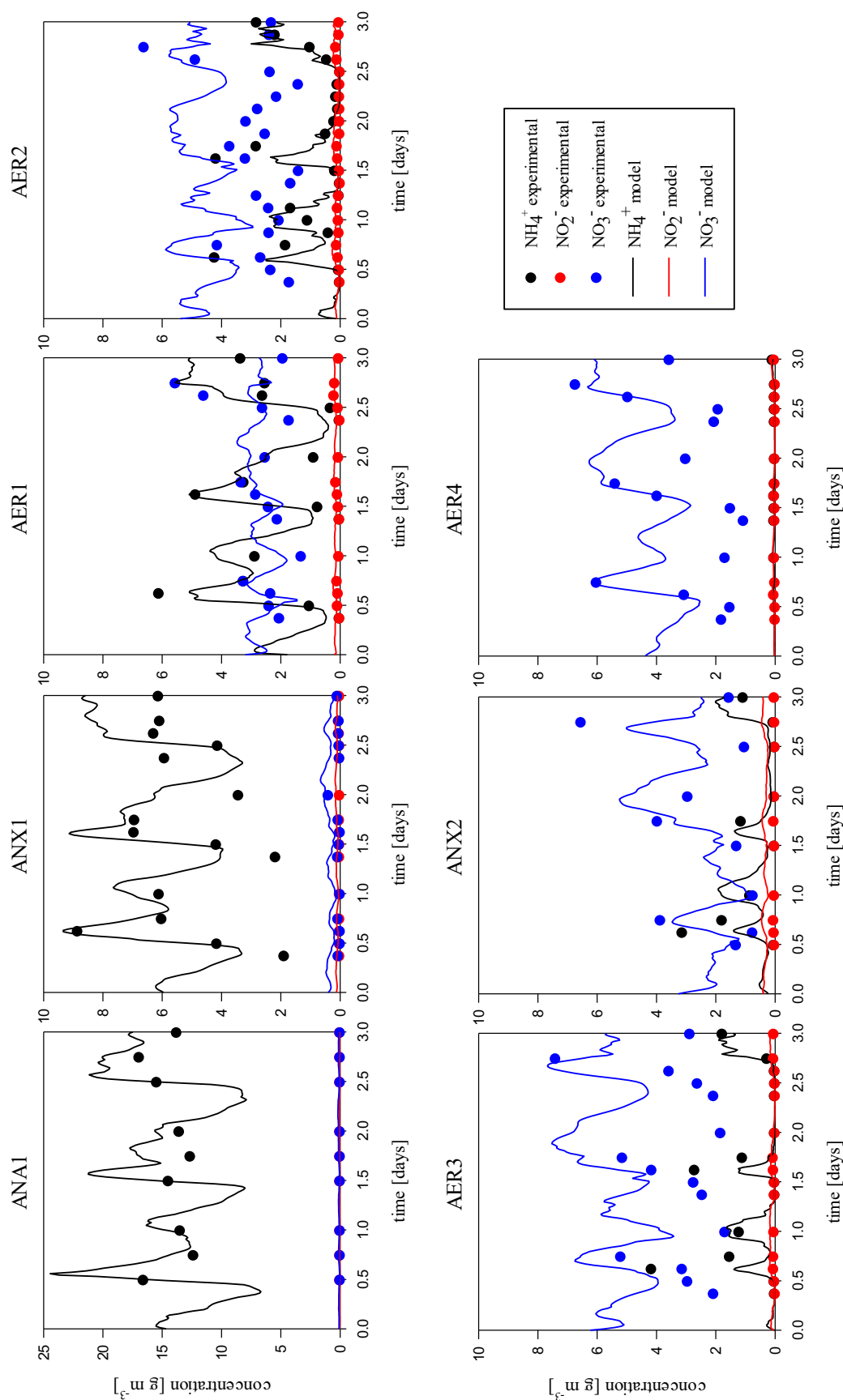


Figure 3.12. Concentrations of ammonium, nitrite and nitrate measured during the experimental campaign and fit obtained during the dynamic calibration of ASM2d-N<sub>2</sub>O.

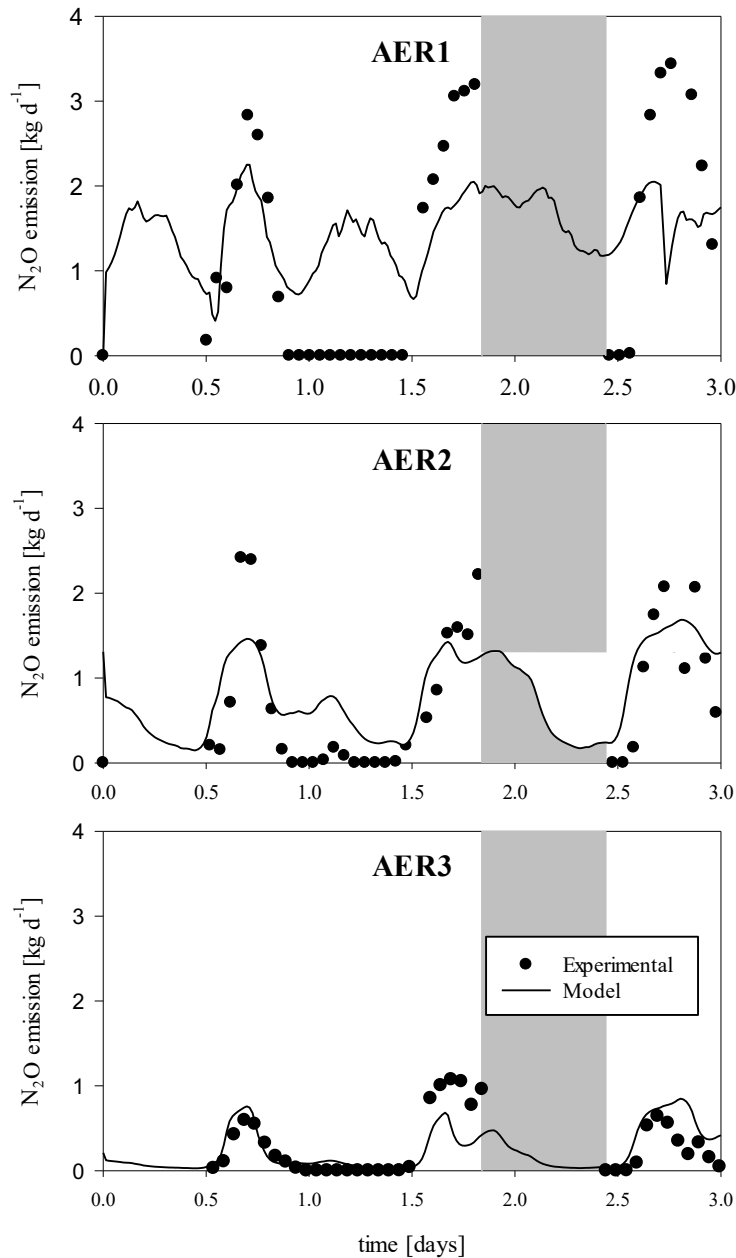


Figure 3.13.  $\text{N}_2\text{O}$  emissions measured during the experimental campaign and fits obtained during the dynamic calibration of ASM2d- $\text{N}_2\text{O}$ . In the grey area no experimental  $\text{N}_2\text{O}$  emission data were available due to a technical failure.

On the other hand, the ASM2d- $\text{N}_2\text{O}$  model was able to capture the dynamics of  $\text{N}_2\text{O}$  emissions from AER1 to AER3 (Figure 3.13) even considering that only one parameter related to biomass producing  $\text{N}_2\text{O}$  was modified ( $q_{\text{AOB\_AMO}}$ ). The largest discrepancies found were in the AER1 compartment, where  $\text{N}_2\text{O}$  model predictions did not show a peak. Moreover, the model predicted that  $\text{N}_2\text{O}$  was emitted during the three days of dynamic simulation whereas the experimental  $\text{N}_2\text{O}$  emissions were, for some time, negligible. This can be explained by:

1) The model predicted a peak of ammonium during day 1.0 and 1.5 that was not experimentally detected (Figure 3.12). The N<sub>2</sub>O emissions during this second daily peak of ammonium were mostly related to the ND pathway, since, as a result of the ammonium accumulation, the model also predicted a slight accumulation of hydroxylamine, which is the electron acceptor substrate for the ND pathway.

2) The model predicted the highest nitrite concentration in AER1, obtaining an average value of 0.17 g N m<sup>-3</sup> during the three days of dynamic simulation. This low nitrite concentration was high enough to boost the ND pathway in this reactor.

ND is the biological N<sub>2</sub>O production pathway responsible for most of emissions during wastewater treatment (Law et al., 2012b; Massara et al., 2018, 2017; Tallec et al., 2006). In fact, the average contribution of the ND pathway to the total N<sub>2</sub>O production in AER1 was 82% and decreased to 78% and 48% in AER2 and AER3, respectively. These values are in agreement with literature ranges for aerobic reactors (Tallec et al., 2006). The NN pathway contributed 6% to the total N<sub>2</sub>O production and the HD pathway contributed mostly in AER3 with 45%, where the DO was the lowest of the aerobic zones (1.2 g O<sub>2</sub> m<sup>-3</sup>). The higher contribution of the HD pathway in AER3 shows that simultaneous nitrification and denitrification occurred in this reactor due to the low DO coupled with low NH<sub>4</sub><sup>+</sup> and high NO<sub>3</sub><sup>-</sup> concentrations. The predicted N<sub>2</sub>O-EF, only considering AER1 to AER3 zones, was 0.55% which is very similar to the measured one (0.41%).

### 3.3.7. Model exploitation

Once the dynamic calibration was done, two scenarios were simulated to investigate the effect of varying the flowrate distribution between both treatment lines (Figure 3.1) on N<sub>2</sub>O emissions and N<sub>2</sub>O-EF. In the first case, an equal flow distribution was simulated, i.e. 50% of the influent flowrate was fed to each line, according to the tracer experiments results (section 3.3.2). The second case was modelled assuming that 40% of the influent flowrate went to the first treatment line and the remaining 60% to the second. Each simulation was done following the same methodology as in the dynamic calibration (section 3.2.7) and with the same model inputs. In addition, it was assumed that the aeration system was able to maintain the same DO concentration despite the increase of N load.

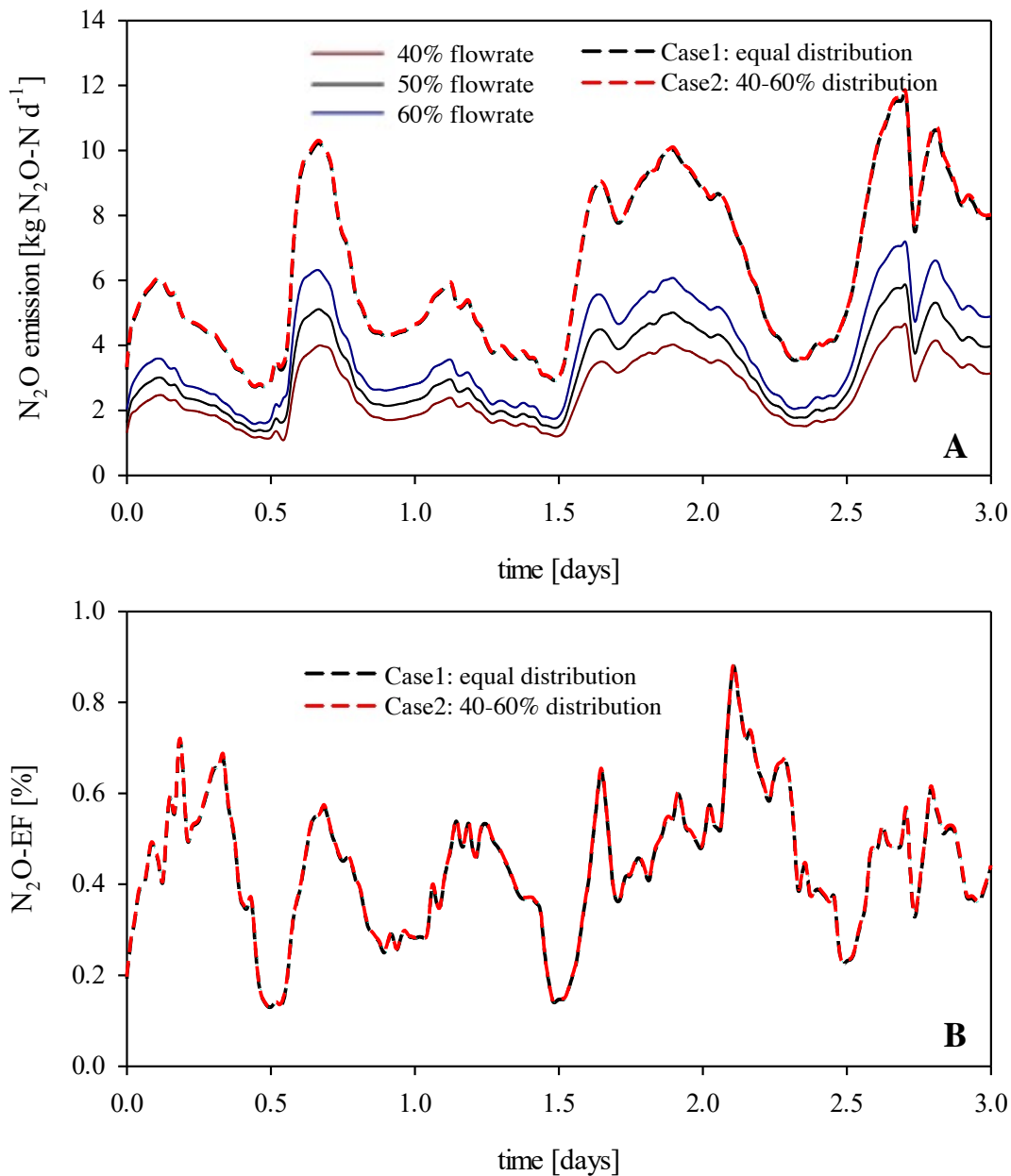


Figure 3.14. Predicted  $N_2O$  emissions in two different flowrate scenarios: Case 1 (equal influent flowrate distribution in both treatment lines) and Case 2 (40-60% influent flowrate distribution). (A)  $N_2O$  emissions in each treatment line for 40%-50%-60% flowrate and total  $N_2O$  emissions. (B) Predicted  $N_2O$ -EF for both cases.

Figure 3.14 shows the predicted  $N_2O$  emissions in each treatment line and the total  $N_2O$  emissions and  $N_2O$ -EF for each case. Figure 3.14A shows that the predicted  $N_2O$  emissions from the treatment lines increased with increasing influent flowrate. The average  $N_2O$  emission rate obtained for an influent flowrate distribution of 40, 50 and 60% were 2.5, 3.2 and 3.8  $kg N_2O-N d^{-1}$  respectively. The same ammonium was obtained in the effluent for all three influent distribution simulations, however, nitrite and nitrate

in the effluent increased with increasing influent flowrate due to the increase on the TKN influent load. Figure 3.14A reveals that the same total N<sub>2</sub>O emissions were predicted for both cases (6.3 kg N<sub>2</sub>O-N d<sup>-1</sup>). This is because the N<sub>2</sub>O emissions increased linearly with increasing influent flowrate and therefore the total N<sub>2</sub>O emissions for both cases were the same. Figure 3.14B also shows that the predicted N<sub>2</sub>O-EF for both lines was the same for each case because the N<sub>2</sub>O emissions increased with the same slope as the TKN removed.

### 3.4. Conclusions

This work is a comprehensive calibration of the ASM2d-N<sub>2</sub>O to a full-scale WWTP including hydraulics with the following main findings:

- Modelling the flow patterns in the plant is essential in view of its calibration. The tracer experiment showed that all reactors of the two treatment lines had a correct hydraulic behaviour, as no dead volumes, flux recycling or by-passes were found. Furthermore, it was demonstrated that an equal flow is flowing to each line.
- RSA was successfully applied to rank the parameters most likely to reduce the CCF. The sensitivity analysis revealed that the top ranked parameters were related to nitrifying organisms.
- Good fits were obtained during the dynamic kinetic calibration of the ASM2d-N<sub>2</sub>O model. The dynamic N-species profiles along the reactors were described with only modifying four kinetic parameters with respect to the default values.
- N<sub>2</sub>O-EF predicted by the ASM2d-N<sub>2</sub>O model was very similar to that measured experimentally and the predicted emission trends were in good agreement with the experimental data.

# **Chapter IV:**

---

**Exploring GHG emissions in the mainstream**

**SCEPPHAR configuration during wastewater resource  
recovery**



## 4. Exploring GHG emissions in the mainstream SCEPPHAR configuration during wastewater resource recovery

### Abstract

The wastewater sector paradigm is shifting from wastewater treatment to resource recovery. In addition, concerns regarding the sustainability during the operation have increased. In this sense, many water utilities have become aware of the potential GHG emissions during the operation of wastewater treatment. This study assesses the nitrous oxide and methane emissions during the long-term operation of a novel WRRF configuration: the mainstream SCEPPHAR. The long-term  $\text{N}_2\text{O}$  and  $\text{CH}_4$  emission factors calculated were in the low range of the literature, 1% and 0.1%, respectively, even with high nitrite accumulation in the case of  $\text{N}_2\text{O}$ . The dynamics and possible sources of production of these emissions are discussed. Finally, different aeration strategies were implemented to study the impact on the  $\text{N}_2\text{O}$  emissions in the nitrifying reactor. The results showed that operating the pilot-plant under different dissolved oxygen (between 1 and 3 g  $\text{O}_2$   $\text{m}^{-3}$ ) did not seem to have an effect on the  $\text{N}_2\text{O}$  emission factor. The intermittent aeration was the aeration strategy that most mitigated the  $\text{N}_2\text{O}$  emissions in the nitrifying reactor, obtaining a reduction of 40% compared to the normal operation of the pilot plant.

### 4.1. Motivations

The aim of this work was to monitor the performance of the mainstream SCEPPHAR pilot plant in its final operation period (i.e. under nitrite shortcut N-removal operation) in view of understanding and assessing the overall GHG emissions through different pilot plant cycles in view of developing novel mitigation control strategies. For this aim, different aeration strategies were implemented and its effect was assessed on both the  $\text{N}_2\text{O}$  liquid concentration and gas emissions. Different operational parameters that seemed to have an effect on the  $\text{N}_2\text{O}$  production and emission were explored and discussed. Finally, the measured GHG emissions were compared to other WRRF configurations and the sources that triggered these emissions were discussed.

### 4.2. Materials and Methods

#### 4.2.1. Pilot plant configuration and influent

The SCEPPHAR pilot scale was located in the municipal WWTP of Manresa (Barcelona, Spain). The influent of the pilot plant was the wastewater of the primary settler effluent of the Manresa WWTP. The average composition of the influent wastewater is shown in Table 4.1.



Table 4.1. Average composition and temperature of the pilot plant.

Variable	Value	Units
PO <sub>4</sub> <sup>3-</sup>	4.1 ± 1.3	g P m <sup>-3</sup>
NH <sub>4</sub> <sup>+</sup>	39.4 ± 10.5	g N m <sup>-3</sup>
NO <sub>2</sub> <sup>-</sup>	0.2 ± 0.4	g N m <sup>-3</sup>
NO <sub>3</sub> <sup>-</sup>	0.2 ± 0.4	g N m <sup>-3</sup>
total COD	300 ± 128	g COD m <sup>-3</sup>
soluble COD	179 ± 62	g COD m <sup>-3</sup>
Temperature	15.6 ± 4.2	°C

The pilot plant consisted of two SBRs (R1-HET and R2-AUT), a precipitation reactor (R3-PRE) and an interchange vessel (R4-INT). The process diagram of the pilot plant is shown in Figure 4.1. The R1-HET reactor was an anaerobic/anoxic/aerobic SBR ( $V=2.5$  m<sup>3</sup>) designed for heterotrophic processes (EBPR, carbon removal and denitrification). The R2-AUT reactor was an aerobic SBR ( $V=2.5$  m<sup>3</sup>) designed for autotrophic nitrification. R3-PRE was a precipitation reactor ( $V=0.15$  m<sup>3</sup>) designed for struvite precipitation. R4-INT was the interchange vessel ( $V=2.5$  m<sup>3</sup>) designed for the exchange of supernatants among R1-HET, R2-AUT and R3-PRE reactors. The pilot plant operated with 70% of volume exchange ratio, resulting in 1.75 m<sup>3</sup> of wastewater treated per cycle of the pilot plant. The pilot plant was operated in cycles of 8- and 12-hour duration, being able to treat 5.2 and 3.5 m<sup>3</sup> of wastewater per day, respectively.

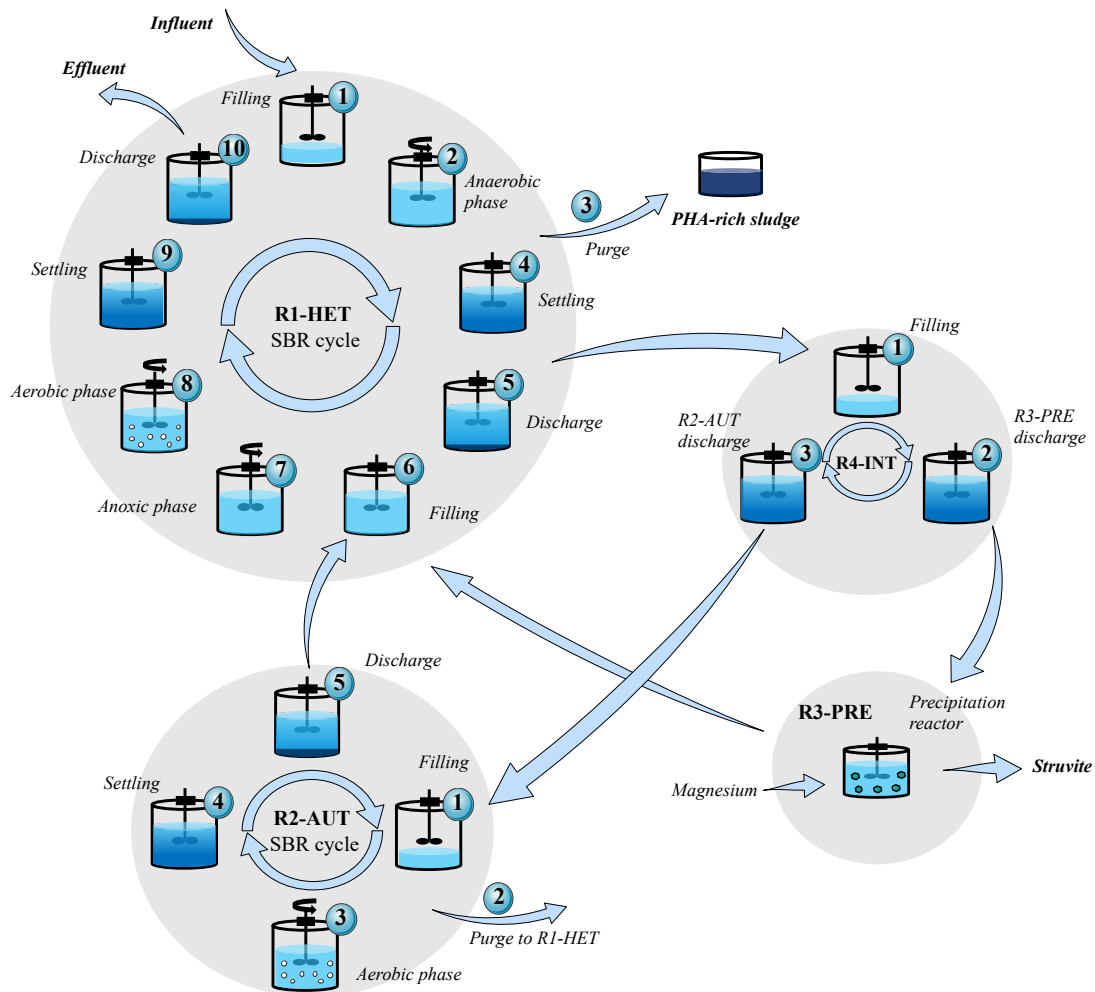


Figure 4.1. SCEPPHAR pilot plant configuration and cycle operation (adapted from Larriba et al., 2020).

Each cycle of the mainstream SCEPPHAR configuration operated in the following sequence (Figure 4.1): the cycle started with the filling of R1-HET, then, an anaerobic phase for promoting COD fermentation, VFA uptake,  $\text{PO}_4^{3-}$  release and PHA accumulation. After an anaerobic purge to obtain a PHA-rich sludge and the settling of the reactor, the supernatant of R1-HET, rich in  $\text{PO}_4^{3-}$  and  $\text{NH}_4^+$ , was transferred to the R4-INT vessel. In R4-INT,  $0.15 \text{ m}^3$  of the supernatant were sent to the R3-PRE reactor to precipitate struvite. The rest of the volume was transferred to the R2-AUT reactor and, once R2-AUT was filled, an aerobic phase with controlled DO took place to promote autotrophic nitrification. After the settling period, the supernatant of R2-AUT, rich in  $\text{PO}_4^{3-}$  and  $\text{NO}_2^-$  was transferred back to R1-HET. The next phase of R1-HET was an anoxic phase in which DPAO took up P while reducing  $\text{NO}_2^-$ . The last phase of R1-HET was aerobic, when PAO captured all the remaining P. After settling, the R1-HET supernatant was discharged to the effluent and the cycle started again. The detailed sequence of the cycles and the duration of each step for the 8- and 12-hour configuration are shown in Table 4.2.

Table 4.2. Configuration of the four reactors of the SCEPPHAR pilot plant with 12 and 8 hours cycle length.

Phase	cycle length = 12 hours		cycle length = 8 hours	
	Time (min)	Duration (min)	Time (min)	Duration (min)
<b>R1-HET</b>				
Feeding from influent	0 - 37	37	0 - 37	37
Anaerobic	37 - 360	323	37 - 180	143
Settling	360 - 385	25	180 - 205	25
Extraction to R4-INT	385 - 413	28	205 - 233	28
Feeding from R2-AUT and R3-PRE	413 - 441	28	233 - 261	28
Anoxic	441 - 541	100	261 - 301	40
Aerobic	541 - 661	120	301 - 421	120
Settling	661 - 691	30	421 - 451	30
Extraction to effluent	691 - 720	29	451 - 480	29
<b>R2-AUT</b>				
Aerobic	37 – 358 <sup>1</sup>	321	0 - 178 <sup>1</sup>	178
Settling	358 <sup>1</sup> - 413	55	178 <sup>1</sup> - 233	55
Extraction to R1-HET	413 - 441	28	233 - 261	28
Feeding from R4-INT	441 - 465	24	261 - 285	24
Purge to R1-HET	465 – 470	5	287 - 290	3
Idle	470 - 37 <sup>2</sup>	287	290 - 480	190
<b>R3-PRE</b>				
Settling	385 – 413	28	205 – 233	28
Extraction to R1-HET	413 - 425	12	233 - 245	12
Feeding from R4-INT	425 – 435	10	245 – 255	10
Precipitation with Mg <sup>2+</sup> addition	435 – 385 <sup>2</sup>	670	255 – 205 <sup>2</sup>	430
<b>R4-INT</b>				
Feeding from R1-HET	385 – 413	28	205 – 233	28
Idle	413 - 425	12	233 - 245	12
Extraction to R3-INT	425 - 435	10	245 - 255	10
Extraction to R2-AUT	441 - 465	24	261 - 285	24
Idle	465 – 385 <sup>2</sup>	640	285 – 205 <sup>2</sup>	400

<sup>1</sup> Maximum value (the actual value is automated from the control system).

<sup>2</sup> Time of the following cycle.

#### 4.2.2. Pilot plant monitoring and control architecture

The pilot plant was highly equipped with online monitoring sensors and automatic control loops. R1-HET, R2-AUT and R4-INT had on-line monitoring of reactor level (Micropilot FMR20, Endress Hauser), which was key for the automation of the interexchange steps

between the reactors. The supernatants were transferred through centrifugal pumps (JP6 B-A-CVBP, Grundfos). R1-HET, R2-AUT and R3-PRE were stirred (HR4A-020/100, Milton Roy Mixing) during the reaction phases of each reactor. R1-HET and R2-AUT were equipped with probes for temperature (Pt1000, Axiomatic), DO (LDO sc, Hach), pH (PC1R1N, Hach) and oxidation-reduction potential (ORP) (RC1R5N, Hach). In addition, R2-AUT was monitored with an online ion-selective electrode for ammonia (AN-ISE sc, Hach). Dosing pumps were used for sludge purge (PS2, Seko) and magnesium and acetic acid addition (Tekna EVO, Seko). DO in R1-HET and R2-AUT was controlled by manipulating the aeration flowrate through electric control valves (Type 3241/3374, Samson Instruments), based on the DO measurement and a proportional-integral (PI) algorithm implemented in the control system. The aeration flow to each reactor was monitored with gas rotameters (Iberfluid). The aerobic phase length in R2-AUT was controlled via the online ammonium sensor, i.e. the control system deactivated the DO PI controller and stopped the aeration when the ammonium was depleted (Larriba et al., 2020).  $N_2O$  and  $CH_4$  gas emissions during the aerobic phases were continuously analysed via an online infra-red gas analyser (VA 3000, Horiba). The typical location of the gas measurement analyser was R2-AUT. However, in some cycles, the analyser monitored R1-HET. The dissolved  $N_2O$  in the liquid phase was monitored in R2-AUT with an on-line microsensor ( $N_2O$ -R, Unisense A/S). All the sensors and the mechanical equipment were connected to a computer (PPC-3170, Advantech) through a data acquisition system (PCI-1711U, PCLD-8710, PCLD-885 I/O, Advantech). The software AddControl developed by the research group was used for automating all the operation, monitoring and control.

#### 4.2.3. Chemical Analysis

Chemical analysis of the influent and effluent COD,  $NH_4^+$ ,  $NO_2^-$ ,  $NO_3^-$  and  $PO_4^{3-}$  concentrations was periodically performed. In addition, one cycle per week was thoroughly monitored. Soluble components were filtered with a  $0.22 \mu m$  filter (Millipore). COD was analysed using Lovibond kits (COD Vario Tube Test LR and COD Vario Tube Test MR) and the MD100 spectrophotometer (Lovibond). Soluble COD ( $COD_s$ ) was measured after the sample filtration while total COD ( $COD_T$ ) was not filtered.  $NH_4^+$  was measured with an ammonium analyser (AMTAXsc, Hach Lange). Phosphate was measured with an analyser based on the Vanadomolybdate yellow method (115 VAC PHOSPHAX sc, Hach-Lange).  $NO_2^-$  and  $NO_3^-$  were analysed with Ion Chromatography (DIONEX ICS-2000). Volatile suspended solids (VSS) and total suspended solids (TSS) were analysed following Standard Methods (APHA, 1995).

#### 4.2.4. GHG emissions and Emission Factor calculations

The  $N_2O$  gas concentration (in  $mg m^{-3}$ ) in the off-gas was calculated with Equation 4.1:

$$C_{N-N_2O} [\text{mg m}^{-3}] = \frac{C_{N-N_2O} [\text{ppmv}] \cdot P [1 \text{ atm}] \cdot MW_{N-N_2O} [28 \text{ g mol}^{-1}]}{R [0.082 \text{ atm L mol}^{-1} \text{ K}^{-1}] \cdot T [\text{K}]} \quad (\text{Eq. 4.1})$$

$C_{N-N_2O}$  [ppmv] and  $T$  [K] are the  $N_2O$  gas concentration and temperature, provided by the Horiba analyser,  $MW_{N-N_2O}$  is the  $N_2O$  molecular weight and  $R$  is the gas constant. The emission flowrate for  $N_2O$  was calculated with Equation 4.2:

$$N_2O \text{ emission rate } [\text{g d}^{-1}] = C_{N-N_2O} [\text{mg m}^{-3}] \cdot Q_{\text{gas}} [\text{m}^3 \text{ d}^{-1}] \cdot \left[ \frac{1 \text{ g}}{1000 \text{ mg}} \right] \quad (\text{Eq. 4.2})$$

Where  $Q_{\text{gas}}$  is the aeration flowrate, given by the data acquisition system of the pilot plant. Finally, the total  $N_2O$  emitted per cycle is calculated with Equation 4.3:

$$N_2O \text{ emitted } [\text{g}] = \sum_{i=1}^n (N_2O \text{ emission rate } [\text{g d}^{-1}] \cdot \Delta t [\text{d}])_i \quad (\text{Eq. 4.3})$$

Where  $\Delta t$  is the time interval for off-gas  $N_2O$  recording (1 minute) and  $n$  is the total number of data points recorded in the cycle.  $CH_4$  emission was analogously calculated using Equation 4.1 for  $CH_4$  concentration (in ppmv), using the  $CH_4$  molecular weight (16  $\text{g mol}^{-1}$ ).

Finally, the  $N_2O$  emission factor ( $N_2O$ -EF) of each cycle was calculated as the percentage of  $N_2O$ -N emitted during the cycle (in R2-AUT or R1-HET) of the total influent  $NH_4^+$ -N load (Equation 4.4). Similarly, The  $CH_4$  emission factor ( $CH_4$ -EF) was calculated as the percentage of influent COD emitted as  $CH_4$  (Equation 4.5).

$$N_2O\text{-EF } [\%] = \frac{N_2O \text{ emitted}}{NH_4^+ - N_{\text{infl}} \cdot VOL_{\text{infl}}} \cdot 100 \quad (\text{Eq. 4.4})$$

$$CH_4\text{-EF } [\%] = \frac{CH_4 \text{ emitted}}{COD_{\text{infl}} \cdot VOL_{\text{infl}}} \cdot 100 \quad (\text{Eq. 4.5})$$

Where  $NH_4^+ - N_{\text{infl}}$  and  $COD_{\text{infl}}$  are the ammoniacal nitrogen and COD influent concentrations, respectively, and  $VOL_{\text{infl}}$  is the influent volume (1.75  $\text{m}^3$ ). In the cycles where the emissions were measured in both R1-HET and R2-AUT, the total emission factor was calculated as the sum of the emission factor in each reactor.

### 4.3. Results

#### 4.3.1. Long term operation of the pilot plant

The SCEPPHAR pilot plant was operated during two years. The operation of the plant was divided into three periods (Larriba et al., 2020):

- Period I corresponded to the start-up of the pilot plant. During this period, operational changes were made to achieve the complete nitrification of  $NH_4^+$  and the EBPR. The start-up had a duration of three months.

- Period II (from day 0 to 225) corresponded to the operation under complete nitrification of ammonium to nitrate and high PAO activity. During this period, the main objective of the pilot plant was accomplished, i.e. meeting the effluent legal discharge limits. The second period had a duration of 225 days.
- Period III (from day 275 to 700) corresponded to the N removal via nitrite while maintaining good PAO activity and meeting the legal discharge limits. Some operational changes were made in this period to achieve short-cut N-removal via nitrite, optimize the plant operation, such as decrease of the cycle length from 12 to 8 hours or the implementation of different aeration strategies.

The results showed in this study belong to the lasts 300 days of operation of period III in which the pilot plant achieved N removal via nitrite and GHG emissions were monitored in selected cycles of the pilot plant.

#### 4.3.2. Process performance of the pilot plant

Figure 4.2 shows the influent and effluent profiles for  $\text{NH}_4^+$ ,  $\text{PO}_4^{3-}$  and COD and the effluent profiles for  $\text{NO}_2^-$  and  $\text{NO}_3^-$  of the pilot plant during the lasts 300 days of operation. The influent  $\text{NO}_2^-$  and  $\text{NO}_3^-$  values are shown in Table 1.  $\text{NH}_4^+$  removal was successful with an average effluent concentration of  $6.0 \pm 7.3 \text{ g NH}_4^+\text{-N m}^{-3}$ . EBPR performance was good during most of the time with an average effluent P of  $0.72 \pm 0.99 \text{ g PO}_4^{3-}\text{-P m}^{-3}$ . The effluent COD average concentration was  $70 \pm 68 \text{ g COD m}^{-3}$ . Effluent  $\text{NO}_2^-$ ,  $\text{NO}_3^-$  and total nitrogen (TN) averaged concentrations were  $3.2 \pm 2.0 \text{ g NO}_2^-\text{-N m}^{-3}$ ,  $0.6 \pm 0.7 \text{ g NO}_3^-\text{-N m}^{-3}$  and  $11.5 \pm 6.8 \text{ g N m}^{-3}$ , respectively. Therefore, the pilot plant was meeting the required discharge legal limits most of the time ( $\text{NH}_4^+ < 4 \text{ g NH}_4^+\text{-N m}^{-3}$ ,  $\text{P} < 1 \text{ g PO}_4^{3-}\text{-P m}^{-3}$ ,  $\text{COD} < 125 \text{ g COD m}^{-3}$  and  $\text{TN} < 10 \text{ g N m}^{-3}$  (EEC Council, 1991)). Furthermore, good removal efficiencies were obtained for TN, P and COD:  $67 \pm 23\%$ ,  $82 \pm 24\%$  and  $76 \pm 18\%$ , respectively. The averaged solids concentration in R1-HET and R2-AUT were similar:  $2.45 \pm 0.28$  and  $2.39 \pm 0.39 \text{ g VSS m}^{-3}$  for VSS in R1-HET and R2-AUT, respectively, and  $2.80 \pm 0.40$  and  $2.86 \pm 0.54 \text{ g TSS m}^{-3}$  for TSS in R1-HET and R2-AUT respectively.

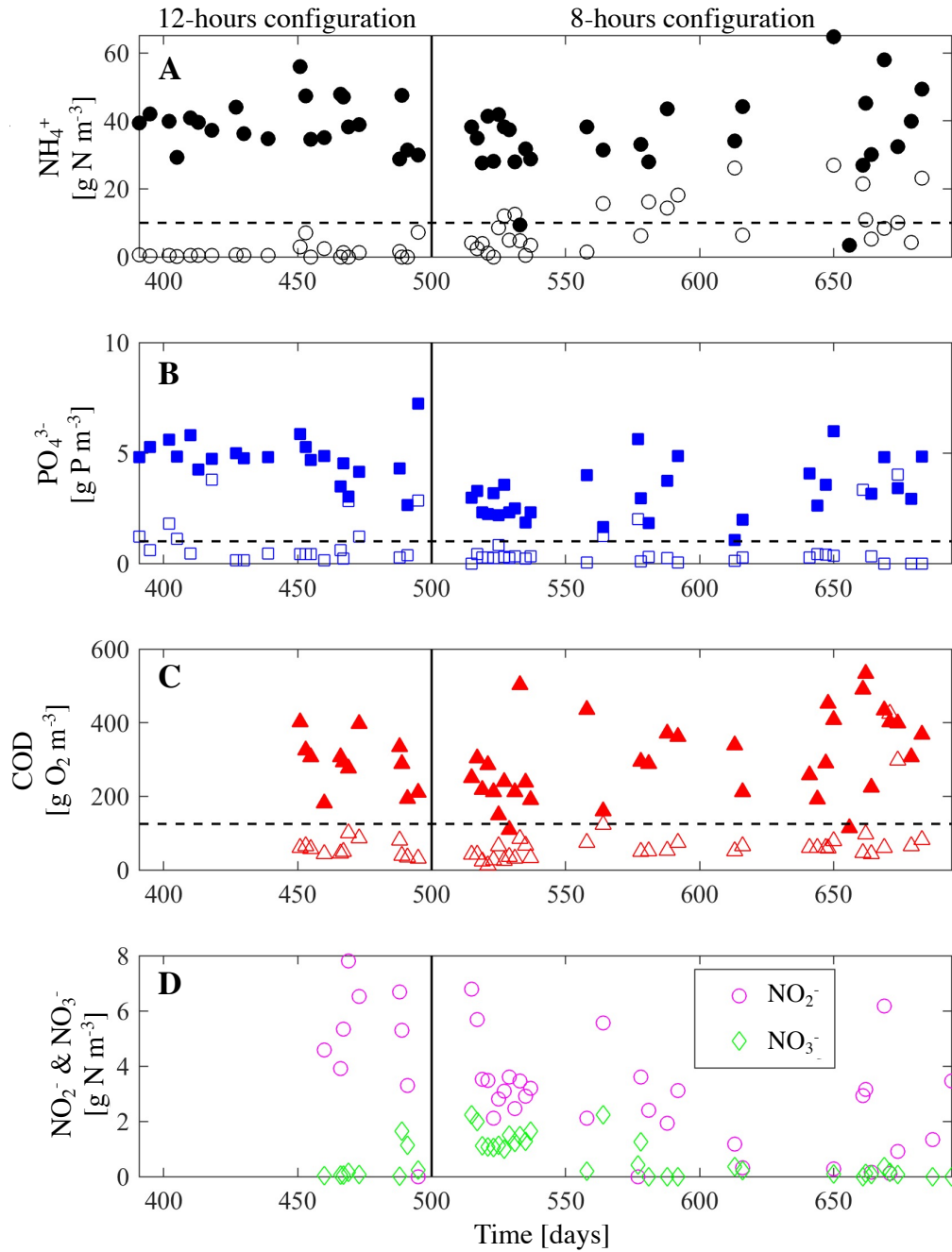


Figure 4.2. SCEPPHAR pilot plant influent and effluent profiles for ammonium (A), phosphate (B) and COD (C) and effluent profiles for nitrite and nitrate (D) during the studied period. Filled symbols represent influent concentration while void symbols represent effluent concentration. Dashed line represents discharge limit for TN (A), P (B) and COD (C).

The pilot plant removal efficiencies for TN, P and COD were maintained when the cycle was shortened to 8 hours (operational day 500, Figure 4.2), while the plant volumetric capacity increased by 50%.

The shortcut N-removal was achieved during the operational period III since the effluent concentration of  $\text{NO}_2^-$  was always higher than the  $\text{NO}_3^-$  concentration (Figure 4.2D). The shortcut N-removal was successfully achieved by applying two operational control strategies simultaneously, both aiming at reducing NOB activity while maintaining high AOB activity, as discussed in Larriba et al., (2020): i) the real-time control length of the aerobic phase in R2-AUT using the on-line  $\text{NH}_4^+$  measurement and ii) operating with a selected sludge retention time (SRT) to remove NOB while retaining AOB. The first strategy is based on stopping the aeration when  $\text{NH}_4^+$  is depleted. Then,  $\text{NO}_2^-$  should be accumulated due to the lack of oxygen and NOB growth would be limited (Guo et al., 2009; Marcelino et al., 2011). The second strategy relied in operating with a selected SRT to remove NOB faster than their growth rate (Jubany et al., 2009), Equation 4.6:

$$\mu_{\text{NOB,app}} < \text{SRT}^{-1} < \mu_{\text{AOB,app}} \quad (\text{Eq. 4.6})$$

Where  $\mu_{\text{NOB,app}}$  and  $\mu_{\text{AOB,app}}$  are the apparent growth rate of NOB and AOB, respectively, i.e. the apparent specific growth rate minus the apparent decay rate for each bacteria. The control of the aeration phase length in several simultaneous cycles in addition with the SRT control led to a gradually decrease of the NOB population and a subsequent increase on  $\text{NO}_2^-$  accumulation at the end of aerobic phases (Larriba et al., 2020).

Figure 4.3 shows an example of the SCEPPHAR cycle operation (day 410), when the pilot plant was operated under a 12-hour cycle configuration. Figure 4.4 shows all the monitored variables of the pilot plant for the same cycle. The influent composition for this cycle was 5.8 g P  $\text{m}^{-3}$  of  $\text{PO}_4^{3-}$  and 41.0 g N  $\text{m}^{-3}$  of  $\text{NH}_4^+$ .

The cycle started with the feeding of R1-HET (step 1 of R1-HET in Figure 4.1 and Table 4.2). The first measurement just after the feeding ended (time = 0.63 hours, Figure 4.4A) was 14.8 g P  $\text{m}^{-3}$  for  $\text{PO}_4^{3-}$ , showing that during the feeding some P was released by PAO. During the second step of R1-HET, the anaerobic phase, the  $\text{PO}_4^{3-}$  concentration increased up to 31.8 g P  $\text{m}^{-3}$  (Figure 4.3A) due to the P-release linked to VFA consumption by PAO. The ORP probe (Figure 4.4D) shows that anaerobic conditions were reached (ORP value below zero) after the feeding of the reactor was completed. The ORP probe signal stabilized at 3 hours of the cycle while complete anaerobic conditions were maintained. When the anaerobic phase ended (at time = 6 hours), part of the biomass was purged (step 3) and the supernatant of the reactor was settled (step 4). Then, the supernatant accounting for 70% of R1-HET volume was transferred to the interchange reactor R4-INT (step 5). The following step of R1-HET (step 6) was the filling of the reactor with the supernatants from R2-AUT (from the previous cycle) and R3-PRE. Then, the anoxic phase started (step 7). At the beginning of the anoxic phase, the  $\text{PO}_4^{3-}$  concentration (Figure 4.3A) decreased to 24.1 g P  $\text{m}^{-3}$  (compared to that the end of the aerobic phase of R2-AUT) due to: i) struvite precipitation decreased the P concentration of the supernatant of R3-PRE returned to R1-HET, ii) slightly decrease on the P concentration due to P-uptake in R2-



AUT (Figure 4.3B) and iii) decrease on P concentration during the filling process of R1-HET due to anoxic conditions. The  $\text{NH}_4^+$  concentration considerably decreased due to the dilution of R1-HET supernatant, since the  $\text{NH}_4^+$  concentration in the supernatant from R2-AUT returned to R1-HET was negligible. During the anoxic phase, the remaining  $\text{NO}_2^-$  was used by DPAO as the electron acceptor. In the presented cycle,  $\text{NO}_2^-$  concentration at the beginning of the anoxic phase was already negligible, meaning that all  $\text{NO}_2^-$  was denitrified during the anoxic filling period of R1-HET. Therefore, the observed P-uptake during the anoxic phase was low ( $2.0 \text{ g PO}_4^{3-}\text{-P m}^{-3}$ ). Soluble COD and  $\text{NH}_4^+$  remained constant during the anoxic phase. The next step of R1-HET reactor was the aerobic phase (step 8). This cycle operated at a DO set point (SP) of  $3 \text{ g O}_2 \text{ m}^{-3}$  with successful P-uptake, obtaining  $0.4 \text{ g PO}_4^{3-}\text{-P m}^{-3}$  at the end of the aerobic phase.  $\text{NH}_4^+$  was oxidised to  $0.5 \text{ g N m}^{-3}$  and  $\text{NO}_3^-$  was not observed in R1-HET.  $\text{NO}_2^-$  concentration at the end of aerobic phase was  $7.9 \text{ g NO}_2^-\text{-N m}^{-3}$  (Figure 4.3A). ORP probe signal sharply increased with the presence of oxygen as electron acceptor (Figure 4.4D). When the aerobic phase ended, aeration and stirring were turned off, supernatant was settled (step 9) and discharged to the effluent (step 10), fully accomplishing discharge limits.

In R2-AUT, the cycle started with the reactor filling with the supernatant of R1-HET (step 1 of R2-AUT in Figure 4.1). Once the reactor was filled, the second step was the purge of the reactor (step 2). The aerobic phase (step 3) started after an idle phase at 0.63 hours of the cycle. Temperature was constant during the aerobic phase (Figure 4.4C), with an average value of  $24.2 \text{ }^\circ\text{C}$ . The  $\text{DO}_{\text{SP}}$  for this cycle was  $3 \text{ g O}_2 \text{ m}^{-3}$ , as in R1-HET (Figure 4.4E). All the  $\text{NH}_4^+$  was oxidised to  $\text{NO}_2^-$  rather than to  $\text{NO}_3^-$ , showing that there was no NOB activity during this cycle. The  $\text{NH}_4^+$  online sensor showed a constant AOR during the aeration of the reactor, with a value of  $8.5 \text{ g NH}_4^+\text{-N m}^{-3} \text{ h}^{-1}$  ( $R^2=0.99$ ). The DO control system opened the aeration valve at the beginning of the aerobic phase (Figure 4.4F) to rapidly achieve the desired  $\text{DO}_{\text{SP}}$  and gradually closed it considering the decrease on the  $\text{NH}_4^+$ . In addition, the aerobic length control turned off the aeration after 2.4 hours of aerobic phase (maximum duration 3 hours), when the ion-selective  $\text{NH}_4^+$  probe signal was  $3 \text{ g NH}_4^+\text{-N m}^{-3}$ . pH slightly decreased due to nitritation (Figure 4.4B). The redox potential increased with the DO and the  $\text{NO}_2^-$  accumulation as electron acceptors (Figure 4.4D). Figure 4.3B reveals some P-removal in R2-AUT ( $4.9 \text{ g PO}_4^{3-}\text{-P m}^{-3}$ ), probably due to interchange of some biomass between reactors and the long idle period of R2-AUT, acting as a post anaerobic zone (Larriba et al., 2020; Wang et al., 2012). The rest of the R2-AUT steps were the settling and discharge to R1-HET (steps 4 and 5, respectively, Figure 4.1).

Finally, the R3-PRE reactor received  $0.15 \text{ m}^3$  of supernatant from R4-INT with high content of  $\text{PO}_4^{3-}$  and  $\text{NH}_4^+$ . P precipitation took place after the air sparging to increase pH and the addition of magnesium solution ( $19 \text{ g Mg}^{2+} \text{ m}^{-3}$  as  $\text{MgCl}_2$ ). Typically, P concentration decreased around 70% (Larriba et al., 2020) in R3-PRE. Finally, the

supernatant of R3-PRE, with low content in  $\text{PO}_4^{3-}$  and  $\text{NH}_4^+$  was sent to R1-HET (Figure 4.1).

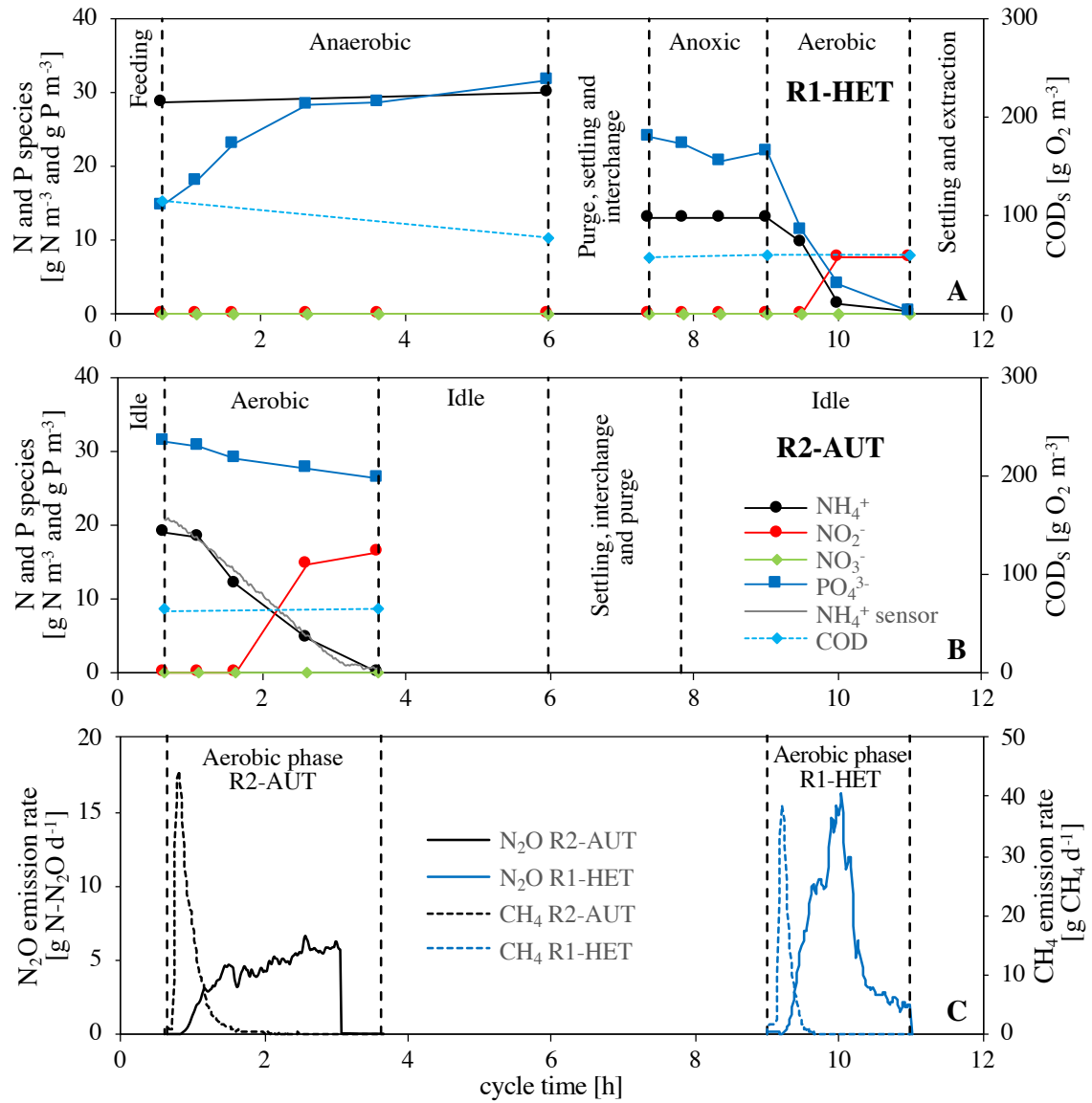


Figure 4.3. Example of SCEPPHAR cycle operation (A and B) and GHG profiles (C) obtained for R1-HET and R2-AUT with a cycle length configuration of 12 hours (cycle belonging to day 410 of operation).

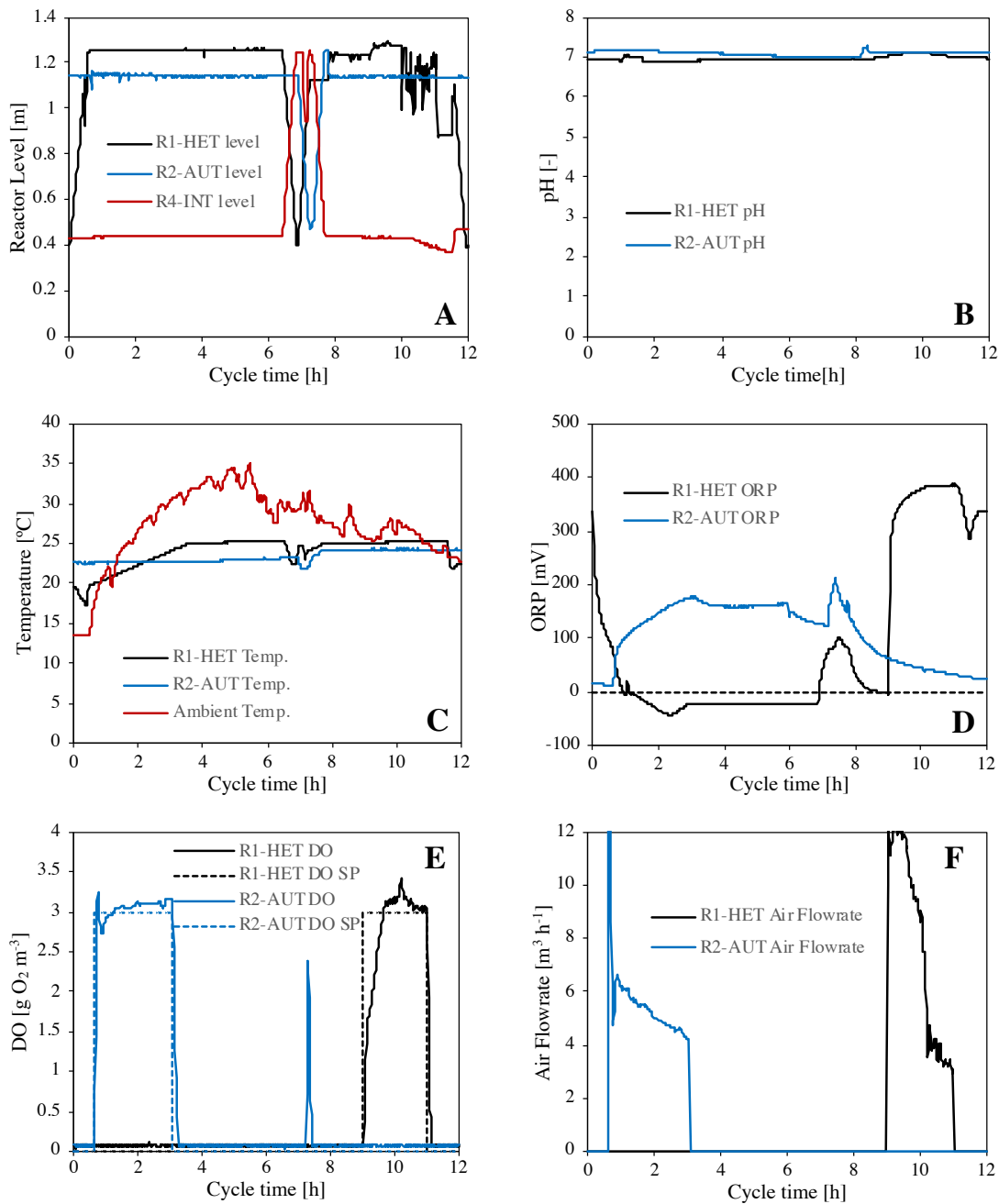


Figure 4.4. Online monitored variables for an example of SCEPPHAR cycle operation with a cycle length configuration of 12 hours (cycle belonging to day 410 of operation).

An example of a fully monitored SCEPPHAR cycle for an 8 hours cycle length configuration on day 557 is shown in Figure 4.5 and Figure 4.6. This cycle was operated at the same  $DO_{SP}$  of  $3 \text{ g O}_2 \text{ m}^{-3}$  (Figure 4.6E). The profiles obtained in Figure 4.5A show that the pilot plant was able to obtain a high effluent quality with reduced anaerobic and anoxic phases length in R1-HET and the observations were similar to those obtained on day 410 (Figure 4.3 and Figure 4.4). However, although  $\text{NH}_4^+$  concentration obtained at the end of aerobic phase of R2-AUT was below discharge limits ( $2.9 \text{ g NH}_4^+\text{-N m}^{-3}$ ), the AOR achieved ( $7.1 \text{ g NH}_4^+\text{-N m}^{-3} \text{ d}^{-1}$ ) was lower than that on day 410 and the aerobic

phase was extended to the maximum length value allowed (3 hours). This fact is probably due to VSS concentration being 14% lower in the 8-hours cycle period than in the 12-hours cycle period.

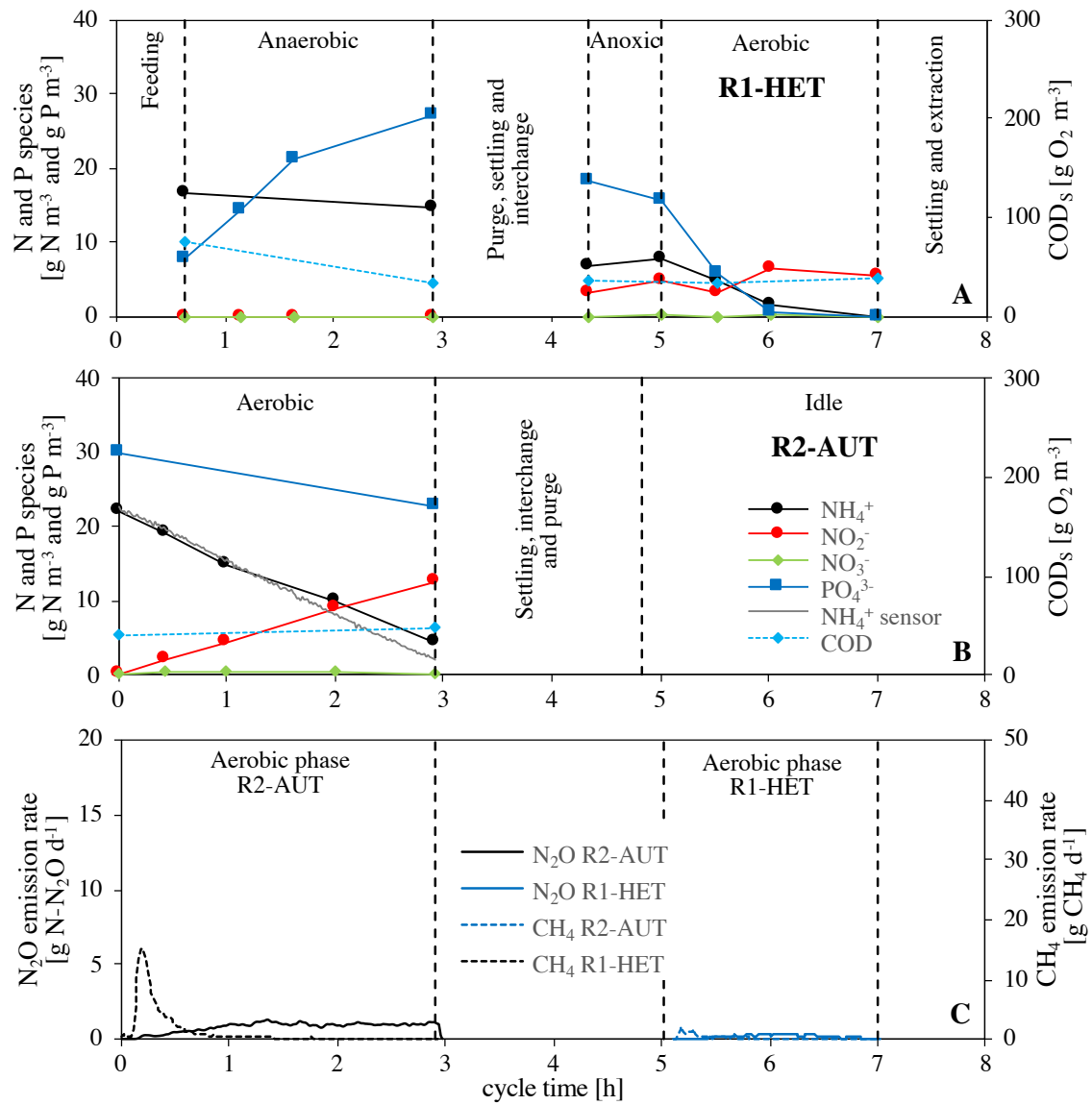


Figure 4.5. Example of SCEPPHAR cycle operation (A and B) and GHG profiles (C) obtained for R1-HET and R2-AUT with a cycle length configuration of 8 hours (cycle belonging to day 557 of operation).

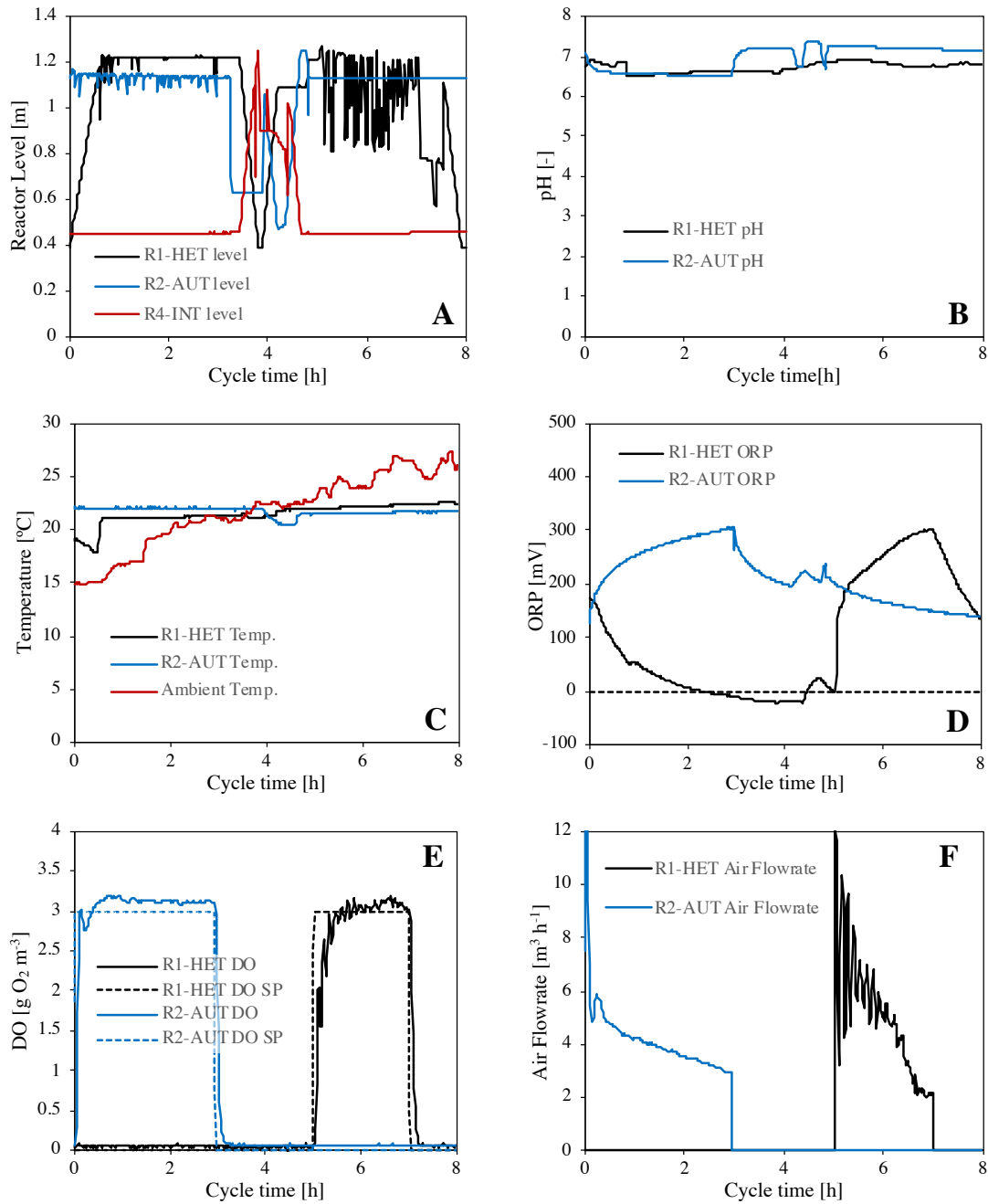


Figure 4.6. Online monitored variables for an example of SCEPPHAR cycle operation with a cycle length configuration of 8 hours (cycle belonging to day 557 of operation).

#### 4.3.3. Overall GHG emissions of the pilot plant

During part of period III,  $N_2O$  and  $CH_4$  emissions were monitored during the aerobic phases of the reactors. Table 4.3 shows the average  $N_2O$  and  $CH_4$  emitted per cycle and the corresponding emission factors (Equation 4.4 and Equation 4.5) obtained for the configurations of 8 and 12 hours. In addition, Figure 4.3C and Figure 4.5C show the  $N_2O$  and  $CH_4$  emission profiles for typical SCEPPHAR cycles of 12 and 8 hours length.

Table 4.3. Averaged N<sub>2</sub>O and CH<sub>4</sub> emissions and emissions factors measured for the cycle length configurations of 12 and 8 hours.

Cycle length	Reactor	N <sub>2</sub> O [g N <sub>2</sub> O-N]	N <sub>2</sub> O-EF [%]	CH <sub>4</sub> [g CH <sub>4</sub> ]	CH <sub>4</sub> -EF [%]
12 hours	R1-HET	0.19 ± 0.18	0.28 ± 0.26	0.25 ± 0.23	0.05 ± 0.04
	R2-AUT	0.44 ± 0.15	0.64 ± 0.22	0.57 ± 0.19	0.11 ± 0.04
	Total	0.64 ± 0.24	0.93 ± 0.34	0.82 ± 0.30	0.16 ± 0.06
8 hours	R1-HET	0.27 ± 0.23	0.39 ± 0.33	0.06 ± 0.03	0.01 ± 0.01
	R2-AUT	0.42 ± 0.37	0.61 ± 0.53	0.36 ± 0.34	0.07 ± 0.06
	Total	0.69 ± 0.43	1.00 ± 0.62	0.42 ± 0.34	0.08 ± 0.06

The GHG emissions were monitored for a total of 43 cycles with 12-hour configuration and 18 cycles for the 8-hour configuration. The cycles in Table 4.3 were those with the usual operation at a DO<sub>SP</sub> of 3 g O<sub>2</sub> m<sup>-3</sup>. Overall, the N<sub>2</sub>O emissions in R2-AUT were higher than those in R1-HET because most of the NH<sub>4</sub><sup>+</sup> was nitrified in R2-AUT (Table 4.3). Low N<sub>2</sub>O emissions (around 0.7 g N<sub>2</sub>O-N per cycle) and N<sub>2</sub>O-EF (around 1.0%) were obtained for both cycle length configurations, showing the capacity of the SCEPPHAR configuration to maintain low emissions in spite of NO<sub>2</sub><sup>-</sup> being accumulated in the reactors. The measured N<sub>2</sub>O emissions and N<sub>2</sub>O-EF were approximately the same operating at 12 and 8 hours since both configurations had the same aerobic phase length and the R2-AUT averaged temperatures were similar for both cycle lengths configurations (21.8 ± 2.6 °C for 8-hour and 22.3 ± 0.8 °C for 12-hour configuration). Figure 4.3C and Figure 4.5C show how N<sub>2</sub>O emissions began when the NH<sub>4</sub><sup>+</sup> was being nitrified and the emissions decreased to zero when both the aeration and the reactor mixing stopped.

Regarding the presented cycles, a total N<sub>2</sub>O emission of 0.87 g N<sub>2</sub>O-N was measured in the typical 12 hours cycle (Figure 4.3), resulting in an N<sub>2</sub>O-EF of 1.3%, while in the 8 hours example cycle (Figure 4.5) it was very low: 0.16% (0.11 g N<sub>2</sub>O-N emitted). The factors affecting these N<sub>2</sub>O emissions are further examined in section 4.3.4, where the different DO control strategies implemented are reported.

Regarding CH<sub>4</sub> emissions, lower variability on the emissions were measured compared to N<sub>2</sub>O emissions, since the aeration strategy has no effect on the CH<sub>4</sub> production. Table 3 shows that CH<sub>4</sub> emissions measured during the operation of the pilot plant were low, with less than 1.0 g CH<sub>4</sub> emitted per cycle and a CH<sub>4</sub>-EF lower than 0.20%. The CH<sub>4</sub> emissions were clearly higher in R2-AUT than in R1-HET and the emission rates showed a peak shape (Figure 4.3C and Figure 4.5C). On one hand, the CH<sub>4</sub> emission rate had an initial peak since CH<sub>4</sub> was not produced during aerobic conditions but the dissolved CH<sub>4</sub> was only stripped from the liquid phase to the gas phase. On the other hand, CH<sub>4</sub>

emissions were higher in R2-AUT compared to R1-HET due to the sequence of wastewater treatment in the SCEPPHAR configuration (Figure 4.1): the aerobic phase of R2-AUT is the first time that air is sparged to the wastewater. Therefore, the emitted  $\text{CH}_4$  in R2-AUT was probably introduced dissolved in the influent wastewater, while a slight amount might be produced during the anaerobic phase in R1-HET.  $\text{CH}_4$  can be produced either in the anaerobic environments of the sewer network, or be present in the reject water from the anaerobic digester (Guisasola et al., 2008; Gutierrez et al., 2014; Rodriguez-Caballero et al., 2014). Therefore, the existing lower  $\text{CH}_4$  emissions in R1-HET during the aerobic phase were due to the 30% of reactor volume that was not interchanged. Table 3 also reveals that the averaged  $\text{CH}_4$  emissions from the 12-hours configuration were 50% higher than those measured through the 8-hours configuration since, in the first case, the anaerobic phase was 55% longer. That supports the hypothesis that part of the  $\text{CH}_4$  emitted in R2-AUT could be produced during the anaerobic phase of R1-HET.

#### 4.3.4. Effect of the aeration strategy on the $\text{N}_2\text{O}$ emissions

This section shows the effect on  $\text{N}_2\text{O}$  emissions of the different aeration strategies implemented during the final operation of the SCEPPHAR pilot plant. During this period, some changes were made on the pilot plant cycle configuration: i) the cycle length was extended to 12 hours, ii) the aerobic phase length of the R2-AUT was incremented to 7.4 hours and iii) the aerobic phase length control through the  $\text{NH}_4^+$  ion selective probe was deactivated. These changes were made to allow a more detailed study of  $\text{N}_2\text{O}$  emissions during nitrification in R2-AUT. In addition, a liquid  $\text{N}_2\text{O}$  probe was installed in R2-AUT to monitor the  $\text{N}_2\text{O}$  concentration in the liquid phase in order to better understand the effect of the different aeration strategies on both  $\text{N}_2\text{O}$  production and emission.

The aeration strategies implemented are divided into: i) Different  $\text{DO}_{\text{SP}}$ , ii) intermittent aeration and iii) steps on the  $\text{DO}_{\text{SP}}$ . This section reports only the results related to R2-AUT reactor, where the soluble  $\text{N}_2\text{O}$  and the  $\text{N}_2\text{O}$  gas emission were measured. During these pilot plant experiments, the operation of R1-HET was the same as showed in Table 2 and the reactor was operated during the aerobic phase with a constant  $\text{DO}_{\text{SP}}$  of  $3 \text{ g O}_2 \text{ m}^{-3}$ .

##### 4.3.4.1. Different $\text{DO}_{\text{SP}}$

The first set of experiments was conducted to assess the effect of different  $\text{DO}_{\text{SP}}$  on the overall  $\text{N}_2\text{O}$  production and emission. The cycles were operated at three different  $\text{DO}_{\text{SP}}$ : 1, 2 and  $3 \text{ g O}_2 \text{ m}^{-3}$ . Figure 4.7 shows the profiles of DO, air flowrate,  $\text{N}_2\text{O}$  emission, soluble  $\text{N}_2\text{O}$  concentration and  $\text{NH}_4^+$  concentration for three particular cycles at a  $\text{DO}_{\text{SP}}$  of 1, 2 and  $3 \text{ g O}_2 \text{ m}^{-3}$ . Table 4.4 shows the obtained average  $\text{N}_2\text{O}$  emissions and  $\text{N}_2\text{O}$ -EF in R2-AUT for the different  $\text{DO}_{\text{SP}}$ .

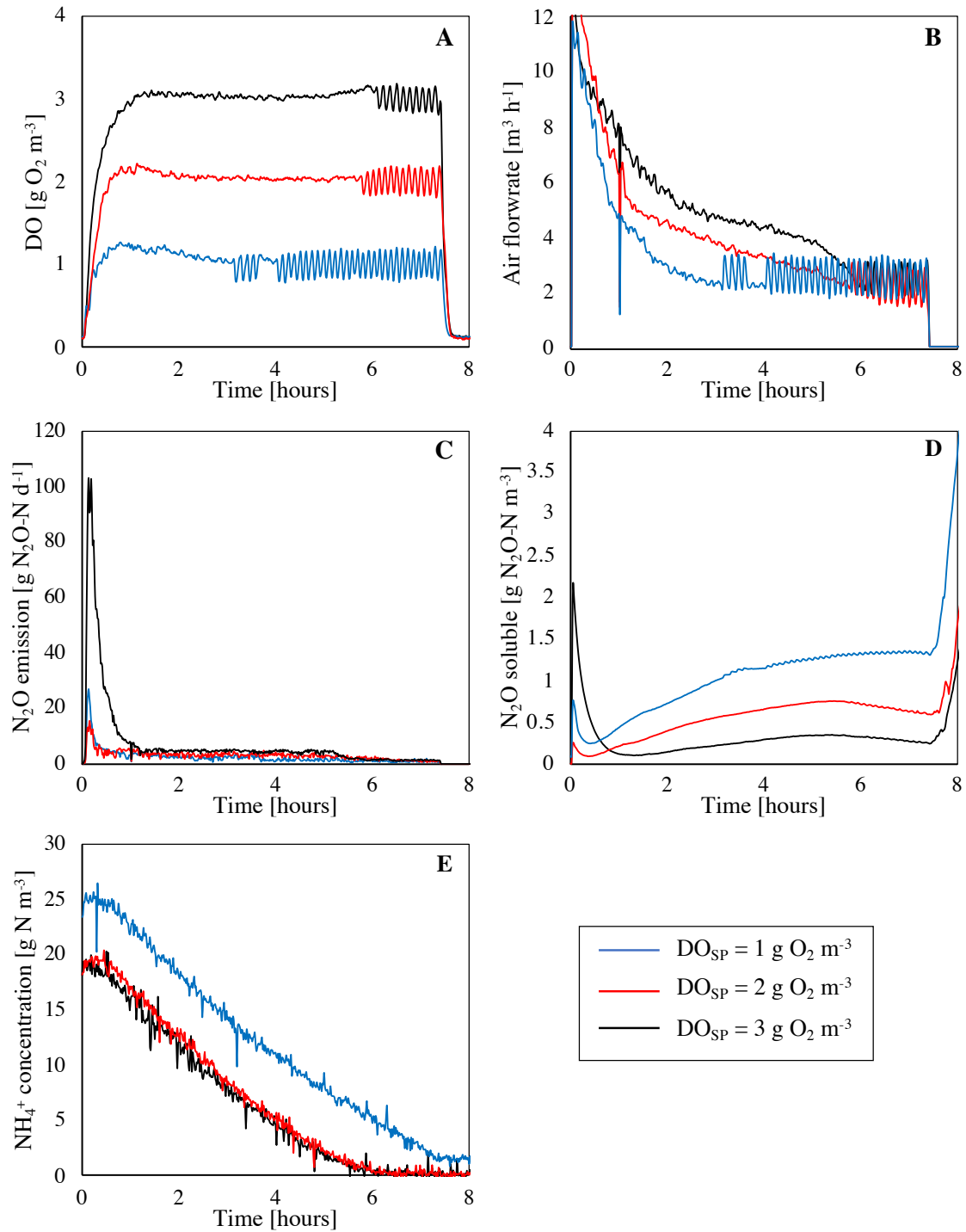


Figure 4.7. Selected monitored variables for three examples of SCEPPHAR operation with extended aeration phase length in R2-AUT using different DO set-points. (A) DO, (B) air flowrate, (C)  $\text{N}_2\text{O}$  emission rate, (D) soluble  $\text{N}_2\text{O}$  concentration and (E) ammonium online concentration.



Table 4.4. Averaged N<sub>2</sub>O emissions and N<sub>2</sub>O-EF measured in R2-AUT per cycle for different DO set-points. n represents the number of cycles operated at each DO set-point.

DO set-point	N <sub>2</sub> O emission [g N <sub>2</sub> O-N]	N <sub>2</sub> O-EF [%]
DO = 1 g O <sub>2</sub> m <sup>-3</sup> (n = 7 cycles)	0.34 ± 0.27	0.50 ± 0.39
DO = 2 g O <sub>2</sub> m <sup>-3</sup> (n = 6 cycles)	0.53 ± 0.30	0.76 ± 0.43
DO = 3 g O <sub>2</sub> m <sup>-3</sup> (n = 34 cycles)	0.43 ± 0.48	0.62 ± 0.70

Figure 4.7A shows that the DO in R2-AUT could be controlled properly at different DO<sub>SP</sub> and Figure 4.7E shows that full NH<sub>4</sub><sup>+</sup> oxidation was achieved regarding of the DO<sub>SP</sub>. The oscillations in DO concentration and air flowrate measured at the end of the aerobic phase (Figure 4.7A and Figure 4.7B) were due to the low linearity of the valve in the low range of actuation (valve opening below 25%), which makes it difficult for the PI controller to maintain a stable DO concentration. The AOR was very similar among the cycles: 3.48, 3.72 and 3.57 g N m<sup>-3</sup> h<sup>-1</sup> (R<sup>2</sup> > 0.98) for DO<sub>SP</sub> of 1, 2 and 3 g O<sub>2</sub> m<sup>-3</sup>, respectively, showing that the AOR was not dependent on DO in the range of values tested. Regarding N<sub>2</sub>O emissions, a different trend in N<sub>2</sub>O emission was observed in each cycle when compared to the examples of pilot plant cycles in Figure 4.3 and Figure 4.5. Figure 4.7C shows that a N<sub>2</sub>O emission peak was obtained for the three cycles at the beginning of the aerobic phase of R2-AUT regardless of the DO<sub>SP</sub>. Then, it decreased rapidly to lower constant emission rate until ammonium depletion. The emission peak accounts from 20% up to 60% of the total N<sub>2</sub>O emission measured per cycle for the cycles operated at 2 and 3 g O<sub>2</sub> m<sup>-3</sup> (Figure 4.7). The N<sub>2</sub>O peak emission was correlated to the N<sub>2</sub>O liquid concentration, since a peak on the N<sub>2</sub>O soluble concentration was also measured in the three cycles (Figure 4.7D) and, moreover, the higher the soluble N<sub>2</sub>O concentration, the higher the N<sub>2</sub>O emission peak. The independency from the DO<sub>SP</sub> on the peak emission rate is due to the aeration control system fully opened the air distribution valve at the beginning of the aerobic phase for the three DO<sub>SP</sub> (Figure 4.7B). Both gas and liquid N<sub>2</sub>O measurements (Figure 4.7C and Figure 4.7D) show that N<sub>2</sub>O was continuously produced during the pilot plant cycle, since soluble N<sub>2</sub>O was being accumulated and N<sub>2</sub>O was continuously emitted. High effect on the stripping of soluble N<sub>2</sub>O and the DO<sub>SP</sub> was found, since although the soluble N<sub>2</sub>O accumulation increased operating at lower DO<sub>SP</sub> (i.e. with lower aeration flowrate), the N<sub>2</sub>O emissions decreased due to the mass transfer coefficient decreased. However, the impact of the stripping effect was not relevant in these cycles since most of the N<sub>2</sub>O emission was found at the beginning of the aerobic phase during the emission peak, where the air flowrate was the same for the three DO<sub>SP</sub>. Finally, Figure 4.7D shows that the N<sub>2</sub>O liquid concentration decreased due to stripping to the gas phase when ammonium was depleted and NO<sub>2</sub><sup>-</sup> was accumulated for the cycles operated at 2 and 3 g O<sub>2</sub> m<sup>-3</sup>. Table 4.4 shows that no correlation was found between the

operating DO and the total N<sub>2</sub>O emissions during the pilot plant cycles operated at different DO<sub>SP</sub> due to the high variability observed on the N<sub>2</sub>O emissions even at the same DO<sub>SP</sub>: the average N<sub>2</sub>O emissions from the cycles operated at DO of 2 g O<sub>2</sub> m<sup>-3</sup> were higher than those obtained operating at a DO of 1 g O<sub>2</sub> m<sup>-3</sup> and lower than those obtained at 3 g O<sub>2</sub> m<sup>-3</sup>. In addition, the variability found in N<sub>2</sub>O emissions for the cycles operating at the same DO<sub>SP</sub> was similar to that calculated for the cycles operated at different DO<sub>SP</sub>. Therefore, in our case, the DO concentration seems to have no effect on the N<sub>2</sub>O emissions of the pilot plant, probably because the same AOR was achieved at different DO concentrations.

#### 4.3.4.2. Intermittent aeration

The second set of experiments was conducted to assess the effect of intermittent aeration on the overall N<sub>2</sub>O production and emission. The intermittent aeration was implemented as an on/off controller where the reactor was aerated at a constant air flowrate and aeration was stopped when the DO measurement increased above 2 g O<sub>2</sub> m<sup>-3</sup> and was turned on again for DO below 1 g O<sub>2</sub> m<sup>-3</sup>. This on/off control was maintained throughout the aerobic phase of R2-AUT. The pilot plant was operated with on/off aeration control under two different air flowrates: 12.5 and 5.0 m<sup>3</sup> h<sup>-1</sup> (100 and 40% of the maximum air flowrate, respectively). Figure 4.8 shows the profiles of DO, air flowrate, N<sub>2</sub>O emission, N<sub>2</sub>O liquid concentration and NH<sub>4</sub><sup>+</sup> concentration for two example cycles with on/off control.

Figure 4.8A shows the variability of the DO concentration for both implemented air flowrates through intermittent aeration. The DO ranged between 0.6 and 2.8 g O<sub>2</sub> m<sup>-3</sup> for the high air flowrate and between 0.6 and 2.0 g O<sub>2</sub> m<sup>-3</sup> when the pilot plant was operated at 40% of the maximum air flowrate and NH<sub>4</sub><sup>+</sup> was not depleted. DO values outside the range 1-2 g O<sub>2</sub> m<sup>-3</sup> were due to the dynamics of the DO sensor and the control valve, even though the on/off controller was sending the command to close the aeration when the measured DO was 2 g O<sub>2</sub> m<sup>-3</sup> and was sending the command to open it when DO was 1 g O<sub>2</sub> m<sup>-3</sup>. The DO concentration at high airflow rate achieved 2 g O<sub>2</sub> m<sup>-3</sup> at 10 minutes of aerobic phase, while it lasted 2 hours in the experiment operated with the low air flowrate of 5 m<sup>3</sup> h<sup>-1</sup> (Figure 4.8B). The duration of the on phases decreased in time for both air flowrates meanwhile the NH<sub>4</sub><sup>+</sup> concentration decreased due to the lower oxygen uptake rate. The same NH<sub>4</sub><sup>+</sup> concentration was measured for both cycles at the beginning of the aerobic phase and both cycles achieved full ammonia oxidation to nitrite. The same AOR was achieved for both cycles (2.70 g N m<sup>-3</sup> h<sup>-1</sup>, R<sup>2</sup> = 0.99), showing that the AOR was not significantly different although the average DO levels were slightly different (1.4 vs 1.8 g O<sub>2</sub> m<sup>-3</sup> for low and high flowrate). The same fact was observed in results of section 4.3.4.1. The NH<sub>4</sub><sup>+</sup> concentration decreased linearly over the time, without any strong variation in the AOR due to the on/off aeration cycles.

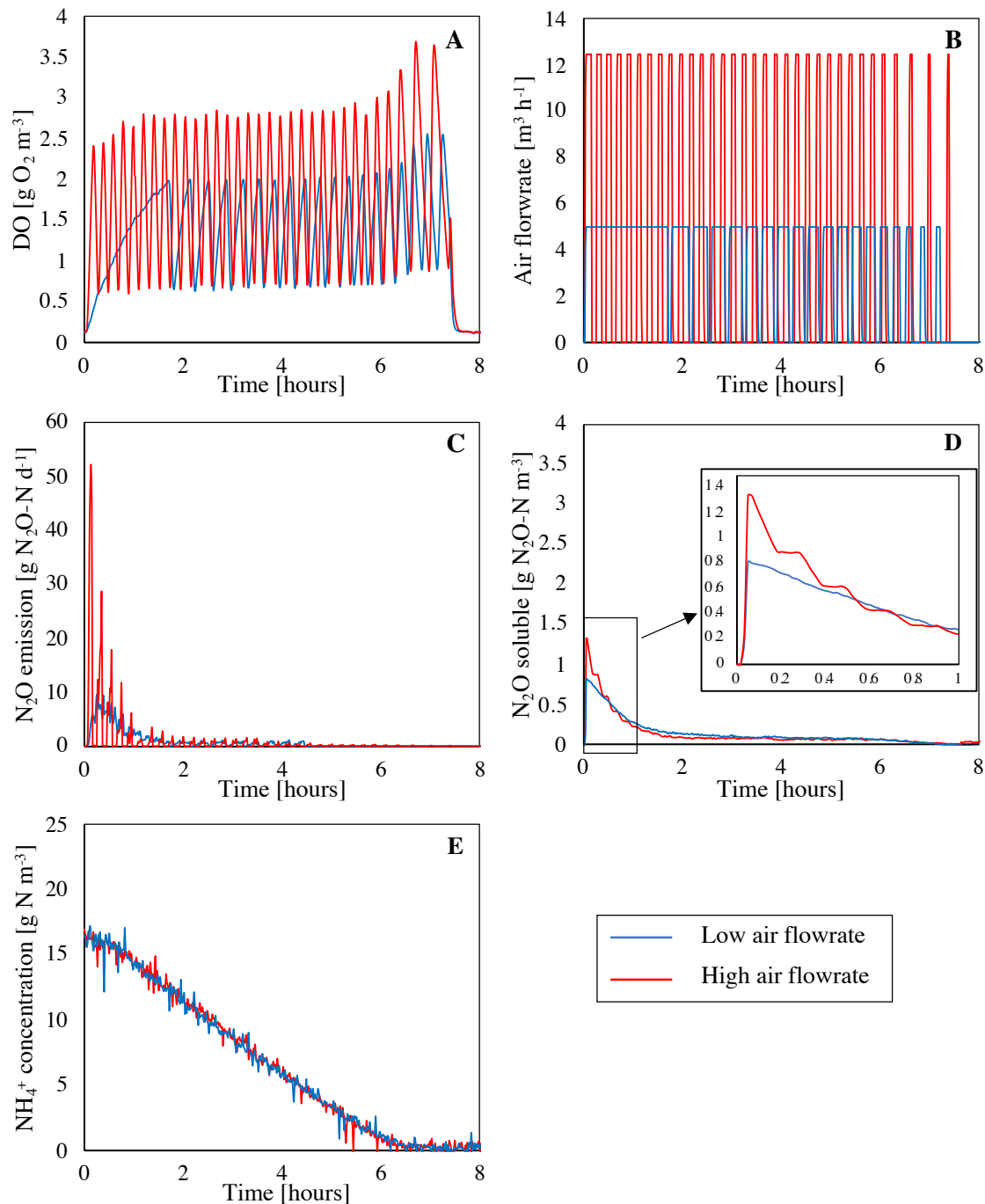


Figure 4.8. Selected monitored variables for two examples of SCEPPHAR operation with extended aeration phase length in R2-AUT and using on/off aeration control at 5.0 and 12.5 m<sup>3</sup> h<sup>-1</sup> of air flowrate. (A) DO, (B) air flowrate, (C) N<sub>2</sub>O emission rate, (D) soluble N<sub>2</sub>O concentration and (E) ammonium online concentration.

Regarding the N<sub>2</sub>O results, a peak of soluble N<sub>2</sub>O was measured in the reactor at the beginning of the aerobic phase for both cycles (Figure 4.8D), as in the cycles operated at different DO<sub>SP</sub> (Figure 4.7, section 4.3.4.1). This peak of soluble N<sub>2</sub>O caused a N<sub>2</sub>O emission peak at the beginning of the aerobic phase (Figure 4.8C), however, the off phases caused the emission to decrease to negligible levels in the high air flowrate

scenario since stripping was suppressed. This behaviour was not observed in the cycle operated at low air flowrate because the emission peak finished before the first off phase. The liquid  $N_2O$  measurements shows that there was no accumulation of  $N_2O$  in the liquid phase during all the aerobic phase for both cycles. The net  $N_2O$  production seemed null since: i) the soluble  $N_2O$  concentration decreased constantly once the initial peak was stripped to the gas phase, and ii) the  $N_2O$  liquid concentration remained constant during the initial peak during the off phase of the cycle operated with the high air flowrate (zoom of Figure 4.8D). Therefore, it is possible that simultaneous nitrification-denitrification was taking place and  $N_2O$  was simultaneously produced and consumed. The R2-AUT  $N_2O$ -EF measured for the cycles operated at  $12.5$  and  $5.0 \text{ m}^3 \text{ h}^{-1}$  were  $0.40$  and  $0.48\%$ , respectively (Figure 4.8). However no correlation was found between the air flowrate and the emitted  $N_2O$ . The averaged R2-AUT  $N_2O$ -EF of all the cycles operated with intermittent aeration strategy (21 cycles) was  $0.40 \pm 0.21\%$ .

#### 4.3.4.3. Steps on the $DO_{SP}$

Finally, the last set of experiments was carried out to assess the effect of varying the  $DO_{SP}$  during the same aerobic phase of R2-AUT on the  $N_2O$  stripping and emissions. Two experiments were conducted: in the first one, the  $DO_{SP}$  was increased every two hours in a stepwise manner, testing values of  $1$ ,  $2$  and  $3 \text{ g O}_2 \text{ m}^{-3}$ . In the second experiment, the same strategy was applied but with values of  $3$ ,  $2$  and  $1 \text{ g O}_2 \text{ m}^{-3}$ . The third step of both experiments lasted until the end of the aerobic phase (3.4 hours). Figure 4.9 shows the profiles of DO, air flowrate,  $N_2O$  emission, soluble  $N_2O$  concentration and  $NH_4^+$  for both experiments.

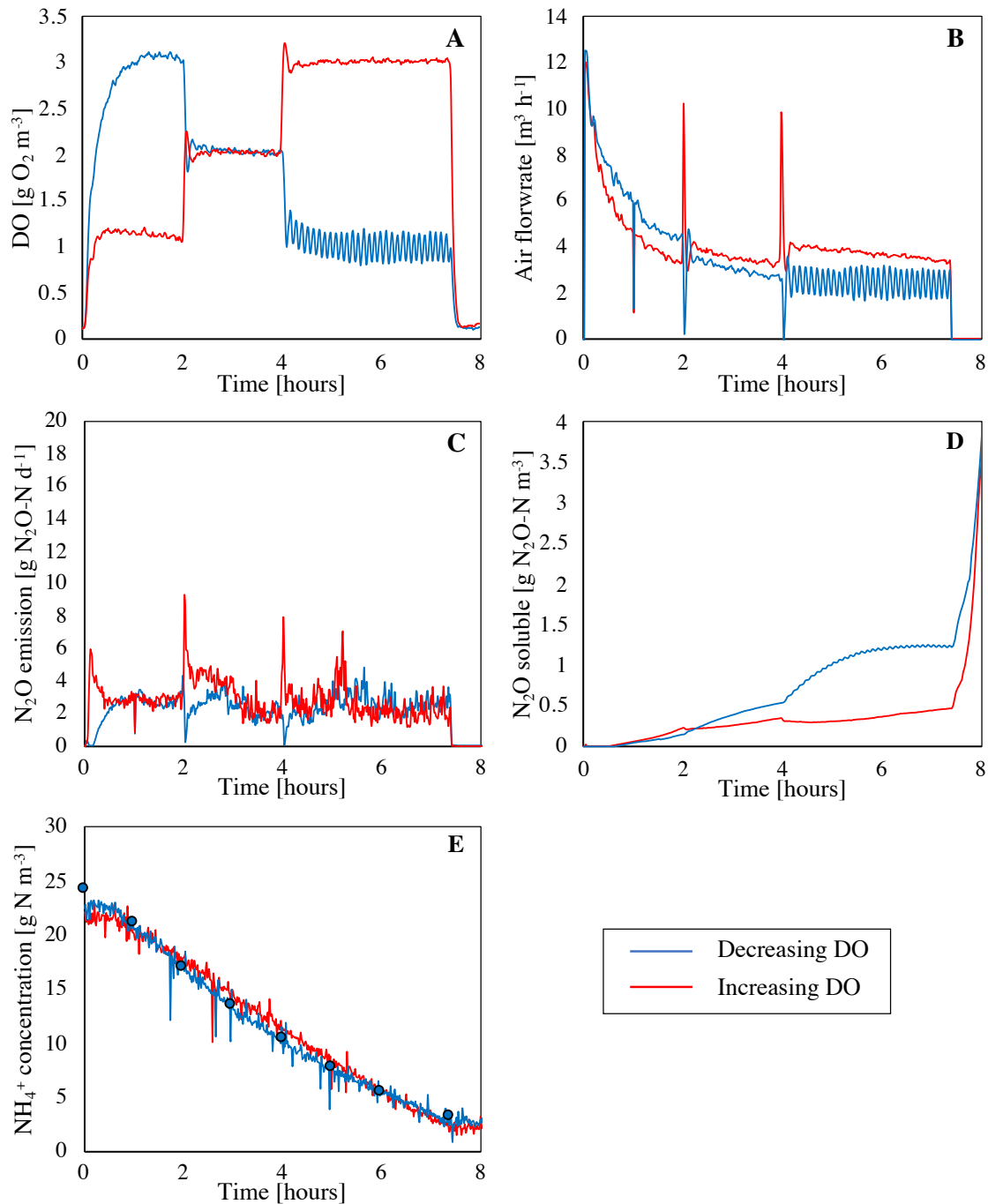


Figure 4.9. Selected monitored variables for two examples of SCEPPHAR operation with extended aeration phase length in R2-AUT and different DO setpoints for the PI controller during the cycle. (A) DO, (B) air flowrate, (C) N<sub>2</sub>O emission rate, (D) soluble N<sub>2</sub>O concentration and (E) ammonium online concentration.

Figure 4.9 shows that the DO PI control loop reacted fast to setpoint changes, modifying the aeration to reach effectively the new setpoint. On the first experiment, the aeration control system opened the valve up to 90% for short periods in order to reach the increased setpoints. On the second experiment, the aeration control system closed the air control valve down to 10% (and even fully closed) after decreasing the setpoint. Similar

$\text{NH}_4^+$  concentrations were measured for both experiments at the beginning of the aerobic phase. Surprisingly, while the AOR of the increasing DO experiment remained constant among the DO steps ( $3.02 \text{ g NH}_4^+\text{-N m}^{-3} \text{ h}^{-1}$ ,  $R^2 = 0.98$ ), the AOR of the decreasing experiment decreased from 3.9 ( $R^2=0.80$ ) to 3.3 ( $R^2=0.90$ ), and  $2.3 \text{ g NH}_4^+\text{-N m}^{-3} \text{ h}^{-1}$  ( $R^2=0.83$ ) in parallel with the new  $\text{DO}_{\text{SP}}$  of 3, 2 and  $1 \text{ g O}_2 \text{ m}^{-3}$ , respectively (Figure 4.9E). Interestingly, neither an initial peak of soluble  $\text{N}_2\text{O}$  nor  $\text{N}_2\text{O}$  emission was measured in any of the DO step experiment, in contrast with other experiments. Both the emission and soluble  $\text{N}_2\text{O}$  profiles seemed to have a strong dependency on the air flowrate applied to R2-AUT. On the one hand, the sudden opening of the air valve linked to a  $\text{DO}_{\text{SP}}$  increase caused also a sudden increase on the  $\text{N}_2\text{O}$  emissions, which decreased after the DO reached the desired setpoint. These emissions led to a decrease in the soluble  $\text{N}_2\text{O}$  concentration. On the other hand, in the second experiment, the  $\text{N}_2\text{O}$  emissions decreased and the soluble  $\text{N}_2\text{O}$  concentration increased every time the  $\text{DO}_{\text{SP}}$  was decreased as the air control valve was closing. Finally,  $\text{N}_2\text{O}$  was continuously produced in both experiments since the accumulation of soluble  $\text{N}_2\text{O}$  increased in both experiments and a constant  $\text{N}_2\text{O}$  emission was measured. The accumulation of soluble  $\text{N}_2\text{O}$  seemed to be correlated with the air flowrate, since the soluble  $\text{N}_2\text{O}$  accumulation increased in every  $\text{DO}_{\text{SP}}$  change in the second experiment: decreasing the air flowrate caused a decrease of  $\text{N}_2\text{O}$  stripping. The  $\text{N}_2\text{O}$ -EF measured in these tests was higher (1.3% when DO was increased and 1.1% when DO was decreased) than that achieved through intermittent aeration, because even though no initial  $\text{N}_2\text{O}$  emission peak was measured,  $\text{N}_2\text{O}$  was continuously produced during the cycles.

#### 4.4. Overall assessment of GHG emissions

##### 4.4.1. Comparison of GHG emissions with other WRRFs

During the last years, several monitoring campaigns to quantify  $\text{N}_2\text{O}$  emissions have been conducted at different full-scale WWTPs. The main objective of the monitoring campaigns was to quantify the  $\text{N}_2\text{O}$  emissions and later to determine the factors affecting these emissions (Ahn et al., 2010; Daelman et al., 2013; Kampschreur et al., 2009b; Law et al., 2012b; Massara et al., 2017). These studies have shown huge variations in the  $\text{N}_2\text{O}$  emissions in WWTPs even under similar conditions, demonstrating that it was very difficult to find a clear trend. The emission factor range for  $\text{N}_2\text{O}$  remained between 0 and 2.5% of the influent N load for most of the municipal full-scale WWTPs (Ribera-Guardia et al., 2019), but  $\text{N}_2\text{O}$ -EF up to 25% was found (Law et al., 2012b). This high variation on the  $\text{N}_2\text{O}$ -EF has been attributed to the different configurations and operational conditions in each WWTP, as well as to the inherent dynamic conditions of the plants, but probably some unknown factors are still to be discovered. Therefore, it was difficult to assess the real causes of the high  $\text{N}_2\text{O}$ -EF variations and, thus, it was difficult to design and implement novel mitigation strategies for the plant.

This study reported the long-term operation and monitoring of the mainstream SCEPPHAR configuration in a pilot scale treating real municipal wastewater. The fact that the pilot plant operated within shortcut N-removal was a priori unattractive in terms of N<sub>2</sub>O emissions, since the accumulation of NO<sub>2</sub><sup>-</sup> is a major cause of N<sub>2</sub>O emissions. However, the average N<sub>2</sub>O-EF calculated during the long-term operation of the pilot plant was  $0.97 \pm 0.70\%$ , which is in the same range for most of municipal WWTPs. This shows the capability of the mainstream SCEPPHAR configuration to obtain a high effluent quality index while reducing aeration costs and COD requirements without increasing N<sub>2</sub>O emissions with respect to conventional nitrification/denitrification.

Regarding CH<sub>4</sub> emissions, the range in municipal WWTPs is typically from 0.02 to 1.13% of the inlet COD (Daelman et al., 2013; Ribera-Guardia et al., 2019; Rodriguez-Caballero et al., 2014). The average CH<sub>4</sub>-EF measured in this study was  $0.12 \pm 0.08\%$  which is in the lower band of the values reported. The sources of CH<sub>4</sub> emissions are mainly attributed to the dissolved CH<sub>4</sub> that contains both the influent wastewater, originated in the sewer network (Guisasola et al., 2008), and the reject water coming from the anaerobic digester (Daelman et al., 2013; Rodriguez-Caballero et al., 2014). Regarding the possible production of CH<sub>4</sub> during the anaerobic phase of R1-HET, textbook knowledge states that methanogenesis is favoured under mesophilic conditions (T around 37 °C), strict anaerobic conditions and non-limiting acetate concentration for acetoclastic methanogens. However, it was experimentally observed that CH<sub>4</sub> emissions decreased by 50% when the anaerobic phase was shortened by 55% suggesting that a non-negligible amount of the emitted CH<sub>4</sub> was produced during the anaerobic phase of the R1-HET cycle. The presence of methanogens in the planktonic biomass can probably be discarded, as this sludge undergoes aerobic conditions during part of the cycle, while methanogens are strictly anaerobic. However, the presence of some methanogens in the possible biofilm of the reactor walls and in the sediments that can accumulated at the bottom of the reactor could explain this slight methane production. The CH<sub>4</sub> present at the end of the anaerobic phase is stripped/emitted during the posterior aerobic phase.

#### 4.4.2. Factors affecting N<sub>2</sub>O emissions

N<sub>2</sub>O emissions occurred throughout all the long-term operation. High variability was detected not only due to the applied operational changes but also when operating the plant under the same operational conditions. The DO<sub>SP</sub> in R2-AUT did not seem to have any effect on the overall N<sub>2</sub>O emissions, since no correlation was found between the DO concentration in R2-AUT and the measured emissions during the operation at different DO<sub>SP</sub> between 1 and 3 g O<sub>2</sub> m<sup>-3</sup> (Figure 4.7 and Table 4.4). This fact is in disagreement with previous experimental reports where a decrease in the DO level led to an increase of the N<sub>2</sub>O emissions (Massara et al., 2017; Peng et al., 2015). A possible explanation that the N<sub>2</sub>O emissions measured in this study did not present a correlation with DO at the

range of DO setpoints implemented is that the lowest  $DO_{SP}$  implemented was  $1 \text{ g O}_2 \text{ m}^{-3}$ , which probably was not low enough to trigger the increase of  $\text{N}_2\text{O}$  production. In this sense, Peng et al., (2015) measured the highest  $\text{N}_2\text{O}$  emissions among different  $\text{NO}_2^-$  accumulations at  $0.35$  and  $0.85 \text{ g O}_2 \text{ m}^{-3}$  through a range of applied DOs from  $0.35$  to  $3.5 \text{ g O}_2 \text{ m}^{-3}$ .

Another interesting observation was that the AOR was neither dependent on the DO concentration, as the same apparent AOR was found during the implementation of different  $DO_{SP}$  during nitrification in R2-AUT. However, the AOR changed during the long-term operation of the pilot plant under different conditions, showing a high variability from  $8.5$  to  $2.3 \text{ g N m}^{-3} \text{ h}^{-1}$ . Therefore, the change on the apparent AOR could be attributed to a decrease in the biomass concentration or to changes in the AOB microbial community. The effect of temperature on AOR was not assessed, since all the presented cycles were operated at a similar temperature. Only in the cycle operating in a decreasing  $DO_{SP}$  step-wise manner (Figure 4.9), the AOR was found to decrease with the decrease of the  $DO_{SP}$ , although it could also be related to the decrease in ammonium concentration along the cycle.

Another issue regarding the high variability of the  $\text{N}_2\text{O}$  emissions was the detected  $\text{N}_2\text{O}$  emission peak at the beginning of the aerobic phase in R2-AUT, that can represent up to the 60% of the total  $\text{N}_2\text{O}$  emitted per cycle. Yu et al., (2010) studied the  $\text{NO}$  and  $\text{N}_2\text{O}$  emissions in a pure culture of AOB and found high  $\text{N}_2\text{O}$  production linked to transient conditions (from anoxic conditions to aerobic conditions) when  $\text{NH}_4^+$  had been accumulated. They concluded that the  $\text{N}_2\text{O}$  production by nitrifying biomass under transient conditions was attributed to a shift in metabolism from low specific activity towards the maximum specific activity (Yu et al., 2010). Therefore, the measured  $\text{N}_2\text{O}$  emission peak at the beginning of the aerobic conditions might be linked to transient conditions, since the aerobic phase of R2-AUT begins after the filling of the reactor with the supernatant of R1-HET reactor, with high  $\text{NH}_4^+$  concentration. This peak was not measured in all the cycles and, therefore, it seems to have a dependency on the conditions of the nitrifying biomass before the aerobic phase. Others works have also found an effect of the transient conditions on the  $\text{N}_2\text{O}$  emissions in full-scale WWTPs (Ahn et al., 2010; Ribera-Guardia et al., 2019).

When describing the influence of the  $DO_{SP}$  on  $\text{N}_2\text{O}$  emissions, it should be noted that a higher  $DO_{SP}$  needs a higher airflow rate in the reactor. The average air flowrate increased from  $3.35 \text{ m}^3 \text{ h}^{-1}$  ( $DO_{SP} = 1$ ) to  $4.08 \text{ m}^3 \text{ h}^{-1}$  ( $DO_{SP} = 2$ ) and  $4.78 \text{ m}^3 \text{ h}^{-1}$  ( $DO_{SP} = 3$ ) i.e. 22% and 43% higher for 2 and 3 with respect to 1. This aeration flowrate increase favours  $\text{N}_2\text{O}$  stripping and may, at least in a short-term, increase  $\text{N}_2\text{O}$  emissions. The operation of the pilot plant through different  $DO_{SP}$ s in R2-AUT revealed the effect of the stripping between liquid and gas phases on the  $\text{N}_2\text{O}$  liquid accumulation and the  $\text{N}_2\text{O}$  measured



emission. Figure 4.7 shows that when the pilot plant was operated at a low DO (i.e. with low aeration flowrate), the accumulation of  $N_2O$  in the liquid increased. This increase could be attributed to the negative effect that decreasing the DO has on  $N_2O$  production through the nitrifier denitrification pathway (Massara et al., 2018, 2017; Peng et al., 2015) or to a decrease in the transfer rate between liquid and gas phase (i.e. the  $N_2O$  mass transfer coefficient decreased due to a decrease in the air flowrate). Hence, although the  $N_2O$  production seems to increase when operating at lower DO, the mass transfer between phases decreases. The accumulated  $N_2O$  at the end of the aerobic phase of R2-AUT does not have a negative effect on the overall  $N_2O$  emissions of the cycle since, once the aerobic phase of R2-AUT is finished, the supernatant of the reactor is sent to R1-HET to perform the anoxic phase, where  $N_2O$  is reduced to  $N_2$ . Therefore, a possible mitigation strategy is to operate at a low DO (down to  $1 \text{ g O}_2 \text{ m}^{-3}$ ), because less  $N_2O$  is emitted due to limited mass transfer rate between phases and the increased accumulation of  $N_2O$  will be subsequently denitrified in R1-HET, and not emitted.

Finally, the aeration strategy implemented that emitted less  $N_2O$  was operating the plant through intermittent aeration. The results of the intermittent aeration showed a decrease of 40% on the  $N_2O$ -EF of R2-AUT compared to normal operation of the pilot plant ( $0.40 \pm 0.21\%$  vs.  $0.64 \pm 0.22\%$ ). A possible explanation is that simultaneous nitrification and denitrification occurred during the off cycles of the aeration since the denitrifying bacteria can denitrify even in a micro-aerobic environments (Massara et al., 2017). Therefore, the non-observed net  $N_2O$  production during the off cycles of initial peak emission, attributed to transient conditions, measured during the implementation of intermittent aeration could be explained by simultaneous nitrification and denitrification occurring in the reactor. Rodriguez-Caballero et al., (2015) also proposed a cycle configuration with intermittent aeration to mitigate the  $N_2O$  emissions from a full-scale SBR treating municipal wastewater.

#### 4.5. Conclusions

This study assesses the plant performance and the GHG emissions of the mainstream SCEPPHAR novel WRRF configuration at pilot scale under real environmental conditions and discusses the effect of different aeration strategies on the  $N_2O$  production and emissions. The main findings are:

- Successful removal efficiencies of C, N and P were achieved for a long-term in the pilot plant under shortcut N-removal operation at 8-hours and 12-hours configuration.
- GHG emissions ( $N_2O$  and  $CH_4$ ) showed high variability.
- Calculated emissions factor for  $N_2O$  and  $CH_4$  were in the low range of typical emission factors measured in conventional full-scale WWTPs, even with high nitrite accumulation, which a priori was unattractive in terms of  $N_2O$  emissions.

- Operating the R2-AUT of the pilot plant at different  $DO_{SPS}$  did not seem to have an effect on the  $N_2O$ -EF of the pilot plant, within the DO ranges applied (1 to  $3 \text{ g O}_2 \text{ m}^{-3}$ ).
- A peak of  $N_2O$  emission was found in many cycles of the pilot plant, attributed to the transient conditions of AOB, at the beginning of the aerobic phase of the R2-AUT operation.
- The aeration strategy implemented that most mitigated the  $N_2O$  emissions in R2-AUT was the intermittent aeration, reducing the  $N_2O$  emissions by 40% compared to normal operation of the plant.



# **Chapter V:**

---

## **A plant-wide model describing GHG emissions and energy/nutrient recovery options for water resource recovery facilities**

**A modified version of this chapter has been prepared for its submission to Water Research as:**

Borja Solís, Albert Guisasola, Xavier Flores-Alsina, Ulf Jeppsson, Juan Antonio Baeza, 2021. A plant-wide model describing GHG emissions and energy/nutrient recovery options for water resource recovery facilities.



## 5. A plant-wide model describing GHG emissions and energy/nutrient recovery options for water resource recovery facilities

### Abstract

In this study, a plant-wide model describing the fate of COD, C, N and P compounds, upgraded to account for (on-site/off-site) greenhouse gas (GHG) emissions, was implemented within the International Water Association (IWA) Benchmarking Simulation Model No. 2 (BSM2) framework. The proposed approach includes the main biological  $N_2O$  production pathways and mechanistically describes  $CO_2$  (biogenic/non-biogenic) emissions in the activated sludge reactors as well as the biogas production ( $CO_2/CH_4$ ) from the anaerobic digester. Indirect GHG emissions for power generation, chemical usage, effluent disposal and sludge storage and reuse are also included using static factors for  $CO_2$ ,  $CH_4$  and  $N_2O$ . Global and individual mass balances were quantified to investigate the fluxes of the different components. Novel control strategies were proposed in order to obtain high plant performance as well as nutrient recovery and mitigation of the GHG emissions in a plant-wide context. The implemented control strategies led to an overall more sustainable and efficient plant performance in terms of better effluent quality, reduced operational cost and lower GHG emissions. The maximum reduction obtained in  $N_2O$  emissions from the biotreatment and total GHG emissions from the water resource recovery facility were 27% and 9%, respectively, compared to the default control strategy.

### 5.1. Motivations

At the beginning of this thesis, the available plant-wide models were not able to describe the GHG emissions of the entire plant when EBPR was implemented. The developments in the previous chapters allowed the prediction of  $N_2O$  emissions from the biological reactor of the water line, but at this stage the calculation of all emissions from the different sub-processes of the plant had not been developed. A first approximation for this calculation was carried out within the UE-Rise C-Foot-Ctrl project in which Genocov was part of. Annex III reports this first approximation, where bibliographic correlations were used to estimate  $N_2O$  and  $CH_4$  emissions at the different points of the plant, including water line and sludge line. Using this extended model, it was possible to study the effect of different operating modes and control strategies on GHG emissions, energy consumption and effluent quality, obtaining some interesting conclusions showing the degree of correlation between these three criteria. However, this type of model based on correlations for the calculation of emissions at the different points of the plant except the biological reactor showed some limitations. In order to obtain a dynamic model capable of describing more rigorously all the processes of a WWTP in terms of GHG emissions ( $N_2O$ ,  $CH_4$  and  $CO_2$ ), energy (consumption and production) and effluent quality, and in which it would be possible to implement control and nutrient recovery strategies, it was

considered appropriate to extend the most advanced benchmarking models of the IWA at that time.

The limitations of the BSM approaches available at that time created the need to define a new extended benchmarking scenario integrating biological COD/N/P removal, GHG emissions, and chemical and physico-chemical models to evaluate different resource recovery scenarios in WRRFs. The main objective of the present work was to develop and evaluate this extension (BSM2-PSFe-GHG) by integrating: i) the biological model ASM2d-N<sub>2</sub>O proposed by Massara et al. (2018) accounting for both enhanced biological phosphorus removal (EBPR) and the most recently reported N<sub>2</sub>O production pathways, ii) potential sources of GHG emissions through the WRRF (updated from Flores-Alsina et al. (2011) and iii) plant-wide modelling of detailed P chemical processes (Solon et al., 2017). Once the BSM2-PSFe-GHG sub-models and their interfaces were developed, a simulation study helped to understand how novel nutrient recovery control strategies can affect GHG emissions in a plant-wide context. In this sense, this work aimed at i) studying the effect on GHG emissions when implementing nutrient recovery control strategies and ii) designing and implementing novel control/operational strategies to optimise plant performance while reducing the GHG emissions.

## 5.2. Materials and Methods

### 5.2.1. BSM2-PSFe-GHG description

#### 5.2.1.1. Biological models

The ASM2d-PSFe-N<sub>2</sub>O model defined in this work merges the BSM2-PSFe approach of Solon et al. (2017) and the ASM2d-N<sub>2</sub>O model of Massara et al. (2018). Hence, it describes simultaneous biological C, N and P removal, as well as the chemical and biological processes related to S and Fe and N<sub>2</sub>O production and emission. Therefore, ASM2d-PSFe-N<sub>2</sub>O presents five new state variables compared to the BSM2-PSFe model (i.e., S<sub>NO<sub>2</sub></sub>, S<sub>NO</sub>, S<sub>N<sub>2</sub>O</sub>, S<sub>NH<sub>2</sub>OH</sub> and X<sub>NOB</sub>). The N<sub>2</sub>O biological pathways adapted from Massara et al. (2018) are:

- i) NH<sub>2</sub>OH oxidation pathway (NN pathway): N<sub>2</sub>O is produced from the reduction of NO by the enzyme “Nor” of AOB coupled with the oxidation of NH<sub>2</sub>OH to NO<sub>2</sub><sup>-</sup> (Pocquet et al., 2016);
- ii) AOB nitrifier denitrification pathway (ND pathway): N<sub>2</sub>O is produced from NO<sub>2</sub><sup>-</sup> reduction to NO and subsequently to N<sub>2</sub>O by AOB. These two processes are lumped in one single reaction as in Pocquet et al., (2016);
- iii) heterotrophic denitrification pathway (DEN pathway): N<sub>2</sub>O is produced as an intermediate of the denitrification processes either by OHO or PAO (W. C. Hiatt and Grady, 2008).

The stoichiometric matrix of the modified ASM2d-PSFe-N<sub>2</sub>O model is provided in Annex II section. The continuity verification of the model was calculated as in Hauduc et al., (2010).

The anaerobic digestion model (ADM) implemented is an extension of the ADM1 model (Batstone et al., 2002), reproducing the biological and chemical interactions between P, S and Fe as reported in previous works (Flores-Alsina et al., 2016; Solon et al., 2017).

#### 5.2.1.2. *Physico-Chemical Models (PCMs)*

BSM2-PSFe-GHG embraces three different PCMs as proposed in the BSM2-PSFe approach (Solon et al., 2017): the pH and ion speciation/pairing model (aqueous phase chemistry model), the multiple mineral precipitation (MMP) model and the gas-liquid mass transfer model.

##### 5.2.1.2.1. *pH and ion speciation/pairing*

A general aqueous phase chemistry model is used in both ASM and ADM, describing the pH variation and ion pairing at each time step (Flores-Alsina et al., 2015; Solon et al., 2015). The acid-base parameters and the activity coefficients are temperature-dependent and all calculations are performed under non-ideal conditions.

The integration of the pH and ion speciation allows to account for weak acid-base conditions within the N<sub>2</sub>O production processes, since the growth rates of nitrifiers ( $X_{AOB}$  and  $X_{NOB}$ ) are functions of their substrates, i.e. free ammonia (FA, NH<sub>3</sub>) and free nitrous acid (FNA, HNO<sub>2</sub>), respectively.

##### 5.2.1.2.2. *Multiple Mineral Precipitation (MMP)*

The precipitation equations are integrated as temperature dependent reversible processes with the saturation index as chemical driving force (Stumm and Morgan, 1996). The precipitation rate depends on the kinetic rate coefficient, the species concentration, the mineral solid phase and the order of the reaction (Kazadi Mbamba et al., 2015a, 2015b; Solon et al., 2017). The MMP model includes the most likely minerals to precipitate during wastewater treatment: calcite (CaCO<sub>3</sub>), hydroxyapatite (Ca<sub>5</sub>(PO<sub>4</sub>)<sub>3</sub>(OH)), amorphous calcium phosphate (Ca<sub>3</sub>(PO<sub>4</sub>)<sub>2</sub>), struvite (MgNH<sub>4</sub>PO<sub>4</sub>·6H<sub>2</sub>O), K-struvite (MgKPO<sub>4</sub>·6H<sub>2</sub>O), newberyite (MgHPO<sub>4</sub>·3H<sub>2</sub>O), magnesite (MgCO<sub>3</sub>) and iron sulphide (FeS). The simplified approach of Hauduc et al. (2015) is implemented to describe the precipitation of hydrous ferric oxides (HFOs), the phosphate adsorption and phosphate co-precipitation to better estimate the phosphorus chemical precipitation.

##### 5.2.1.2.3. *Gas-liquid transfer*



In the ASM2d-PSFe-N<sub>2</sub>O model, the gas-liquid transfer processes are described for the gas components: CO<sub>2</sub>, O<sub>2</sub>, NO, N<sub>2</sub>O, N<sub>2</sub> and H<sub>2</sub>S. The gas-liquid transfer is based on Fick's first law (Equation 5.1), which states that the transfer rate ( $\rho_i$ ) is proportional to the global mass transfer coefficient ( $k_L a_i$ ) and the driving force is the difference between the saturation concentration and the concentration of the gas in the liquid phase. The saturation concentration is calculated through Henry's law, which states that there is a proportionality ( $K_{H,i}$ ) between the saturation concentration of the gas dissolved in the liquid and the partial pressure of the gas ( $P_i$ ).

$$\rho_i = k_L a_i \cdot (K_{H,i} \cdot P_i - C_i) \quad (\text{Eq. 5.1})$$

The mass transfer coefficient for each gas ( $i = \text{CO}_2, \text{O}_2, \text{NO}, \text{N}_2\text{O}, \text{N}_2$  and  $\text{H}_2\text{S}$ ) is calculated from Equation 5.2 as the square root of the ratio of the diffusivities of the gaseous component in the liquid ( $D_i$ ) to that of oxygen ( $D_{\text{O}_2}$ ) and proportional to the mass transfer coefficient of the reference compound oxygen (Lizarralde et al., 2015).

$$k_L a_i = k_L a_{\text{O}_2} \cdot \left( \frac{D_i}{D_{\text{O}_2}} \right)^{1/2} \quad (\text{Eq. 5.2})$$

The gas-liquid transfer processes in ADM are included for the following gas components: H<sub>2</sub>O, CO<sub>2</sub>, H<sub>2</sub>, CH<sub>4</sub> and H<sub>2</sub>S, and are implemented as described by Batstone et al., (2002).

### 5.2.2. Model integration

The different sub-models (ASM2d-PSFe-N<sub>2</sub>O, ADM and PCMs) in BSM2-PSFe-GHG were integrated using model interfaces. The ASM→ADM and ADM→ASM interfaces are based on the continuity-based interfacing method (Nopens et al., 2009) to ensure elemental mass and charge conservation. The interfaces consider instantaneous processes (i.e. PROCESS<sub>AS-AD</sub>) and state variable conversions (i.e. CONV<sub>AS-AD</sub>). The ASM→ADM interface PROCESS<sub>AS-AD</sub> involves: (1) the removal of COD demanding compounds (NH<sub>2</sub>OH, O<sub>2</sub>, NO<sub>3</sub><sup>-</sup>, NO<sub>2</sub><sup>-</sup>, NO and N<sub>2</sub>O) with the associated growth of biomass, and (2) the decay of biomass (OHO, PAO, AOB and NOB) to produce proteins (X<sub>pr</sub>), lipids (X<sub>li</sub>), carbohydrates (X<sub>ch</sub>) and inert particulate organics (X<sub>I</sub>). The CONV<sub>AS-AD</sub> involve (1) the conversion of soluble fermentable organics (S<sub>F</sub>) to amino acids (S<sub>aa</sub>), sugars (S<sub>su</sub>) and fatty acids (S<sub>fa</sub>); (2) the conversion of biodegradable particulate organics (X<sub>S</sub>) to X<sub>pr</sub>, X<sub>li</sub> and X<sub>ch</sub>; and (3) the direct mapping of acetate (S<sub>A</sub> to S<sub>ac</sub>) and inert soluble and particulate organics (S<sub>I</sub> and X<sub>I</sub>) (Solon et al., 2017). Regarding the ADM→ASM interface, a comprehensive description of the involved processes and conversion can be found in Flores-Alsina et al. (2016). Finally, the PCMs integration into ASM and ADM models was made following the procedures detailed in the original works (Flores-Alsina et al., 2015; Solon et al., 2017, 2015).

### 5.2.3. Plant layout and ancillary processes

BSM2-PSFe-GHG was implemented in the same plant layout as the BSM2-PSFe (Solon et al., 2017). The WRRF consists of a primary clarifier (PRIM), an activated sludge section (AS), a secondary clarifier (SEC), a sludge thickener (THK), an anaerobic digester (AD), a dewatering unit (DEW) and finally a storage tank (ST) (Figure 5.1). Additional models were considered to simulate the ancillary processes PRIM, SEC, THK, DEW and ST. The PRIM (900 m<sup>3</sup>) was modelled according to Otterpohl and Freund (1992) with different settling velocities for biodegradable and non-biodegradable compounds (Wentzel et al., 2006). The AS had an A<sup>2</sup>/O configuration consisting of 7 tanks in series: Tanks 1 and 2 were anaerobic (ANAER1 and ANAER2) with a total volume of 2000 m<sup>3</sup>; tanks 3 and 4 were anoxic (ANOX1 and ANOX2) with a total volume of 3000 m<sup>3</sup> while tanks 5, 6 and 7 were aerobic (AER1, AER2 and AER3) with a total volume of 9000 m<sup>3</sup>. The SEC (surface of 1500 m<sup>2</sup> and height of 4 m) was modelled according to the double exponential settling velocity function of Takács et al. (1991) in a ten-layer one-dimensional settler. The THK and DEW units were modelled as ideal units, with no biological activity and a constant percentage of TSS in the concentrated sludge flows. The AD had a working volume of 3400 m<sup>3</sup> and a headspace volume of 300 m<sup>3</sup>. The ST was modelled as a non-reactive, ideally mixed tank of 160 m<sup>3</sup>. Additional information about the plant design and default operational conditions can be found in Gernaey et al. (2014) and Solon et al. (2017).

The influent was generated following the principles proposed by Gernaey et al. (2011). Finally, the sensors and actuators were modelled with response time, delay and white noise to avoid creating unrealistic control applications (Rieger et al., 2003).

#### 5.2.4. Estimation of GHG emissions

Different GHG compounds (CO<sub>2</sub>, CH<sub>4</sub> and N<sub>2</sub>O) type of emissions (biogenic and non-biogenic) and sources of emissions (direct or indirect) were accounted for in BSM2-PSFe-GHG. Estimates not explicitly calculated by the sub-models were estimated following the comprehensive methodology suggested by Flores-Alsina et al. (2014, 2011). The different sources of GHG emissions considered throughout the WRRF are:

- *Direct secondary treatment GHG emissions:* CO<sub>2</sub> generated from biomass respiration, CO<sub>2</sub> generated from BOD<sub>5</sub> oxidation, CO<sub>2</sub> credit from nitrification and N<sub>2</sub>O generated during biological N-removal. CO<sub>2</sub> emissions are explicitly accounted for by ASM2d-PSFe-N<sub>2</sub>O and PCMs (i.e. pH and ion speciation/pairing and gas-liquid transfer models), by including IC instead of alkalinity as a state variable (Flores-Alsina et al., 2015). N<sub>2</sub>O was emitted via the NN and ND pathways of AOB and DEN pathway of heterotrophic organisms (Massara et al., 2018).
- *Sludge processing GHG emissions:* GHG emissions during sludge processing are generated in the anaerobic digester. CO<sub>2</sub> and CH<sub>4</sub> emissions are explicitly

calculated by the modified ADM1 model (Flores-Alsina et al., 2016; Solon et al., 2017). Fugitive emissions from AD and co-generation units are included as a total of 2.7% of the produced biogas that was slipped and un-combusted (Magnus Arnell, 2016). The remaining biogas is combusted in the gas-engine turbine and all the CH<sub>4</sub> is converted to CO<sub>2</sub>, generating electricity and heat. The CO<sub>2</sub> produced in the AD and the CO<sub>2</sub> produced in the combustion are released into the atmosphere. Finally, dissolved CH<sub>4</sub> (and H<sub>2</sub>) in the digester effluent is assumed to be fully stripped in the following process units and emitted to the atmosphere. These emissions are accounted for in the AD (important to maintain mass balances).

- *Net power-related GHG emissions:* Net power is the difference between energy consumption and production. Energy production is the electricity produced by the AD turbine and it is calculated using a factor for the energy content of CH<sub>4</sub> (50 014 MJ (kg CH<sub>4</sub>)<sup>-1</sup>) and assuming an efficiency of 43% for electricity generation (Flores-Alsina et al., 2011). Energy consumption involves pumping, mixing, aeration and heating and is calculated using the OCI, see section 5.2.5. A value of 0.359 kg CO<sub>2</sub> kWh<sup>-1</sup> is selected for the CO<sub>2</sub> emission from net power production (European production mix) (IEA, 2011.).
- *Embedded GHG emissions from chemicals use:* The possible addition of chemicals in the WRRF produces embedded indirect GHG emissions. The specific chemicals considered are: i) methanol dosage as external carbon source with a static factor of 1.54 kg CO<sub>2</sub> (kg methanol)<sup>-1</sup> (Flores-Alsina et al., 2011), ii) FeCl<sub>3</sub> for P precipitation, 0.16 kg CO<sub>2</sub> (kg FeCl<sub>3</sub>)<sup>-1</sup>, iii) NaOH to raise the pH, 1.24 kg CO<sub>2</sub> (kg NaOH)<sup>-1</sup> and iv) Mg(OH)<sub>2</sub> to favour the struvite precipitation, 1.17 kg CO<sub>2</sub> (kg Mg(OH)<sub>2</sub>)<sup>-1</sup> (Gustavsson and Tumlin, 2013).
- *GHG emissions from effluent disposal:* N<sub>2</sub>O is produced in the effluent recipient due to the partial conversion of the remaining TN. An emission factor of 5 g per kg TN discharged to recipient is obtained from the N<sub>2</sub>O emissions corresponding to disposal in lakes and rivers (Arnell, 2016).
- *Sludge storage, disposal and reuse:* Direct emissions from sludge storage are estimated by assuming uncovered storage for 12 months as 8.68 kg CH<sub>4</sub> per ton of VS and 1.1% of TN in sludge is emitted as N<sub>2</sub>O (Arnell, 2016). After the sludge storage, it is transported for disposal and reuse, causing indirect emissions of CO<sub>2</sub>, CH<sub>4</sub> and N<sub>2</sub>O. The CO<sub>2</sub> emissions associated with the transport of biosolids are quantified by multiplying the truck movements by the distance of reuse. CO<sub>2</sub> emissions from mineralization are calculated based on the sludge mass multiplied by the carbon concentration and the conversion factor from C to CO<sub>2</sub>. N<sub>2</sub>O emissions are calculated based on a static factor of 0.01 kg N-N<sub>2</sub>O per kg of TN. In total, three different sludge disposal alternatives are included: Agriculture (38% sludge disposal, 150km from the WRRF), Compost (45% sludge, 20 km) and

Forestry (17% sludge, 144 km) (Arnell, 2016; Bridle et al., 2008; Flores-Alsina et al., 2011).

Finally, all GHG emissions are converted into units of CO<sub>2</sub> equivalents (CO<sub>2e</sub>) by the Global Warming Potentials (GWP). The GWP for a 100-year time horizon for N<sub>2</sub>O and CH<sub>4</sub> are 298 kg CO<sub>2e</sub> per kg N<sub>2</sub>O and 34 kg CO<sub>2e</sub> per kg CH<sub>4</sub>, respectively (IPCC, 2013).

#### 5.2.5. Evaluation criteria

Three performance indices were used to assess the plant performance for the different control/operational strategies. Besides the classical evaluation criteria based on the effluent quality index (EQI) and the OCI (Gernaey et al., 2014; Nopens et al., 2010), total GHG emissions (in CO<sub>2e</sub>) were added as an additional criterion, as first proposed by Flores-Alsina et al., (2014). This value enables the understanding of the synergies and trade-offs that different nutrient recovery control strategies can have on overall GHG emissions. On the other hand, EQI represents the overall pollution leaving the plant and is calculated as a weighted sum of effluent TSS, COD, BOD, TKN, NO<sub>x</sub> (oxidized forms of nitrogen, including NO<sub>3</sub><sup>-</sup>, NO<sub>2</sub><sup>-</sup>, NO, N<sub>2</sub>O and NH<sub>2</sub>OH) and organic and inorganic P (Solon et al., 2017). The OCI is calculated as a weighted sum of the costs related to aeration, pumping, mixing and heating energy, external carbon source, sludge production, chemicals as well as the potential benefits of methane production and nutrients recovered (e.g. struvite). A detailed description of the EQI and OCI calculations can be found in Solon et al., (2017). Finally, other legal criteria such as the percentage of time the plant is in violation (TIV), i.e. when effluent concentrations are above discharge limits for selected nutrients in the effluent were also used to evaluate the plant performance.

#### 5.2.6. Control strategies and sensors characteristics

Table 5.1 summarises the individual controllers and control strategies combining different controllers that were applied in this work. The default scenario (A<sub>0</sub>) is the open-loop configuration (Gernaey et al., 2014), thus the air flow rate supplied to the aerobic reactors (value of the mass transfer coefficient k<sub>L</sub>a) and the purge flow rate were kept constant. The performance of each implemented control strategy is evaluated by comparison with A<sub>0</sub> by means of the evaluation criteria indices. The control strategies A<sub>1</sub> to A<sub>3</sub> are based on the improvement of the water quality (reduction of EQI and TIV for N and P species) by optimizing the aeration strategy, the sludge age in winter or by including nutrient recovery. Finally, the control strategies A<sub>4</sub> and A<sub>5</sub> are mainly focused on reducing the GHG emissions while maintaining good effluent quality and low operating costs.

All dynamic simulations (609 days) are preceded by a steady state simulation (300 days) but only data generated during the last 364 days of dynamic simulations are used to evaluate the implemented control strategies.

DO and T sensors are considered with a response time of 1 min (sensor class A, Rieger et al., 2003). The ammonium sensor is assumed to have a time delay of 10 min and zero mean white noise with standard deviation of  $0.5 \text{ g N m}^{-3}$  (sensor class B0). The aeration and purge pumping actuators are modelled assuming a time delay of 4 min.

Phosphate sensors are considered with the same characteristics as the ammonium sensor (sensor class B0): 10 min of time delay and zero mean white noise with  $0.5 \text{ g P m}^{-3}$  of standard deviation. The pumping systems of  $Q_{\text{FeCl}_3}$  and  $Q_{\text{Mg(OH)}_2}$  have a response time of 10 min.

The nitrite sensor is modelled with a time delay of 10 min and zero mean white noise with standard deviation of  $0.5 \text{ g N m}^{-3}$ .

The soluble  $\text{N}_2\text{O}$  sensor characteristics are based on those of the  $\text{N}_2\text{O}$ -R microsensor of Unisense ([www.unisense.com/N2O](http://www.unisense.com/N2O)): 1 min of time delay (rounded from 45 s of the commercial sensor) and zero mean white noise with standard deviation of  $0.01 \text{ g N m}^{-3}$ .

Table 5.1. Characteristics of the implemented controllers and control strategies.

Controller→	DO	$\text{NH}_4^+$	MLSS	$\text{PO}_4^{3-}$	Magnesium	Nitrite	$\text{N}_2\text{O}$
<b>Characteristics↓</b>							
Measured variable(s)	$\text{S}_{\text{O}_2}$ in AER2	$\text{S}_{\text{NH}_4}$ in AER2	$X_{\text{TSS}}$ and T in AER2	$\text{S}_{\text{PO}_4}$ in AER3	Effluent $\text{S}_{\text{PO}_4}$ in REC unit	$\text{S}_{\text{NO}_2}$ in AER2	$\text{S}_{\text{N}_2\text{O}}$ in AER2
Controlled variable	$\text{S}_{\text{O}_2}$ in AER2	$\text{S}_{\text{NH}_4}$ in AER2	$X_{\text{TSS}}$ in AER2	$\text{S}_{\text{PO}_4}$ in AER3	$X_{\text{Mg(OH)}_2}$ in REC unit	$\text{S}_{\text{NO}_2}$ in AER2	$\text{S}_{\text{N}_2\text{O}}$ in AER2
Set-point	-	$2 \text{ g N m}^{-3}$	$3000 \text{ g m}^{-3}$ (if $T > 15 \text{ }^\circ\text{C}$ ) $4000 \text{ g m}^{-3}$ (if $T < 15 \text{ }^\circ\text{C}$ )	$1.0 \text{ g P m}^{-3}$	$50 \text{ g P m}^{-3}$	$0.5 \text{ g N m}^{-3}$	$0.01 \text{ g N m}^{-3}$
Manipulated variable	$k_{\text{L}}a$ in AER1, 2 & 3	$\text{S}_{\text{O}_2}$ set-point in AER2	$Q_{\text{w}}$	$Q_{\text{FeCl}_3}$	$Q_{\text{Mg(OH)}_2}$	$\text{S}_{\text{O}_2}$ set-point in AER2	$\text{S}_{\text{O}_2}$ set-point in AER2
Control algorithm	PI	Cascaded PI	Cascaded PI	PI	PI	Cascaded PI	Cascaded PI
<b>Control strategy</b>							
<b>A<sub>0</sub></b>							
<b>A<sub>1</sub></b>	X	X	X				
<b>A<sub>2</sub></b>	X	X	X	X			
<b>A<sub>3</sub></b>	X	X	X		X		
<b>A<sub>4</sub></b>	X	X	X		X	X	
<b>A<sub>5</sub></b>	X	X	X		X		X

## 5.3. Results

### 5.3.1. Steady State Simulations

Figure 5.1 shows the total GHG emissions, combined with the fractionation of GHG emissions (on-plant and off-plant), and the overall and individual mass balances for C, N and P as well as the pH under steady-state conditions for the  $A_0$  scenario. Among the total GHG emissions, 65% consisted of  $\text{CO}_2$  (which 63% of the total  $\text{CO}_2$  emissions was

biogenic CO<sub>2</sub> emitted in the biotreatment), 29% of N<sub>2</sub>O (21% of the total N<sub>2</sub>O emitted was produced in the biotreatment section through N-removal) and 6% of CH<sub>4</sub>. The low CH<sub>4</sub> emissions were due to all the produced CH<sub>4</sub> in the AD was burnt in the gas engine unit and, therefore, transformed to CO<sub>2</sub> and energy. Most of the GHG emissions were direct emissions (80%), i.e. produced in the WRRF. The predicted indirect GHG emissions were mainly produced due to sludge disposal and reuse, since the CO<sub>2</sub> emissions produced due to electricity production were mitigated from the electricity generated in the cogeneration unit of CH<sub>4</sub> and no imbedded GHG emissions from chemicals use were produced.

Regarding the fate of C, the inlet C ends up in three different forms: i) 51.3% is emitted as CO<sub>2</sub>: 32.8% in the AS section as biogenic CO<sub>2</sub>, due to the organic matter oxidation and biomass respiration and 18.5% as combustion and leakages of biogas in the AD (this represents 38.7% of the inlet C to the digester), ii) 23.1% dissolved in the effluent mainly in the form of S<sub>IC</sub> (80%) and S<sub>I</sub> (13.4%) and iii) 25.5% is disposed of in the sludge as particulate organics and biomass.

In the case of N, the inlet N ends up in three different phases: i) 49% is discharged in the effluent mainly as S<sub>NO3</sub> (31.4%) and dissolved S<sub>N2</sub> (56.5%), ii) 21.4% ends up in the gas phase of the biological reactors, mainly as N<sub>2</sub>, but with 1.0% of the inlet N as N-N<sub>2</sub>O, which is within the ranges reported by Massara et al., (2017) and Ahn et al. (2010) who obtained values of 0-3.3% of N<sub>2</sub>O emission in 12 different WWTPs, and iii) the remaining 29.6% of the inlet N is disposed in the sludge, mainly as biomass and entrapped in particulate organics. One important outcome of this A<sub>0</sub> operation is its feasibility to accomplish N removal despite its lack of active control, since the values of TKN (2.8 g N m<sup>-3</sup>) and TN (11.0 g N m<sup>-3</sup>) in the effluent for A<sub>0</sub> are below the BSM discharge limits (TKN<sub>limit</sub> = 4 g N m<sup>-3</sup>, TN<sub>limit</sub> = 18 g N m<sup>-3</sup>). The analysis of this scenario also shows the important effects of some recycled streams, such as the overflows of the thickener and the dewatering unit, which increase the N influent load to the plant by 21.5%.

Regarding the P results, only 22.3% of the influent P leaves the plant through the water line, mainly as soluble orthophosphate S<sub>PO4</sub> (43.6%) and X<sub>PP</sub> (39.7%) that overflows in the secondary settler. The obtained effluent TP concentration is 2.37 g P m<sup>-3</sup>, above the BSM discharge limit of TP<sub>limit</sub> = 2.0 g P m<sup>-3</sup>. The remaining 77.7% of inlet P remain in the waste sludge, pointing out the possibility of recovering P from the anaerobic digestate. Moreover, the recycles of the thickener overflows and the reject water, 7.7 and 229.9 kg P d<sup>-1</sup> respectively, increase the influent P load by 95%.

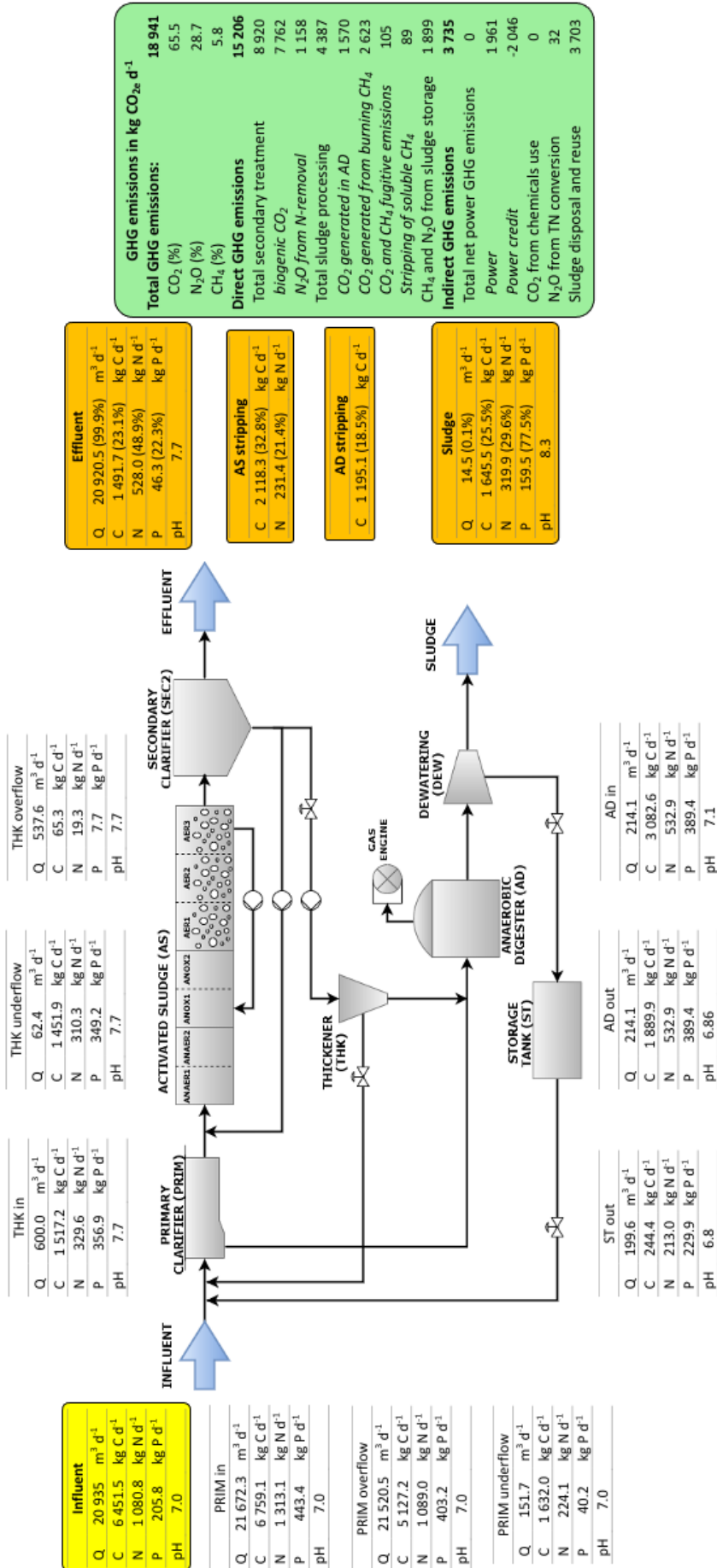


Figure 5.1. Layout of the WRRF from the BSM2-PSFe-GHG. GHG emissions (green box) and overall and individual mass balances (C, N and P) and pH for the main streams of the WRRF are indicated in the tables (steady state results for A<sub>0</sub> open loop configuration). Inlet and outlet streams of the mass balances are highlighted in yellow and orange, respectively.

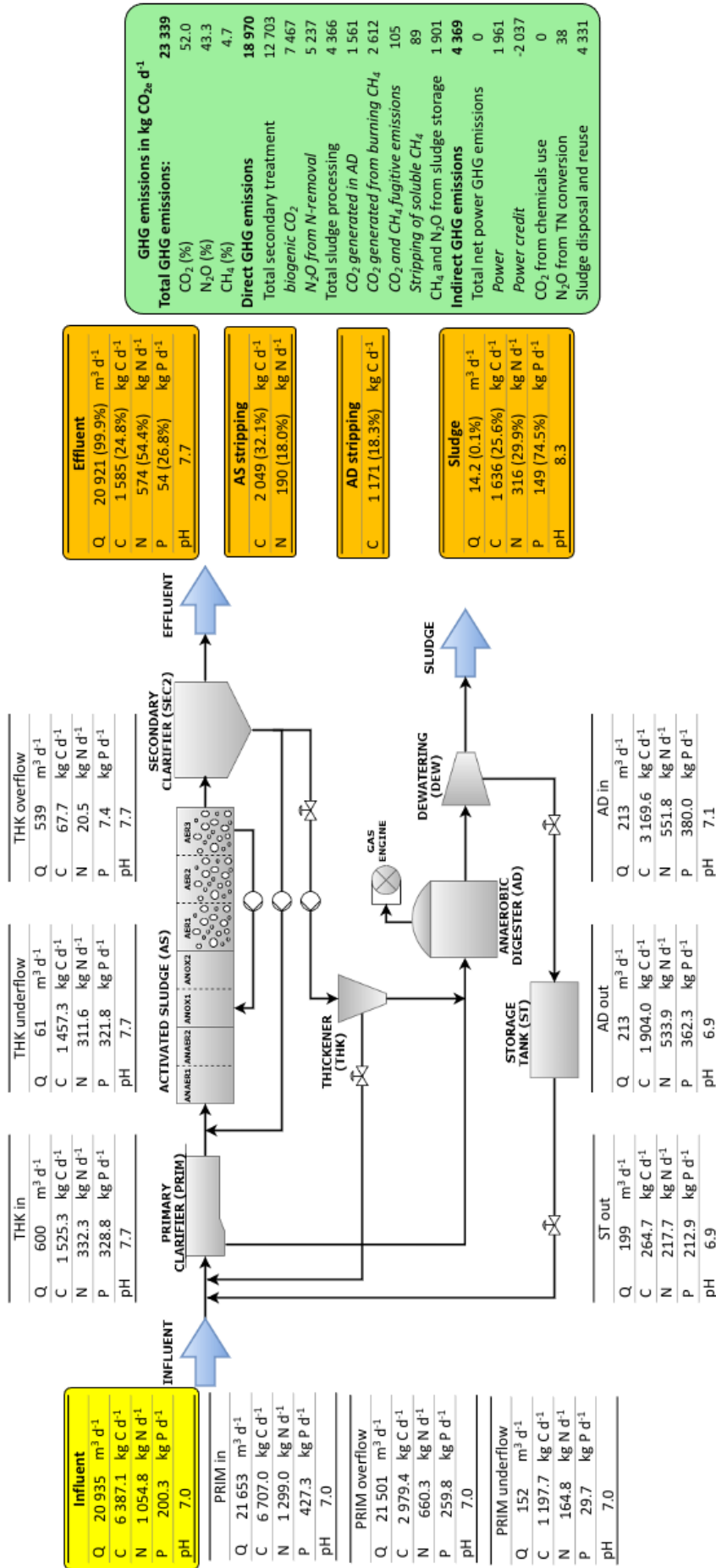


Figure 5.2. GHG emissions (green box) and overall and individual mass balances (C, N and P) and pH for the main streams of the WRRF obtained in A<sub>0</sub> (averaged from last 364 days of dynamic simulation). Inlet and outlet streams are highlighted in yellow and orange, respectively.



### 5.3.2. Dynamic Simulations

The dynamic simulation results of the default  $A_0$  scenario and the runs with implemented control strategies  $A_1$ - $A_5$  are summarized in Table 5.2. In the case of  $A_0$ , the effluent obtained is acceptable in terms of effluent average concentrations during the evaluated period. However, the percentages of TIV for ammonium and P are high (35.3% and 40.5%, respectively) and thus, there is a niche for a performance improvement using control strategies. Table 5.2 also shows that 22.5% of the total GHG emissions come from  $N_2O$  during biological N removal, which represents a  $N_2O$  emission factor ( $N_2O$ -EF) of 2.10%. This emission factor could be reduced by analysing which biological pathways are producing most of the  $N_2O$  and, then, designing adequate mitigation strategies. The source of the GHG emissions and overall and individual mass (Q, C, N and P) and pH for the main streams of the WRRF obtained for control strategy  $A_0$  in the dynamic simulation are shown in Figure 5.2. In the following sections, the results for each implemented control strategy (Table 5.1) are presented and discussed.

Table 5.2. Performance evaluation criteria for each control strategy.

Control strategy →	$A_0$	$A_1$	$A_2$	$A_3$	$A_4$	$A_5$	units
$N_{kjeldahl}$	5.8	3.6	3.5	3.8	3.6	3.6	g N m <sup>-3</sup>
$N_{total}$	13.0	11.3	11.4	10.6	10.9	10.9	g N m <sup>-3</sup>
$P_{inorg}$	1.0	1.0	0.5	0.1	0.1	0.1	g P m <sup>-3</sup>
$P_{total}$	2.5	2.4	1.8	0.9	0.9	0.9	g P m <sup>-3</sup>
TIV $SNH_4$ (= 4 g N m <sup>-3</sup> )	35.3	0.2	0.6	0.2	0.1	0.1	%
TIV $N_{total}$ (= 18 g N m <sup>-3</sup> )	0.2	0.0	0.0	0.0	0.0	0.0	%
TIV $P_{total}$ (= 2 g P m <sup>-3</sup> )	40.5	34.1	20.0	0.3	0.3	0.3	%
<b>EQI</b>	<b>11 769</b>	<b>10 338</b>	<b>9 074</b>	<b>7 129</b>	<b>7 240</b>	<b>7 238</b>	<b>kg p.u. d<sup>-1</sup></b>
$E_{aeration}$	4 000	4 445	4 838	4 031	4 126	4 237	kWh d <sup>-1</sup>
$E_{production}^a$	5 674	5 791	5 897	5 906	5 829	5 860	kWh d <sup>-1</sup>
$SP_{disposal}$	4 033	4 068	4 532	3 643	3 632	3 641	kg TSS d <sup>-1</sup>
$Q_{FeCl_3}^b$	0	0	88	0	0	0	kg Fe d <sup>-1</sup>
$Q_{Mg(OH)_2}^b$	0	0	0	80	80	80	kg Mg d <sup>-1</sup>
$S_{recovered}^c$	0	0	0	442	442	442	kg struv d <sup>-1</sup>
<b>OCI</b>	<b>11 864</b>	<b>12 306</b>	<b>16 109</b>	<b>10 045</b>	<b>10 224</b>	<b>10 362</b>	<b>-</b>
Emitted CO <sub>2</sub> biogenic	7 467	7 510	7 616	7 470	7 569	7 527	kg CO <sub>2e</sub> d <sup>-1</sup>
Emitted N <sub>2</sub> O N-removal	5 237	4 681	4 685	4 312	3 987	3 832	kg CO <sub>2e</sub> d <sup>-1</sup>
$N_2O$ -EF total	2.10	1.33	1.35	1.27	1.17	1.11	%
Total emissions biotreatment	12 703	12 191	12 301	11 782	11 556	11 359	kg CO <sub>2e</sub> d <sup>-1</sup>
AD emissions	4 366	4 462	4 528	4 252	4 238	4 261	kg CO <sub>2e</sub> d <sup>-1</sup>
<b>Total GHG emissions</b>	<b>23 339</b>	<b>22 494</b>	<b>22 844</b>	<b>22 363</b>	<b>21 333</b>	<b>21 164</b>	<b>kg CO<sub>2e</sub> d<sup>-1</sup></b>

Control strategy →	A <sub>0</sub>	A <sub>1</sub>	A <sub>2</sub>	A <sub>3</sub>	A <sub>4</sub>	A <sub>5</sub>	units
Direct GHG emissions	18 970	18 582	18 796	17 743	17 491	17 326	kg CO <sub>2e</sub> d <sup>-1</sup>
Indirect GHG emissions	4 369	3 912	4 049	4 620	3 842	3 837	kg CO <sub>2e</sub> d <sup>-1</sup>

<sup>a</sup> Energy production. The electricity generated by the turbine, calculated as the energy content of methane gas.

<sup>b</sup> Relative costs for FeCl<sub>3</sub>, Mg(OH)<sub>2</sub> and recovered struvite are the same as in Solon et al. (2017).

<sup>c</sup> S<sub>recovered</sub> refers to recovered struvite.

### 5.3.2.1. Control strategy A<sub>1</sub>: Ammonium cascade & waste controller

The A<sub>1</sub> control strategy involves three controllers. The first control loops include two controllers following a cascade configuration, currently known as aeration-based ammonium controller (ABAC). In this configuration, the DO controller of the secondary feedback control loop is in charge of maintaining the DO concentration in AER2 by manipulating the aeration flow ( $k_L a$  value), while the primary feedback control loop manipulates the DO set-point in AER2 using the ammonium concentration in AER2 as the controlled variable. The ammonium set-point in AER2 reactor is fixed at 2 g N m<sup>-3</sup>. An additional control loop with a feedback controller acts on the purge flow ( $Q_w$ ) to maintain the desired  $X_{TSS}$  concentration in AER3. The  $X_{TSS}$  set-point depends on the temperature (Table 5.1). The  $X_{TSS}$  concentration is increased from 3 000 to 4 000 g TSS m<sup>-3</sup> during winter conditions (i.e.  $T < 15$  °C) to establish a longer sludge retention time (SRT) and to maintain the nitrification capacity (Solon et al., 2017; Vanrolleghem et al., 2010). Figure 5.3 shows the schematics of the control loops implemented in A<sub>1</sub>. The source of the GHG emissions and the overall and individual mass (Q, C, N and P) and pH for the main streams of the WRRF obtained for control strategy A<sub>1</sub> are shown in Figure 5.4.

Table 5.2 shows that there is a reduction in N<sub>2</sub>O emissions due to the increase of the DO-setpoint, which decreases the nitrite concentration compared to A<sub>0</sub> and leads to a reduction of N<sub>2</sub>O emissions through the ND pathway. Figure 5.5a shows that there are two different trends in N<sub>2</sub>O emission rates depending on the season. On the one hand, the aeration demand is low during summer (day 254 to 357 and day 549 to 609), the DO ranges between 1 and 2 g O<sub>2</sub> m<sup>-3</sup> and nitrite is accumulating in the reactors (Figure 5.5g). This causes N<sub>2</sub>O emissions via the ND pathway of AOBs to increase (Figure 5.5d). On the other hand, during winter conditions, aeration increases and nitrite levels decrease, which deactivates the ND pathway. However, the production of N<sub>2</sub>O by the NN and NET pathways increases because the cascade NH<sub>4</sub><sup>+</sup> control has difficulty in maintaining the desired NH<sub>4</sub><sup>+</sup> concentration during winter (see Figure 5.5d and Figure 5.5g) considering the applied constraints in the DO set-point to avoid unrealistic control applications (minimum of 0 g O<sub>2</sub> m<sup>-3</sup> and maximum of 6 g O<sub>2</sub> m<sup>-3</sup>). The GHG emissions from the biotreatment (CO<sub>2</sub> biogenic plus N<sub>2</sub>O from N removal) and the total GHG emissions

decreased (4.0% and 3.6%, respectively), due to the decrease in N<sub>2</sub>O emissions. The variation of the waste flow rates during summer and winter led to an improvement in the AD performance, since more methane was produced ( $E_{\text{production}}$  increased), which however led to an increase in AD emissions due to increased combustion of biogas.

EQI improved in A<sub>1</sub> due to lower effluent N concentrations: TKN decreased from 5.8 to 3.6 g N m<sup>-3</sup> (A<sub>0</sub> vs A<sub>1</sub>) and the TIV of ammonium decreased from 35.3 to 0.2%. The average P concentration remained the same and the total P concentration in the effluent decreased by only 0.1 g P m<sup>-3</sup> compared to A<sub>0</sub>. The OCI increased compared to A<sub>0</sub> mainly due to increased aeration costs during the winter period (i.e. when the temperature is below 15°C, between days 357 and 549 of the simulation), since a higher DO set-point is required to maintain the desired ammonium concentration (Figure 5.5g).

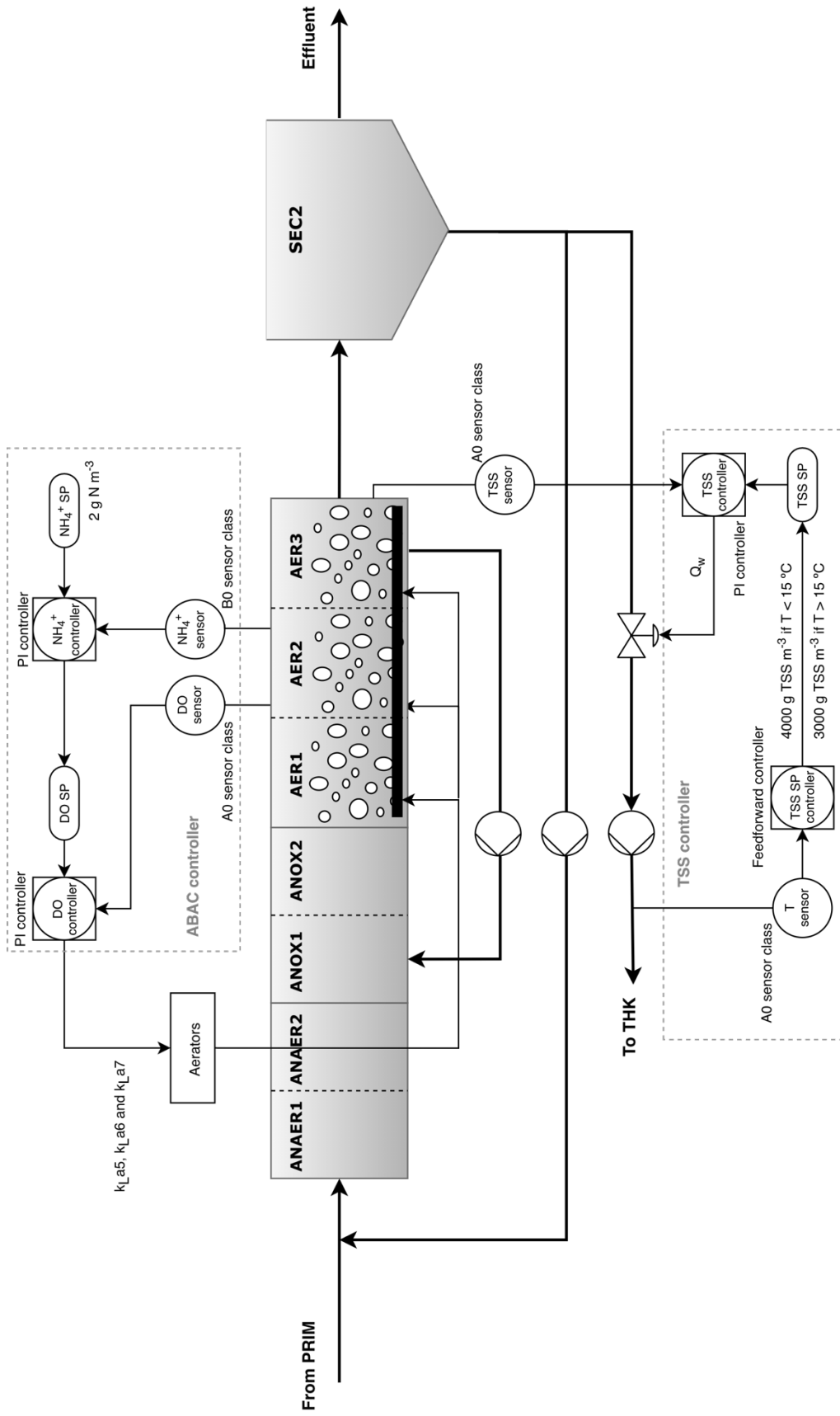


Figure 5.3. Schematics of the control loops implemented for control strategy A<sub>1</sub>.

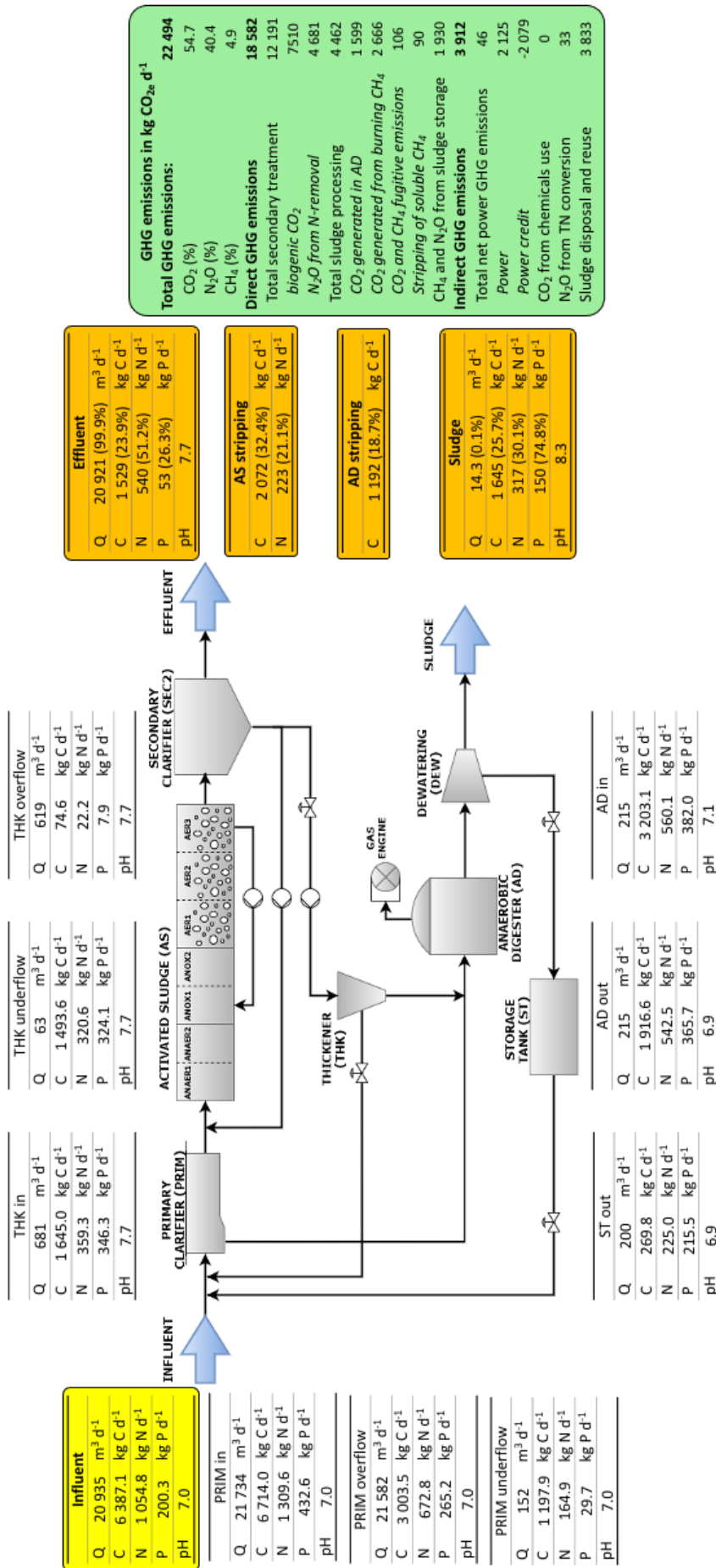


Figure 5.4. GHG emissions (green box) and overall and individual mass balances (C, N and P) and pH for the main streams of the WRRF obtained in A<sub>1</sub> (averaged from last 364 days of dynamic simulation). Inlet and outlet streams are highlighted in yellow and orange, respectively.

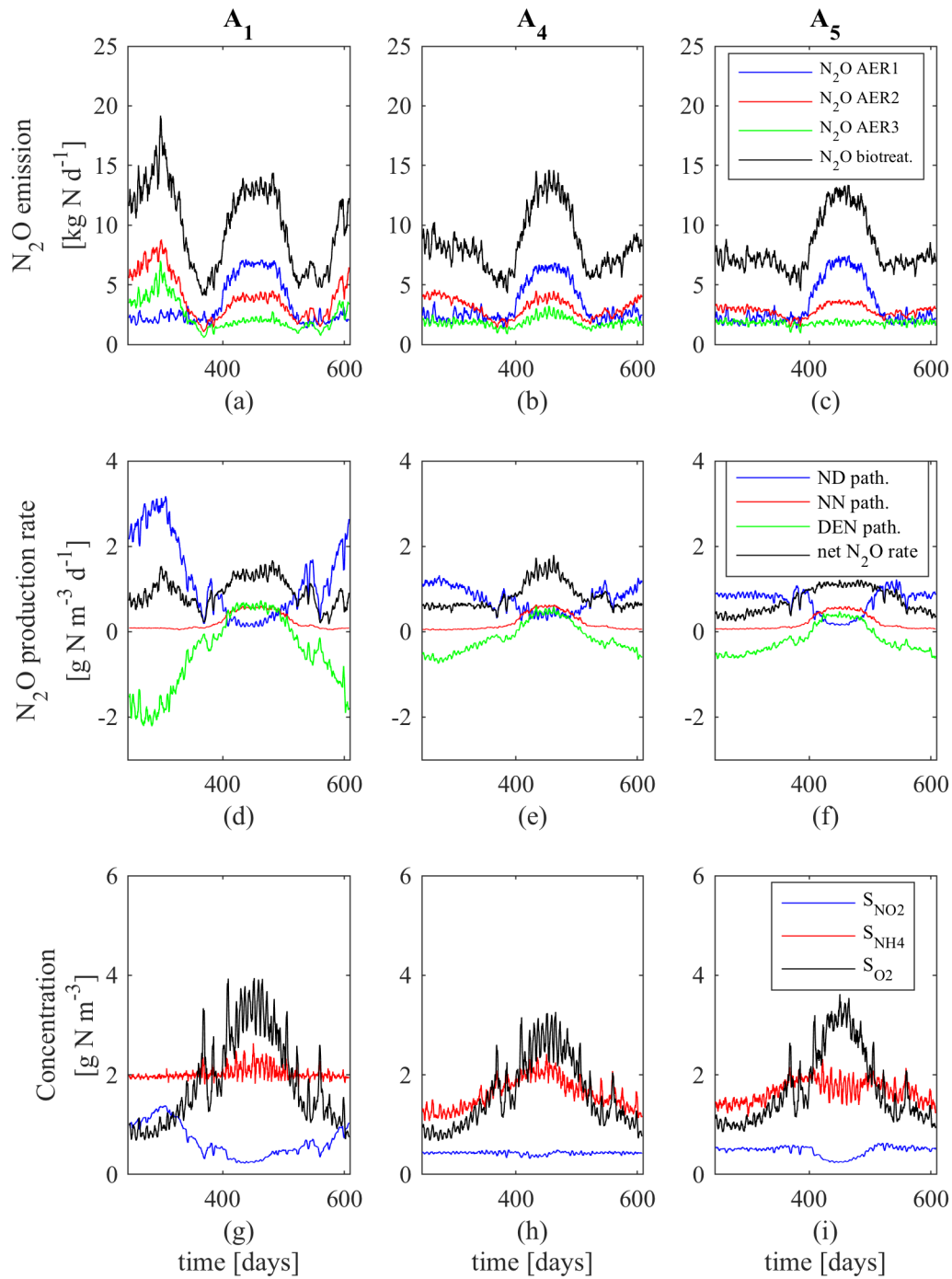


Figure 5.5. Dynamic profiles of control strategies  $A_1$  (a), (d) and (g),  $A_4$  (b), (e) and (h) and  $A_5$  (c), (f) and (i). (a), (b) and (c)  $N_2O$  emissions in the AS unit; (d), (e) and (f)  $N_2O$  production rates in AER2 reactor and, (g), (h) and (i) nitrite, ammonium and DO concentrations in AER2 reactor. A 3-day exponential filter is used to improve visualization of the results.

### 5.3.2.2. Control strategy A<sub>2</sub>: Fe chemical precipitation of PO<sub>4</sub><sup>3-</sup>

Control strategy A<sub>2</sub> aims at reducing the effluent P concentration via its chemical precipitation with Fe by adsorption and co-precipitation of phosphate species onto HFOs. A<sub>2</sub> includes A<sub>1</sub> and a PI controller that regulates the FeCl<sub>3</sub> addition in AER3 reactor to maintain the P concentration in AER3 reactor at the desired set-point of 1 g P m<sup>-3</sup> (Table 5.1). The average S<sub>PO4</sub> concentration in scenario A<sub>0</sub> already was 1 g P·m<sup>-3</sup>, but high P peaks were observed in the effluent. The objective of A<sub>2</sub> is mitigating these P peaks avoiding the high TIV = 40.5% observed. Figure 5.6 shows the schematics of the control loops implemented in A<sub>2</sub>. The source of the GHG emissions and the overall and individual mass (Q, C, N and P) and pH for the main streams of the WRRF obtained for control strategy A<sub>2</sub> are shown in Figure 5.7.

Regarding GHG emissions, total emissions in A<sub>2</sub> increased slightly due to i) more biogenic CO<sub>2</sub> was emitted: PAO activity decreased because there was less phosphate in the anaerobic reactor, resulting in a higher fraction of COD removed by heterotrophic biomass; this biomass produces more inorganic carbon than PAO when removing COD, ii) higher production of biogas and therefore higher emissions from the AD: the iron species enhance primary clarification and more COD is redirected to the AD system and iii) indirect CO<sub>2</sub> emitted by the use of FeCl<sub>3</sub>. The observed N<sub>2</sub>O emissions were the same as in control strategy A<sub>1</sub> because the N fluxes were not affected by the addition of iron (see Table 5.2).

A<sub>2</sub> led to a lower concentration of P in the effluent and, consequently, the TIV of total P decreased from 40.5% with A<sub>0</sub> to 20.0% with A<sub>2</sub> and the EQI was reduced by about 23% (Table 5.2). The phosphate controller was able to reduce the S<sub>PO4</sub> peaks in the AER3 reactor with the addition of Fe, compared to control strategy A<sub>0</sub> (Table 5.2). However, the controller was not able to maintain the S<sub>PO4</sub> at the desired set-point. The average FeCl<sub>3</sub> flow rate throughout the evaluation period was 88 kg Fe/d, which led to a considerable increase of the operational cost, mainly due to the iron dosage (2400 \$ (Ton Fe)<sup>-1</sup>, (Solon et al., 2017)).

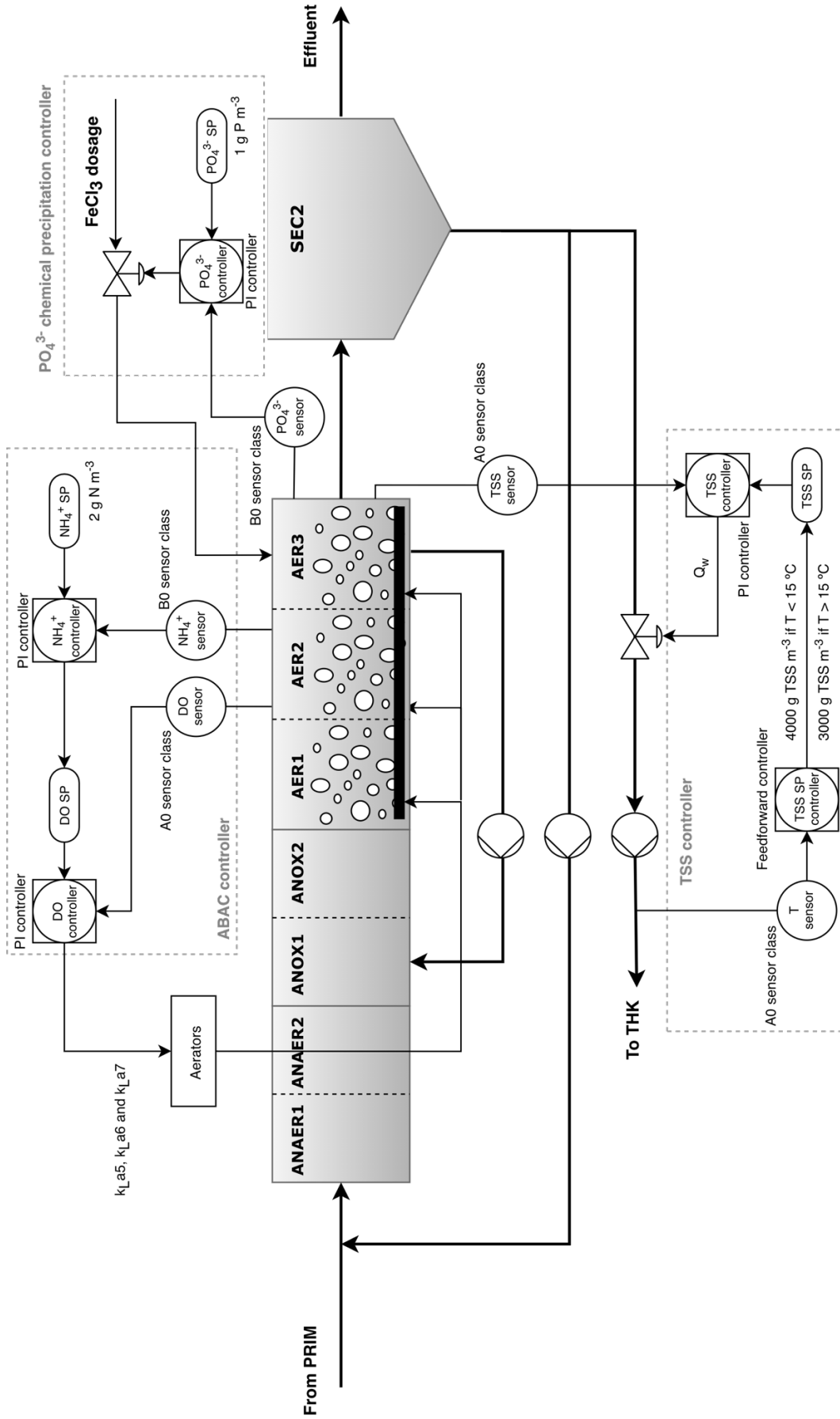


Figure 5.6. Schematics of the control loops implemented for control strategy A<sub>2</sub>.



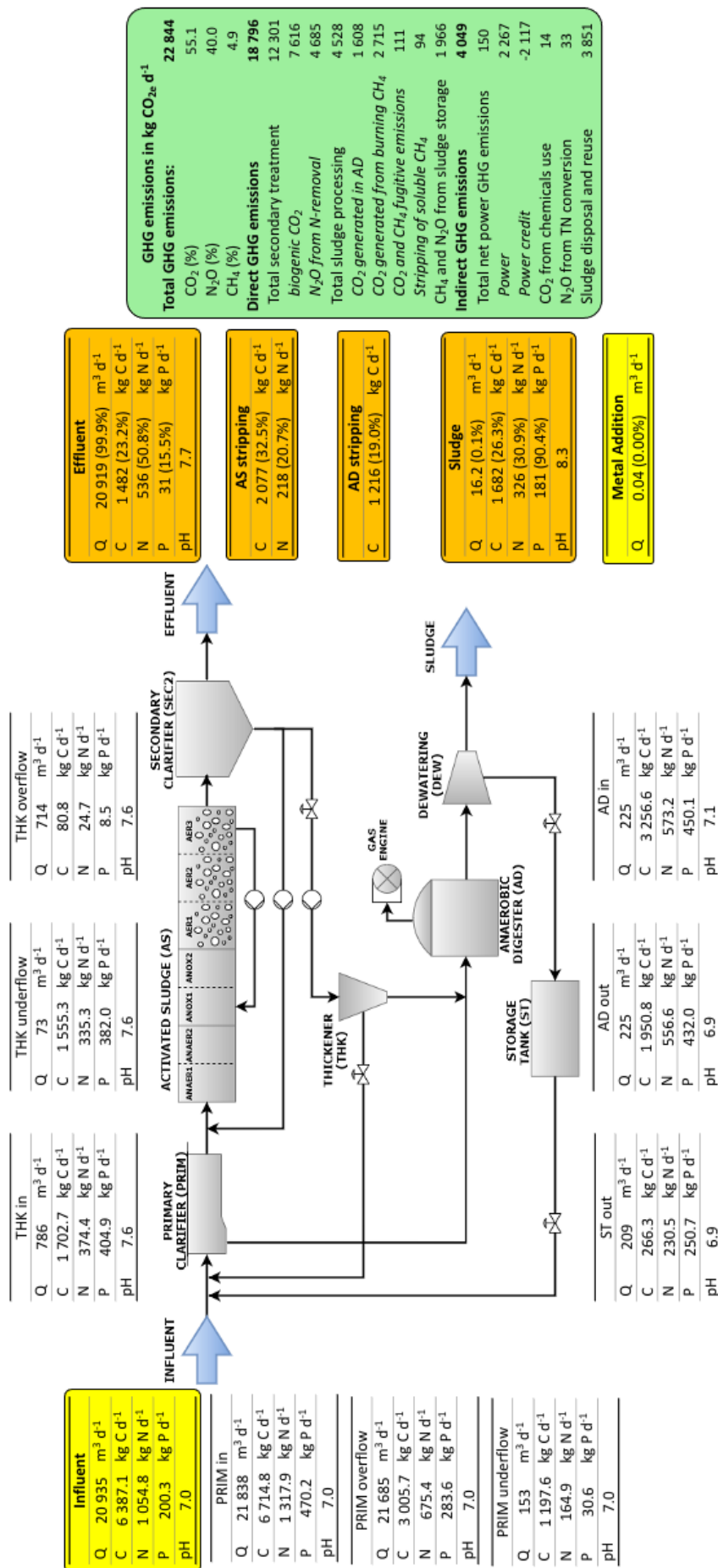


Figure 5.7. GHG emissions (green box) and overall and individual mass balances (C, N and P) and pH for the main streams of the WRRF obtained in A<sub>2</sub> (averaged from last 364 days of dynamic simulation). Inlet and outlet streams are highlighted in yellow and orange, respectively.

### 5.3.2.3. Control strategy $A_3$ : Struvite recovery

Control strategy  $A_3$  complements  $A_1$  by including P-recovery as struvite in the digester supernatant. The layout of the WRRF was modified by including a recovery unit (REC) based on struvite precipitation (see Figure 5.8). The REC unit includes a crystallizer to support struvite precipitation, a storage tank for magnesium hydroxide ( $Mg(OH)_2$ ) and a dewatering unit (Kazadi Mbamba et al., 2016; Solon et al., 2017). A PI controller was added to control the effluent P from the recovery unit at a set-point of  $50 \text{ g P m}^{-3}$  by manipulating the  $Mg(OH)_2$  flow rate ( $Q_{Mg(OH)_2}$ ). Figure 5.8 shows the schematics of the control loops implemented in  $A_3$ . The source of the GHG emissions and the overall and individual mass (Q, C, N and P) and pH for the main streams of the WRRF obtained for control strategy  $A_3$  are shown in Figure 5.9.

Table 5.2 shows that GHG emissions from the whole WRRF decreased. The P load and N in the reject water decreased due to struvite crystallisation: the reject water P load was reduced from  $232.3 \text{ kg P d}^{-1}$  ( $A_1$ ) to  $11.2 \text{ kg P d}^{-1}$  ( $A_3$ ), which resulted in a 95% reduction in the influent P load to the biological reactors. The struvite recovered was  $442 \text{ kg d}^{-1}$ , which resulted in  $99.8 \text{ kg P d}^{-1}$  (48.5% of the total P influent load) and  $45.0 \text{ kg N d}^{-1}$  recovered (4.2% of the total N influent load), respectively.  $N_2O$  emissions decreased slightly because the influent N load to the AS unit decreased and, thus, P-recovery as struvite also had a potential benefit on GHG emissions due to more diluted streams.

Table 5.2 shows that the average effluent P concentrations in  $A_3$  were lower than those in strategies  $A_0$  to  $A_2$ : the WRRF was able to discharge P below the legal limits most of the time (TIV of 0.3%) and EQI decreased by a significant 31% with respect to  $A_1$ . Table 5.2 also shows that OCI decreased 18% compared to  $A_1$ , i.e. struvite recovery is technoeconomically feasible considering only the operational costs associated with the addition of Mg and struvite revenues in a current market scenario. More struvite could be recovered by lowering the phosphate set-point of the controller, since there was still a surplus of  $11.2 \text{ kg d}^{-1}$  of inorganic P available to be precipitated as struvite (Figure 5.10a). However, this would imply a higher cost of  $Mg(OH)_2$  and with the selected setpoint it was enough to meet P discharge limits. Struvite can be precipitated in a wide range of pH (between 7 and 11) with an optimum pH range between 8.0 and 9.5. The addition of  $Mg(OH)_2$  was enough to increase pH from 7.1 to 8.3 (Figure 5.10b) favouring struvite precipitation without requiring an additional aeration unit for  $CO_2$  stripping nor the addition of more alkalinity such as NaOH (Kazadi Mbamba et al., 2016; Solon et al., 2017). Further studies are required to assess the capital costs associated with struvite recovery and additional transport costs (these costs were not considered in the evaluation criteria)

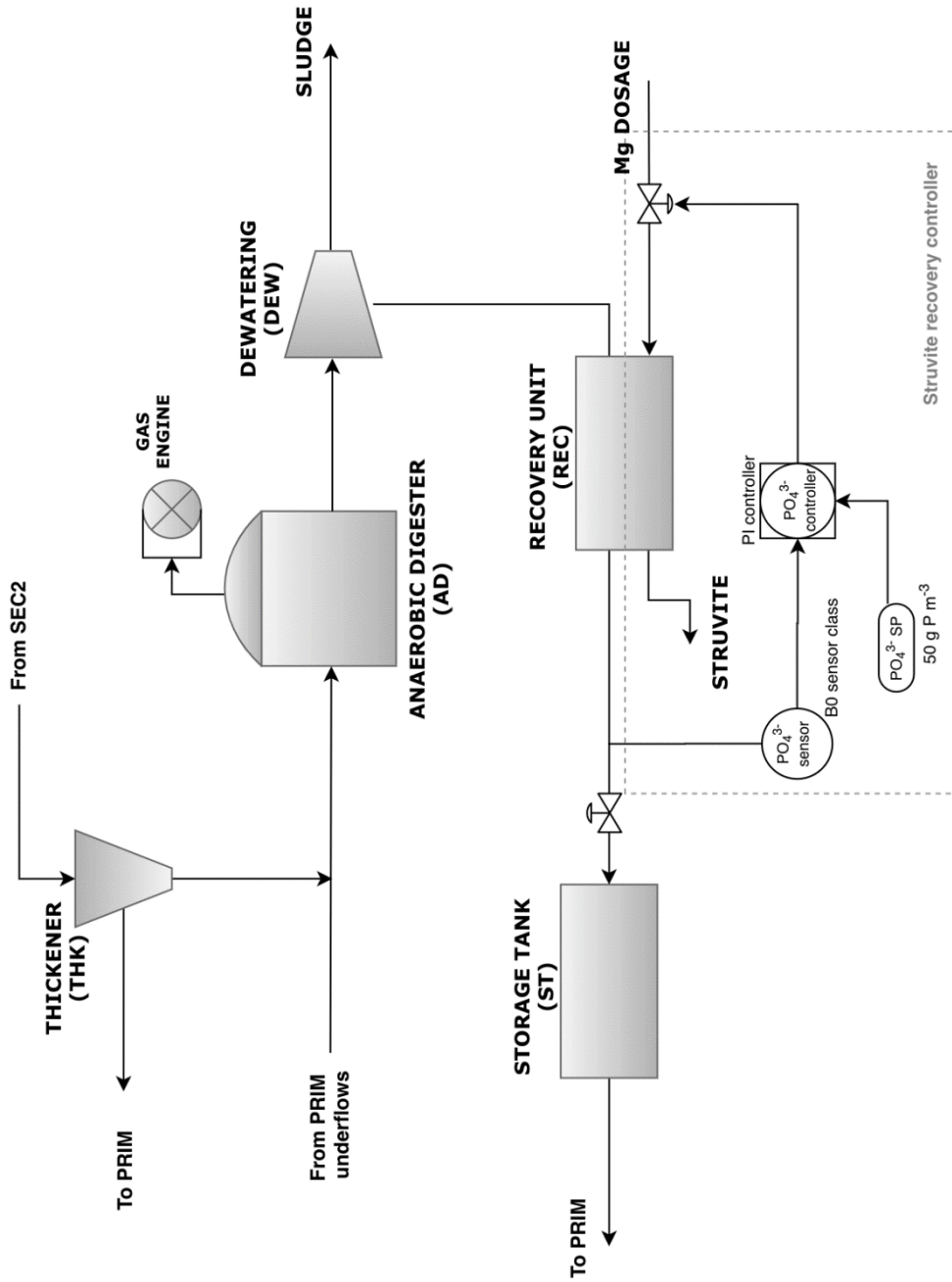


Figure 5.8. Schematics of the control loop implemented in the sludge line for control strategy A<sub>3</sub>. The control loops implemented in the water line are the same as in control strategy A<sub>1</sub> (Figure 5.3).

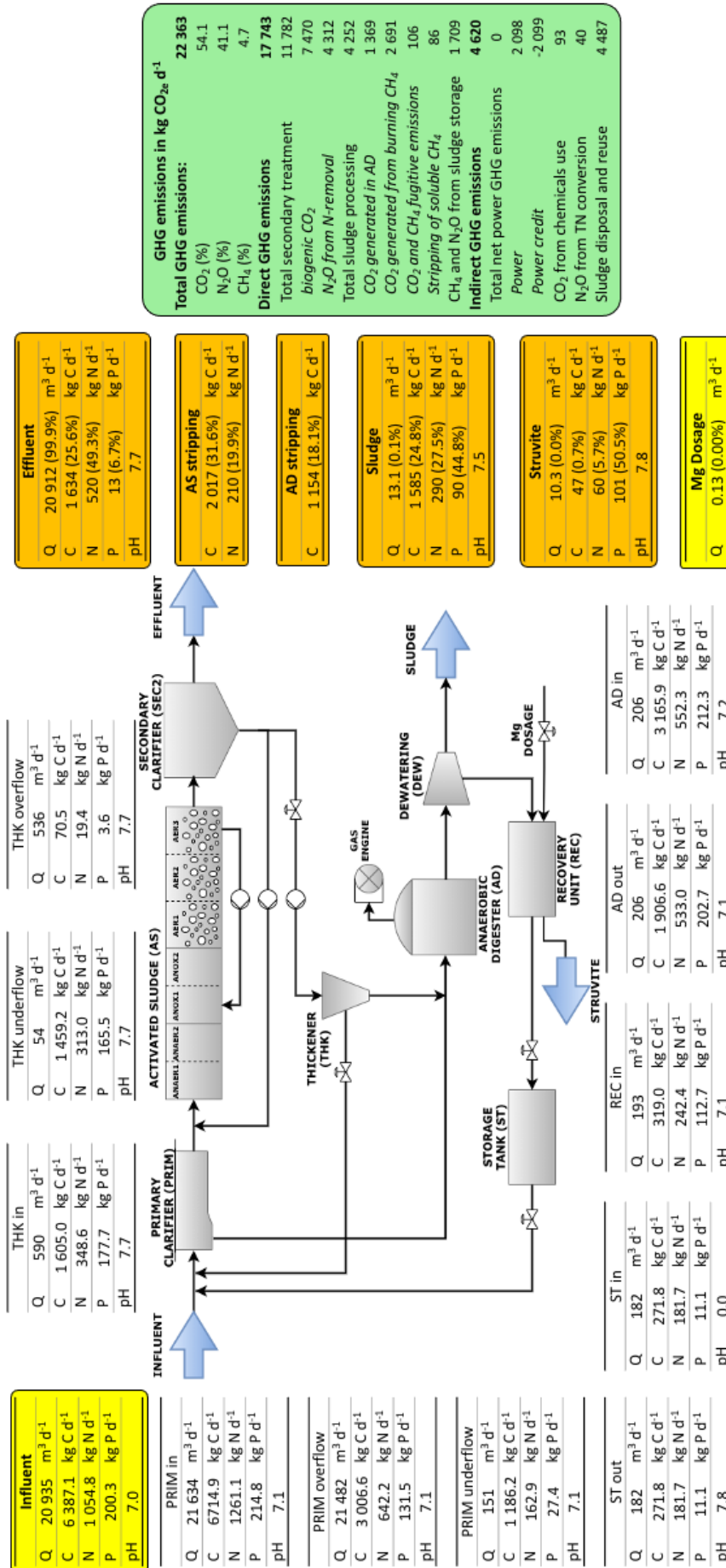


Figure 5.9. GHG emissions (green box) and overall and individual mass balances (C, N and P) and pH for the main streams of the WRRF obtained in A<sub>3</sub> (averaged from last 364 days of dynamic simulation). Inlet and outlet streams are highlighted in yellow and orange, respectively.

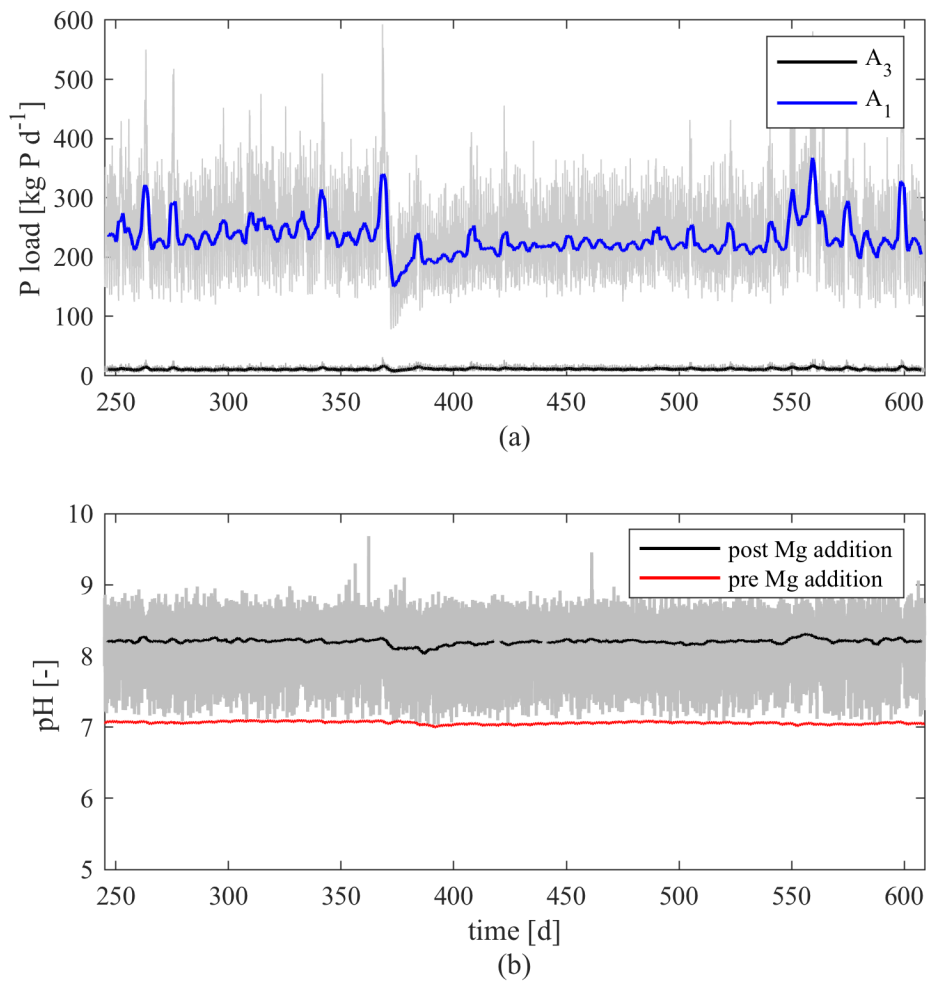


Figure 5.10. a) total P effluent load of the recovery unit (returns to water line) for control strategies  $A_1$  and  $A_3$ . b) Simulated pH values of the recovery unit influent prior and post magnesium addition for control strategy  $A_3$ . A 3-day exponential filter is used to improve the visualization of the results. Raw data is showed in grey.

#### 5.3.2.4. Control strategy $A_4$ : Ammonium & nitrite cascade controllers and struvite recovery

Control strategy  $A_4$  aims at reducing GHG emissions with a particular emphasis on  $\text{N}_2\text{O}$  emissions derived from biological N removal.  $A_4$  extends  $A_3$  with a cascade PI nitrite controller in AER2 reactor. Nitrite concentration was maintained at the desired set-point by manipulating the set-point of the DO controller in conjunction with the ammonium cascade PI controller. Both controllers calculated an adequate DO set-point and the maximum value was chosen (see Table 5.1 for the characteristics of the controllers). The set-point signal of both controllers was filtered with a first-order exponential filter with a time constant of 15 min to avoid numerical instabilities during solver integration. Figure 5.11 shows the schematics of the control loops implemented in  $A_4$ . The source of the

GHG emissions and the overall and individual mass (Q, C, N and P) and pH for the main streams of the WRRF obtained for control strategy  $A_4$  are shown in Figure 5.12.

$A_4$  led to the minimum GHG emissions with respect to the previously implemented strategies ( $A_0$  to  $A_3$ ): the  $N_2O$  emissions were reduced by 7.5% compared to  $A_3$ . The implementation of the nitrite PI cascade led to a reduction of the  $N_2O$  emissions during the summer conditions compared to  $A_1$  (Figure 5.5a and Figure 5.5b), since one of the substrates of the ND pathway, i.e. nitrite, was minimized (Figure 5.5b and Figure 5.5d). The  $N_2O$  emissions during winter conditions remained the same as in  $A_1$  because the ammonium PI cascade was preferentially fixing the DO set-point. The nitrification capacity should be increased in order to further reduce the  $N_2O$  emissions during winter by, for example, increasing the DO levels or the MLSS concentration, with the trade-off of further increasing the operational costs.

$A_4$  led to a slight increase in the effluent N concentration and TIV in comparison to  $A_3$  (2.8% increase in total N compared to  $A_3$ ) due to more ammonium being nitrified in  $A_4$  compared to  $A_3$  (effluent TKN decreased by 5%) and the effluent nitrate concentration increased. In this sense, the implementation of ammonium and nitrite cascade controllers also led to a slight increase in OCI by 1.8%, compared to  $A_3$ , since the applied DO set-point was always the maximum of ammonium and nitrite controllers and the aeration costs incremented by 2.3% compared to  $A_3$ . The same amount of struvite was obtained as in  $A_3$  because the fluxes of P in the sludge line remained unaffected. Figure 5.5i shows that during summer conditions (i.e. T above 15 °C) the DO set-point is mostly defined by the nitrite controller ( $NH_4^+$  is below the set-point of 2 g N m<sup>-3</sup> and  $NO_2^-$  concentration is around the set-point of 0.5 g N m<sup>-3</sup>). The  $NH_4^+$  controller is only activated during the daily peaks when the influent N load is high (in summer the DO set-point is defined by the  $NH_4^+$  controller only 23% of the time). On the other hand, during winter conditions the DO set-point is defined most of the time (62%) by the  $NH_4^+$  controller to ensure complete nitrification.

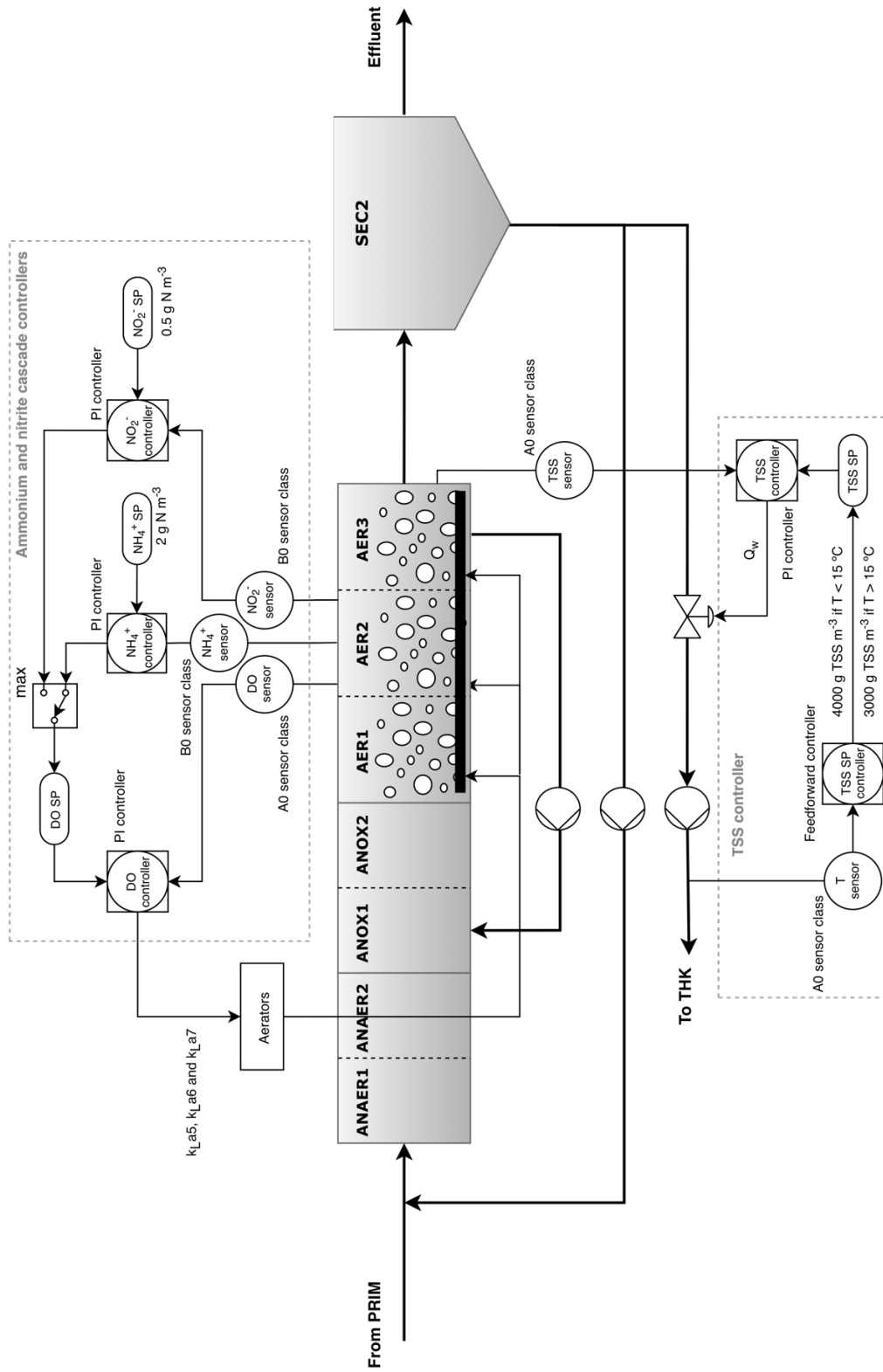


Figure 5.11. Schematics of the control loops implemented for control strategy  $A_4$  for the water line. The control loop implemented in the sludge line is the same as in control strategy  $A_3$  (Figure 5.8).

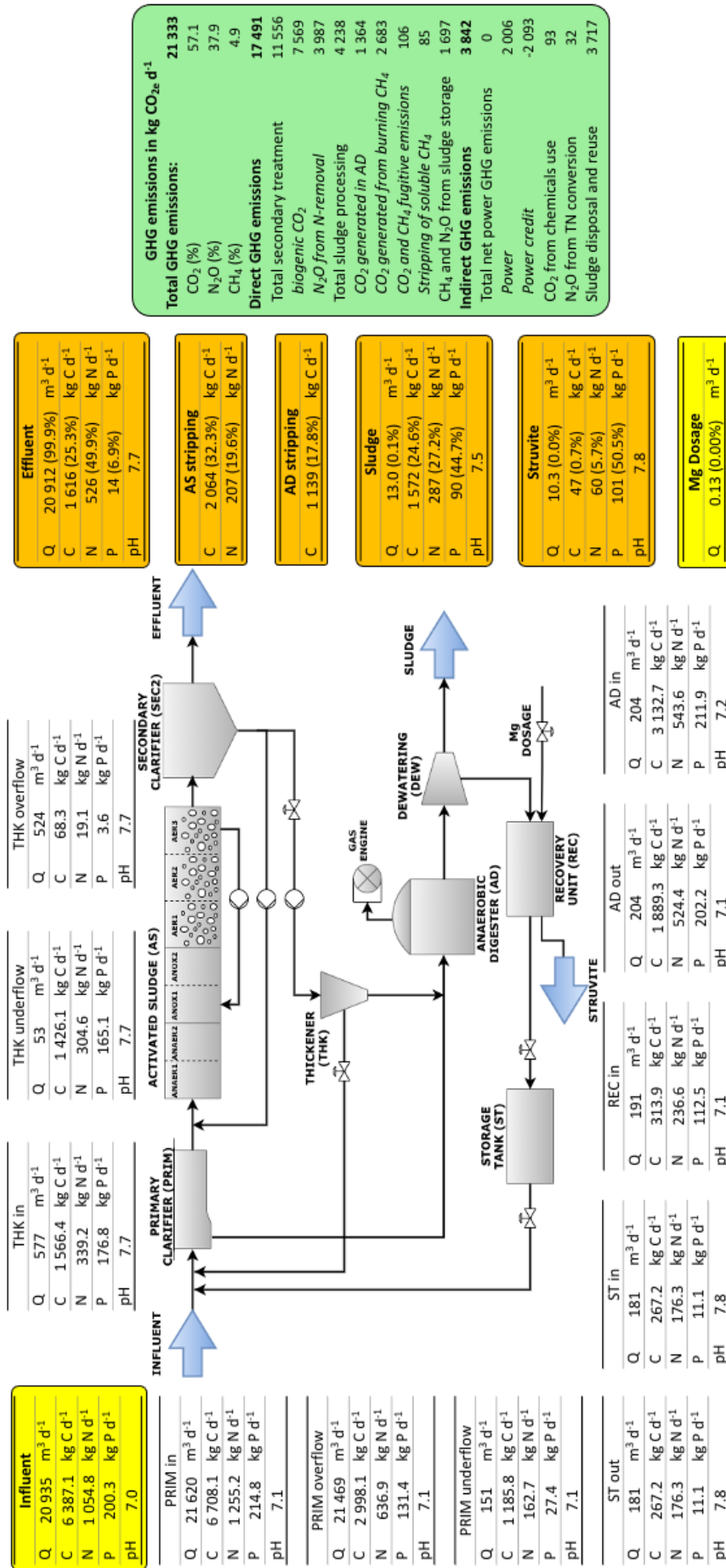


Figure 5.12. GHG emissions (green box) and overall and individual mass balances (C, N and P) and pH for the main streams of the WRRF obtained in A<sub>4</sub> (averaged from last 364 days of dynamic simulation). Inlet and outlet streams are highlighted in yellow and orange, respectively.



#### 5.3.2.5. Control strategy A<sub>5</sub>: Ammonium & nitrous oxide cascade controllers and struvite recovery

A<sub>5</sub> is a modification of A<sub>4</sub> that also aimed at reducing N<sub>2</sub>O emissions. New sensors have appeared in the market that enable the monitoring of soluble N<sub>2</sub>O concentration in the reactors with high accuracy and, thus, allow designing novel mitigation strategies. For this reason, A<sub>5</sub> included a cascade PI controller based on the measurement and control of N<sub>2</sub>O concentration in AER2. In a similar way to A<sub>4</sub>, N<sub>2</sub>O and NH<sub>4</sub><sup>+</sup> controllers calculated S<sub>O<sub>2</sub></sub> set-points for the DO controller and the chosen value was the maximum (Table 5.1). Figure 5.13 shows the schematics of the control loops implemented in A<sub>5</sub>. The source of the GHG emissions and the overall and individual mass (Q, C, N and P) and pH for the main streams of the WRRF obtained for control strategy A<sub>5</sub> are shown in Figure 5.14.

The GHG emissions obtained were the lowest among all the control strategies implemented (Table 5.2), with a 13% reduction in N<sub>2</sub>O emissions compared to A<sub>1</sub>, and a 1% reduction compared to A<sub>4</sub>. Figure 5.15 shows the concentration of soluble N<sub>2</sub>O in AER2 predicted in A<sub>4</sub> and A<sub>5</sub>. N<sub>2</sub>O concentration in A<sub>5</sub> was much more constant due to the N<sub>2</sub>O PI cascade controller, which actively imposed the DO set-point when the N<sub>2</sub>O concentration in AER2 was too high. Only in the transition period from summer to winter (T around 15°C), the cascade PI controllers of A<sub>4</sub> achieved lower N<sub>2</sub>O concentrations (and lower N<sub>2</sub>O emissions) than in A<sub>5</sub>. This was due to the N<sub>2</sub>O PI of A<sub>5</sub> being deactivated and the DO setpoint was being fixed by the NH<sub>4</sub><sup>+</sup> controller. On the other hand, during summer and winter, i.e. T above ~16°C and T below ~14°C, the cascade controllers of A<sub>5</sub> achieved lower N<sub>2</sub>O soluble concentration in AER2 (Figure 5.15) and lower global N<sub>2</sub>O emissions (Figure 5.5b and Figure 5.5c).

The effluent concentrations and the TIV obtained for A<sub>5</sub> were the same as for A<sub>4</sub>, therefore, a high effluent quality was obtained. However, the OCI was 1.3% higher than A<sub>4</sub>, since slightly more oxygen was required to maintain the N<sub>2</sub>O set-point: the DO set-point was set by the N<sub>2</sub>O cascade PI in A<sub>5</sub> 58% of the time whereas the DO set-point was fixed by the nitrite controller in A<sub>4</sub> 56% of the time.

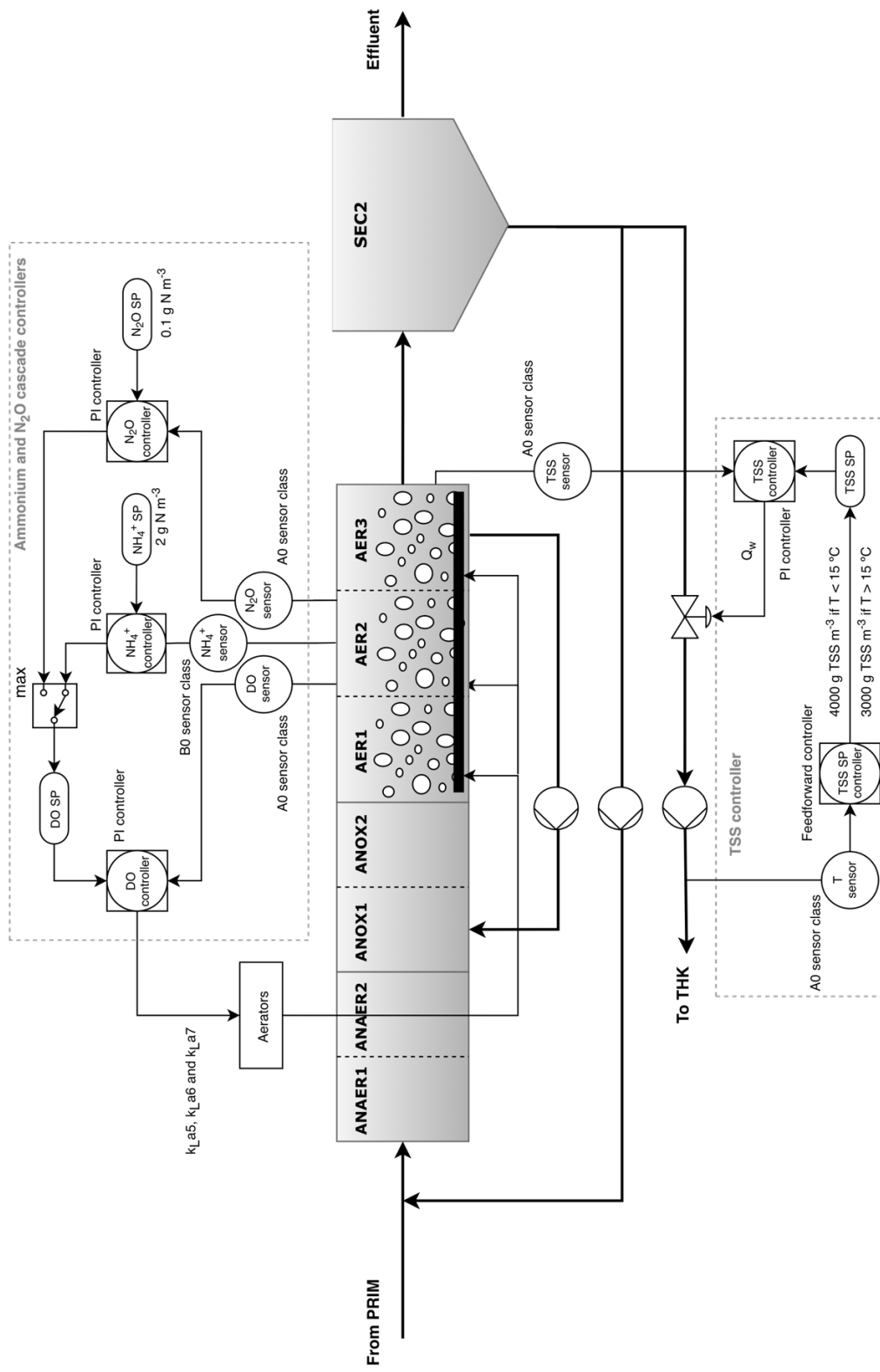


Figure 5.13. Schematics of the control loops implemented for control strategy A<sub>5</sub> for the water line. The control loop implemented in the sludge line is the same as in control strategy A<sub>3</sub> (Figure 5.8).

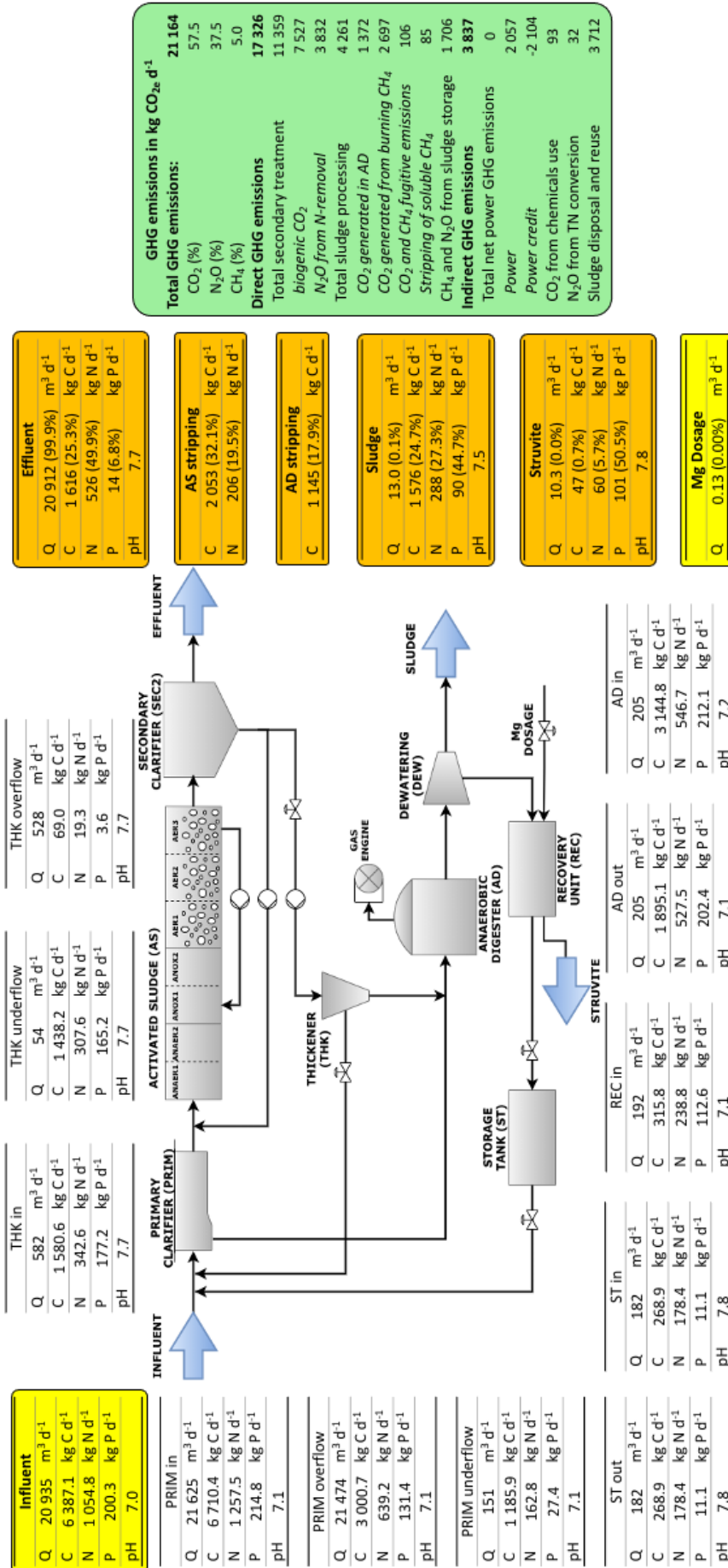


Figure 5.14. GHG emissions (green box) and overall and individual mass balances (C, N and P) and pH for the main streams of the WRRF obtained in A<sub>5</sub> (averaged from last 364 days of dynamic simulation). Inlet and outlet streams are highlighted in yellow and orange, respectively.

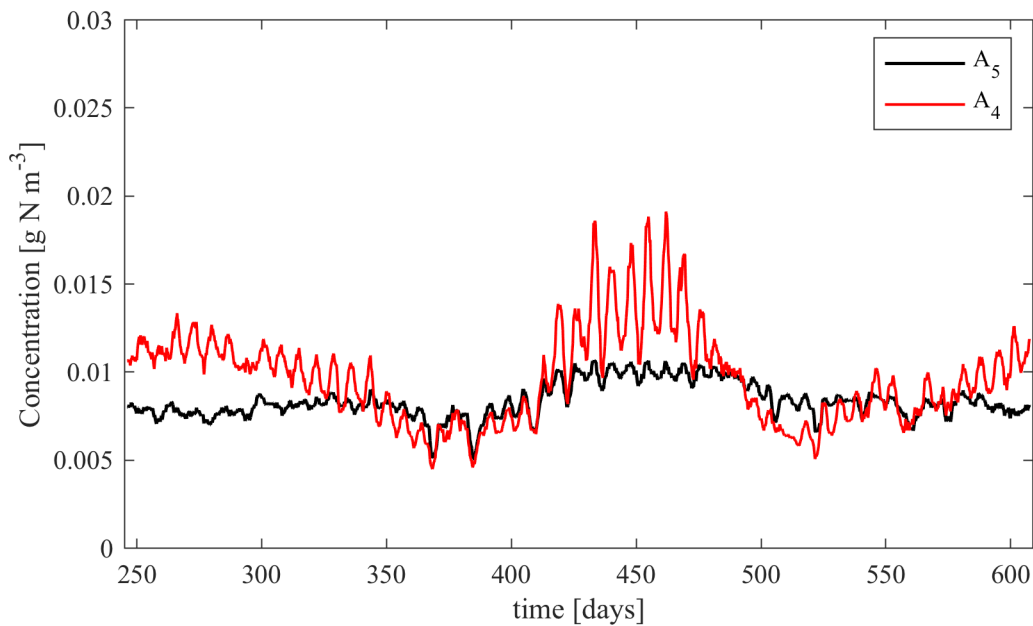


Figure 5.15. Simulated soluble  $\text{N}_2\text{O}$  concentration in AER2 for  $A_4$  and  $A_5$ . A 3-day exponential filter is used to improve the visualization of the results.

#### 5.3.2.6. Comparison of the evaluation criteria for the control strategies implemented

Figure 5.16 compares EQI, OCI, biogenic  $\text{N}_2\text{O}$  emissions and total GHG emissions for each control strategy implemented. The data are normalised considering 100% for the values obtained with the reference operation  $A_0$ . All control strategies led to a more sustainable overall plant performance, since all of them obtained a better effluent quality (i.e. lower EQI) and lower GHG emissions compared to default scenario. Regarding operational costs, the ammonium cascade controller ( $A_1$ ) increased the OCI by 4% compared to  $A_0$  due to the intense aeration demands. The chemical P precipitation strategy ( $A_2$ ) increased the OCI by 36% compared to  $A_0$  due to the high cost of  $\text{FeCl}_3$  dosage. On the other hand, struvite precipitation in the reject water (control strategy  $A_3$ ) was the most successful strategy in terms of EQI and OCI, leading to a reduction in EQI of 40% compared to  $A_0$  and 31% compared to  $A_1$ , and a reduction in OCI of 11% and 14% compared to  $A_0$  and  $A_1$ , respectively, due to: 1) the potential benefits of struvite sales and 2) the reduction in influent load of P and N, which led to lower aeration demand. Control strategies  $A_4$  and  $A_5$  obtained higher reduction in  $\text{N}_2\text{O}$  emission from N-removal compared to  $A_0$ . Control strategies  $A_4$  and  $A_5$  merged the ammonium cascade controller of  $A_1$  with another nitrite or soluble  $\text{N}_2\text{O}$  cascade controller and the struvite precipitation of  $A_3$ . Both control strategies led to higher operational costs than  $A_3$ , 1.8 and 2.8%, respectively, due to the increased aeration demand imposed by the cascade controllers.  $A_5$  seems to have a better performance since it led to a reduction of the emitted  $\text{N}_2\text{O}$  in

the biotreatment of 27% but at the expense of higher costs (i.e. 1.3% higher in  $A_5$  compared to  $A_4$ ). There is therefore a compromise between operational costs and GHG emissions, since operational costs increased slightly in both strategies compared to  $A_3$ , where the main difference between the objectives of  $A_3$  compared to  $A_4$  and  $A_5$  was the reduction of GHG emissions, and moreover,  $A_4$  and  $A_5$  achieved the same EQI.

Finally, Figure 5.16 shows that the largest reduction in total GHG emissions was 9% compared to  $A_0$ , despite the fact that the main aim of the novel control strategies is  $N_2O$  reduction. Other sources of GHG emissions were not reduced, such as indirect emissions (electricity, chemical usage, sludge storage and reuse) which represented about 20% of the total GHG emissions, and other direct GHG sources that were not controllable, such as biogenic  $CO_2$  and methane combustion, which together represented around 50% of the total GHG emissions (Table 5.2).

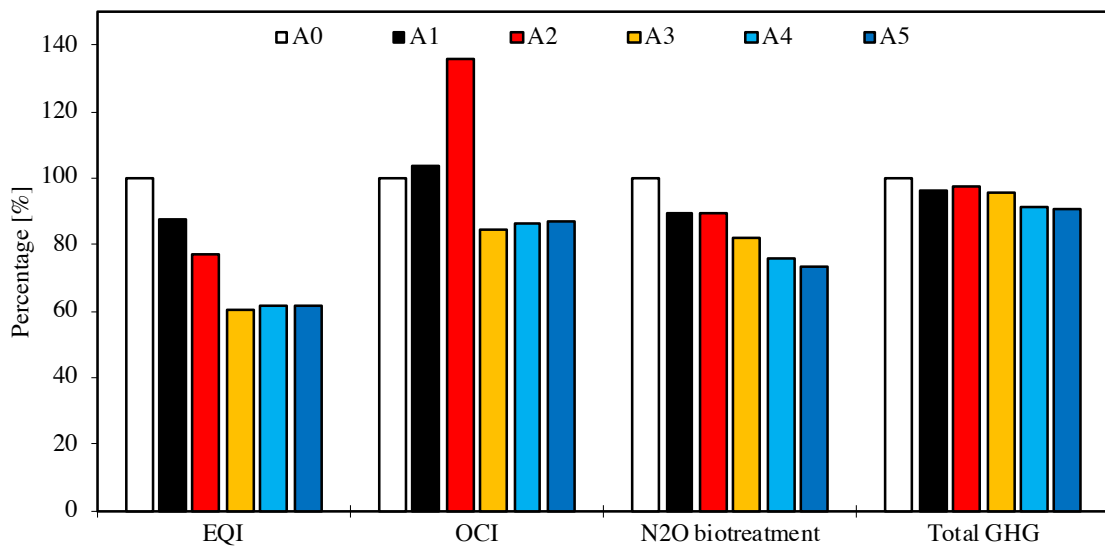


Figure 5.16. Comparison of the evaluation criteria for the control strategies implemented. Data is shown in relative percentage compared to control strategy  $A_0$ .

#### 5.4. Comparison with other works and limitations of the proposed methodology

The proposed BSM2-PSFe-GHG plant-wide model and the implemented control strategies results represent an improvement to the current BSM modelling framework BSM2-PSFe (Solon et al., 2017) by adding the GHG production and emission during nutrient removal and recovery operational/control strategies. In this sense, the BSM2-PSFe-GHG provides a new tool that shows, in a plant-wide context, the trade-offs that different novel control strategies had on the sustainability of the WRRF. On the other hand, the BSM2-PSFe-GHG updates previous works addressed to characterize GHG emissions, with a particular emphasis on  $N_2O$  emissions, which were designed for different plant-wide models (Flores-Alsina et al., 2014, 2011; Sweetapple et al., 2014)

by: i) adding the GHG emissions to the most recent BSM modelling framework capable of simulating nutrient recovery strategies (Solon et al., 2017), ii) adding all the known biological N<sub>2</sub>O pathways reported in the ASM2d-N<sub>2</sub>O model (Massara et al., 2018), iii) improving the calculation of CO<sub>2</sub> emissions by including the general aqueous phase model (Flores-Alsina et al., 2015; Solon et al., 2017) and iv) updating the sources of direct and indirect GHG emissions (Flores-Alsina et al., 2011; Arnell, 2016).

The results reported for each control strategy were unified into three main groups (EQI, OCI and GHG) as proposed by Flores-Alsina et al. (2014). This enabled a fairer evaluation of the different strategies, since none of the criteria depended on the others. Other works have proposed to unify the multicriteria into a single cost function by transforming effluent quality into monetary units by defining tariffs or taxes when the concentrations in the effluent are above a certain limit (Guerrero et al., 2012; Stare et al., 2007), or applying a defined weighted average of the different evaluation criteria (Machado et al., 2020). The benefits of the latter approach are that control strategies are compared with a single index. In this work, a unified cost function could be defined if GHG emissions were also translated into monetary units, by imposing tariffs due to high emissions. Special attention should be paid to defining the different weights of the cost function, since an optimisation of the cost function could lead to high GHG emissions or to poor effluent quality with low operational costs.

P recovery as struvite (strategies A<sub>3</sub> onwards) showed an improvement in the operational costs due to the potential revenues from struvite; however, these results should be taken with caution as the assumed price of struvite (200 \$ ton<sup>-1</sup> as in Solon et al. (2017)) is very uncertain. In addition, struvite recovery improved effluent quality due to reduced P and N loading in the sludge line recycles and that also decreases operational costs. In fact, the OCI would also improve by 17.6%, compared to A<sub>1</sub>, assuming no benefit from struvite sales. Finally, P recovery as struvite also showed a reduction in GHG emissions from the AS unit, mainly due to the decrease in the N influent load. Other important assumptions were made in the crystallizer unit model, such as ideal solids separation and simplified precipitate dissolution (Solon et al., 2017). In addition, potential pipe clogging in REC unit due to struvite precipitation was not considered and is known to be a major issue during P recovery as struvite. These limitations in the crystallizer model should be addressed in future work to obtain a better estimation of struvite recovery.

One limitation of BSM2-PSFe-GHG is that capital expenditure was not included in the evaluation criteria and the comparison between control strategies was only subject to operational costs. Adding the capital costs of equipment, sensors, civil, electrical and piping will provide a more complete assessment (Solon et al., 2017). For example, integrating P-recovery as struvite recovery implies a modification of the plant layout or adding a REC unit and all related equipment. That would result in a higher capital

investment when retrofitting or upgrading the WRRF. On the other hand, P precipitation by Fe addition (control strategy A<sub>2</sub>), showed higher operational costs than A<sub>3</sub> but this strategy “only” implies adding an extra dosing tank to the existing plant layout.

The proposed control strategies showed the logical steps that a WRRF manager should take to improve effluent quality (A<sub>1</sub> to A<sub>3</sub>) and, afterwards, to reduce GHG emissions (A<sub>4</sub> and A<sub>5</sub>). However, each of the control strategies could be optimized:

- i) the location of the Fe addition in A<sub>2</sub> can be optimised to reduce operational costs as already reported (Kazadi Mbamba et al., 2019);
- ii) each of the set-point values can be optimized as in Guerrero et al. (2011) in order to decrease the EQI and OCI, and to minimise GHG emissions. For instance, the reduction of the NH<sub>4</sub><sup>+</sup> set-point value from 2.0 to 1.0 g N m<sup>-3</sup> in A<sub>1</sub> (Table 5.1) led to a 45% reduction in N<sub>2</sub>O emissions, while the OCI increased by 4% and the EQI by 14%.
- iii) N<sub>2</sub>O emissions in the AS unit could be reduced by adding DO, NH<sub>4</sub><sup>+</sup>, NO<sub>2</sub><sup>-</sup> or N<sub>2</sub>O sensors and controllers in each aerobic reactor to better control the WRRF as in Santín et al. (2017), who also aimed at reducing GHG emissions during wastewater treatment by using the BSM2G modelling framework (Flores-Alsina et al., 2011). This strategy enabled a more robust DO control and, therefore, a more robust control of N<sub>2</sub>O emissions. However, the addition of multiple controllers in each aerobic reactor results in a more complex control structure for the biological reactors and would increase the capital and maintenance costs of the associated sensors, instruments and controllers.

## 5.5. Conclusions

In this study a novel plant-wide model that integrates the latest advances in energy and nutrient recovery modelling for an accurate description of N<sub>2</sub>O- and EBPR-related processes is proposed. Five control strategies are evaluated in view of optimising plant performance, minimizing GHG emissions and implementing nutrient recovery. The main findings of the work are:

- Overall and individual mass balances quantify the distribution of C, N and P in the whole WRRF.
- Direct and indirect GHG emissions for CO<sub>2</sub>, N<sub>2</sub>O and CH<sub>4</sub> were quantified in the whole WRRF.
- All five control strategies led to an overall more efficient and sustainable plant performance.
- P-recovery as struvite led to more diluted streams in the biological reactors which reduced GHG emissions in the biotreatment by 17% compared to default configuration.

- The lowest N<sub>2</sub>O and overall GHG emissions were achieved when ammonium and soluble nitrous oxide in the aerobic reactors were controlled, achieving a reduction of 24% and 27% for N<sub>2</sub>O, respectively, and 9% for total GHG, compared to the default configuration.





## **Chapter VI:**

---

## **General Conclusions and Future Work**



## 6. General Conclusions and Future Work

### 6.1. General Conclusions

The overall results obtained in this thesis have contributed to a deeper understanding of the factors triggering N<sub>2</sub>O emissions in wastewater treatment, both experimentally (in a full-scale WWTP and through a novel pilot-plant WRRF configuration) and through modelling. In addition, this thesis has extended the last reported Benchmark Simulation Model by integrating the prediction module of GHG emissions into a novel BSM platform able to model nutrient recovery strategies.

The novel ASM2d-N<sub>2</sub>O model was successfully calibrated for a full-scale WWTP under dynamic conditions, including the calibration of the WWTP hydraulics. Therefore, it can be concluded that available N<sub>2</sub>O models can be applied and calibrated to case specific studies. The key findings of this work are:

- Modelling the flow patterns in the plant is essential for an accurate model calibration. The tracer experiment showed that all reactors of both treatment lines had correct hydraulic behaviour, as no dead volumes, flux recycling or by-passes were found. Furthermore, it was demonstrated that each line received an equal flow.
- Global sensitivity analysis through regional sensitivity analysis method was successfully applied to rank the parameters most likely to reduce the calibration cost function. The sensitivity analysis revealed that the top ranked parameters were related to nitrifying organisms.
- Good fits were obtained during the dynamic kinetic calibration of the ASM2d-N<sub>2</sub>O model. The nutrient profile along the reactors was accurately described only by modifying four kinetic parameters, and showing that ASM2d-N<sub>2</sub>O maintains the predictability of ASM2d for nutrient removal.
- The N<sub>2</sub>O-EF predicted by the ASM2d-N<sub>2</sub>O model was very similar to that measured experimentally and the predicted GHG emission profiles trends were in good agreement with the experimental data.

The plant performance and the GHG emissions of the novel mainstream SCEPPHAR WRRF configuration were assessed at pilot scale and under real environmental conditions. The study showed the good long-term nutrient removal efficiency and the monitoring of the GHG emissions of the pilot plant when operating under shortcut nitrogen removal. Several potential mitigation strategies of N<sub>2</sub>O emissions were implemented in the nitrifying reactor through different aeration control strategies. The main findings of this work are:

- Successful removal efficiencies of C, N and P were achieved for a long-term period in the pilot plant when operating under shortcut N-removal in 8-hour and 12-hour configurations.
- GHG emissions ( $\text{N}_2\text{O}$  and  $\text{CH}_4$ ) showed a high variability.
- Calculated emission factors for  $\text{N}_2\text{O}$  and  $\text{CH}_4$  were in the low range of typical emission factors measured in conventional full-scale WWTPs, despite the high nitrite accumulation measured in the nitrifying reactor of the pilot plant, which a priori might seem conducive to increased  $\text{N}_2\text{O}$  emissions.
- Operating the R2-AUT of the pilot plant at different  $\text{DO}_{\text{SPS}}$  did not seem to have an effect on the  $\text{N}_2\text{O}$ -EF of the pilot plant, within the applied DO ranges (1 to  $3 \text{ g O}_2 \text{ m}^{-3}$ ).
- A peak of  $\text{N}_2\text{O}$  emission was found in many cycles of the pilot plant, attributed to the transient conditions of AOB, at the beginning of the aerobic phase of the R2-AUT operation.
- The aeration strategy implemented that most mitigated  $\text{N}_2\text{O}$  emissions in R2-AUT was the intermittent aeration with an on/off DO controller, reducing  $\text{N}_2\text{O}$  emissions by 40% compared to normal plant operation.

A plant-wide model describing the fate of COD, C, N and P compounds and describing on-site and off-site GHG emissions was implemented in the BSM2 framework. The developed BSM2-PSFe-GHG model integrates the latest advances in energy and nutrient recovery modelling for an accurate description of  $\text{N}_2\text{O}$ - and EBPR-related processes. The biokinetic model in BSM2-PSFe was extended with the  $\text{N}_2\text{O}$  biological production pathways of the ASM2d- $\text{N}_2\text{O}$  model. Five control strategies were implemented in view of optimising plant performance, nutrient recovery and minimization of GHG emissions. The main conclusions drawn during the BSM work are:

- Overall and individual mass balances quantify the distribution of C, N and P in the whole WRRF.
- Direct and indirect GHG emissions of  $\text{CO}_2$ ,  $\text{N}_2\text{O}$  and  $\text{CH}_4$  were quantified in the whole WRRF.
- All five control strategies tested led to an overall more efficient and sustainable plant performance.
- P-recovery as struvite led to more P and N diluted streams in the biological reactors which reduced GHG emissions in the biotreatment by 17% compared to default configuration.
- The lowest  $\text{N}_2\text{O}$  and overall GHG emissions were achieved when ammonium and soluble nitrous oxide in the aerobic reactors were controlled, achieving a reduction of 24% and 27% for  $\text{N}_2\text{O}$ , respectively, and 9% for total GHG, compared to the default configuration.

## 6.2. Future Work

During the development of this thesis, some opportunities for future research topics were identified in each of the chapter of results: the calibration of the ASM2d-N<sub>2</sub>O model to fit full-scale dynamic data, the monitoring, assessment and mitigation of GHG emissions from the mainstream SCEPPHAR configuration and the implementation of GHG emissions in a plant-wide model.

The comprehensive calibration of the hydraulics and kinetics of the Girona WWTP was performed during three days of experimental campaign and, although the dynamics of the nutrients removal and GHG emissions in each of the reactors of one biotreatment line of the Girona WWTP were captured, the seasonal effects due to temperature changes and changes on the operational conditions were not captured. Therefore, there is an opportunity for future research on the calibration of the ASM2d-N<sub>2</sub>O model to fit larger dynamic data on the Girona WWTP. In addition, a validation of the kinetic parameters calibration is mandatory.

Future work on modelling the long term operation of the mainstream SCEPPHAR pilot-plant and the GHG emissions will validate the ASM2d-N<sub>2</sub>O model. New experiments on the mainstream SCEPPHAR could be done to calibrate the ASM2d-N<sub>2</sub>O model to the dynamics of the pilot plant and the N<sub>2</sub>O liquid and gas concentration. In addition, the modelling of the mainstream SCEPPHAR operation can simplify the development of mitigation strategies of GHG emissions. The ASM2d-N<sub>2</sub>O model can be increased to account for the CH<sub>4</sub> emissions in future research to develop model-based CH<sub>4</sub> mitigation strategies.

The increase in model complexity and associated parameters on the developed BSM2-PSFe-GHG platform creates an opportunity for future research on calibration and validation of the ASM2d-PSFe-GHG model. Novel nutrient recovery and mitigation of GHG emissions could be developed in the proposed BSM2 model such as increasing the biogas production, increasing the P or N recovery strategies and developing new strategies to mitigate the N<sub>2</sub>O emissions. There is also an opportunity to develop novel control strategies to mitigate the indirect or off-site GHG emissions of the plant-wide model. A life cycle analysis model could also be implemented in the developed BSM2-PSFe-GHG to assess the global environmental impact of the WRRRF operation. Another opportunity for future research is needed in the BSM to evaluate the investments costs of the equipment to compare fairly control and operational strategies that involves the addition of unit processes to facilitate resource recovery strategies.



## **Chapter VII:**

---

## **References**





## 7. References

- Ahn, J.H., Kim, S., Park, H., Rahm, B., Pagilla, K., Chandran, K., 2010. N<sub>2</sub>O emissions from activated sludge processes, 2008-2009: Results of a national monitoring survey in the united states. *Environ. Sci. Technol.* 44, 4505–4511. <https://doi.org/10.1021/es903845y>
- APHA, 1995. Standard methods for the examination of water and wastewater.
- Ardern, E., Lockett, W.T., 1914. Experiments on the oxidation of sewage without the aid of filters. *J. Soc. Chem. Ind.* 33, 523–539. <https://doi.org/10.1002/jctb.5000331005>
- Arnell, M., 2016. Performance Assessment of Wastewater Treatment Plants - Multi-objective Analysis Using Plant-Wide Models. PhD thesis. Lund University. Sweden.
- Arnell, M., Astals, S., Åmand, L., Batstone, D.J., Jensen, P.D., Jeppsson, U., 2016. Modelling anaerobic co-digestion in Benchmark Simulation Model No. 2: Parameter estimation, substrate characterisation and plant-wide integration. *Water Res.* 98, 138–146. <https://doi.org/10.1016/j.watres.2016.03.070>
- Baeza, J.A., Guerrero, J., Guisasola, A., 2017. Optimising a novel SBR configuration for enhanced biological phosphorus removal and recovery (EBPR2). *Desalin. Water Treat.* 68. <https://doi.org/https://doi.org/10.5004/dwt.2017.20468>
- Bao, Z., Ribera-Guardia, A., Spinelli, M., Sun, D., Pijuan, M., 2018. The effect of temperature shifts on N<sub>2</sub>O and NO emissions from a partial nitrification reactor treating reject wastewater. *Chemosphere* 212, 162–169. <https://doi.org/10.1016/j.chemosphere.2018.08.090>
- Barat, R., Serralta, J., Ruano, M. V., Jiménez, E., Ribes, J., Seco, A., Ferrer, J., 2013. Biological nutrient removal model no. 2 (BNRM2): A general model for wastewater treatment plants. *Water Sci. Technol.* 67, 1481–1489. <https://doi.org/10.2166/wst.2013.004>
- Barbu, M., Vilanova, R., Meneses, M., Santin, I., 2017. On the evaluation of the global impact of control strategies applied to wastewater treatment plants. *J. Clean. Prod.* 149, 396–405. <https://doi.org/10.1016/j.jclepro.2017.02.018>
- Barnard, J., 1976. A review of biological phosphorus removal in the activated sludge process. *Water Sa* 2, 136–144.
- Batstone, D.J., Vavilin, V., Keller, J., Angelidaki, I., Kalyuzhnyi, S.V., Pavlostathis, S.G., Rozzi, A., Sanders, W.T.M., Siegrist, H., Vavilin, V.A., 2002. Anaerobic Digestion Model No. 1. IWA Sci. Tech. Rep. n.13, IWA Publ. London, UK. 45, 65–73.
- Bernhard, A., 2010. The Nitrogen Cycle: Processes, Players, and Human Impact. *Nat. Educ. Knowl.* 3, (10):25.
- Bridle, T., Shaw, A., Cooper, S., Yap, K.C., Third, K., Domurad, M., 2008. Estimation of green-house gas emissions from wastewater treatment plants, in: *Proceedings of IWA World Water Congress. Vienna, Austria, September 7-12, 2008.*
- Brun, R., Kühni, M., Siegrist, H., Gujer, W., Reichert, P., 2002. Practical identifiability of ASM2d parameters - Systematic selection and tuning of parameter subsets. *Water Res.* 36, 4113–4127. [https://doi.org/10.1016/S0043-1354\(02\)00104-5](https://doi.org/10.1016/S0043-1354(02)00104-5)
- Bunce, J.T., Ndam, E., Ofiteru, I.D., Moore, A., Graham, D.W., 2018. A review of phosphorus removal technologies and their applicability to small-scale domestic wastewater treatment systems. *Front. Environ. Sci.* 6, 1–15. <https://doi.org/10.3389/fenvs.2018.00008>
- Bürger, R., Diehl, S., Farås, S., Nopens, I., Torfs, E., 2013. A consistent modelling methodology for

- secondary settling tanks: A reliable numerical method. *Water Sci. Technol.* 68, 192–208. <https://doi.org/10.2166/wst.2013.239>
- C**han, C., Guisasola, A., Baeza, J.A., 2020. Correlating the biochemical methane potential of bio-P sludge with its polyhydroxyalkanoate content. *J. Clean. Prod.* 242, 118495. <https://doi.org/10.1016/j.jclepro.2019.118495>
- Cieślak, B., Konieczka, P., 2017. A review of phosphorus recovery methods at various steps of wastewater treatment and sewage sludge management. The concept of “no solid waste generation” and analytical methods. *J. Clean. Prod.* 142, 1728–1740. <https://doi.org/10.1016/j.jclepro.2016.11.116>
- Coen, F., Petersen, B., Vanrolleghem, P.A., Vanderhaegen, B., Henze, M., 1998. Model-based characterisation of hydraulic, kinetic and influent properties of an industrial WWTP. *Water Sci. Technol.* 37, 317–326. [https://doi.org/10.1016/S0273-1223\(98\)00352-7](https://doi.org/10.1016/S0273-1223(98)00352-7)
- Comas, J., Rodríguez-Roda, I., Gernaey, K. V., Rosen, C., Jeppsson, U., Poch, M., 2008. Risk assessment modelling of microbiology-related solids separation problems in activated sludge systems. *Environ. Model. Softw.* 23, 1250–1261. <https://doi.org/10.1016/j.envsoft.2008.02.013>
- Cordell, D., Rosemarin, A., Schröder, J.J., Smit, A.L., 2011. Towards global phosphorus security: A systems framework for phosphorus recovery and reuse options. *Chemosphere* 84, 747–758. <https://doi.org/10.1016/j.chemosphere.2011.02.032>
- D**aelman, M.R.J., Van Voorthuizen, E.M., Van Dongen, L.G.J.M., Volcke, E.I.P., Van Loosdrecht, M.C.M., 2013. Methane and nitrous oxide emissions from municipal wastewater treatment - Results from a long-term study. *Water Sci. Technol.* 67, 2350–2355. <https://doi.org/10.2166/wst.2013.109>
- Daelman, M.R.J., van Voorthuizen, E.M., van Dongen, U.G.J.M., Volcke, E.I.P., van Loosdrecht, M.C.M., 2012. Methane emission during municipal wastewater treatment. *Water Res.* 46, 3657–3670. <https://doi.org/10.1016/j.watres.2012.04.024>
- Domingo-Félez, C., Calderó-Pascual, M., Plósz, B.G., Smets, B.F., Sin, G., Plósz, B.G., 2017. Calibration of the comprehensive NDHA-N<sub>2</sub>O dynamics model for nitrifier-enriched biomass using targeted respirometric assays. *Water Res.* 126, 29–39. <https://doi.org/10.1016/j.watres.2017.09.013>
- Domingo-Félez, C., Smets, B.F., 2016. A consilience model to describe N<sub>2</sub>O production during biological N removal. *Environ. Sci. Water Res. Technol.* 2, 923–930. <https://doi.org/10.1039/c6ew00179c>
- Downs, J.J., Vogel, E.F., 1993. A plant-wide industrial process control problem. *Comput. Chem. Eng.* 17, 245–255. [https://doi.org/10.1016/0098-1354\(93\)80018-I](https://doi.org/10.1016/0098-1354(93)80018-I)
- E**EC Council, 1991. Council Directive of 21 May 1991 concerning urban waste water treatment (91/271/EEC). *Off. J. Eur. Communities*.
- F**lores-Alsina, X., Arnell, M., Amerlinck, Y., Corominas, L., Gernaey, K. V., Guo, L., Lindblom, E., Nopens, I., Porro, J., Shaw, A., Snip, L., Vanrolleghem, P.A., Jeppsson, U., 2014. Balancing effluent quality, economic cost and greenhouse gas emissions during the evaluation of (plant-wide) control/operational strategies in WWTPs. *Sci. Total Environ.* 466–467, 616–624. <https://doi.org/10.1016/j.scitotenv.2013.07.046>
- Flores-Alsina, X., Comas, J., Rodríguez-Roda, I., Gernaey, K. V., Rosen, C., 2009. Including the effects of filamentous bulking sludge during the simulation of wastewater treatment plants using a risk assessment model. *Water Res.* 43, 4527–4538.

<https://doi.org/10.1016/j.watres.2009.07.033>

- Flores-Alsina, X., Corominas, L., Snip, L., Vanrolleghem, P.A., 2011. Including greenhouse gas emissions during benchmarking of wastewater treatment plant control strategies. *Water Res.* 45, 4700–4710. <https://doi.org/10.1016/j.watres.2011.04.040>
- Flores-Alsina, X., Kazadi Mbamba, C., Solon, K., Vrecko, D., Tait, S., Batstone, D.J., Jeppsson, U., Gernaey, K. V., 2015. A plant-wide aqueous phase chemistry module describing pH variations and ion speciation/pairing in wastewater treatment process models. *Water Res.* 85, 255–265. <https://doi.org/10.1016/j.watres.2015.07.014>
- Flores-Alsina, X., Solon, K., Kazadi Mbamba, C., Tait, S., Gernaey, K. V., Jeppsson, U., Batstone, D.J., 2016. Modelling phosphorus (P), sulfur (S) and iron (Fe) interactions for dynamic simulations of anaerobic digestion processes. *Water Res.* 95, 370–382. <https://doi.org/10.1016/j.watres.2016.03.012>
- Foley, J., de Haas, D., Yuan, Z., Lant, P., 2010. Nitrous oxide generation in full-scale biological nutrient removal wastewater treatment plants. *Water Res.* 44, 831–844. <https://doi.org/10.1016/j.watres.2009.10.033>
- G**ernaey, K. V., Flores-Alsina, X., Rosen, C., Benedetti, L., Jeppsson, U., 2011. Dynamic influent pollutant disturbance scenario generation using a phenomenological modelling approach. *Environ. Model. Softw.* 26, 1255–1267. <https://doi.org/10.1016/j.envsoft.2011.06.001>
- Gernaey, K. V., Jeppsson, U., Vanrolleghem, P.A., Copp, J.B., 2014. Benchmarking of Control Strategies for Wastewater Treatment Plants, *Water Intelligence Online*. <https://doi.org/10.2166/9781780401171>
- Gernaey, K. V., Van Loosdrecht, M.C.M., Henze, M., Lind, M., Jørgensen, S.B., 2004. Activated sludge wastewater treatment plant modelling and simulation: State of the art. *Environ. Model. Softw.* 19, 763–783. <https://doi.org/10.1016/j.envsoft.2003.03.005>
- Grau, P., de Gracia, M., Vanrolleghem, P.A., Ayesa, E., 2007. A new plant-wide modelling methodology for WWTPs. *Water Res.* 41, 4357–4372. <https://doi.org/10.1016/j.watres.2007.06.019>
- Guerrero, J., Guisasola, A., Comas, J., Rodríguez-Roda, I., Baeza, J.A., 2012. Multi-criteria selection of optimum WWTP control setpoints based on microbiology-related failures, effluent quality and operating costs. *Chem. Eng. J.* 188, 23–29. <https://doi.org/10.1016/j.cej.2012.01.115>
- Guerrero, J., Guisasola, A., Vilanova, R., Baeza, J.A., 2011. Improving the performance of a WWTP control system by model-based setpoint optimisation. *Environ. Model. Softw.* 26, 492–497. <https://doi.org/10.1016/j.envsoft.2010.10.012>
- Guisasola, A., Chan, C., Larriba, O., Lippo, D., Suárez-Ojeda, M.E., Baeza, J.A., 2019. Long-term stability of an enhanced biological phosphorus removal system in a phosphorus recovery scenario. *J. Clean. Prod.* 214, 308–318. <https://doi.org/10.1016/j.jclepro.2018.12.220>
- Guisasola, A., de Haas, D., Keller, J., Yuan, Z., 2008. Methane formation in sewer systems. *Water Res.* 42, 1421–1430. <https://doi.org/10.1016/j.watres.2007.10.014>
- Guisasola, A., Petzet, S., Baeza, J.A., Carrera, J., Lafuente, F.J., 2007. Inorganic carbon limitations on nitrification: experimental assessment and modelling. *Water Res.* 41, 277–86. <https://doi.org/10.1016/j.watres.2006.10.030>
- Guo, J.H., Peng, Y.Z., Wang, S.Y., Zheng, Y.N., Huang, H.J., Ge, S.J., 2009. Effective and robust partial nitrification to nitrite by real-time aeration duration control in an SBR treating domestic wastewater. *Process Biochem.* 44, 979–985. <https://doi.org/10.1016/j.procbio.2009.04.022>

- Guo, L., Vanrolleghem, P.A., 2014. Calibration and validation of an activated sludge model for greenhouse gases no. 1 (ASMG1): Prediction of temperature-dependent N<sub>2</sub>O emission dynamics. *Bioprocess Biosyst. Eng.* 37, 151–163. <https://doi.org/10.1007/s00449-013-0978-3>
- Gustavsson, D.J.I., Tumlin, S., 2013. Carbon footprints of Scandinavian wastewater treatment plants. *Water Sci. Technol.* 68, 887–893. <https://doi.org/10.2166/wst.2013.318>
- Gutierrez, O., Sudarjanto, G., Ren, G., Ganigué, R., Jiang, G., Yuan, Z., 2014. Assessment of pH shock as a method for controlling sulfide and methane formation in pressure main sewer systems. *Water Res.* 48, 569–578. <https://doi.org/10.1016/j.watres.2013.10.021>
- H**auduc, H., Rieger, L., Takács, I., Héduit, A., Vanrolleghem, P.A., Gillot, S., 2010. A systematic approach for model verification: Application on seven published activated sludge models. *Water Sci. Technol.* 61, 825–839. <https://doi.org/10.2166/wst.2010.898>
- Hauduc, H., Takács, I., Smith, S., Szabo, A., Murthy, S., Daigger, G.T., Spérandio, M., 2015. A dynamic physicochemical model for chemical phosphorus removal. *Water Res.* 73, 157–170. <https://doi.org/10.1016/j.watres.2014.12.053>
- Hauduc, H., Wadhawan, T., Takács, I., Johnson, B., Bott, C., Ward, M., 2019. Incorporating sulfur reactions and interactions with iron and phosphorus into a general plant-wide model. *Water Sci. Technol.* 79, 26–34. <https://doi.org/10.2166/wst.2018.482>
- Heil, J., Wolf, B., Brüggemann, N., Emmenegger, L., Tuzson, B., Vereecken, H., Mohn, J., 2014. Site-specific <sup>15</sup>N isotopic signatures of abiotically produced N<sub>2</sub>O. *Geochim. Cosmochim. Acta* 139, 72–82. <https://doi.org/10.1016/j.gca.2014.04.037>
- Henze, M., Grady, C.P.L., Gujer, W., Marais, G.V., Matsuo, T., 1987. Activated Sludge Model No. 1. IWA Sci. Tech. Rep. n.1, IWA Publ. London, UK.
- Henze, M., Gujer, W., Mino, T., van Loosdrecht, M., van Loosdrecht, M.C.M., 2000. Activated Sludge Models ASM1, ASM2, ASM2d and ASM3. IWA Sci. Tech. Rep. n.9, IWA Publ. London, UK. 5. <https://doi.org/10.2166/9781780402369>
- Henze, M., Van Loosdrecht, M.C.M., Ekama, G., Brdjanovic, D., 2008. Biological Wastewater Treatment. Principles, Modelling and Design. IWA Publishing, London, UK.
- Hiatt, W. C., Grady, C.P.L., 2008. An Updated Process Model for Carbon Oxidation, Nitrification, and Denitrification. *Water Environ. Res.* 80, 2145–2156. <https://doi.org/10.2175/106143008X304776>
- Hiatt, W C, Grady, C.P.L., 2008. An Updated Process Model for Carbon Oxidation, Nitrification, and Denitrification. *Water Environ. Res.* 80, 2145–2156. <https://doi.org/10.2175/106143008X304776>
- I**EA, 2011. Emissions from fuel combustion. Highlights. Technical report. International Energy Agency, Paris, France., n.d.
- IPCC, 2013: Climate Change 2013: The Physical Science Basis. Contribution of Working Group I to the Fifth Assessment Report of the Intergovernmental Panel on Climate Change [Stocker, T.F., D. Qin, G.-K. Plattner, M. Tignor, S.K. Allen, J. Boschung, A.
- IPCC, 2014: Climate change 2014: synthesis report . contribution of working groups I, II and III to the fifth assessment report of the intergovernmental panel on climate change, core writing team, R.K. Pachauri and L.A. Meyer. IPCC, Geneva, Switzerland.
- J**eppsson, U., Alex, J., Batstone, D.J., Benedetti, L., Comas, J., Copp, J.B., Corominas, L., Flores-Alsina, X., Gernaey, K. V., Nopens, I., Pons, M.N., Rodríguez-Roda, I., Rosen, C., Steyer, J.P.,

- Vanrolleghem, P.A., Volcke, E.I.P., Vrecko, D., 2013. Benchmark simulation models, quo vadis? *Water Sci. Technol.* 68, 1–15. <https://doi.org/10.2166/wst.2013.246>
- Jeppsson, U., Pons, M.N., Nopens, I., Alex, J., Copp, J.B., Gernaey, K. V., Rosen, C., Steyer, J.P., Vanrolleghem, P.A., 2007. Benchmark simulation model no 2: General protocol and exploratory case studies. *Water Sci. Technol.* 56, 67–78. <https://doi.org/10.2166/wst.2007.604>
- Jubany, I., Carrera, J., Lafuente, J., Baeza, J.A., 2008. Start-up of a nitrification system with automatic control to treat highly concentrated ammonium wastewater: Experimental results and modeling. *Chem. Eng. J.* 144, 407–419. <https://doi.org/10.1016/j.cej.2008.02.010>
- Jubany, I., Lafuente, J., Baeza, J.A., Carrera, J., 2009. Total and stable washout of nitrite oxidizing bacteria from a nitrifying continuous activated sludge system using automatic control based on Oxygen Uptake Rate measurements. *Water Res.* 43, 2761–2772. <https://doi.org/10.1016/J.WATRES.2009.03.022>
- K**ampschreur, M.J., Poldermans, R., Kleerebezem, R., Van Der Star, W.R.L., Haarhuis, R., Abma, W.R., Jetten, M.S.M., Van Loosdrecht, M.C.M., 2009a. Emission of nitrous oxide and nitric oxide from a full-scale single-stage nitrification-anammox reactor. *Water Sci. Technol.* 60, 3211–3217. <https://doi.org/10.2166/wst.2009.608>
- Kampschreur, M.J., Temmink, H., Kleerebezem, R., Jetten, M.S.M., Van Loosdrecht, M.C.M., 2009b. Nitrous oxide emission during wastewater treatment. *Water Res.* 43, 4093–4103. <https://doi.org/10.1016/j.watres.2009.03.001>
- Kazadi Mbamba, C., Batstone, D.J., Flores-Alsina, X., Tait, S., 2015a. A generalised chemical precipitation modelling approach in wastewater treatment applied to calcite. *Water Res.* 68, 342–353. <https://doi.org/10.1016/j.watres.2014.10.011>
- Kazadi Mbamba, C., Flores-Alsina, X., John Batstone, D., Tait, S., 2016. Validation of a plant-wide phosphorus modelling approach with minerals precipitation in a full-scale WWTP. *Water Res.* 100, 169–183. <https://doi.org/10.1016/j.watres.2016.05.003>
- Kazadi Mbamba, C., Lindblom, E., Flores-Alsina, X., Tait, S., Anderson, S., Saagi, R., Batstone, D.J., Gernaey, K. V., Jeppsson, U., 2019. Plant-wide model-based analysis of iron dosage strategies for chemical phosphorus removal in wastewater treatment systems. *Water Res.* 155, 12–25. <https://doi.org/10.1016/j.watres.2019.01.048>
- Kazadi Mbamba, C., Tait, S., Flores-Alsina, X., Batstone, D.J., 2015b. A systematic study of multiple minerals precipitation modelling in wastewater treatment. *Water Res.* 85, 359–370. <https://doi.org/10.1016/j.watres.2015.08.041>
- L**arriba, O., Rovira-Cal, E., Juznic-Zonta, Z., Guisasola, A., Baeza, J.A., 2020. Evaluation of the integration of P recovery, polyhydroxyalkanoate production and short cut nitrogen removal in a mainstream wastewater treatment process. *Water Res.* 172, 115474. <https://doi.org/10.1016/j.watres.2020.115474>
- Law, Y., Ni, B.J., Lant, P., Yuan, Z., 2012a. N<sub>2</sub>O production rate of an enriched ammonia-oxidising bacteria culture exponentially correlates to its ammonia oxidation rate. *Water Res.* 46, 3409–3419. <https://doi.org/10.1016/j.watres.2012.03.043>
- Law, Y., Ye, L., Pan, Y., Yuan, Z., 2012b. Nitrous oxide emissions from wastewater treatment processes. *Philos. Trans. R. Soc. B Biol. Sci.* 367, 1265–1277. <https://doi.org/10.1098/rstb.2011.0317>
- Lijó, L., Malamis, S., González-García, S., Fatone, F., Moreira, M.T., Katsou, E., 2017. Technical and environmental evaluation of an integrated scheme for the co-treatment of wastewater and domestic organic waste in small communities. *Water Res.* 109, 173–185.

<https://doi.org/10.1016/j.watres.2016.10.057>

- Lizarralde, I., Fernández-Arévalo, T., Brouckaert, C., Vanrolleghem, P., Ikumi, D.S., Ekama, G.A., Ayesa, E., Grau, P., 2015. A new general methodology for incorporating physico-chemical transformations into multi-phase wastewater treatment process models. *Water Res.* 74, 239–256. <https://doi.org/10.1016/j.watres.2015.01.031>
- Lizarralde, I., Fernández-Arévalo, T., Manas, A., Ayesa, E., Grau, P., 2019. Model-based optimization of phosphorus management strategies in Sur WWTP, Madrid. *Water Res.* 153, 39–52. <https://doi.org/10.1016/j.watres.2018.12.056>
- M**achado, V.C., Lafuente, J., Baeza, J.A., 2020. Systematic comparison framework for selecting the best retrofitting alternative for an existing water resource recovery facility. *Water Environ. Res.* 92, 2072–2085. <https://doi.org/10.1002/wer.1368>
- Machado, V.C., Lafuente, J., Baeza, J.A., 2013. Activated sludge model 2d calibration with full-scale WWTP data: Comparing model parameter identifiability with influent and operational uncertainty. *Bioprocess Biosyst. Eng.* 37, 1271–1287. <https://doi.org/10.1007/s00449-013-1099-8>
- Mannina, G., Ekama, G., Caniani, D., Cosenza, A., Esposito, G., Gori, R., Garrido-Baserba, M., Rosso, D., Olsson, G., 2016. Greenhouse gases from wastewater treatment - A review of modelling tools. *Sci. Total Environ.* 551–552, 254–270. <https://doi.org/10.1016/j.scitotenv.2016.01.163>
- Marcelino, M., Wallaert, D., Guisasola, A., Baeza, J.A., 2011. A two-sludge system for simultaneous biological C, N and P removal via the nitrite pathway. *Water Sci. Technol.* 64, 1142–1147. <https://doi.org/10.2166/wst.2011.398>
- Massara, T.M., Malamis, S., Guisasola, A., Baeza, J.A., Noutsopoulos, C., Katsou, E., 2017. A review on nitrous oxide (N<sub>2</sub>O) emissions during biological nutrient removal from municipal wastewater and sludge reject water. *Sci. Total Environ.* 596–597, 106–123. <https://doi.org/10.1016/j.scitotenv.2017.03.191>
- Massara, T.M., Solís, B., Guisasola, A., Katsou, E., Baeza, J.A., 2018. Development of an ASM2d-N<sub>2</sub>O model to describe nitrous oxide emissions in municipal WWTPs under dynamic conditions. *Chem. Eng. J.* 335, 185–196. <https://doi.org/10.1016/j.cej.2017.10.119>
- Mavinic, D., S., Turk, O., 1987. Benefits of using selective inhibition to remove nitrogen from highly nitrogenous wastes. *Environ. Technol. Lett.* 8, 419–426. <https://doi.org/10.1080/09593338709384500>
- Mayer, B.K., Baker, L.A., Boyer, T.H., Drechsel, P., Gifford, M., Hanjra, M.A., Parameswaran, P., Stoltzfus, J., Westerhoff, P., Rittmann, B.E., 2016. Total Value of Phosphorus Recovery. *Environ. Sci. Technol.* 50, 6606–6620. <https://doi.org/10.1021/acs.est.6b01239>
- Metcalf & Eddy, I., 2014. *Wastewater engineering: treatment and resource recovery*, 5th ed. McGraw-Hill Education, New York, NY, USA.
- Metcalf & Eddy, I., 2003. *Wastewater engineering: treatment and reuse*, 4th ed. McGraw-Hill, New York, NY, USA.
- N**i, B.J., Ye, L., Law, Y., Byers, C., Yuan, Z., 2013a. Mathematical modeling of nitrous oxide (N<sub>2</sub>O) emissions from full-scale wastewater treatment plants. *Environ. Sci. Technol.* 47, 7795–7803. <https://doi.org/10.1021/es4005398>
- Ni, B.J., Yuan, Z., 2015. Recent advances in mathematical modeling of nitrous oxides emissions from wastewater treatment processes. *Water Res.* 87, 336–346. <https://doi.org/10.1016/j.watres.2015.09.049>

- Ni, B.J., Yuan, Z., Chandran, K., Vanrolleghem, P.A., Murthy, S., 2013b. Evaluating four mathematical models for nitrous oxide production by autotrophic ammonia-oxidizing bacteria. *Biotechnol. Bioeng.* 110, 153–163. <https://doi.org/10.1002/bit.24620>
- Nopens, I., Batstone, D.J., Copp, J.B., Jeppsson, U., Volcke, E., Alex, J., Vanrolleghem, P.A., 2009. An ASM/ADM model interface for dynamic plant-wide simulation. *Water Res.* 43, 1913–1923. <https://doi.org/10.1016/j.watres.2009.01.012>
- Nopens, I., Benedetti, L., Jeppsson, U., Pons, M.N., Alex, J., Copp, J.B., Gernaey, K. V., Rosen, C., Steyer, J.P., Vanrolleghem, P.A., 2010. Benchmark Simulation Model No 2: Finalisation of plant layout and default control strategy. *Water Sci. Technol.* 62, 1967–1974. <https://doi.org/10.2166/wst.2010.044>
- O**ehmen, A., Lemos, P.C., Carvalho, G., Yuan, Z., Keller, J., Blackall, L.L., Reis, M.A.M., 2007. Advances in enhanced biological phosphorus removal: From micro to macro scale. *Water Res.* 41, 2271–2300. <https://doi.org/10.1016/j.watres.2007.02.030>
- Olivet, D., Valls, J., Gordillo, M.À., Freixó, À., Sánchez, A., 2005. Application of residence time distribution technique to the study of the hydrodynamic behaviour of a full-scale wastewater treatment plant plug-flow bioreactor. *J. Chem. Technol. Biotechnol.* 80, 425–432. <https://doi.org/10.1002/jctb.1201>
- Otterpohl, R., Freund, M., 1992. Dynamic models for clarifiers of activated sludge plants with dry and wet weather flows. *Water Sci. Technol.* 26, 1391–1400. <https://doi.org/10.2166/wst.1992.0582>
- P**an, Y., Ni, B.J., Bond, P.L., Ye, L., Yuan, Z., 2013a. Electron competition among nitrogen oxides reduction during methanol-utilizing denitrification in wastewater treatment. *Water Res.* 47, 3273–3281. <https://doi.org/10.1016/j.watres.2013.02.054>
- Pan, Y., Ni, B.J., Yuan, Z., 2013b. Modeling electron competition among nitrogen oxides reduction and N<sub>2</sub>O accumulation in denitrification. *Environ. Sci. Technol.* 47, 11083–11091. <https://doi.org/10.1021/es402348n>
- Peng, L., Ni, B.J., Erler, D., Ye, L., Yuan, Z., 2014. The effect of dissolved oxygen on N<sub>2</sub>O production by ammonia-oxidizing bacteria in an enriched nitrifying sludge. *Water Res.* 66, 12–21. <https://doi.org/10.1016/j.watres.2014.08.009>
- Peng, L., Ni, B.J., Ye, L., Yuan, Z., 2015. The combined effect of dissolved oxygen and nitrite on N<sub>2</sub>O production by ammonia oxidizing bacteria in an enriched nitrifying sludge. *Water Res.* 73, 29–36. <https://doi.org/10.1016/j.watres.2015.01.021>
- Pianosi, F., Beven, K., Freer, J., Hall, J.W., Rougier, J., Stephenson, D.B., Wagener, T., 2016. Sensitivity analysis of environmental models: A systematic review with practical workflow. *Environ. Model. Softw.* 79, 214–232. <https://doi.org/10.1016/j.envsoft.2016.02.008>
- Pocquet, M., Wu, Z., Queinnec, I., Spérandio, M., 2016. A two pathway model for N<sub>2</sub>O emissions by ammonium oxidizing bacteria supported by the NO/N<sub>2</sub>O variation. *Water Res.* 88, 948–959. <https://doi.org/10.1016/j.watres.2015.11.029>
- Purkhold, U., Pommerening-Röser, A., Juretschko, S., Schmid, M.C., Koops, H.P., Wagner, M., 2000. Phylogeny of all recognized species of ammonia oxidizers based on comparative 16S rRNA and amoA sequence analysis: Implications for molecular diversity surveys. *Appl. Environ. Microbiol.* 66, 5368–5382. <https://doi.org/10.1128/AEM.66.12.5368-5382.2000>
- R**avishankara, A.R., Daniel, J.S., Portmann, R.W., 2009. Nitrous oxide (N<sub>2</sub>O): The dominant ozone-depleting substance emitted in the 21st century. *Science* (80- ). 326, 123–125. <https://doi.org/10.1126/science.1176985>



- Remy, C., Jossa, P., 2015. Life Cycle Assessment of Selected Processes for P Recovery from Sewage Sludge, Sludge Liquor or Ash. Deliverable 9.2 of P-REX Project. Sustainable Sewage Sludge Management Fostering Phosphorus Recovery and Energy Efficiency.
- Ribera-Guardia, A., Bosch, L., Corominas, L., Pijuan, M., 2019. Nitrous oxide and methane emissions from a plug-flow full-scale bioreactor and assessment of its carbon footprint. *J. Clean. Prod.* 212, 162–172. <https://doi.org/10.1016/j.jclepro.2018.11.286>
- Richardson, D., Felgate, H., Watmough, N., Thomson, A., Baggs, E., 2009. Mitigating release of the potent greenhouse gas N<sub>2</sub>O from the nitrogen cycle - could enzymic regulation hold the key? *Trends Biotechnol.* <https://doi.org/10.1016/j.tibtech.2009.03.009>
- Rieger, L., Alex, J., Winkler, S., Boehler, M., Thomann, M., Siegrist, H., 2003. Progress in sensor technology--progress in process control? Part 1: sensor property investigation and classification. *Water Sci. Technol.* 47, 103–12.
- Rodriguez-Caballero, A., Aymerich, I., Marques, R., Poch, M., Pijuan, M., 2015. Minimizing N<sub>2</sub>O emissions and carbon footprint on a full-scale activated sludge sequencing batch reactor. *Water Res.* 71, 1–10. <https://doi.org/10.1016/j.watres.2014.12.032>
- Rodriguez-Caballero, A., Aymerich, I., Poch, M., Pijuan, M., 2014. Evaluation of process conditions triggering emissions of green-house gases from a biological wastewater treatment system. *Sci. Total Environ.* 493, 384–391. <https://doi.org/10.1016/j.scitotenv.2014.06.015>
- Saltelli, A., Ratto, M., Andres, T., Campolongo, F., Cariboni, J., Gatelli, D., Saisana, M., Tarantola, S., 2008. *Global Sensitivity Analysis: The Primer*, International Statistical Review. [https://doi.org/10.1111/j.1751-5823.2008.00062\\_17.x](https://doi.org/10.1111/j.1751-5823.2008.00062_17.x)
- Saltelli, A., Ratto, M., Tarantola, S., Campolongo, F., 2005. Sensitivity analysis for chemical models. *Chem. Rev.* 105, 2811–2827. <https://doi.org/10.1021/cr040659d>
- Saltelli, A., Ratto, M., Tarantola, S., Campolongo, F., 2004. Sensitivity analysis practice: A guide to scientific models, *Reliability Engineering and System Safety.* <https://doi.org/10.1016/j.ress.2005.11.014>
- Santín, I., Barbu, M., Pedret, C., Vilanova, R., 2018. Fuzzy logic for plant-wide control of biological wastewater treatment process including greenhouse gas emissions. *ISA Trans.* 77, 146–166. <https://doi.org/10.1016/j.isatra.2018.04.006>
- Santín, I., Barbu, M., Pedret, C., Vilanova, R., 2017. Control strategies for nitrous oxide emissions reduction on wastewater treatment plants operation. *Water Res.* 125, 466–477. <https://doi.org/10.1016/j.watres.2017.08.056>
- Seco, A., Ruano, M. V., Ruiz-Martinez, A., Robles, A., Barat, R., Serralta, J., Ferrer, J., 2020. Plant-wide modelling in wastewater treatment: Showcasing experiences using the Biological Nutrient Removal Model. *Water Sci. Technol.* 81, 1700–1714. <https://doi.org/10.2166/wst.2020.056>
- Shu, L., Schneider, P., Jegatheesan, V., Johnson, J., 2006. An economic evaluation of phosphorus recovery as struvite from digester supernatant. *Bioresour. Technol.* 97, 2211–2216. <https://doi.org/10.1016/j.biortech.2005.11.005>
- Slikers, A.O., Derwort, N., Gomez, J.L.C., Strous, M., Kuenen, J.G., Jetten, M.S.M., 2002. Completely autotrophic nitrogen removal over nitrite in one single reactor. *Water Res.* 36, 2475–2482. [https://doi.org/10.1016/S0043-1354\(01\)00476-6](https://doi.org/10.1016/S0043-1354(01)00476-6)
- Soler-Jofra, A., Stevens, B., Hoekstra, M., Picioreanu, C., Sorokin, D., van Loosdrecht, M.C.M., Pérez, J., 2016. Importance of abiotic hydroxylamine conversion on nitrous oxide emissions during nitrification of reject water. *Chem. Eng. J.* 287, 720–726. <https://doi.org/10.1016/j.cej.2015.11.073>

- Solon, K., Flores-Alsina, X., Kazadi Mbamba, C., Ikumi, D., Volcke, E.I.P., Vaneekhaute, C., Ekama, G., Vanrolleghem, P.A., Batstone, D.J., Gernaey, K. V., Jeppsson, U., 2017. Plant-wide modelling of phosphorus transformations in wastewater treatment systems: Impacts of control and operational strategies. *Water Res.* 113, 97–110. <https://doi.org/10.1016/j.watres.2017.02.007>
- Solon, K., Flores-Alsina, X., Mbamba, C.K., Volcke, E.I.P., Tait, S., Batstone, D., Gernaey, K. V., Jeppsson, U., 2015. Effects of ionic strength and ion pairing on (plant-wide) modelling of anaerobic digestion. *Water Res.* 70, 235–245. <https://doi.org/10.1016/j.watres.2014.11.035>
- Stare, A., Vrečko, D., Hvala, N., Strmčnik, S., 2007. Comparison of control strategies for nitrogen removal in an activated sludge process in terms of operating costs: A simulation study. *Water Res.* 41, 2004–2014. <https://doi.org/10.1016/j.watres.2007.01.029>
- Stumm, W., Morgan, J.J., 1996. *Aquatic Chemistry: Chemical Equilibria and Rates in Natural Waters*, 3rd ed. John Wiley and Sons, New York, NY, USA.
- Su, Q., Domingo-Félez, C., Zhang, Z., Blum, J.M., Jensen, M.M., Smets, B.F., 2019. The effect of pH on N<sub>2</sub>O production in intermittently-fed nitrification reactors. *Water Res.* 156, 223–231. <https://doi.org/10.1016/j.watres.2019.03.015>
- Sweetapple, C., Fu, G., Butler, D., 2015. Does carbon reduction increase sustainability? A study in wastewater treatment. *Water Res.* 87, 522–530. <https://doi.org/10.1016/j.watres.2015.06.047>
- Sweetapple, C., Fu, G., Butler, D., 2014. Multi-objective optimisation of wastewater treatment plant control to reduce greenhouse gas emissions. *Water Res.* 55, 52–62. <https://doi.org/10.1016/j.watres.2014.02.018>
- Takács, I., Patry, G.G., Nolasco, D., 1991. A dynamic model of the clarification-thickening process. *Water Res.* 25, 1263–1271. [https://doi.org/10.1016/0043-1354\(91\)90066-Y](https://doi.org/10.1016/0043-1354(91)90066-Y)
- Tallec, G., Garnier, J., Billen, G., Gossais, M., 2006. Nitrous oxide emissions from secondary activated sludge in nitrifying conditions of urban wastewater treatment plants: Effect of oxygenation level. *Water Res.* 40, 2972–2980. <https://doi.org/10.1016/j.watres.2006.05.037>
- Torà, J. a, Lafuente, F.J., Baeza, J.A., Carrera, J., 2010. Combined effect of inorganic carbon limitation and inhibition by free ammonia and free nitrous acid on ammonia oxidizing bacteria. *Bioresour. Technol.* 101, 6051–8. <https://doi.org/10.1016/j.biortech.2010.03.005>
- Valverde-Pérez, B., Ramin, E., Smets, B.F., Plósz, B.G., 2015. EBP2R - An innovative enhanced biological nutrient recovery activated sludge system to produce growth medium for green microalgae cultivation. *Water Res.* 68, 821–830. <https://doi.org/10.1016/j.watres.2014.09.027>
- Van Loosdrecht, M.C.M., Brdjanovic, D., 2014. Anticipating the next century of wastewater treatment. *Science (80-. )*. 344, 1452–1453. <https://doi.org/10.1126/science.1255183>
- Vaneekhaute, C., Claeys, F.H.A., Tack, F.M.G., Meers, E., Belia, E., Vanrolleghem, P.A., 2018. Development, implementation, and validation of a generic nutrient recovery model (NRM) library. *Environ. Model. Softw.* 99, 170–209. <https://doi.org/10.1016/j.envsoft.2017.09.002>
- Vanrolleghem, P.A., Corominas, L., Flores-Alsina, X., 2010. Real-Time Control and Effluent Ammonia Violations Induced by Return Liquor Overloads. *Proc. Water Environ. Fed.* 2010, 7101–7108. <https://doi.org/10.2175/193864710798207503>
- Vanrolleghem, P.A., Insel, G., Petersen, B., Sin, G., De Pauw, D., Nopens, I., Dovermann, H., Weijers, S., Gernaey, K., 2003. A comprehensive model calibration procedure for Activated Sludge Models, in: *WEFTEC 76th Annual Technical Exhibition and Conference*, October 11-15. Los Angeles, California.

- Wang, D., Li, X., Yang, Q., Zheng, W., Wu, Y., Zeng, T., Zeng, G., 2012. Improved biological phosphorus removal performance driven by the aerobic/extended-idle regime with propionate as the sole carbon source. *Water Res.* 46, 3868–3878. <https://doi.org/10.1016/j.watres.2012.04.036>
- Wentzel, M.C., Ekama, G.A., Sötemann, S.W., 2006. Mass balance-based plant-wide wastewater treatment plant models - Part 1: Biodegradability of wastewater organics under anaerobic conditions. *Water SA* 32, 269–275. <https://doi.org/10.4314/wsa.v32i3.5261>
- Wett, B., Rauch, W., 2003. The role of inorganic carbon limitation in biological nitrogen removal of extremely ammonia concentrated wastewater. *Water Res.* 37, 1100–1110.
- Wunderlin, P., Lehmann, M.F., Siegrist, H., Tuzson, B., Joss, A., Emmenegger, L., Mohn, J., 2013. Isotope signatures of N<sub>2</sub>O in a mixed microbial population system: Constraints on N<sub>2</sub>O producing pathways in wastewater treatment. *Environ. Sci. Technol.* 47, 1339–1348. <https://doi.org/10.1021/es303174x>
- Wunderlin, P., Mohn, J., Joss, A., Emmenegger, L., Siegrist, H., 2012. Mechanisms of N<sub>2</sub>O production in biological wastewater treatment under nitrifying and denitrifying conditions. *Water Res.* 46, 1027–1037. <https://doi.org/10.1016/j.watres.2011.11.080>
- WWAP, 2017. The United Nations World Water Development Report 2017. Wastewater: The Untapped Resource. Paris, UNESCO.
- Yu, R., Kampschreur, M.J., van Loosdrecht, M.C.M., Chandran, K., 2010. Mechanisms and Specific Directionality of Autotrophic Nitrous Oxide and Nitric Oxide Generation during Transient Anoxia. *Environ. Sci. Technol.* 44, 1313–1319.
- Zhang, W., Wang, D., Jin, Y., 2018. Effects of inorganic carbon on the nitrous oxide emissions and microbial diversity of an anaerobic ammonia oxidation reactor. *Bioresour. Technol.* 250, 124–130. <https://doi.org/10.1016/j.biortech.2017.11.027>
- Zumft, W.G., 1997. Cell biology and molecular basis of denitrification. *Microbiol. Mol. Biol. Rev.* 61, 533–616. <https://doi.org/10.1128/61.4.533-616.1997>

# **Annex**

---



### Annex I: ASM2d-N<sub>2</sub>O model description

This annex section shows the ASM2d-N<sub>2</sub>O model description. A detailed description of the model can be found in the original publication (Massara et al., 2018). Table A1.1 shows the state variables. Table A1.2 shows all the parameters involved in ASM2d-N<sub>2</sub>O, with the updated calibrated parameters obtained in Chapter III. The kinetic rates expressions are shown in Table A1.3. Finally, the ASM2d-N<sub>2</sub>O stoichiometry is shown in Table A1.4 to Table A1.9.

Table A1.1. State variables of the ASM2d-N<sub>2</sub>O.

State variable	Units	Description
S <sub>O2</sub>	g O <sub>2</sub> m <sup>-3</sup>	Dissolved Oxygen
S <sub>F</sub>	g COD m <sup>-3</sup>	Readily biodegradable substrate
S <sub>A</sub>	g COD m <sup>-3</sup>	Fermentation product
S <sub>NH4</sub>	g N m <sup>-3</sup>	Ammonium nitrogen
S <sub>NH2OH</sub>	g N m <sup>-3</sup>	Hydroxylamine nitrogen
S <sub>N2O</sub>	g N m <sup>-3</sup>	Nitrous oxide nitrogen
S <sub>NO</sub>	g N m <sup>-3</sup>	Nitric oxide nitrogen
S <sub>NO2</sub>	g N m <sup>-3</sup>	Nitrite nitrogen
S <sub>NO3</sub>	g N m <sup>-3</sup>	Nitrate nitrogen
S <sub>PO4</sub>	g P m <sup>-3</sup>	Orthophosphate phosphorus
S <sub>I</sub>	g COD m <sup>-3</sup>	Inert, non-biodegradable soluble organic compounds
S <sub>ALK</sub>	mol HCO <sub>3</sub> <sup>-</sup> m <sup>-3</sup>	Alkalinity
S <sub>N2</sub>	g N m <sup>-3</sup>	Nitrogen gas
X <sub>I</sub>	g COD m <sup>-3</sup>	Inert, non-biodegradable particulate organic compounds
X <sub>S</sub>	g COD m <sup>-3</sup>	Slowly biodegradable substrates
X <sub>H</sub>	g COD m <sup>-3</sup>	Heterotrophic biomass
X <sub>PAO</sub>	g COD m <sup>-3</sup>	Polyphosphate accumulating organisms, PAO
X <sub>PP</sub>	g P m <sup>-3</sup>	Stored polyphosphate of PAO
X <sub>PHA</sub>	g COD m <sup>-3</sup>	Stored poly-hydroxyalkanoates of PAO
X <sub>AOB</sub>	g COD m <sup>-3</sup>	Ammonia oxidizing bacteria, AOB
X <sub>NOB</sub>	g COD m <sup>-3</sup>	Nitrite oxidizing bacteria, NOB
X <sub>TSS</sub>	g TSS m <sup>-3</sup>	Total Suspended Solids, TSS
X <sub>MeOH</sub>	g Fe(OH) <sub>3</sub> m <sup>-3</sup>	Ferric Hydroxide
X <sub>MeP</sub>	g FePO <sub>4</sub> m <sup>-3</sup>	Ferric Phosphate

Table A1.2. Kinetic and stoichiometric parameters of ASM2d-N<sub>2</sub>O.

<b>Symbol</b>	<b>Value</b>	<b>Units</b>	<b>Description</b>	<b>Reference</b>
<b>Stoichiometric Parameters and conversion factors</b>				
Y <sub>H</sub>	0.625	g COD (g COD) <sup>-1</sup>	Yield coefficient for heterotrophic organisms	(Henze et al., 2000)
Y <sub>PHA</sub>	0.2	g COD (g P) <sup>-1</sup>	Polyhydroxyalkanoate (PHA) requirement for Polyphosphate (PP) storage	(Henze et al., 2000)
Y <sub>PAO</sub>	0.625	g COD (g COD) <sup>-1</sup>	Yield coefficient for PAO	(Henze et al., 2000)
Y <sub>PO4</sub>	0.4	g P (g COD) <sup>-1</sup>	PP requirement (PO <sub>4</sub> release) per PHA stored	(Henze et al., 2000)
Y <sub>AOB</sub>	0.18	g COD (g COD) <sup>-1</sup>	Yield coefficient for the Ammonia Oxidizing Bacteria (AOB)	(Jubany et al., 2008)
Y <sub>NOB</sub>	0.08	g COD (g COD) <sup>-1</sup>	Yield coefficient for the Nitrite Oxidizing Bacteria (NOB)	(Jubany et al., 2008)
f <sub>SI</sub>	0	g COD (g COD) <sup>-1</sup>	Production of S <sub>I</sub> in hydrolysis	(Henze et al., 2000)
f <sub>XI</sub>	0.1	g COD (g COD) <sup>-1</sup>	Fraction of X <sub>I</sub> generated in biomass lysis	(Henze et al., 2000)
n <sub>G</sub>	1	dimensionless	Anoxic growth factor	(W C Hiatt and Grady, 2008)
i <sub>N,SI</sub>	0.01	g N (g COD) <sup>-1</sup>	N content of inert soluble COD S <sub>I</sub>	(Henze et al., 2000)
i <sub>N,SF</sub>	0.03	g N (g COD) <sup>-1</sup>	N content of fermentable substrates S <sub>F</sub>	(Henze et al., 2000)
i <sub>N,XI</sub>	0.02	g N (g COD) <sup>-1</sup>	N content of inert particulate COD X <sub>I</sub>	(Henze et al., 2000)
i <sub>N,XS</sub>	0.04	g N (g COD) <sup>-1</sup>	N content of slowly biodegradable substrate X <sub>S</sub>	(Henze et al., 2000)
i <sub>N,BM</sub>	0.07	g N (g COD) <sup>-1</sup>	N content of biomass	(Henze et al., 2000)
i <sub>P,SI</sub>	0	g P (g COD) <sup>-1</sup>	P content of inert soluble COD S <sub>I</sub>	(Henze et al., 2000)
i <sub>P,SF</sub>	0.01	g P (g COD) <sup>-1</sup>	P content of fermentable substrates S <sub>F</sub>	(Henze et al., 2000)
i <sub>P,XI</sub>	0.01	g P (g COD) <sup>-1</sup>	P content of inert particulate COD X <sub>I</sub>	(Henze et al., 2000)
i <sub>P,XS</sub>	0.01	g P (g COD) <sup>-1</sup>	P content of slowly biodegradable substrate X <sub>S</sub>	(Henze et al., 2000)
i <sub>P,BM</sub>	0.02	g P (g COD) <sup>-1</sup>	P content of biomass	(Henze et al., 2000)
i <sub>TSS,XI</sub>	0.75	g TSS (g COD) <sup>-1</sup>	TSS to COD ratio for X <sub>I</sub>	(Henze et al., 2000)
i <sub>TSS,XS</sub>	0.75	g TSS (g COD) <sup>-1</sup>	TSS to COD ratio for X <sub>S</sub>	(Henze et al., 2000)
i <sub>TSS,BM</sub>	0.9	g TSS (g COD) <sup>-1</sup>	TSS to COD ratio for biomass	(Henze et al., 2000)
<b>Hydrolysis processes</b>				
K <sub>O<sub>2</sub>,H</sub>	0.2	g O <sub>2</sub> m <sup>-3</sup>	Saturation/inhibition coefficient for O <sub>2</sub>	(Henze et al., 2000)
K <sub>X,H</sub>	0.1	g X <sub>S</sub> (g X <sub>H</sub> ) <sup>-1</sup>	Saturation coefficient for particulate COD	(Henze et al., 2000)

Symbol	Value	Units	Description	Reference
$\mu_{NO_3\_H}$	0.6	Dimensionless	Anoxic hydrolysis reduction factor	(Henze et al., 2000)
$\mu_{NO_2\_H}$	0.6	Dimensionless	Anoxic hydrolysis reduction factor	(Massara et al., 2018)
$K_{NO_3\_H}$	0.5	$g\ N\ m^{-3}$	Saturation/inhibition coefficient for $NO_3^-$	(Henze et al., 2000)
$K_{NO_2\_H}$	0.5	$g\ N\ m^{-3}$	Saturation/inhibition coefficient for $NO_2^-$	(Massara et al., 2018)
$\mu_{Fe\_H}$	0.4	Dimensionless	Anaerobic hydrolysis reduction factor	(Henze et al., 2000)
<b>Heterotrophic biomass, <math>X_H</math></b>				
$\mu_H$	6	$g\ X_H\ (g\ X_H)^{-1}d^{-1}$	Maximum growth rate on substrate	(Henze et al., 2000)
$K_{O_2}$	0.2	$g\ O_2\ m^{-3}$	Saturation/inhibition coefficient for $O_2$	(Henze et al., 2000)
$K_F$	4	$g\ COD\ m^{-3}$	Saturation coefficient for growth on $S_F$	(Henze et al., 2000)
$K_{NH_4}$	0.05	$g\ N\ m^{-3}$	Saturation coefficient for $NH_4^+$ (nutrient)	(Henze et al., 2000)
$K_P$	0.01	$g\ P\ m^{-3}$	Saturation coefficient for $PO_4^{3-}$ (nutrient)	(Henze et al., 2000)
$K_{ALK}$	0.1	$mole\ HCO_3^-\ m^{-3}$	Saturation coefficient for alkalinity ( $HCO_3^-$ )	(Henze et al., 2000)
$K_A$	4	$g\ COD\ m^{-3}$	Saturation coefficient for growth on acetate $S_A$	(Henze et al., 2000)
$K_{NO_3}$	0.5	$g\ N\ m^{-3}$	Saturation/inhibition coefficient for $NO_3^-$	(Henze et al., 2000)
$K_{NO_2}$	0.5	$g\ N\ m^{-3}$	Saturation/inhibition coefficient for $NO_2^-$	(Massara et al., 2018)
$\mu_{NO_3\_D}$	0.8	Dimensionless	Reduction factor for denitrification	(Henze et al., 2000)
$q_{Fe}$	3	$g\ S_F\ (g\ X_H)^{-1}d^{-1}$	Maximum rate for fermentation	(Henze et al., 2000)
$K_{Fe\_H}$	4	$g\ COD\ m^{-3}$	Saturation coefficient for fermentation of $S_F$	(Henze et al., 2000)
$b_H$	0.4	$d^{-1}$	Rate constant for lysis and decay	(Henze et al., 2000)
$\mu_{G3}$	0.16	Dimensionless	Anoxic growth factor ( $NO_2^- \rightarrow NO$ )	(W C Hiatt and Grady, 2008)
$\mu_{G4}$	0.35	Dimensionless	Anoxic growth factor ( $NO \rightarrow N_2O$ )	(W C Hiatt and Grady, 2008)
$\mu_{G5}$	0.35	Dimensionless	Anoxic growth factor ( $N_2O \rightarrow N_2$ )	(W C Hiatt and Grady, 2008)
$K_{S3}$	20	$mg\ COD\ L^{-1}$	Half-saturation coefficient for substrate	(W C Hiatt and Grady, 2008)
$K_{S4}$	20	$mg\ COD\ L^{-1}$	Half-saturation coefficient for substrate	(W C Hiatt and Grady, 2008)
$K_{S5}$	40	$mg\ COD\ L^{-1}$	Half-saturation coefficient for substrate	(W C Hiatt and Grady, 2008)
$K_{NO_2\_Den}$	0.2	$mg\ N\ L^{-1}$	Half-saturation coefficient for $NO_2-N$	(W C Hiatt and Grady, 2008)
$K_{OH4}$	0.1	$mg\ O_2\ L^{-1}$	Half-saturation coefficient for $O_2$	(W C Hiatt and Grady, 2008)



Symbol	Value	Units	Description	Reference
K <sub>N2O_Den</sub>	0.05	mg N L <sup>-1</sup>	Half-saturation coefficient for N <sub>2</sub> O-N	(W C Hiatt and Grady, 2008)
K <sub>O<sub>2</sub>H</sub>	0.1	mg O <sub>2</sub> L <sup>-1</sup>	Half-saturation coefficient for O <sub>2</sub>	(W C Hiatt and Grady, 2008)
K <sub>NO_Den</sub>	0.05	mg N L <sup>-1</sup>	Half-saturation coefficient for NO-N	(W C Hiatt and Grady, 2008)
K <sub>O<sub>2</sub>H</sub>	0.1	mg O <sub>2</sub> L <sup>-1</sup>	Half-saturation coefficient for O <sub>2</sub>	(W C Hiatt and Grady, 2008)
K <sub>I3NO</sub>	0.5	mg N L <sup>-1</sup>	NO inhibition coefficient (NO <sub>2</sub> <sup>-</sup> →NO)	(W C Hiatt and Grady, 2008)
K <sub>I4NO</sub>	0.3	mg N L <sup>-1</sup>	NO inhibition coefficient (NO→N <sub>2</sub> O)	(W C Hiatt and Grady, 2008)
K <sub>I5NO</sub>	0.075	mg N L <sup>-1</sup>	NO inhibition coefficient (N <sub>2</sub> O→N <sub>2</sub> )	(W C Hiatt and Grady, 2008)
<b>Phosphorus Accumulating Organisms, X<sub>PAO</sub></b>				
K <sub>A_P</sub>	4	g COD m <sup>-3</sup>	Saturation coefficient for growth on acetate S <sub>A</sub>	(Henze et al., 2000)
K <sub>ALK_P</sub>	0.1	mole HCO <sub>3</sub> <sup>-</sup> m <sup>-3</sup>	Saturation coefficient for alkalinity (HCO <sub>3</sub> <sup>-</sup> )	(Henze et al., 2000)
q <sub>PP</sub>	1.5	g X <sub>PP</sub> (g X <sub>PAO</sub> ) <sup>-1</sup> d <sup>-1</sup>	Rate constant for storage of X <sub>PP</sub>	(Henze et al., 2000)
K <sub>O<sub>2</sub>_P</sub>	0.2	g O <sub>2</sub> m <sup>-3</sup>	Saturation/inhibition coefficient for O <sub>2</sub>	(Henze et al., 2000)
K <sub>P_P</sub>	0.2	g P m <sup>-3</sup>	Saturation coefficient for P in storage of PP	(Henze et al., 2000)
K <sub>PHA_P</sub>	0.01	g X <sub>PHA</sub> (g X <sub>PAO</sub> ) <sup>-1</sup>	Saturation coefficient for PHA	(Henze et al., 2000)
K <sub>MAX_P</sub>	0.34	g X <sub>PP</sub> (g X <sub>PAO</sub> ) <sup>-1</sup>	Maximum ratio of X <sub>PP</sub> /X <sub>PAO</sub>	(Henze et al., 2000)
K <sub>PP_P</sub>	0.01	g X <sub>PP</sub> (g X <sub>PAO</sub> ) <sup>-1</sup>	Saturation coefficient for PP	(Henze et al., 2000)
K <sub>I<sub>PP</sub>_P</sub>	0.02	g X <sub>PP</sub> (g X <sub>PAO</sub> ) <sup>-1</sup>	Inhibition coefficient for PP storage	(Henze et al., 2000)
K <sub>PO<sub>4</sub>_P</sub>	0.01	g P m <sup>-3</sup>	Saturation coefficient for PO <sub>4</sub> <sup>3-</sup>	(Henze et al., 2000)
r <sub>NO<sub>3</sub>_P</sub>	0.6	Dimensionless	Anoxic hydrolysis reduction factor	(Henze et al., 2000)
r <sub>NO<sub>2</sub>_P</sub>	0.6	Dimensionless	Anoxic hydrolysis reduction factor	(Massara et al., 2018)
K <sub>NO<sub>3</sub>_P</sub>	0.5	g N m <sup>-3</sup>	Saturation/inhibition coefficient for NO <sub>3</sub> <sup>-</sup>	(Henze et al., 2000)
K <sub>NO<sub>2</sub>_P</sub>	0.5	g N m <sup>-3</sup>	Saturation/inhibition coefficient for NO <sub>2</sub> <sup>-</sup>	(Massara et al., 2018)
μ <sub>PAO</sub>	1	d <sup>-1</sup>	Maximum growth rate of PAO	(Henze et al., 2000)
b <sub>PAO</sub>	0.2	d <sup>-1</sup>	Rate for lysis of X <sub>PAO</sub>	(Henze et al., 2000)
b <sub>PP</sub>	0.2	d <sup>-1</sup>	Rate for lysis of X <sub>PP</sub>	(Henze et al., 2000)
b <sub>PHA</sub>	0.2	d <sup>-1</sup>	Rate for lysis of X <sub>PHA</sub>	(Henze et al., 2000)
<b>Nitrifying organisms, X<sub>AOB</sub> and X<sub>NOB</sub></b>				

Symbol	Value	Units	Description	Reference
$q_{AOB\_AMO}$	5.2008	$\text{g N (g COD)}^{-1} \text{d}^{-1}$	Maximum rate for the AMO reaction	(Pocquet et al., 2016)
$K_{O2\_AOB1}$	1	$\text{g O}_2 \text{m}^{-3}$	AOB affinity constant for $\text{O}_2$ (AMO reaction)	(Pocquet et al., 2016)
$K_{NH4\_AOB}$	0.2	$\text{g N m}^{-3}$	AOB affinity constant for $\text{NH}_4^+$	(Pocquet et al., 2016)
$K_{O2\_AOB2}$	0.6	$\text{g O}_2 \text{m}^{-3}$	AOB affinity constant for $\text{O}_2$ (HAO reaction)	(Pocquet et al., 2016)
$K_{NH2OH\_AOB}$	0.3	$\text{g N m}^{-3}$	AOB affinity constant for $\text{NH}_2\text{OH}$	(Domingo-Félez et al., 2017)
$q_{AOB\_HAO}$	5.2008	$\text{g N (g COD)}^{-1} \text{d}^{-1}$	Maximum rate for HAO reaction	(Pocquet et al., 2016)
$K_{NO\_AOB\_HAO}$	0.0003	$\text{g N m}^{-3}$	AOB affinity constant for NO (from HAO)	(Pocquet et al., 2016)
$q_{AOB\_N2O\_NN}$	0.0078	$\text{g N (g COD)}^{-1} \text{d}^{-1}$	Maximum $\text{N}_2\text{O}$ production rate by $\text{NH}_2\text{OH}$ oxidation pathway	(Pocquet et al., 2016)
$K_{NO\_AOB\_NN}$	0.008	$\text{g N m}^{-3}$	AOB affinity constant for NO (from NirK)	(Pocquet et al., 2016)
$K_{O2\_AOB\_ND}$	0.5	$\text{g O}_2 \text{m}^{-3}$	AOB constant for $\text{O}_2$ effect on the nitrifier denitrification pathway	(Pocquet et al., 2016)
$K_{I\_O2\_AOB}$	0.8	$\text{g O}_2 \text{m}^{-3}$	$\text{N}_2\text{O}$ constant for production inhibition by $\text{O}_2$	(Pocquet et al., 2016)
$K_{HNO2\_AOB}$	0.004	$\text{g N m}^{-3}$	AOB affinity constant for $\text{HNO}_2$	(Pocquet et al., 2016)
$q_{AOB\_N2O\_ND}$	1.3008	$\text{g N (g COD)}^{-1} \text{d}^{-1}$	Maximum $\text{N}_2\text{O}$ production rate by the nitrifier denitrification pathway	(Pocquet et al., 2016)
$K_{ALK\_AOB}$	0.1	$\text{mole HCO}_3^- \text{m}^{-3}$	Saturation coefficient for alkalinity ( $\text{HCO}_3^-$ )	Current study
$K_{P\_AOB}$	0.01	$\text{g P m}^{-3}$	Saturation coefficient for $\text{PO}_4^{3-}$ (nutrient)	(Massara et al., 2018)
$\mu_{NOB}$	0.67	$\text{d}^{-1}$	Maximum NOB growth rate	Current study
$K_{O2\_NOB}$	0.13	$\text{g O}_2 \text{m}^{-3}$	Half-saturation coefficient for $\text{O}_2$	Current study
$K_{ALK\_NOB}$	0.1	$\text{mole HCO}_3^- \text{m}^{-3}$	Saturation coefficient for alkalinity ( $\text{HCO}_3^-$ )	(Massara et al., 2018)
$K_{NO2\_NOB}$	0.13	$\text{g N m}^{-3}$	Saturation coefficient for $\text{NO}_2^-$	Current study
$K_{P\_NOB}$	0.01	$\text{g P m}^{-3}$	Saturation coefficient for $\text{PO}_4^{3-}$ (nutrient)	(Massara et al., 2018)
$b_{AOB}$	0.096	$\text{d}^{-1}$	Decay rate of AOB	(W C Hiatt and Grady, 2008)
$b_{NOB}$	0.096	$\text{d}^{-1}$	Decay rate of NOB	(W C Hiatt and Grady, 2008)
<b>Precipitation of P with Fe(OH)<sub>3</sub></b>				
$k_{RED}$	0.6	$\text{d}^{-1}$	Rate constant for redissolution	(Henze et al., 2000)
$K_{ALK\_PR}$	0.5	$\text{mole HCO}_3^- \text{m}^{-3}$	Saturation coefficient for alkalinity ( $\text{HCO}_3^-$ )	(Henze et al., 2000)
<b>Temperature related parameters: <math>\theta_1 = a_i^{(T_{\text{temperature}} - 20)}</math></b>				
$a_i$	1	Dimensionless	Chemical precipitation processes (no Temp. dependency)	(Henze et al., 2000)

Symbol	Value	Units	Description	Reference
a <sub>2</sub>	1.04	Dimensionless	Hydrolysis processes and PAO (low Temp. dependency)	(Henze et al., 2000)
a <sub>3</sub>	1.07	Dimensionless	Heterotrophic organisms and fermentation (medium Temp. dependency)	(Henze et al., 2000)
a <sub>4</sub>	1.11	Dimensionless	Nitrifying organisms (high Temp. dependency)	(Henze et al., 2000)

Table A1.3. Kinetic rates expressions of the ASM2d-N<sub>2</sub>O. Extracted from Massara et al., (2018).

j	Process	Reaction Rate [d <sup>-1</sup> ]
<b>Hydrolysis processes</b>		
1	Aerobic hydrolysis	$K_H \cdot \frac{S_{O_2}}{K_{O_2,H} + S_{O_2}} \cdot \frac{X_S/X_H}{K_{X,H} + X_S/X_H} \cdot X_H \cdot \theta_2$
2	Anoxic hydrolysis (NO <sub>3</sub> <sup>-</sup> )	$\eta_{NO_3,H} \cdot K_H \cdot \frac{K_{O_2,H}}{K_{O_2,H} + S_{O_2}} \cdot \frac{S_{NO_3}}{K_{NO_3,H} + S_{NO_3}} \cdot \frac{X_S/X_H}{K_{X,H} + X_S/X_H} \cdot X_H \cdot \theta_2$
3	Anoxic hydrolysis (NO <sub>2</sub> <sup>-</sup> )	$\eta_{NO_2,H} \cdot K_H \cdot \frac{K_{O_2,H}}{K_{O_2,H} + S_{O_2}} \cdot \frac{S_{NO_2}}{K_{NO_2,H} + S_{NO_2}} \cdot \frac{X_S/X_H}{K_{X,H} + X_S/X_H} \cdot X_H \cdot \theta_2$
4	Anaerobic hydrolysis	$\eta_{Fe,H} \cdot K_H \cdot \frac{K_{O_2,H}}{K_{O_2,H} + S_{O_2}} \cdot \frac{K_{NO_2,H}}{K_{NO_2,H} + (S_{NO_2} + S_{NO_3})} \cdot \frac{X_S/X_H}{K_{X,H} + X_S/X_H} \cdot X_H \cdot \theta_2$
<b>Heterotrophs Organisms</b>		
5	Aerobic growth on S <sub>F</sub>	$\mu_H \cdot \frac{S_F}{K_F + S_F} \cdot \frac{S_A + S_F}{S_A + S_F} \cdot \frac{S_{O_2}}{K_{O_2} + S_{O_2}} \cdot \frac{S_{NH_4}}{K_{NH_4} + S_{NH_4}} \cdot \frac{S_{PO_4}}{K_{PO_4} + S_{PO_4}} \cdot \frac{S_{ALK}}{K_{ALK} + S_{ALK}} \cdot X_H \cdot \theta_3$
6	Aerobic growth on S <sub>A</sub>	$\mu_H \cdot \frac{S_A}{K_A + S_A} \cdot \frac{S_A}{S_A + S_F} \cdot \frac{S_{O_2}}{K_{O_2} + S_{O_2}} \cdot \frac{S_{NH_4}}{K_{NH_4} + S_{NH_4}} \cdot \frac{S_{PO_4}}{K_{PO_4} + S_{PO_4}} \cdot \frac{S_{ALK}}{K_{ALK} + S_{ALK}} \cdot X_H \cdot \theta_3$
7	Anoxic growth on S <sub>F</sub> (Denitrification NO <sub>3</sub> <sup>-</sup> - NO <sub>2</sub> <sup>-</sup> )	$\eta_{NO_3,D} \cdot \mu_H \cdot \frac{S_F}{K_F + S_F} \cdot \frac{S_F}{S_A + S_F} \cdot \frac{K_{O_2}}{K_{O_2} + S_{O_2}} \cdot \frac{S_{NO_3}}{K_{NO_3} + S_{NO_3}} \cdot \frac{S_{NH_4}}{K_{NH_4} + S_{NH_4}} \cdot \frac{S_{PO_4}}{K_{PO_4} + S_{PO_4}} \cdot \frac{S_{ALK}}{K_{ALK} + S_{ALK}} \cdot X_H \cdot \theta_3$
8	Anoxic growth on S <sub>F</sub> (Denitrification NO <sub>2</sub> <sup>-</sup> - NO)	$\eta_{G3} \cdot \mu_H \cdot \frac{S_F}{K_{S3} + S_F} \cdot \frac{S_F}{S_A + S_F} \cdot \frac{S_{NO_2}}{K_{NO_2,Den} + S_{NO_2}} \cdot \frac{K_{OH3}}{K_{OH3} + S_{O_2}} \cdot \frac{S_{NH_4}}{K_{NH_4} + S_{NH_4}} \cdot \frac{S_{PO_4}}{K_{PO_4} + S_{PO_4}} \cdot \frac{S_{ALK}}{K_{ALK} + S_{ALK}} \cdot X_H \cdot \theta_3$
9	Anoxic growth on S <sub>F</sub> (Denitrification NO - N <sub>2</sub> O)	$\eta_{G4} \cdot \mu_H \cdot \frac{S_F}{K_{S4} + S_F} \cdot \frac{S_F}{S_A + S_F} \cdot \frac{S_{NO}}{K_{NO,Den} + S_{NO} + S_{NO}^2/K_{I4NO}} \cdot \frac{K_{OH4}}{K_{OH4} + S_{O_2}} \cdot \frac{S_{NH_4}}{K_{NH_4} + S_{NH_4}} \cdot \frac{S_{PO_4}}{K_{PO_4} + S_{PO_4}} \cdot \frac{S_{ALK}}{K_{ALK} + S_{ALK}} \cdot X_H \cdot \theta_3$

j	Process	Reaction Rate [d <sup>-1</sup> ]
10	Anoxic growth on S <sub>F</sub> (Denitrification N <sub>2</sub> O - N <sub>2</sub> )	$\eta_{G5} \cdot \mu_H \cdot \frac{S_F}{K_{S5} + S_F} \cdot \frac{S_A}{K_A + S_A} \cdot \frac{S_{N_2O}}{K_{N_2O,Den} + S_{N_2O}} \cdot \frac{K_{OH5}}{K_{OH5} + S_{O_2}} \cdot \frac{S_{NH_4}}{K_{NH_4} + S_{NH_4}} \cdot \frac{S_{PO_4}}{K_{PO_4} + S_{PO_4}} \cdot \frac{S_{SALK}}{K_{ALK} + S_{ALK}} \cdot X_H \cdot \theta_3$
11	Anoxic growth on S <sub>A</sub> (Denitrification NO <sub>3</sub> <sup>-</sup> - NO <sub>2</sub> <sup>-</sup> )	$\eta_{NO_3,D} \cdot \mu_H \cdot \frac{S_A}{K_A + S_A} \cdot \frac{S_A}{S_A + S_F} \cdot \frac{K_{O_2}}{K_{O_2} + S_{O_2}} \cdot \frac{S_{NO_3}}{K_{NO_3} + S_{NO_3}} \cdot \frac{S_{NH_4}}{K_{NH_4} + S_{NH_4}} \cdot \frac{S_{PO_4}}{K_{PO_4} + S_{PO_4}} \cdot \frac{S_{SALK}}{K_{ALK} + S_{ALK}} \cdot X_H \cdot \theta_3$
12	Anoxic growth on S <sub>A</sub> (Denitrification NO <sub>2</sub> - NO)	$\eta_{G3} \cdot \mu_H \cdot \frac{S_A}{K_{S3} + S_A} \cdot \frac{S_A}{S_A + S_F} \cdot \frac{S_{NO_2}}{K_{NO_2,Den} + S_{NO_2}} \cdot \frac{K_{OH3}}{K_{OH3} + S_{O_2}} \cdot \frac{S_{NH_4}}{K_{NH_4} + S_{NH_4}} \cdot \frac{S_{PO_4}}{K_{PO_4} + S_{PO_4}} \cdot \frac{S_{SALK}}{K_{ALK} + S_{ALK}} \cdot X_H \cdot \theta_3$
13	Anoxic growth on S <sub>A</sub> (Denitrification NO - N <sub>2</sub> O)	$\eta_{G4} \cdot \mu_H \cdot \frac{S_A}{K_{S4} + S_A} \cdot \frac{S_A}{S_A + S_F} \cdot \frac{S_{NO}}{K_{NO,Den} + S_{NO} + S_{NO}^2/K_{I4NO}} \cdot \frac{K_{OH4}}{K_{OH4} + S_{O_2}} \cdot \frac{S_{NH_4}}{K_{NH_4} + S_{NH_4}} \cdot \frac{S_{PO_4}}{K_{PO_4} + S_{PO_4}} \cdot \frac{S_{SALK}}{K_{ALK} + S_{ALK}} \cdot X_H \cdot \theta_3$
14	Anoxic growth on S <sub>A</sub> (Denitrification N <sub>2</sub> O - N <sub>2</sub> )	$\eta_{G5} \cdot \mu_H \cdot \frac{S_A}{K_{S5} + S_A} \cdot \frac{S_A}{S_A + S_F} \cdot \frac{S_{N_2O}}{K_{N_2O,Den} + S_{N_2O}} \cdot \frac{K_{OH5}}{K_{OH5} + S_{O_2}} \cdot \frac{S_{NH_4}}{K_{NH_4} + S_{NH_4}} \cdot \frac{S_{PO_4}}{K_{PO_4} + S_{PO_4}} \cdot \frac{S_{SALK}}{K_{ALK} + S_{ALK}} \cdot X_H \cdot \theta_3$
15	Fermentation	$q_{fe} \cdot \frac{K_{O_2}}{K_{O_2} + S_{O_2}} \cdot \frac{K_{NO_2}}{K_{NO_2} + (S_{NO_3} + S_{NO_2})} \cdot \frac{S_F}{K_{Fe,H} + S_F} \cdot \frac{S_{ALK}}{K_{ALK} + S_{ALK}} \cdot X_H \cdot \theta_3$
16	Lysis	$b_H \cdot X_H \cdot \theta_3$
<b>Phosphorus Accumulating Organisms (PAO)</b>		
17	Storage of X <sub>PHA</sub>	$q_{PHA} \cdot \frac{S_A}{K_{A,P} + S_A} \cdot \frac{S_{ALK}}{K_{ALK,P} + S_{ALK}} \cdot \frac{X_{PP}/X_{PAO}}{K_{PP,P} + X_{PP}/X_{PAO}} \cdot X_{PAO} \cdot \theta_2$
18	Aerobic storage of X <sub>PP</sub>	$q_{PP} \cdot \frac{S_{O_2}}{K_{O_2,P} + S_{O_2}} \cdot \frac{S_{PO_4}}{K_{PO_4,P} + S_{PO_4}} \cdot \frac{S_{ALK}}{K_{ALK,P} + S_{ALK}} \cdot \frac{X_{PHA}/X_{PAO}}{K_{PHA,P} + X_{PHA}/X_{PAO}} \cdot \frac{K_{MAX,P} - X_{PP}/X_{PAO}}{K_{IPP,P} + K_{MAX,P} - X_{PP}/X_{PAO}} \cdot X_{PAO} \cdot \theta_2$
19	Anoxic storage of X <sub>PP</sub> (NO <sub>3</sub> <sup>-</sup> - NO <sub>2</sub> <sup>-</sup> )	$\eta_{NO_3,P} \cdot q_{PP} \cdot \frac{S_{NO_3}}{K_{NO_3,P} + S_{NO_3}} \cdot \frac{K_{O_2,P}}{K_{O_2,P} + S_{O_2}} \cdot \frac{S_{PO_4}}{K_{PO_4,P} + S_{PO_4}} \cdot \frac{S_{ALK}}{K_{ALK,P} + S_{ALK}} \cdot \frac{X_{PHA}/X_{PAO}}{K_{PHA,P} + X_{PHA}/X_{PAO}} \cdot \frac{K_{MAX,P} - X_{PP}/X_{PAO}}{K_{IPP,P} + K_{MAX,P} - X_{PP}/X_{PAO}} \cdot X_{PAO} \cdot \theta_2$
20	Anoxic storage of X <sub>PP</sub> (NO <sub>2</sub> <sup>-</sup> - NO)	$\eta_{G3} \cdot q_{PP} \cdot \frac{S_{NO_2}}{K_{NO_2,Den} + S_{NO_2}} \cdot \frac{K_{OH3}}{K_{OH3} + S_{O_2}} \cdot \frac{S_{PO_4}}{K_{PO_4,P} + S_{PO_4}} \cdot \frac{S_{ALK}}{K_{ALK,P} + S_{ALK}} \cdot \frac{X_{PHA}/X_{PAO}}{K_{PHA,P} + X_{PHA}/X_{PAO}} \cdot \frac{K_{MAX,P} - X_{PP}/X_{PAO}}{K_{IPP,P} + K_{MAX,P} - X_{PP}/X_{PAO}} \cdot X_{PAO} \cdot \theta_2$
21	Anoxic storage of X <sub>PP</sub> (NO - N <sub>2</sub> O)	$\eta_{G4} \cdot q_{PP} \cdot \frac{S_{NO}}{K_{NO,Den} + S_{NO} + S_{NO}^2/K_{I4NO}} \cdot \frac{K_{OH4}}{K_{OH4} + S_{O_2}} \cdot \frac{S_{PO_4}}{K_{PO_4,P} + S_{PO_4}} \cdot \frac{S_{ALK}}{K_{ALK,P} + S_{ALK}} \cdot \frac{X_{PHA}/X_{PAO}}{K_{PHA,P} + X_{PHA}/X_{PAO}} \cdot \frac{K_{MAX,P} - X_{PP}/X_{PAO}}{K_{IPP,P} + K_{MAX,P} - X_{PP}/X_{PAO}} \cdot X_{PAO}$
22	Anoxic storage of X <sub>PP</sub> (N <sub>2</sub> O - N <sub>2</sub> )	$\eta_{G5} \cdot q_{PP} \cdot \frac{S_{N_2O}}{K_{N_2O,Den} + S_{N_2O}} \cdot \frac{K_{OH5}}{K_{OH5} + S_{O_2}} \cdot \frac{S_{PO_4}}{K_{PO_4,P} + S_{PO_4}} \cdot \frac{S_{ALK}}{K_{ALK,P} + S_{ALK}} \cdot \frac{X_{PHA}/X_{PAO}}{K_{PHA,P} + X_{PHA}/X_{PAO}} \cdot \frac{K_{MAX,P} - X_{PP}/X_{PAO}}{K_{IPP,P} + K_{MAX,P} - X_{PP}/X_{PAO}} \cdot X_{PAO} \cdot \theta_2$

j	Process	Reaction Rate [d <sup>-1</sup> ]
23	Aerobic growth of X <sub>PAO</sub>	$\mu_{PAO} \cdot \frac{S_{O_2}}{K_{O_2,P} + S_{O_2}} \cdot \frac{S_{PO_4}}{K_{PO_4,P} + S_{PO_4}} \cdot \frac{S_{NH_4}}{K_{NH_4} + S_{NH_4}} \cdot \frac{S_{SALK}}{K_{ALK,P} + S_{SALK}} \cdot \frac{X_{PHA}/X_{PAO}}{K_{PHA,P} + X_{PHA}/X_{PAO}} \cdot X_{PAO} \cdot \theta_2$
24	Anoxic growth of X <sub>PAO</sub> (NO <sub>3</sub> <sup>-</sup> - NO <sub>2</sub> )	$\eta_{NO_3,P} \cdot \mu_{PAO} \cdot \frac{S_{NO_3}}{K_{NO_3,P} + S_{NO_3}} \cdot \frac{K_{O_2,P}}{K_{O_2,P} + S_{O_2}} \cdot \frac{S_{PO_4}}{K_{PO_4,P} + S_{PO_4}} \cdot \frac{S_{NH_4}}{K_{NH_4} + S_{NH_4}} \cdot \frac{S_{SALK}}{K_{ALK,P} + S_{SALK}} \cdot \frac{X_{PHA}/X_{PAO}}{K_{PHA,P} + X_{PHA}/X_{PAO}} \cdot X_{PAO} \cdot \theta_2$
25	Anoxic growth of X <sub>PAO</sub> (NO <sub>2</sub> <sup>-</sup> - NO)	$\eta_{G3} \cdot \mu_{PAO} \cdot \frac{S_{NO_2}}{K_{NO_2,Den} + S_{NO_2}} \cdot \frac{K_{OH3}}{K_{OH3} + S_{O_2}} \cdot \frac{S_{PO_4}}{K_{PO_4,P} + S_{PO_4}} \cdot \frac{S_{NH_4}}{K_{NH_4} + S_{NH_4}} \cdot \frac{S_{SALK}}{K_{ALK,P} + S_{SALK}} \cdot \frac{X_{PHA}/X_{PAO}}{K_{PHA,P} + X_{PHA}/X_{PAO}} \cdot X_{PAO} \cdot \theta_2$
26	Anoxic growth of X <sub>PAO</sub> (NO - N <sub>2</sub> O)	$\eta_{G4} \cdot \mu_{PAO} \cdot \frac{S_{NO}}{K_{NO,Den} + S_{NO} + S_{NO}^2/K_{I4NO}} \cdot \frac{K_{OH4}}{K_{OH4} + S_{O_2}} \cdot \frac{S_{PO_4}}{K_{PO_4,P} + S_{PO_4}} \cdot \frac{S_{NH_4}}{K_{NH_4} + S_{NH_4}} \cdot \frac{S_{SALK}}{K_{ALK,P} + S_{SALK}} \cdot \frac{X_{PHA}/X_{PAO}}{K_{PHA,P} + X_{PHA}/X_{PAO}} \cdot X_{PAO} \cdot \theta_2$
27	Anoxic growth of X <sub>PAO</sub> (N <sub>2</sub> O - N <sub>2</sub> )	$\eta_{G5} \cdot \mu_{PAO} \cdot \frac{S_{N_2O}}{K_{N_2O,Den} + S_{N_2O}} \cdot \frac{K_{OH5}}{K_{OH5} + S_{O_2}} \cdot \frac{S_{PO_4}}{K_{PO_4,P} + S_{PO_4}} \cdot \frac{S_{NH_4}}{K_{NH_4} + S_{NH_4}} \cdot \frac{S_{SALK}}{K_{ALK,P} + S_{SALK}} \cdot \frac{X_{PHA}/X_{PAO}}{K_{PHA,P} + X_{PHA}/X_{PAO}} \cdot X_{PAO} \cdot \theta_2$
28	Lysis of X <sub>PAO</sub>	$b_{PAO} \cdot X_{PAO} \cdot \frac{S_{SALK}}{K_{ALK,P} + S_{SALK}} \cdot \theta_2$
29	Lysis of X <sub>PP</sub>	$b_{PP} \cdot X_{PP} \cdot \frac{S_{SALK}}{K_{ALK,P} + S_{SALK}} \cdot \theta_2$
30	Lysis of X <sub>PHA</sub>	$b_{PHA} \cdot X_{PHA} \cdot \frac{S_{SALK}}{K_{ALK,P} + S_{SALK}} \cdot \theta_2$
<b>Nitrifying Organisms (AOB and NOB)</b>		
31	NH <sub>3</sub> oxidation to NH <sub>2</sub> OH with O <sub>2</sub> consumption	$q_{AOB,AMO} \cdot \frac{S_{O_2}}{K_{O_2,AOB1} + S_{O_2}} \cdot \frac{S_{NH_4}}{K_{NH_4,AOB} + S_{NH_4}} \cdot X_{AOB} \cdot \theta_4$
32	NH <sub>2</sub> OH oxidation to NO coupled with O <sub>2</sub> reduction	$\mu_{AOB,HAO} \cdot \frac{S_{O_2}}{K_{O_2,AOB2} + S_{O_2}} \cdot \frac{S_{NH_2OH}}{K_{NH_2OH,AOB} + S_{NH_2OH}} \cdot \frac{S_{NH_4}}{S_{NH_4} + 10^{-12}} \cdot \frac{S_{PO_4}}{K_{P,AOB} + S_{PO_4}} \cdot \frac{S_{SALK}}{K_{ALK,AOB} + S_{SALK}} \cdot X_{AOB} \cdot \theta_4$
33	NO oxidation to NO <sub>2</sub> <sup>-</sup> coupled with O <sub>2</sub> reduction	$q_{AOB,HAO} \cdot \frac{S_{O_2}}{K_{O_2,AOB2} + S_{O_2}} \cdot \frac{S_{NO}}{K_{NO,AOB} + S_{NO}} \cdot X_{AOB} \cdot \theta_4$
34	NO reduction to N <sub>2</sub> O coupled with NH <sub>2</sub> OH to NO <sub>2</sub> (N <sub>2</sub> O from NN)	$q_{AOB,N_2O,NN} \cdot \frac{S_{NH_2OH}}{K_{NH_2OH,AOB} + S_{NH_2OH}} \cdot \frac{S_{NO}}{K_{NO,AOB,NN} + S_{NO}} \cdot X_{AOB} \cdot \theta_4$
35	HNO <sub>2</sub> reduction to N <sub>2</sub> O coupled with NH <sub>2</sub> OH to NO <sub>2</sub> <sup>-</sup> (N <sub>2</sub> O from ND)	$q_{AOB,N_2O,ND} \cdot \frac{S_{NH_2OH}}{K_{NH_2OH,AOB} + S_{NH_2OH}} \cdot \frac{S_{HNO_2}}{K_{HNO_2,AOB} + S_{HNO_2}} \cdot f_{SO_2} \cdot X_{AOB} \cdot \theta_4$

j	Process	Reaction Rate [d <sup>-1</sup> ]
		with $f_{SO_2} = \frac{S_{O_2}}{K_{O_2,AOB,ND} + (1 - 2 \cdot \sqrt{K_{O_2,AOB,ND}/K_{I,O_2,AOB}}) \cdot S_{O_2} + S_{O_2}^2 / K_{I,O_2,AOB}}$
36	Aerobic growth of $X_{NOB}$	$\mu_{NOB} \cdot \frac{S_{O_2}}{K_{O_2,NOB} + S_{O_2}} \cdot \frac{S_{NO_2}}{K_{NO_2,NOB} + S_{NO_2}} \cdot \frac{S_{PO_4}}{K_{P,NOB} + S_{PO_4}} \cdot \frac{S_{ALK}}{K_{ALK,NOB} + S_{ALK}} \cdot X_{NOB} \cdot \theta_4$
37	Lysis of $X_{AOB}$	$b_{AOB} \cdot X_{AOB} \cdot \theta_4$
38	Lysis of $X_{NOB}$	$b_{NOB} \cdot X_{NOB} \cdot \theta_4$
<b>Phosphorus Precipitation and Redissolution</b>		
39	Precipitation	$K_{PRE} \cdot S_{PO_4} \cdot X_{MeOH} \cdot \theta_1$
40	Redissolution	$K_{RED} \cdot X_{MeP} \cdot \frac{S_{ALK}}{K_{ALK,PR} + S_{ALK}} \cdot \theta_1$

Table A1.4. Conversion factor matrix of ASM2d-N<sub>2</sub>O (Massara et al., 2018).

Component → Composition ↓	S <sub>O2</sub>	S <sub>F</sub>	S <sub>A</sub>	S <sub>NH4</sub>	S <sub>NH3OH</sub>	S <sub>N2O</sub>	S <sub>NO</sub>	S <sub>NO2</sub>	S <sub>NO3</sub>	S <sub>PO4</sub>	S <sub>I</sub>	S <sub>ALK</sub>	S <sub>N2</sub>	X <sub>I</sub>	X <sub>S</sub>	X <sub>H</sub>	X <sub>PAO</sub>	X <sub>PP</sub>	X <sub>PHA</sub>	X <sub>AOB</sub>	X <sub>NOB</sub>	X <sub>TSS</sub>	X <sub>MeOH</sub>	X <sub>MeP</sub>	
<b>COD</b>	-1	1	1		-8/7	-16/7	-20/7	-24/7	-32/7	1		-24/14	1	1	1	1	1	1	1	1	1	1	1	1	1
<b>N</b>		i <sub>NSF</sub>	1	1	1	1	1	1	1	i <sub>NSI</sub>	i <sub>NSI</sub>	i <sub>NSI</sub>	1	i <sub>NXI</sub>	i <sub>NXS</sub>	i <sub>NBM</sub>	i <sub>NBM</sub>	i <sub>NBM</sub>	i <sub>NBM</sub>	i <sub>NBM</sub>	i <sub>NBM</sub>	i <sub>NBM</sub>	i <sub>NBM</sub>	i <sub>NBM</sub>	i <sub>NBM</sub>
<b>P</b>		i <sub>PSF</sub>								1	i <sub>PSI</sub>	i <sub>PSI</sub>	i <sub>PXI</sub>	i <sub>PXS</sub>	i <sub>PBM</sub>	i <sub>PBM</sub>	i <sub>PBM</sub>	1	1	i <sub>PBM</sub>	i <sub>PBM</sub>	i <sub>PBM</sub>	i <sub>PBM</sub>	0.21	
<b>Charge</b>			-1/64	1/14				-1/14	-1/14	-1.5/31	-1							-1/31							
<b>TSS</b>														i <sub>TSSXI</sub>	i <sub>TSSXS</sub>	i <sub>TSSBM</sub>	i <sub>TSSBM</sub>	i <sub>TSSBM</sub>	3.23	0.6	i <sub>TSSBM</sub>	i <sub>TSSBM</sub>	-1	1	1

Table A1.5. Part A of stoichiometric matrix of ASM2d-N<sub>2</sub>O (Hydrolysis processes). Stoichiometry for S<sub>NH4</sub>, S<sub>PO4</sub>, S<sub>ALK</sub> and X<sub>TSS</sub> are calculated from conservation.

Part A: Hydrolysis Processes										
Comp. → Process ↓	S <sub>F</sub>	S <sub>NH4</sub>	S <sub>PO4</sub>	S <sub>I</sub>	S <sub>ALK</sub>	X <sub>S</sub>	X <sub>TSS</sub>			
P1	1-f <sub>SI</sub>	V <sub>1,NH4</sub>	V <sub>1,PO4</sub>	f <sub>SI</sub>	V <sub>1,ALK</sub>	-1	V <sub>1,TSS</sub>			
P2	1-f <sub>SI</sub>	V <sub>2,NH4</sub>	V <sub>2,PO4</sub>	f <sub>SI</sub>	V <sub>2,ALK</sub>	-1	V <sub>2,TSS</sub>			
P3	1-f <sub>SI</sub>	V <sub>3,NH4</sub>	V <sub>3,PO4</sub>	f <sub>SI</sub>	V <sub>3,ALK</sub>	-1	V <sub>3,TSS</sub>			
P4	1-f <sub>SI</sub>	V <sub>4,NH4</sub>	V <sub>4,PO4</sub>	f <sub>SI</sub>	V <sub>4,ALK</sub>	-1	V <sub>4,TSS</sub>			

Table A1.6. Part B of stoichiometric matrix of ASM2d-N<sub>2</sub>O (Heterotrophic organisms processes). Stoichiometry for S<sub>NH4</sub>, S<sub>PO4</sub>, S<sub>ALK</sub> and X<sub>TSS</sub> are calculated from conservation.

Part B: Heterotrophic organisms															
Comp. → Process ↓	S <sub>O2</sub>	S <sub>F</sub>	S <sub>A</sub>	S <sub>NH4</sub>	S <sub>N2O</sub>	S <sub>N2</sub>	S <sub>N2O</sub>	S <sub>NO3</sub>	S <sub>PO4</sub>	S <sub>ALK</sub>	S <sub>N2</sub>	X <sub>I</sub>	X <sub>S</sub>	X <sub>H</sub>	X <sub>TSS</sub>
P5	1-(1/Y <sub>H</sub> )	-1/Y <sub>H</sub>		V <sub>5,NH4</sub>					V <sub>5,PO4</sub>	V <sub>5,ALK</sub>				1	V <sub>5,TSS</sub>
P6	1-(1/Y <sub>H</sub> )	-1/Y <sub>H</sub>		V <sub>6,NH4</sub>					V <sub>6,PO4</sub>	V <sub>6,ALK</sub>				1	V <sub>6,TSS</sub>
P7	-1/(Y <sub>H</sub> ·n <sub>G</sub> )			V <sub>7,NH4</sub>			$\frac{1 - Y_H \cdot n_G}{8/7 \cdot Y_H \cdot n_G}$	$-\frac{1 - Y_H \cdot n_G}{8/7 \cdot Y_H \cdot n_G}$	V <sub>7,PO4</sub>	V <sub>7,ALK</sub>				1	V <sub>7,TSS</sub>
P8	-1/(Y <sub>H</sub> ·n <sub>G</sub> )			V <sub>8,NH4</sub>			$-\frac{1 - Y_H \cdot n_G}{4/7 \cdot Y_H \cdot n_G}$		V <sub>8,PO4</sub>	V <sub>8,ALK</sub>				1	V <sub>8,TSS</sub>
P9	-1/(Y <sub>H</sub> ·n <sub>G</sub> )			V <sub>9,NH4</sub>			$-\frac{1 - Y_H \cdot n_G}{4/7 \cdot Y_H \cdot n_G}$		V <sub>9,PO4</sub>	V <sub>9,ALK</sub>				1	V <sub>9,TSS</sub>
P10	-1/(Y <sub>H</sub> ·n <sub>G</sub> )			V <sub>10,NH4</sub>			$-\frac{1 - Y_H \cdot n_G}{4/7 \cdot Y_H \cdot n_G}$		V <sub>10,PO4</sub>	V <sub>10,ALK</sub>				1	V <sub>10,TSS</sub>
P11	-1/(Y <sub>H</sub> ·n <sub>G</sub> )			V <sub>11,NH4</sub>			$\frac{1 - Y_H \cdot n_G}{8/7 \cdot Y_H \cdot n_G}$	$-\frac{1 - Y_H \cdot n_G}{8/7 \cdot Y_H \cdot n_G}$	V <sub>11,PO4</sub>	V <sub>11,ALK</sub>				1	V <sub>11,TSS</sub>

Part B: Heterotrophic organisms														
Comp. → Process ↓	S <sub>O2</sub>	S <sub>A</sub>	S <sub>NH4</sub>	S <sub>N2O</sub>	S <sub>N0</sub>	S <sub>N02</sub>	S <sub>N03</sub>	S <sub>PO4</sub>	S <sub>ALK</sub>	S <sub>N2</sub>	X <sub>I</sub>	X <sub>S</sub>	X <sub>H</sub>	X <sub>TSS</sub>
P12		-1/(Y <sub>H</sub> ·n <sub>G</sub> )	V <sub>12,NH4</sub>	$\frac{1 - Y_H \cdot n_G}{4/7 \cdot Y_H \cdot n_G}$	$-\frac{1 - Y_H \cdot n_G}{4/7 \cdot Y_H \cdot n_G}$		V <sub>12,PO4</sub>	V <sub>12,ALK</sub>					1	V <sub>12,TSS</sub>
P13		-1/(Y <sub>H</sub> ·n <sub>G</sub> )	V <sub>13,NH4</sub>	$\frac{1 - Y_H \cdot n_G}{4/7 \cdot Y_H \cdot n_G}$	$-\frac{1 - Y_H \cdot n_G}{4/7 \cdot Y_H \cdot n_G}$		V <sub>13,PO4</sub>	V <sub>13,ALK</sub>					1	V <sub>13,TSS</sub>
P14		-1/(Y <sub>H</sub> ·n <sub>G</sub> )	V <sub>14,NH4</sub>	$\frac{1 - Y_H \cdot n_G}{4/7 \cdot Y_H \cdot n_G}$	$-\frac{1 - Y_H \cdot n_G}{4/7 \cdot Y_H \cdot n_G}$		V <sub>14,PO4</sub>	V <sub>14,ALK</sub>	$\frac{1 - Y_H \cdot n_G}{4/7 \cdot Y_H \cdot n_G}$				1	V <sub>14,TSS</sub>
P15		1	V <sub>15,NH4</sub>				V <sub>15,PO4</sub>	V <sub>15,ALK</sub>						V <sub>15,TSS</sub>
P16			V <sub>16,NH4</sub>				V <sub>16,PO4</sub>	V <sub>16,ALK</sub>	f <sub>XI</sub>	1-f <sub>XI</sub>			-1	V <sub>16,TSS</sub>

Table A1.7. Part C of stoichiometric matrix of ASM2d-N<sub>2</sub>O (PAO processes). Stoichiometry for S<sub>NH4</sub>, S<sub>PO4</sub>, S<sub>ALK</sub> and X<sub>TSS</sub> are calculated from conservation.

Part C: Polyphosphate accumulating organisms (PAO) processes															
Comp. → Process ↓	S <sub>O2</sub>	S <sub>A</sub>	S <sub>NH4</sub>	S <sub>N2O</sub>	S <sub>N0</sub>	S <sub>N02</sub>	S <sub>N03</sub>	S <sub>PO4</sub>	S <sub>ALK</sub>	S <sub>N2</sub>	X <sub>I</sub>	X <sub>S</sub>	X <sub>PP</sub>	X <sub>PHA</sub>	X <sub>TSS</sub>
P17		-1	V <sub>17,NH4</sub>				Y <sub>PO4</sub>	V <sub>17,ALK</sub>					-Y <sub>PO4</sub>	1	V <sub>17,TSS</sub>
P18	-Y <sub>PHA</sub>		V <sub>18,NH4</sub>				-1	V <sub>18,ALK</sub>					1	-Y <sub>PHA</sub>	V <sub>18,TSS</sub>
P19			V <sub>19,NH4</sub>			Y <sub>PHA</sub> /(8/7)		-1	V <sub>19,ALK</sub>				1	-Y <sub>PHA</sub>	V <sub>19,TSS</sub>
P20			V <sub>20,NH4</sub>	Y <sub>PHA</sub> /(4/7)		-Y <sub>PHA</sub> /(4/7)		-1	V <sub>20,ALK</sub>				1	-Y <sub>PHA</sub>	V <sub>20,TSS</sub>
P21			V <sub>21,NH4</sub>	Y <sub>PHA</sub> /(4/7)		-Y <sub>PHA</sub> /(4/7)		-1	V <sub>21,ALK</sub>				1	-Y <sub>PHA</sub>	V <sub>21,TSS</sub>
P22			V <sub>22,NH4</sub>	-Y <sub>PHA</sub> /(4/7)				-1	V <sub>22,ALK</sub>	Y <sub>PHA</sub> /(4/7)			1	-Y <sub>PHA</sub>	V <sub>22,TSS</sub>
P23	1-(1/Y <sub>PAO</sub> )		V <sub>23,NH4</sub>				-i <sub>P,BM</sub>	V <sub>23,ALK</sub>					1	-1/Y <sub>PAO</sub>	V <sub>23,TSS</sub>
P24			V <sub>24,NH4</sub>			$\frac{1 - Y_{PAO} \cdot n_G}{8/7 \cdot Y_{PAO} \cdot n_G}$	-i <sub>P,BM</sub>	V <sub>24,ALK</sub>					1	-1/Y <sub>PAO</sub>	V <sub>24,TSS</sub>



Part C: Polyphosphate accumulating organisms (PAO) processes														
Comp. →	S <sub>O2</sub>	S <sub>A</sub>	S <sub>NH4</sub>	S <sub>N2O</sub>	S <sub>N2O</sub>	S <sub>N2O</sub>	S <sub>N2O</sub>	S <sub>N2O</sub>	S <sub>N2O</sub>	S <sub>N2O</sub>	S <sub>N2O</sub>	S <sub>N2O</sub>	S <sub>N2O</sub>	X <sub>TSS</sub>
Process ↓														
<b>P25</b>		V <sub>25,NH4</sub>		$\frac{1 - Y_{PAO} \cdot \eta_G}{4/7 \cdot Y_{PAO} \cdot \eta_G}$	$-\frac{1 - Y_{PAO} \cdot \eta_G}{4/7 \cdot Y_{PAO} \cdot \eta_G}$									V <sub>25,TSS</sub>
<b>P26</b>		V <sub>26,NH4</sub>		$\frac{1 - Y_{PAO} \cdot \eta_G}{4/7 \cdot Y_{PAO} \cdot \eta_G}$	$-\frac{1 - Y_{PAO} \cdot \eta_G}{4/7 \cdot Y_{PAO} \cdot \eta_G}$									V <sub>26,TSS</sub>
<b>P27</b>		V <sub>27,NH4</sub>		$\frac{1 - Y_{PAO} \cdot \eta_G}{4/7 \cdot Y_{PAO} \cdot \eta_G}$	$-\frac{1 - Y_{PAO} \cdot \eta_G}{4/7 \cdot Y_{PAO} \cdot \eta_G}$									V <sub>27,TSS</sub>
<b>P28</b>		V <sub>28,NH4</sub>												V <sub>28,TSS</sub>
<b>P29</b>		V <sub>29,NH4</sub>												V <sub>29,TSS</sub>
<b>P30</b>	1	V <sub>30,NH4</sub>												V <sub>30,TSS</sub>

Table A1.8. Part D of stoichiometric matrix of ASM2d-N<sub>2</sub>O (nitrifying organisms processes). Stoichiometry for S<sub>NH4</sub>, S<sub>PO4</sub>, S<sub>ALK</sub> and X<sub>TSS</sub> are calculated from conservation.

Part D: Nitrifying organisms (AOB and NOB)														
Comp. →	S <sub>O2</sub>	S <sub>NH4</sub>	S <sub>NH2OH</sub>	S <sub>N2O</sub>	S <sub>N2O</sub>	S <sub>N2O</sub>	S <sub>N2O</sub>	S <sub>N2O</sub>	S <sub>N2O</sub>	S <sub>N2O</sub>	S <sub>N2O</sub>	S <sub>N2O</sub>	S <sub>N2O</sub>	X <sub>TSS</sub>
Process ↓														
<b>P31</b>	-8/7	-1	1											V <sub>31,TSS</sub>
<b>P32</b>	$-\frac{12/7 - Y_{AOB}}{Y_{AOB}}$	-i <sub>N,BM</sub>	-1/Y <sub>AOB</sub>			1/Y <sub>AOB</sub>							1	V <sub>32,TSS</sub>
<b>P33</b>	-4/7													V <sub>33,TSS</sub>
<b>P34</b>			-1	4	-4	1								V <sub>34,TSS</sub>
<b>P35</b>			-1	2	-1									V <sub>35,TSS</sub>
<b>P36</b>	$-\frac{8/7 - Y_{NOB}}{Y_{NOB}}$	-i <sub>N,BM</sub>											1	V <sub>36,TSS</sub>
<b>P37</b>		V <sub>37,NH4</sub>												V <sub>37,TSS</sub>
<b>P38</b>		V <sub>38,NH4</sub>												V <sub>38,TSS</sub>

Table A1.9. Part E of stoichiometric matrix of ASM2d-N<sub>2</sub>O (Chemical P precipitation processes).

Part E: Chemical P precipitation						
Comp. →	S <sub>PO4</sub>	S <sub>ALK</sub>	X <sub>ISS</sub>	X <sub>MeOH</sub>	X <sub>MeP</sub>	
Process ↓						
P39	-1	V <sub>39,ALK</sub>	V <sub>39,TSS</sub>	-3.45	4.87	
P40	1	V <sub>40,ALK</sub>	V <sub>40,TSS</sub>	3.45	-4.87	



**Annex II: ASM2d-PSFe-N<sub>2</sub>O stoichiometric matrix**

This annex section shows the stoichiometric matrix, the composition matrix and the stoichiometric and conversion parameters of the ASM2d-PSFe-N<sub>2</sub>O model implemented in the proposed BSM2-PSFe-GHG plant-wide model, presented in Chapter V. The added state variables and processes compared to the ASM2d-PSFe (Solon et al., 2017) are shown in grey and are adapted from the ASM2d-N<sub>2</sub>O model (Massara et al., 2018). Table A2.1 shows the stoichiometric parameters and the conversion factors of the model. Table A2.2 shows the composition matrix of the state variable and Table A2.3 to Table A2.9 show the stoichiometric matrix of ASM2d-PSFe- N<sub>2</sub>O.

Table A2.1. Stoichiometric and conversion factors parameters for the ASM2d-PSFe-N<sub>2</sub>O.

Symbol	Value	Units	Description	Reference
$Y_H$	0.625	g COD (gCOD) <sup>-1</sup>	Yield coefficient for OHO	(Henze et al., 2000)
$Y_{PHA}$	0.2	g COD (g P) <sup>-1</sup>	PHA requirement for PP storage	(Henze et al., 2000)
$Y_{PAO}$	0.625	g COD (gCOD) <sup>-1</sup>	Yield coefficient for PAO	(Henze et al., 2000)
$Y_{PO_4}$	0.4	g P (g COD) <sup>-1</sup>	PP requirement (PO <sub>4</sub> release) per PHA stored	(Henze et al., 2000)
$Y_{AOB}$	0.18	g COD (gCOD) <sup>-1</sup>	Yield coefficient for AOB	(Jubany et al., 2008)
$Y_{NOB}$	0.08	g COD (gCOD) <sup>-1</sup>	Yield coefficient for NOB	(Jubany et al., 2008)
$Y_{SRB}$	0.05	g COD (gCOD) <sup>-1</sup>	Yield coefficient for SRB	(Solon et al., 2017)
$f_{SI}$	0	g COD (gCOD) <sup>-1</sup>	Production of S <sub>I</sub> in hydrolysis	(Henze et al., 2000)
$f_{XI}$	0.1	g COD (gCOD) <sup>-1</sup>	Fraction of X <sub>I</sub> generated in biomass lysis	(Henze et al., 2000)
$n_G$	1	dimensionless	Anoxic growth factor	(W C Hiatt and Grady, 2008)
$i_{C\_SI}$	0.36178	g C (g COD) <sup>-1</sup>	C content of inert soluble COD S <sub>I</sub>	(Solon et al., 2017)
$i_{C\_SF}$	0.31843	g C (g COD) <sup>-1</sup>	C content of fermentable substrates S <sub>F</sub>	(Solon et al., 2017)
$i_{C\_SA}$	0.37500	g C (g COD) <sup>-1</sup>	C content of acetate S <sub>A</sub>	(Solon et al., 2017)
$i_{C\_XI}$	0.36178	g C (g COD) <sup>-1</sup>	C content of inert particulate COD X <sub>I</sub>	(Solon et al., 2017)
$i_{C\_XS}$	0.31843	g C (g COD) <sup>-1</sup>	C content of slowly biodegradable COD X <sub>S</sub>	(Solon et al., 2017)
$i_{C\_BM}$	0.36612	g C (g COD) <sup>-1</sup>	C content of biomass	(Solon et al., 2017)
$i_{C\_XPHA}$	0.30000	g C (g COD) <sup>-1</sup>	C content of PHA	(Solon et al., 2017)
$i_{N\_SF}$	0.03352	g N (g COD) <sup>-1</sup>	N content of fermentable substrates S <sub>F</sub>	(Solon et al., 2017)
$i_{N\_SI}$	0.06003	g N (g COD) <sup>-1</sup>	N content of inert soluble COD S <sub>I</sub>	(Solon et al., 2017)
$i_{N\_XI}$	0.06003	g N (g COD) <sup>-1</sup>	N content of inert particulate COD X <sub>I</sub>	(Solon et al., 2017)
$i_{N\_XS}$	0.03352	g N (g COD) <sup>-1</sup>	N content of X <sub>S</sub>	(Solon et al., 2017)
$i_{N\_BM}$	0.08615	g N (g COD) <sup>-1</sup>	N content of biomass	(Solon et al., 2017)
$i_{P\_SF}$	0.00559	g P (g COD) <sup>-1</sup>	P content of fermentable substrates S <sub>F</sub>	(Solon et al., 2017)
$i_{P\_SI}$	0.00649	g P (g COD) <sup>-1</sup>	P content of inert soluble COD S <sub>I</sub>	(Solon et al., 2017)
$i_{P\_XI}$	0.00649	g P (g COD) <sup>-1</sup>	P content of inert particulate COD X <sub>I</sub>	(Solon et al., 2017)
$i_{P\_XS}$	0.00559	g P (g COD) <sup>-1</sup>	P content of X <sub>S</sub>	(Solon et al., 2017)
$i_{P\_BM}$	0.02154	g P (g COD) <sup>-1</sup>	P content of biomass	(Solon et al., 2017)
$i_{TSS,XI}$	0.75	g TSS (gCOD) <sup>-1</sup>	TSS to COD ratio for X <sub>I</sub>	(Henze et al., 2000)
$i_{TSS,XS}$	0.75	g TSS (gCOD) <sup>-1</sup>	TSS to COD ratio for X <sub>S</sub>	(Henze et al., 2000)

Symbol	Value	Units	Description	Reference
$i_{TSS,BM}$	0.9	g TSS (gCOD) <sup>-1</sup>	TSS to COD ratio for biomass	(Henze et al., 2000)
$i_{TSS,XPHA}$	0.6	g TSS (gCOD) <sup>-1</sup>	TSS to COD ratio for PHA	(Henze et al., 2000)
$i_{TSS,XPP}$	3.23	g TSS (g P) <sup>-1</sup>	TSS to P ratio for PP	(Henze et al., 2000)
$i_{K,XPP}$	0.4204	g K (g P) <sup>-1</sup>	K to P ratio for PP	(Solon et al., 2017)
$i_{Mg,XPP}$	0.2614	g Mg (g P) <sup>-1</sup>	Mg to P ratio for PP	(Solon et al., 2017)

Table A2.2. Composition matrix for the ASM2d-PSFe-N<sub>2</sub>O model.

Content→ Component↓	COD <sub>i</sub>	C <sub>i</sub>	N <sub>i</sub>	P <sub>i</sub>	K <sub>i</sub>	Mg <sub>i</sub>	S <sub>i</sub>	Fe <sub>i</sub>
SO <sub>2</sub>	-1							
S <sub>F</sub>	1	$i_{C,SF}$	$i_{N,SF}$	$i_{P,SF}$				
S <sub>A</sub>	1	$i_{C,SA}$						
S <sub>I</sub>	1	$i_{C,SI}$	$i_{N,SI}$	$i_{P,SI}$				
S <sub>NH4</sub>			1					
S <sub>NH2OH</sub>	-8/7		1					
S <sub>N2O</sub>	-16/7		1					
S <sub>NO</sub>	-20/7		1					
S <sub>NO2</sub>	-24/7		1					
S <sub>NO3</sub>	-32/7		1					
S <sub>N2</sub>	-24/14		1					
S <sub>PO4</sub>				1				
S <sub>IC</sub>		1						
X <sub>I</sub>	1	$i_{C,XI}$	$i_{N,XI}$	$i_{P,XI}$				
X <sub>S</sub>	1	$i_{C,XS}$	$i_{N,XS}$	$i_{P,XS}$				
X <sub>H</sub>	1	$i_{C,BM}$	$i_{N,BM}$	$i_{P,BM}$				
X <sub>PAO</sub>	1	$i_{C,BM}$	$i_{N,BM}$	$i_{P,BM}$				
X <sub>PP</sub>				1	$i_{K,XPP}$	$i_{Mg,XPP}$		
X <sub>PHA</sub>	1	$i_{C,XPHA}$						
X <sub>AOB</sub>	1	$i_{C,BM}$	$i_{N,BM}$	$i_{P,BM}$				
X <sub>NOB</sub>	1	$i_{C,BM}$	$i_{N,BM}$	$i_{P,BM}$				
S <sub>K</sub>					1			
S <sub>Mg</sub>						1		
S <sub>SO4</sub>							1	
S <sub>Fe(II)</sub>	0.1433							1
S <sub>Fe(III)</sub>								1
S <sub>IS</sub>	2						1	
X <sub>S0</sub>	1.5						1	
X <sub>SRB</sub>	1	$i_{C,BM}$	$i_{N,BM}$	$i_{P,BM}$				

<b>Content→</b> <b>Component↓</b>	<b>COD<sub>i</sub></b>	<b>C<sub>i</sub></b>	<b>N<sub>i</sub></b>	<b>P<sub>i</sub></b>	<b>K<sub>i</sub></b>	<b>Mg<sub>i</sub></b>	<b>Si</b>	<b>Fe<sub>i</sub></b>
X <sub>HFO,L</sub>								1
X <sub>HFO,H</sub>								1
X <sub>HFO,L,P</sub>				0.1722				1
X <sub>HFO,H,P</sub>				0.6667				1
X <sub>HFO,H,P,old</sub>				0.6667				1
X <sub>HFO,L,P,old</sub>				0.1722				1
X <sub>HFO,old</sub>								1

Table A2.3. Part A of stoichiometric matrix of ASM2d-PSFe-N<sub>2</sub>O (Hydrolysis processes). Stoichiometry for S<sub>NH4</sub>, S<sub>PO4</sub>, and S<sub>IC</sub> are calculated from conservation.

Part A: Hydrolysis processes									
j	Process ↓	S <sub>F</sub>	S <sub>I</sub>	S <sub>NH4</sub>	S <sub>PO4</sub>	S <sub>IC</sub>	X <sub>S</sub>	X <sub>I</sub>	X <sub>H</sub>
1	Aerobic hydrolysis	1-f <sub>SI</sub>	f <sub>SI</sub>	V <sub>1,NH4</sub>	V <sub>1,NH4</sub>	V <sub>1,NH4</sub>	-1		
2	Anoxic hydrolysis (NO <sub>3</sub> <sup>-</sup> )	1-f <sub>SI</sub>	f <sub>SI</sub>	V <sub>1,NH4</sub>	V <sub>1,NH4</sub>	V <sub>1,NH4</sub>	-1		
3	Anoxic hydrolysis (NO <sub>2</sub> <sup>-</sup> )	1-f <sub>SI</sub>	f <sub>SI</sub>	V <sub>1,NH4</sub>	V <sub>1,NH4</sub>	V <sub>1,NH4</sub>	-1		
4	Anaerobic hydrolysis	1-f <sub>SI</sub>	f <sub>SI</sub>	V <sub>1,NH4</sub>	V <sub>1,NH4</sub>	V <sub>1,NH4</sub>	-1		

Table A2.4. Part B of stoichiometric matrix of ASM2d-PSFe-N<sub>2</sub>O (heterotrophic organisms processes). Stoichiometry for S<sub>NH4</sub>, S<sub>PO4</sub>, and S<sub>IC</sub> are calculated from conservation.

Part B: Heterotrophic organisms processes														
j	Process ↓	S <sub>O2</sub>	S <sub>F</sub>	S <sub>A</sub>	S <sub>NH4</sub>	S <sub>N2O</sub>	S <sub>NO</sub>	S <sub>NO2</sub>	S <sub>NO3</sub>	S <sub>NO4</sub>	S <sub>IC</sub>	X <sub>I</sub>	X <sub>S</sub>	X <sub>H</sub>
5	Aerobic growth on S <sub>F</sub>	$\frac{1-Y_H}{Y_H}$	$\frac{1}{Y_H}$		V <sub>5,NH4</sub>					V <sub>5,PO4</sub>	V <sub>5,IC</sub>			1
6	Aerobic growth on S <sub>A</sub>	$\frac{1-Y_H}{Y_H}$		$-\frac{1}{Y_H}$	V <sub>6,NH4</sub>					V <sub>6,PO4</sub>	V <sub>6,IC</sub>			1
7	Anoxic growth on S <sub>F</sub> (NO <sub>3</sub> <sup>-</sup> → NO <sub>2</sub> <sup>-</sup> )	$-\frac{1}{Y_H \cdot n_G}$	$\frac{1}{Y_H \cdot n_G}$		V <sub>7,NH4</sub>			$\frac{1-Y_H \cdot n_G}{1.14 \cdot Y_H \cdot n_G}$	$-\frac{1-Y_H \cdot n_G}{1.14 \cdot Y_H \cdot n_G}$	V <sub>7,PO4</sub>	V <sub>7,IC</sub>			1
8	Anoxic growth on S <sub>F</sub> (NO <sub>2</sub> <sup>-</sup> → NO)	$-\frac{1}{Y_H \cdot n_G}$	$\frac{1}{Y_H \cdot n_G}$		V <sub>8,NH4</sub>		$\frac{1-Y_H \cdot n_G}{0.57 \cdot Y_H \cdot n_G}$	$-\frac{1-Y_H \cdot n_G}{0.57 \cdot Y_H \cdot n_G}$		V <sub>8,PO4</sub>	V <sub>8,IC</sub>			1
9	Anoxic growth on S <sub>F</sub> (NO → N <sub>2</sub> O)	$-\frac{1}{Y_H \cdot n_G}$	$\frac{1}{Y_H \cdot n_G}$		V <sub>9,NH4</sub>		$\frac{1-Y_H \cdot n_G}{0.57 \cdot Y_H \cdot n_G}$	$-\frac{1-Y_H \cdot n_G}{0.57 \cdot Y_H \cdot n_G}$		V <sub>9,PO4</sub>	V <sub>9,IC</sub>			1
10	Anoxic growth on S <sub>F</sub> (N <sub>2</sub> O → N <sub>2</sub> )	$-\frac{1}{Y_H \cdot n_G}$	$\frac{1}{Y_H \cdot n_G}$		V <sub>10,NH4</sub>		$\frac{1-Y_H \cdot n_G}{0.57 \cdot Y_H \cdot n_G}$	$-\frac{1-Y_H \cdot n_G}{0.57 \cdot Y_H \cdot n_G}$		V <sub>10,PO4</sub>	V <sub>10,IC</sub>			1
11	Anoxic growth on S <sub>A</sub> (NO <sub>3</sub> <sup>-</sup> → NO <sub>2</sub> <sup>-</sup> )		$-\frac{1}{Y_H \cdot n_G}$	$\frac{1}{Y_H \cdot n_G}$	V <sub>11,NH4</sub>			$\frac{1-Y_H \cdot n_G}{1.14 \cdot Y_H \cdot n_G}$	$-\frac{1-Y_H \cdot n_G}{1.14 \cdot Y_H \cdot n_G}$	V <sub>11,PO4</sub>	V <sub>11,IC</sub>			1
12	Anoxic growth on S <sub>A</sub> (NO <sub>2</sub> <sup>-</sup> → NO)		$-\frac{1}{Y_H \cdot n_G}$	$\frac{1}{Y_H \cdot n_G}$	V <sub>12,NH4</sub>		$\frac{1-Y_H \cdot n_G}{0.57 \cdot Y_H \cdot n_G}$	$-\frac{1-Y_H \cdot n_G}{0.57 \cdot Y_H \cdot n_G}$		V <sub>12,PO4</sub>	V <sub>12,IC</sub>			1
13	Anoxic growth on S <sub>A</sub> (NO → N <sub>2</sub> O)		$-\frac{1}{Y_H \cdot n_G}$	$\frac{1}{Y_H \cdot n_G}$	V <sub>13,NH4</sub>		$\frac{1-Y_H \cdot n_G}{0.57 \cdot Y_H \cdot n_G}$	$-\frac{1-Y_H \cdot n_G}{0.57 \cdot Y_H \cdot n_G}$		V <sub>13,PO4</sub>	V <sub>13,IC</sub>			1
14	Anoxic growth on S <sub>A</sub> (N <sub>2</sub> O → N <sub>2</sub> )		$-\frac{1}{Y_H \cdot n_G}$	$\frac{1}{Y_H \cdot n_G}$	V <sub>14,NH4</sub>		$\frac{1-Y_H \cdot n_G}{0.57 \cdot Y_H \cdot n_G}$	$-\frac{1-Y_H \cdot n_G}{0.57 \cdot Y_H \cdot n_G}$		V <sub>14,PO4</sub>	V <sub>14,IC</sub>			1

Part B: Heterotrophic organisms processes															
j	Process ↓	S <sub>O2</sub>	S <sub>F</sub>	S <sub>A</sub>	S <sub>NH4</sub>	S <sub>N2O</sub>	S <sub>NO</sub>	S <sub>NO2</sub>	S <sub>NO3</sub>	S <sub>N2</sub>	S <sub>PO4</sub>	S <sub>IC</sub>	X <sub>I</sub>	X <sub>S</sub>	X <sub>II</sub>
15	Fermentation	-1	1		V <sub>15,NH4</sub>						V <sub>15,PO4</sub>	V <sub>15,IC</sub>			
16	Lysis of X <sub>II</sub>				V <sub>16,NH4</sub>						V <sub>16,PO4</sub>	V <sub>16,IC</sub>	f <sub>XI</sub>	1-f <sub>XI</sub>	-1

Table A2.5. Part C of stoichiometric matrix of ASM2d-PSFe-N<sub>2</sub>O (PAO processes). Stoichiometry for S<sub>NH4</sub>, S<sub>PO4</sub>, and S<sub>IC</sub> are calculated from conservation.

Part C: Polyphosphate accumulating organisms (PAO) processes																
j	Process ↓	S <sub>O2</sub>	S <sub>A</sub>	S <sub>N2O</sub>	S <sub>NO</sub>	S <sub>NO2</sub>	S <sub>NO3</sub>	S <sub>N2</sub>	S <sub>PO4</sub>	X <sub>I</sub>	X <sub>S</sub>	X <sub>PAO</sub>	X <sub>PP</sub>	X <sub>PHA</sub>	S <sub>K</sub>	S <sub>Mg</sub>
17	Storage of X <sub>PHA</sub>								Y <sub>PO4</sub>				-Y <sub>PO4</sub>	1	Y <sub>PO4</sub> ·i <sub>K,XPP</sub>	Y <sub>PO4</sub> ·i <sub>Mg,XPP</sub>
18	Aerobic storage of X <sub>PP</sub>			-Y <sub>PHA</sub>					-1				1	-Y <sub>PHA</sub>	-i <sub>K,XPP</sub>	-i <sub>Mg,XPP</sub>
19	Anoxic storage of X <sub>PP</sub> (NO <sub>3</sub> <sup>-</sup> to NO <sub>2</sub> <sup>-</sup> )					$\frac{Y_{PHA} \cdot n_G}{1.14}$	$\frac{Y_{PHA} \cdot n_G}{-1.14}$		-1				1	-Y <sub>PHA</sub> ·n <sub>G</sub>	-i <sub>K,XPP</sub>	-i <sub>Mg,XPP</sub>
20	Anoxic storage of X <sub>PP</sub> (NO <sub>2</sub> <sup>-</sup> to NO)					$\frac{Y_{PHA} \cdot n_G}{0.57}$	$\frac{Y_{PHA} \cdot n_G}{-0.57}$		-1				1	-Y <sub>PHA</sub> ·n <sub>G</sub>	-i <sub>K,XPP</sub>	-i <sub>Mg,XPP</sub>
21	Anoxic storage of X <sub>PP</sub> (NO to N <sub>2</sub> O)					$\frac{Y_{PHA} \cdot n_G}{0.57}$	$\frac{Y_{PHA} \cdot n_G}{-0.57}$		-1				1	-Y <sub>PHA</sub> ·n <sub>G</sub>	-i <sub>K,XPP</sub>	-i <sub>Mg,XPP</sub>
22	Anoxic storage of X <sub>PP</sub> (N <sub>2</sub> O to N <sub>2</sub> )					$\frac{Y_{PHA} \cdot n_G}{-0.57}$	$\frac{Y_{PHA} \cdot n_G}{0.57}$		-1				1	-Y <sub>PHA</sub> ·n <sub>G</sub>	-i <sub>K,XPP</sub>	-i <sub>Mg,XPP</sub>
23	Aerobic growth of X <sub>PAO</sub>			$\frac{1-Y_{PAO}}{Y_{PAO}}$					-i <sub>P,BM</sub>			1		$\frac{1}{Y_{PAO}}$		
24	Anoxic growth of X <sub>PAO</sub> (NO <sub>3</sub> <sup>-</sup> to NO <sub>2</sub> <sup>-</sup> )					$\frac{1-Y_{PAO} \cdot n_G}{1.14 \cdot Y_{PAO} \cdot n_G}$	$\frac{1-Y_{PAO} \cdot n_G}{1.14 \cdot Y_{PAO} \cdot n_G}$		-i <sub>P,BM</sub>			1		$\frac{1}{Y_{PAO} \cdot n_G}$		
25	Anoxic growth of X <sub>PAO</sub> (NO <sub>2</sub> <sup>-</sup> to NO)					$\frac{1-Y_{PAO} \cdot n_G}{0.57 \cdot Y_{PAO} \cdot n_G}$	$\frac{1-Y_{PAO} \cdot n_G}{-0.57 \cdot Y_{PAO} \cdot n_G}$		-i <sub>P,BM</sub>			1		$\frac{1}{Y_{PAO} \cdot n_G}$		
26	Anoxic growth of X <sub>PAO</sub> (NO to N <sub>2</sub> O)					$\frac{1-Y_{PAO} \cdot n_G}{0.57 \cdot Y_{PAO} \cdot n_G}$	$\frac{1-Y_{PAO} \cdot n_G}{-0.57 \cdot Y_{PAO} \cdot n_G}$		-i <sub>P,BM</sub>			1		$\frac{1}{Y_{PAO} \cdot n_G}$		
27	Anoxic growth of X <sub>PAO</sub> (N <sub>2</sub> O → N <sub>2</sub> )					$\frac{1-Y_{PAO} \cdot n_G}{-0.57 \cdot Y_{PAO} \cdot n_G}$	$\frac{1-Y_{PAO} \cdot n_G}{0.57 \cdot Y_{PAO} \cdot n_G}$		-i <sub>P,BM</sub>			1		$\frac{1}{Y_{PAO} \cdot n_G}$		
28	Lysis of X <sub>PAO</sub>							V <sub>28,PO4</sub>	f <sub>XI</sub>	1-f <sub>XI</sub>						
29	Lysis of X <sub>PP</sub>							1							i <sub>K,XPP</sub>	i <sub>Mg,XPP</sub>
30	Lysis of X <sub>PHA</sub>															



Table A2.6. Part D of stoichiometric matrix of ASM2d-PSFe-N<sub>2</sub>O (nitrifying organisms processes). Stoichiometry for S<sub>NH4</sub>, S<sub>PO4</sub>, and S<sub>IC</sub> are calculated from conservation.

Part D: Nitrifying organisms processes (AOB and NOB)														
j	Process ↓	S <sub>O2</sub>	S <sub>NH4</sub>	S <sub>NH2OH</sub>	S <sub>N2O</sub>	S <sub>NO</sub>	S <sub>NO2</sub>	S <sub>NO3</sub>	S <sub>PO4</sub>	S <sub>IC</sub>	X <sub>I</sub>	X <sub>S</sub>	X <sub>AOB</sub>	X <sub>NOB</sub>
31	NH <sub>3</sub> oxidation to NH <sub>2</sub> OH with O <sub>2</sub> consumption	-1.14	-1	1										
32	NH <sub>2</sub> OH to NO coupled with O <sub>2</sub> reduction (X <sub>AOB</sub> growth)	$-\frac{1.71 \cdot Y_{AOB}}{Y_{AOB}}$	$V_{32,NH4}$	$-\frac{1}{Y_{AOB}}$	$\frac{1}{Y_{AOB}}$			$V_{32,PO4}$	$V_{32,IC}$				1	
33	NO oxidation to NO <sub>2</sub> <sup>-</sup> coupled with O <sub>2</sub> reduction	-0.57			-1	1								
34	NO to N <sub>2</sub> O coupled with NH <sub>2</sub> OH to NO <sub>2</sub> <sup>-</sup> (N <sub>2</sub> O from NN pathway)		-1	4	-4	1								
35	HNO <sub>2</sub> to N <sub>2</sub> O coupled with NH <sub>2</sub> OH to NO <sub>2</sub> <sup>-</sup> (N <sub>2</sub> O from ND pathway)		-1	2	-1									
36	Aerobic growth of X <sub>NOB</sub>	$-\frac{1.14 \cdot Y_{NOB}}{Y_{NOB}}$	$V_{36,NH4}$		$-\frac{1}{Y_{NOB}}$	$\frac{1}{Y_{NOB}}$		$V_{36,PO4}$	$V_{36,IC}$					1
37	Lysis of X <sub>AOB</sub>		$V_{37,NH4}$					$V_{37,PO4}$	$V_{37,IC}$	$f_{XI}$	$1-f_{XI}$		-1	
38	Lysis of X <sub>NOB</sub>		$V_{38,NH4}$					$V_{38,PO4}$	$V_{38,IC}$	$f_{XI}$	$1-f_{XI}$		-1	

Table A2.7. Part E of stoichiometric matrix of ASM2d-PSFe-N<sub>2</sub>O (SRB processes). Stoichiometry for S<sub>NH4</sub>, S<sub>PO4</sub>, and S<sub>IC</sub> are calculated from conservation.

Part E: Sulfate Reduction Bacteria processes (SRB)														
j	Process ↓	S <sub>O2</sub>	S <sub>F</sub>	S <sub>A</sub>	S <sub>NH4</sub>	S <sub>NO2</sub>	S <sub>NO3</sub>	S <sub>N2</sub>	S <sub>PO4</sub>	S <sub>IC</sub>	X <sub>I</sub>	X <sub>S</sub>	S <sub>S0</sub>	X <sub>SRB</sub>
39	Reduction of S <sub>SO4</sub> to S <sub>IS</sub> on S <sub>F</sub>	$-\frac{1}{Y_{HSRB}}$			$V_{39,NH4}$			$V_{39,PO4}$	$V_{39,IC}$		$\frac{1-Y_{HSRB}}{2Y_{HSRB}}$	$\frac{1-Y_{HSRB}}{2Y_{HSRB}}$		1
40	Reduction of S <sub>SO4</sub> to S <sub>IS</sub> on S <sub>A</sub>	$-\frac{1}{Y_{HSRB}}$			$V_{40,NH4}$			$V_{40,PO4}$	$V_{40,IC}$		$\frac{1-Y_{HSRB}}{2Y_{HSRB}}$	$\frac{1-Y_{HSRB}}{2Y_{HSRB}}$		1
41	Oxidation of S <sub>IS</sub> to S <sub>S0</sub> using S <sub>O2</sub>	-1										-2	2	
42	Oxidation of S <sub>IS</sub> to S <sub>S0</sub> using S <sub>NO2</sub>					-0.2917		0.2917				-1	1	
43	Oxidation of S <sub>IS</sub> to S <sub>S0</sub> using S <sub>NO3</sub>					-0.1750		0.1750				-1	1	

Part E: Sulfate Reduction Bacteria processes (SRB)																
j	Process ↓	S <sub>O2</sub>	S <sub>F</sub>	S <sub>A</sub>	S <sub>NH4</sub>	S <sub>NO2</sub>	S <sub>NO3</sub>	S <sub>N2</sub>	S <sub>PO4</sub>	S <sub>IC</sub>	X <sub>I</sub>	X <sub>S</sub>	S <sub>SO4</sub>	S <sub>IS</sub>	S <sub>SO</sub>	X <sub>SRB</sub>
44	Oxidation of S <sub>SO</sub> to S <sub>SO4</sub> using S <sub>O2</sub>	-1.5											1			-1
45	Oxidation of S <sub>SO</sub> to S <sub>SO4</sub> using S <sub>NO2</sub>					-0.8750		0.8750					1			-1
46	Oxidation of S <sub>SO</sub> to S <sub>SO4</sub> using S <sub>NO3</sub>					-0.5250		0.5250					1			-1
47	Decay of X <sub>SRB</sub>				V <sub>47,NH4</sub>				V <sub>47,PO4</sub>	V <sub>47,IC</sub>	f <sub>XI</sub>	1-f <sub>XI</sub>				-1

Table A2.8. Part F of stoichiometric matrix of ASM2d-PSFe-N<sub>2</sub>O (Iron processes). Stoichiometry for S<sub>IC</sub> is calculated from conservation.

Part F: Iron-related processes													
j	Process ↓	S <sub>O2</sub>	S <sub>A</sub>	S <sub>NO2</sub>	S <sub>NO3</sub>	S <sub>N2</sub>	S <sub>IC</sub>	S <sub>Fe(II)</sub>	S <sub>IS</sub>	X <sub>SO</sub>	X <sub>HFO,L</sub>	X <sub>HFO,H</sub>	
48	Oxidation of S <sub>Fe(II)</sub> to S <sub>Fe(III)</sub> on S <sub>O2</sub>	-0.1433						-1			0.3103	0.6897	
49	Oxidation of S <sub>Fe(II)</sub> to S <sub>Fe(III)</sub> on S <sub>NO2</sub>			-0.0836		0.0836		-1			0.3103	0.6897	
50	Oxidation of S <sub>Fe(II)</sub> to S <sub>Fe(III)</sub> on S <sub>NO3</sub>				-0.0501	0.0501		-1			0.3103	0.6897	
51	Reduction of X <sub>HFO,L</sub> to S <sub>Fe(II)</sub> using S <sub>IS</sub>							1	-0.2865	0.2865	-1		
52	Reduction of X <sub>HFO,H</sub> to S <sub>Fe(II)</sub> using S <sub>IS</sub>							1	-0.2865	0.2865	-1		
53	Reduction of X <sub>HFO,L</sub> to S <sub>Fe(II)</sub> using S <sub>A</sub>		-0.1433				V <sub>53,IC</sub>	1			-1		
54	Reduction of X <sub>HFO,H</sub> to S <sub>Fe(II)</sub> using S <sub>A</sub>		-0.1433				V <sub>54,IC</sub>	1			-1		

Table A2.9. Part G of stoichiometric matrix of ASM2d-PSFe-N<sub>2</sub>O (HFO precipitation model processes).

Part G: HFO precipitation model									
j	Process ↓	SP04	X <sub>HFO,L</sub>	X <sub>HFO,H</sub>	X <sub>HFO,L,P</sub>	X <sub>HFO,H,P</sub>	X <sub>HFO,H,P,old</sub>	X <sub>HFO,L,P,old</sub>	X <sub>HFO,old</sub>
Fe1	Aging of X <sub>HFO,H</sub>		1	-1					
Fe2	Aging of X <sub>HFO,L</sub>		-1						1
Fe3	Fast binding of P to active X <sub>HFO,H</sub>	-1		-1.5	1.5				
Fe4	Slow sorption of P to active X <sub>HFO,L</sub>	-1	-5.8065		5.8065				
Fe5	Aging of X <sub>HFO,H,P</sub>					-1	1		
Fe6	Aging of X <sub>HFO,H,L</sub>				-1			1	
Fe7	Dissolution of X <sub>HFO,H</sub> and release of P	0.6667		1		-1			
Fe8	Dissolution of X <sub>HFO,L</sub> and release of P	0.1722	1					-1	

### **Annex III: Evaluation of potential operational and control strategies in a plant-wide WWTP model to mitigate GHG emissions**

#### **Abstract**

This work is part of the EU RISE project C-FOOT-CTRL aiming at developing online tools to monitor, control and mitigate GHG emissions in WWTPs. This work shows the development of the WWTP model that is integrated in the C-FOOT-CTRL software tool, the development of the evaluation criteria for the reduction of the GHG emissions and the development and implementation in the WWTP model of potential mitigation of GHG emissions. A system analysis was performed to identify the effect that different operational strategies (DO, SRT and primary clarifier solids removal efficiency) had on the GHG emissions, the effluent quality and the energy consumption. Four control strategies were implemented and analysed through two different scenarios. The results show that the control strategy that most mitigates the GHG emissions and with an adequate effluent quality was the control strategy based on a cascade-feed forward DO control loop, where the DO SP is modified according to the ammonium influent load, together with a control loop based on adding external organic matter into the anoxic reactor to maintain a low level of nitrous oxide species (NO<sub>x</sub>) in this reactor.

#### **A3.1. Motivations**

This work is part of the European Union's RISE project C-FOOT-CTRL ([www.cfootcontrol.gr](http://www.cfootcontrol.gr)), entitled: Developing online tools to monitor, control and mitigate GHG emissions in WWTPs (grant agreement No 645769). The goal of the C-FOOT-CTRL project was to develop a new software tool able to conduct online monitoring, control and mitigation of GHG production and emissions in WWTPs. The developed software tool comprised three components: the online data acquisition system, the database and the dynamic model. Specifically, this annex presents: i) the development of the carbon footprint model, referring to Deliverable 3.1 of the project; ii) the development of the methodology followed to assess the mitigation of GHG emissions in the dynamic model, referring to Deliverable 7.1 of the project and iii) the development of mitigation strategies to reduce GHG emissions and the study of the effects of its implementation by modelling tools, referring to Deliverable 7.2 of the project.

Therefore, the aims of this work were: i) the development of the dynamic plant-wide WWTP model, able to predict the plant carbon footprint in view of its integration with the novel C-FOOT-CTRL software tool; ii) the development of the methodology followed to assess the reduction of the GHG emissions predicted by the dynamic model and iii) the development and implementation of potential mitigation strategies of GHG emissions in the developed WWTP model.

## A3.2. Materials and Methods

### A3.2.1. Plant layout and dynamic model description

The general layout of the WWTP is presented in Figure A3.1, while the number of units, dimensions and flowrates of the simulated WWTP are detailed in Table A3.1. The biological treatment had an A<sup>2</sup>/O configuration consisting of 7 tanks in series: tank 1 was anaerobic, tank 2 was anoxic and tanks 3 to 7 were aerobic.

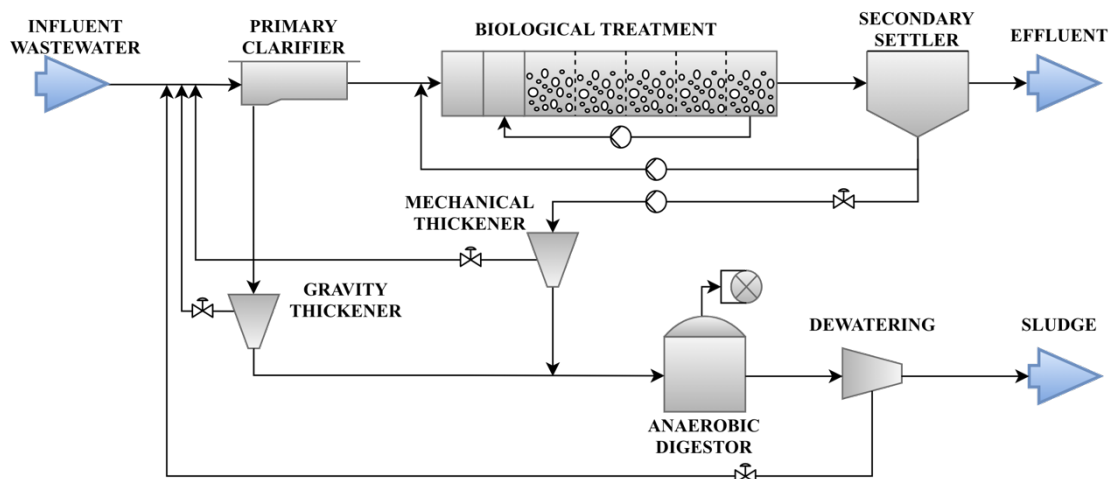


Figure A3.1. Layout used in the model to describe the simulated WWTP.

Table A3.1. Characteristics of the simulated WWTP.

<b>Primary Clarifier (PC):</b>		
- Number of PC	[-]	1
- Area of PC tank	[m <sup>2</sup> ]	1500
<b>Biological Reactor:</b>		
<b>Anaerobic reactor:</b>		
- Number of anaerobic reactors	[-]	1
- Volume	[m <sup>3</sup> ]	7880
<b>Anoxic reactor:</b>		
- Number of anoxic reactors	[-]	1
- Volume	[m <sup>3</sup> ]	11032
<b>Aerobic reactor:</b>		
- Number of aerobic reactors	[-]	5
- Volume	[m <sup>3</sup> ]	15559
- Volume aerobic 1	[m <sup>3</sup> ]	3716
- Volume aerobic 2	[m <sup>3</sup> ]	3716
- Volume aerobic 3	[m <sup>3</sup> ]	3716
- Volume aerobic 4	[m <sup>3</sup> ]	3716
- Volume aerobic 5	[m <sup>3</sup> ]	695
<b>Internal Recirculation (R7 to R2):</b>		
- Ratio $Q_{R1}/Q_{in}^*$	[-]	4

<b>Secondary settler:</b>		
- Number of settlers	[-]	1
- Area of each settler	[m <sup>2</sup> ]	6000
- Height	[m]	4.5
<b>External recirculation flowrate:</b>		
- Ratio $Q_{RE}/Q_{in}^*$	[-]	1
<b>Wastage flowrate:</b>		
- Ratio $Q_w/Q_{in}^*$	[-]	**
<b>Gravity thickener:</b>		
- Number of thickeners	[-]	1
- Area of each thickener	[m <sup>2</sup> ]	100
<b>Mechanical thickener:</b>		
- Number of thickeners	[-]	1
- Area of each thickener	[m <sup>2</sup> ]	100
<b>Anaerobic digester:</b>		
- Number of digesters	[-]	1
- Volume of each digester	[m <sup>3</sup> ]	6000
<b>Dewatering unit:</b>		
- Number of tanks	[-]	1
- Surface of each tank	[m <sup>2</sup> ]	100
* $Q_{in}$ is referred to influent flowrate		
** Wastage flowrate ( $Q_w$ ) is determined with the desired SRT		

The PC was ideally simulated performing mass balances based on the efficiency of the unit, assuming a constant ratio of sludge flowrate to influent flowrate and a constant percentage of TSS removal.

The kinetic model implemented in the biological reactor simulation was the ASM2d-N<sub>2</sub>O of Massara et al., (2018). The ASM2d-N<sub>2</sub>O model is able to describe organic matter, N and P removal and N<sub>2</sub>O production and quantification. The ASM2d-N<sub>2</sub>O state variables, kinetic rate expressions and stoichiometry is shown in Annex I section. The model was updated in this work in order to account for biogenic CO<sub>2</sub> emissions, by means of the stoichiometry of inorganic carbon (IC) of the state variables (Solon et al., 2017). The conversion factors for IC used are presented in Table A3.2.

Table A3.2. Conversion factors for IC and model state variables.

Param.	Value [g C.(g COD) <sup>-1</sup> ]	Description	Source
$i_{C,SF}$	0.318	C content of fermentable substrates $S_F$	(Solon et al., 2017)
$i_{C,SA}$	0.375	C content of fermentation products $S_A$	(Solon et al., 2017)
$i_{C,SI}$	0.362	C content of inert soluble COD $S_I$	(Solon et al., 2017)
$i_{C,XI}$	0.362	C content of inert particulate COD $X_I$	(Solon et al., 2017)
$i_{C,XS}$	0.318	C content of slowly biodegradable COD $X_S$	(Solon et al., 2017)

Param.	Value [g C.(g COD) <sup>-1</sup> ]	Description	Source
i <sub>C,BM</sub>	0.366	C content of biomass, X <sub>H</sub> , X <sub>PAO</sub> , X <sub>AOB</sub> and X <sub>NOB</sub>	(Solon et al., 2017)
i <sub>C,XPHA</sub>	0.300	C content of PHA, X <sub>PHA</sub>	(Solon et al., 2017)

The secondary settler was modelled using the double exponential velocity function of Takács et al., (1991) in a ten-layer one-dimensional settler, with the feeding entering in the fifth layer and using the default model parameters. The thickeners and the dewatering units were modelled as ideal units, with a constant percentage of TSS in the sludge flows. Finally, the anaerobic digester was modelled in a simplified way assuming an anaerobic decomposition rate for primary and secondary sludges and through mass balances. It was assumed that 0.8 m<sup>3</sup> of biogas are produced for each kg of volatile solid that is removed, with an average calorific value for biogas of 5500 Kcal m<sup>-3</sup>. Additional details of the simulations of the units processes can be found in Deliverable 3.1 of the C-FOOT-CTRL project.

#### A3.2.2. WWTP influent characteristics and fractionation

The influent of the WWTP is considered constant throughout all the simulated time. Table A3.3 present the influent flowrate, analytical concentrations and other operational parameters.

Table A3.3. Influent of WWTP. Flowrate, temperature, pH and concentrations.

Variable	Units	Value
Influent flowrate	[m <sup>3</sup> d <sup>-1</sup> ]	62000
COD	[g COD m <sup>-3</sup> ]	628.8
BOD <sub>5</sub>	[g BOD <sub>5</sub> m <sup>-3</sup> ]	240
TKN	[g N m <sup>-3</sup> ]	66.92
TN	[g N m <sup>-3</sup> ]	66.92
NH <sub>4</sub> <sup>+</sup>	[g N m <sup>-3</sup> ]	40
TP	[g P m <sup>-3</sup> ]	15.88
Phosphates	[g P-PO <sub>4</sub> <sup>3-</sup> m <sup>-3</sup> ]	10
TSS	[g TSS m <sup>-3</sup> ]	348.42
Temperature	[°C]	20
pH	[-]	7

The characterization of the influent, i.e. the transformation of the analytical measures of contaminants into model state variable are given in Table A3.4.

Table A3.4. Characterization of the WWTP influent.

State Variable	Units	Value
S <sub>O2</sub>	[g COD m <sup>-3</sup> ]	0
S <sub>F</sub>	[g COD m <sup>-3</sup> ]	100
S <sub>A</sub>	[g COD m <sup>-3</sup> ]	40
S <sub>NH4</sub>	[g N m <sup>-3</sup> ]	40
S <sub>NH2OH</sub>	[g N m <sup>-3</sup> ]	0
S <sub>N2O</sub>	[g N m <sup>-3</sup> ]	0
S <sub>NO</sub>	[g N m <sup>-3</sup> ]	0
S <sub>NO2</sub>	[g N m <sup>-3</sup> ]	0
S <sub>NO3</sub>	[g N m <sup>-3</sup> ]	0
S <sub>PO4</sub>	[g P m <sup>-3</sup> ]	10
S <sub>I</sub>	[g COD m <sup>-3</sup> ]	30
S <sub>ALK</sub>	[mole HCO <sub>3</sub> <sup>-</sup> m <sup>-3</sup> ]	15
S <sub>N2</sub>	[g N m <sup>-3</sup> ]	0
X <sub>I</sub>	[g COD m <sup>-3</sup> ]	30
X <sub>S</sub>	[g COD m <sup>-3</sup> ]	400
X <sub>H</sub>	[g COD m <sup>-3</sup> ]	28.8
X <sub>PAO</sub>	[g COD m <sup>-3</sup> ]	0
X <sub>PP</sub>	[g P m <sup>-3</sup> ]	0
X <sub>PHA</sub>	[g COD m <sup>-3</sup> ]	0
X <sub>AOB</sub>	[g COD m <sup>-3</sup> ]	0
X <sub>NOB</sub>	[g COD m <sup>-3</sup> ]	0
X <sub>TSS</sub>	[g TSS m <sup>-3</sup> ]	348.42
X <sub>MeOH</sub>	[g TSS m <sup>-3</sup> ]	0
X <sub>MeP</sub>	[g TSS m <sup>-3</sup> ]	0

### A3.2.3. WWTP energy consumption

The energy consumption in a WWTP depends on the operational conditions and the equipment used. In the developed model, the simulation of the energy consumption is based on the number of installed equipment ( $n$ ), the rated power of each equipment (RP) and the operational time of the equipment (OT) (Equation A3.1):

$$E = n \cdot RP \cdot OT \quad [\text{kWh d}^{-1}] \quad (\text{Eq. A3.1})$$

The considered equipment for the energy consumption calculation in the dynamic model includes the inlet, intermediate, recirculation and wastage pumps, the associated equipment of the primary sedimentation tank, the mixing and aeration of the biological reactors, the rotating bridge of the secondary settler, the associated equipment of the sludge thickening and dewatering, the energy consumption due to the heating of the



anaerobic digester and the energy credit due to electricity generation due to biogas production. Additional details about the calculation of energy consumption of each unit process can be found in Deliverable 3.1. of the C-FOOT-CTRL project.

#### *A3.2.4. Estimation of GHG emissions*

The GHG emissions of the WWTP are divided into direct and indirect emissions. In the dynamic model CO<sub>2</sub>, N<sub>2</sub>O and CH<sub>4</sub> emissions are predicted in each unit process. The direct emissions accounted for in the dynamic model were due to the biological treatment and the biogas production, while for the indirect emissions it was assumed that they are due to energy consumption of the WWTP, chemicals usage, effluent discharge and sludge disposal. All the GHG are expressed as CO<sub>2</sub> equivalents by transforming the mass of each GHG by their global warming potential factor (IPCC, 2014).

For the biological reactor, the ASM2d-N<sub>2</sub>O model (Massara et al., 2018) mechanistically describes the N<sub>2</sub>O emissions. The biogenic CO<sub>2</sub> emissions are calculated by the addition of the stoichiometry of the IC and assuming that all the produced IC is stripped in the aerobic reactors. In the anaerobic digester the total GHG emissions concerning the produced biogas include the use of the biogas for the production of heat and electrical energy (emitted as CO<sub>2</sub>) and the leaks from the digester. Additional details on the estimation of the GHG emissions can be found in Deliverable 3.1 and Deliverable 7.2 of the C-FOOT-CTRL project.

#### *A3.2.5. Evaluation criteria*

Three performance indices were used to select the scenarios that best mitigate GHG emissions: i) the total GHG emissions of the WWTP, ii) the Effluent Quality Index (EQI) and iii) the total energy consumption of the WWTP.

These three performance indices are calculated per cubic meter of treated influent, in order to make comparisons between different WWTPs. The objective of the mitigation strategies is to reduce the first performance index, i.e. the GHG emissions, while reducing the total energy consumption and the EQI if possible.

- Total GHG emissions is the main index to understand the extent of GHG mitigation. The Total GHG emissions are reported as CO<sub>2</sub> equivalent per cubic meter of treated influent and are the sum of all the emissions calculated in each unit of the WWTP and the off-site emissions.
- The EQI measures the overall pollution removal efficiency and it is a value adapted from the standard BSM2 (Nopens et al., 2010). The EQI is an aggregated weighted index of all pollution loads: TSS, COD, BOD<sub>5</sub>, total Kjeldahl nitrogen (TKN), oxidized forms of nitrogen (NO<sub>x</sub>) and Total Phosphorus (TP) leaving the

WWTP. The EQI is reported in units of kg of pollution units (PU) per cubic meter of treated influent.

- The total energy consumption performance index refers to the operational costs of the WWTPs to treat each cubic meter of the influent. The total energy consumption is the sum of the energy consumption of all the individual subunits of the WWTP. For the calculations of the total energy consumption of the WWTP please refer to Deliverable 3.1 reference. The total energy consumption is reported as kWh m<sup>-3</sup>.

#### A3.2.6. System Analysis

The systems analysis aims at studying the effect of some operational parameters on the performance indices selected for comparison. Then, adequate control strategies for GHG mitigation GHG will be designed. Three different operational parameters are analysed: the Sludge Retention Time (SRT), the Dissolved Oxygen (DO) concentration in the aerobic compartments and the solids removal efficiency in the Primary Clarifier (PC). In a sensitivity study, the desired operational variable is changed between a minimum and a maximum value, with the rest of parameters kept constant. The results show how this operational parameter affects to the effluent quality, the energy consumption and the GHG emissions. Table A3.5 shows the different parameters evaluated in the system analyses of this study.

Table A3.5. List of the system analysis performed in this study.

<b>SRT:</b>
- SRT (days) = 3, 5, 6, 7, 8, 9, 10, 11, 12, 13, 14, 15, 20, 25 and 30
- DO Set Point = 2 g O <sub>2</sub> m <sup>-3</sup>
- PC solids removal efficiency = 40%
<b>DO:</b>
- DO Set Points (g O <sub>2</sub> m <sup>-3</sup> ) = 0.5, 0.6, 0.7, 0.8, 0.9, 1.0, 1.1, 1.2, 1.3, 1.4, 1.5, 1.6, 1.7, 1.8, 1.9, 2.0, 2.5, 3.0, 4.0 and 5.0.
- SRT = 10 days
- PC solids removal efficiency = 40%
<b>PC solids removal efficiency:</b>
- PC efficiency (%) = 40, 50, 60, 70, 80 and 90
- SRT = 10 days
- DO Set Points = 2 g O <sub>2</sub> m <sup>-3</sup>

#### A3.2.7. Scenarios and simulations procedure

Two different scenarios are designed to study the effect that different control strategies have on the performance indices: the GHG emissions, the EQI and the energy consumption. The scenarios and the description of the scenarios are presented in Table A3.6.

Table A3.6. Scenarios list and description.

Scenario number	Scenario description	Procedure
Scenario 1	Low increase of the influent $\text{NH}_4^+$ load	At time 10 days, the influent N- $\text{NH}_4$ is increased by $5 \text{ g N-NH}_4^+ \text{ m}^{-3}$ .
Scenario 2	High increase of the influent $\text{NH}_4^+$ load	At time 10 days, the influent N- $\text{NH}_4$ is increased by $10 \text{ g N-NH}_4^+ \text{ m}^{-3}$ .

The scenario set-up for the mitigation strategies study is the following:

- 1) The initial conditions for the scenario run are based on the steady state results for the default control strategy of the WWTP.
- 2) The scenario tested is based on an initial constant influent and at time 10 days a disturbance based on an increase in the ammonium concentration in the influent is applied.
- 3) One simulation is performed with the dynamic model for each one of the control strategies proposed.
- 4) The simulation is maintained until a new steady state is achieved with each control strategy.

The results of each performance index are evaluated with the aim of reducing the three performance indices, focusing on the reduction of the total GHG emissions.

#### A3.2.8. Control strategies implemented

Four different control strategies are studied for the scenarios showed in Table A3.6. The different control strategies and the individual control loops that are implemented in the dynamic model are shown in the following sections. The set points of the control loops are selected through the system analysis results.

##### A3.2.8.1. Closed loop 0 (CL0)

The default control strategy of the WWTP (CL0) will be considered as the base case. Then, we will analyse how the new control strategies mitigates the GHG as well as the impact on the EQI and the energy consumption. The individual control loops are shown in Table A3.7.

Table A3.7. Individual control loops description for CL0 control strategy.

Controlled Variable	Manipulated Variable	Set Point (SP)	Description
DO aerobic reactor 1	$k_{La}$ of the aerobic reactor 1 (equivalent to air flowrate)	$2.0 \text{ g O}_2 \text{ m}^{-3}$	PI control to maintain the desired DO concentration in the aerobic reactor 1
DO aerobic reactor 2	$k_{La}$ of the aerobic reactor 2	$2.0 \text{ g O}_2 \text{ m}^{-3}$	PI control to maintain the desired DO concentration in the aerobic reactor 2

Controlled Variable	Manipulated Variable	Set Point (SP)	Description
DO aerobic reactor 3	$k_{La}$ of the aerobic reactor 3	2.0 g O <sub>2</sub> m <sup>-3</sup>	PI control to maintain the desired DO concentration in the aerobic reactor 3
DO aerobic reactor 4	$k_{La}$ of the aerobic reactor 4	2.0 g O <sub>2</sub> m <sup>-3</sup>	PI control to maintain the desired DO concentration in the aerobic reactor 4
SRT	WAS flow (Q <sub>w</sub> )	10 days	PI control to maintain the desired SRT in the activated sludge.

#### A3.2.8.2. Closed loop 1 (CL1)

The CL1 control strategy is based on the CL0, but the set points of the DO concentration of the aerobic reactors depend on the ammonium load at the influent. The individual control loops are shown in Table A3.8.

Table A3.8. Individual control loops description for CL1 control strategy.

Controlled Variable	Manipulated Variable	Set Point (SP)	Description
DO aerobic reactor 1	$k_{La}$ of the aerobic reactor 1 (equivalent to air flowrate)	2 or 3 gO <sub>2</sub> m <sup>-3</sup>	Cascade-feedforward control to maintain the desired DO concentration in the aerobic reactor 1. The SP is changed according to the influent NH <sub>4</sub> concentration. When the NH <sub>4</sub> concentration is the same or lower as in the system analysis (40 g N m <sup>-3</sup> ) the DO SP is 2.0 g O <sub>2</sub> m <sup>-3</sup> . When the NH <sub>4</sub> concentration increases, the DO SP increases to 3 g O <sub>2</sub> m <sup>-3</sup> .
DO aerobic reactor 2	$k_{La}$ of the aerobic reactor 2	2 or 3 gO <sub>2</sub> m <sup>-3</sup>	Same as DO aerobic reactor 1
DO aerobic reactor 3	$k_{La}$ of the aerobic reactor 3	2 or 3 gO <sub>2</sub> m <sup>-3</sup>	Same as DO aerobic reactor 1
DO aerobic reactor 4	$k_{La}$ of the aerobic reactor 4	2 or 3 gO <sub>2</sub> m <sup>-3</sup>	Same as DO aerobic reactor 1
SRT	WAS flow (Q <sub>w</sub> )	10 days	PI control to maintain the desired SRT in the activated sludge.

#### A3.2.8.3. Closed loop 2 (CL2)

The CL2 control strategy is based on CL0, but in this control strategy a new control loop is added to maintain the concentration of oxidized forms of nitrogen (NO<sub>x</sub>=NO<sub>3</sub><sup>-</sup>+NO<sub>2</sub><sup>-</sup>) in the anoxic reactor at a fixed value. The manipulated variable is the flow of external

carbon source, which is added to improve denitrification. This strategy reduces the amount of  $\text{NO}_3^-$  and  $\text{NO}_2^-$  that enter to the first aerobic reactor. The individual control loops are detailed in Table A3.9.

Table A3.9. Individual control loops description for CL2 control strategy.

Controlled Variable	Manipulated Variable	Set Point (SP)	Description
DO aerobic reactor 1	$k_{L,a}$ of the aerobic reactor 1 (equivalent to air flowrate)	2.0 g $\text{O}_2$ $\text{m}^{-3}$	PI control to maintain the desired DO concentration in the aerobic reactor 1
DO aerobic reactor 2	$k_{L,a}$ of the aerobic reactor 2	2.0 g $\text{O}_2$ $\text{m}^{-3}$	PI control to maintain the desired DO concentration in the aerobic reactor 2
DO aerobic reactor 3	$k_{L,a}$ of the aerobic reactor 3	2.0 g $\text{O}_2$ $\text{m}^{-3}$	PI control to maintain the desired DO concentration in the aerobic reactor 3
DO aerobic reactor 4	$k_{L,a}$ of the aerobic reactor 4	2.0 g $\text{O}_2$ $\text{m}^{-3}$	PI control to maintain the desired DO concentration in the aerobic reactor 4
SRT	WAS flow ( $Q_w$ )	10 days	PI control to maintain the desired SRT in the activated sludge.
$\text{NO}_3^- + \text{NO}_2^-$ in anoxic reactor	Methanol flow added in the anoxic reactor	0.1 g N- $\text{NO}_x$ $\text{m}^{-3}$	PI control to maintain the desired $\text{NO}_x$ concentration in the anoxic zone. More methanol flow is added to the anoxic reactor to favour the denitrification.

#### A3.2.8.4. Closed loop 3 (CL3)

The CL3 control strategy is a sum of the CL1 and CL2. Readily organic matter is added in the anoxic reactor to promote the denitrification when the influent N load is increased and the DO set points are changed depending on the influent  $\text{NH}_4$  concentration. The individual control loops are detailed in Table A3.10.

Table A3.10. Individual control loops description for CL3 control strategy.

Controlled Variable	Manipulated Variable	Set Point (SP)	Description
DO aerobic reactor 1	$k_{L,a}$ of the aerobic reactor 1 (equivalent to air flowrate)	2 or 3 g $\text{O}_2$ $\text{m}^{-3}$	Cascade-feed forward control to maintain the desired DO concentration in the aerobic reactor 1. The SP is changed according to the influent $\text{NH}_4$ concentration. When the $\text{NH}_4$ concentration is the same or lower as in the system analysis (40 g N $\text{m}^{-3}$ ) the DO SP is 2 g $\text{O}_2$ $\text{m}^{-3}$ .

Controlled Variable	Manipulated Variable	Set Point (SP)	Description
			When the $\text{NH}_4$ concentration increases, the DO SP increases to $3 \text{ g O}_2 \text{ m}^{-3}$ .
DO aerobic reactor 2	$k_{\text{La}}$ of the aerobic reactor 2	2 or $3 \text{ gO}_2 \text{ m}^{-3}$	Same as DO aerobic reactor 1
DO aerobic reactor 3	$k_{\text{La}}$ of the aerobic reactor 3	2 or $3 \text{ gO}_2 \text{ m}^{-3}$	Same as DO aerobic reactor 1
DO aerobic reactor 4	$k_{\text{La}}$ of the aerobic reactor 4	2 or $3 \text{ gO}_2 \text{ m}^{-3}$	Same as DO aerobic reactor 1
SRT	WAS flow ( $Q_w$ )	10 days	PI control to maintain the desired SRT in the activated sludge.
$\text{NO}_3^- + \text{NO}_2^-$ in anoxic reactor	Methanol flow added in anoxic reactor	$0.1 \text{ g NO}_x \text{ m}^{-3}$	PI control to maintain the desired $\text{NO}_x$ concentration in the anoxic zone. More methanol flow is added in the anoxic reactor to favour the denitrification.

### A3.3. Results

#### A3.3.1. System Analysis

##### A3.3.1.1. Sludge Retention Time

Figure A3.2a shows that, for SRT lower than 3 days, the EQI obtained is the highest, with a value of  $1.9 \text{ kg pollution units m}^{-3}$ , because neither the Biological Nitrogen Removal (BNR) nor the Enhanced Biological Phosphorus Removal (EBPR) are performed (Figure A3.3). For SRTs between 5 and 8 days, the EQI decreases since EBPR is achieved, obtaining Total Phosphorus (TP) concentrations in the effluent below the legal limits of discharge of  $1 \text{ g P m}^{-3}$ . Finally, at an SRT of 9 days, there is a sharp decrease of EQI because both BNR and EBPR are achieved, obtaining Total Nitrogen (TN) concentrations in the effluent below the legal limits of discharge of  $10 \text{ g N m}^{-3}$ . The minimum EQI obtained is  $0.22 \text{ kg pollution unit m}^{-3}$  for an operating SRT of 10 days. At SRTs higher than 10 days, the EQI obtained slightly increases because the soluble  $\text{PO}_4^{3-}$  concentrations and hence the TP concentrations at the effluent increases. As the SRT increases, the wastage activated sludge (WAS) flow decreases and less P is removed through the sludge.

Regarding the energy consumption (Figure A3.2b), the results show that the minimum value is obtained at the minimum SRT of 3 days ( $0.26 \text{ kWh m}^{-3}$ ) and that the energy consumption increases proportionally to the SRT up to a maximum of  $0.37 \text{ kWh m}^{-3}$  observed at the highest SRT tested of 30 days. For SRT below 8 days, the energy consumption remains practically constant since nitrification is not achieved and, therefore, aeration is only related to organic matter oxidation. As the SRT increases and,

thus, nitrification is achieved, the energy consumption increases notably since more oxygen is needed for nitrification (SRT higher than 9 days). Short-cut nitrogen removal (i.e. nitrification and nitrite-denitrification) occurs at some extent at SRT between 9 and 15 days. This implies lower oxygen demand than conventional biological nitrogen removal and that part of the nitrogen effluent is nitrite (Figure A3.4). However, at higher values, the nitrification/denitrification processes are complete processes and ammonium is oxidised to nitrate (Figure A3.4) and hence aeration demand is higher. From SRTs of 15 days onwards, the energy consumption increases because more aeration is needed at higher biomass concentrations.

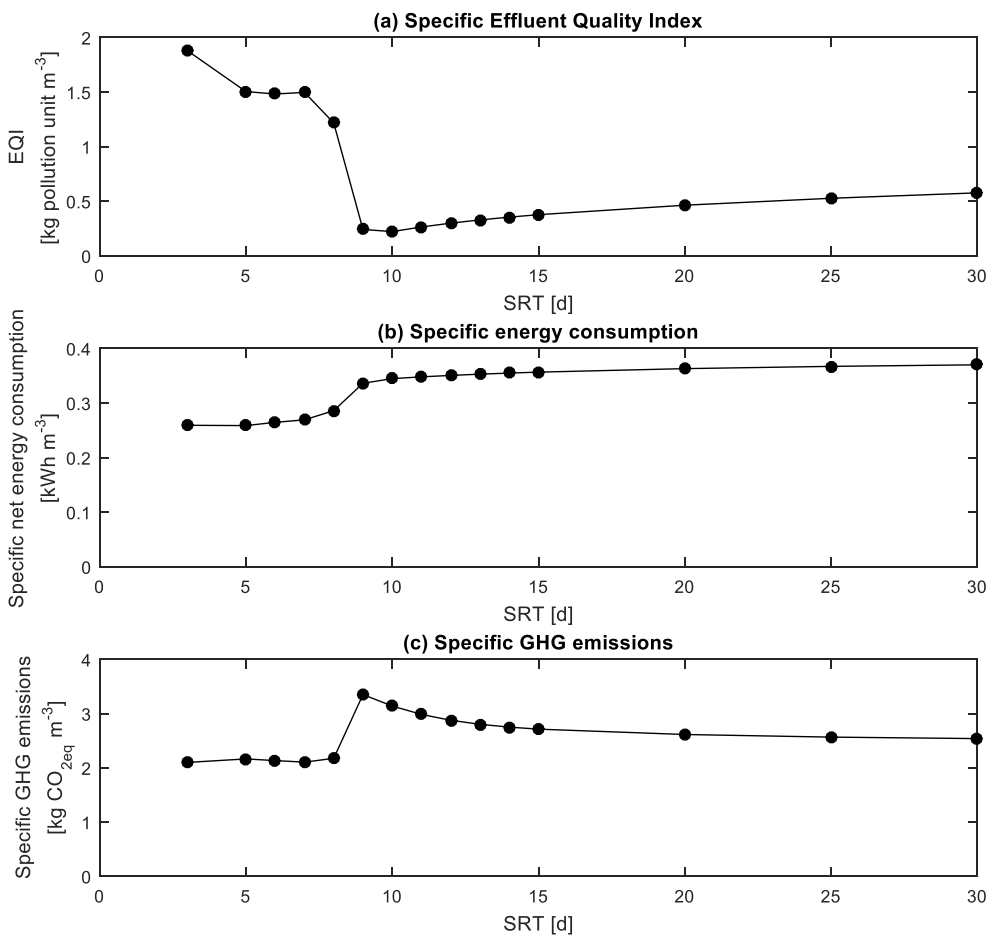


Figure A3.2. Performance indices for the SRT system analysis. Effluent Quality Index (a), total energy consumption (b) and total GHG emissions (c).

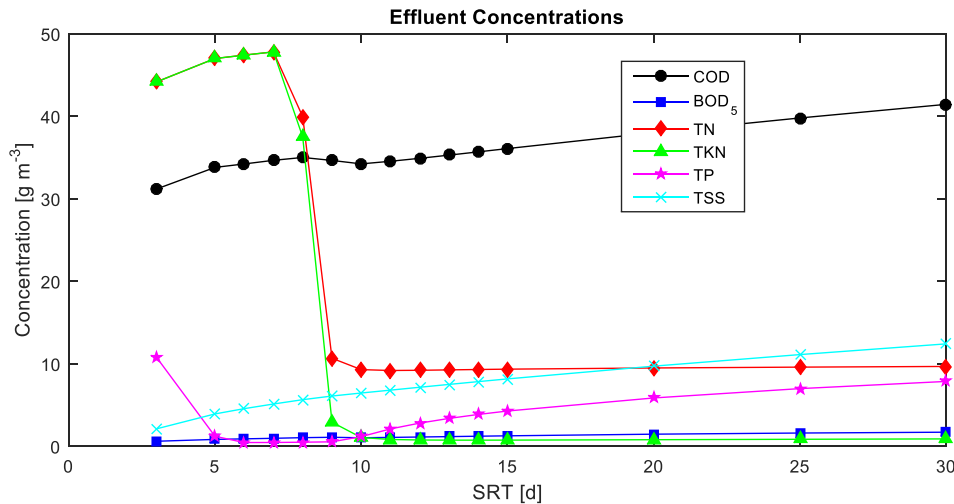


Figure A3.3. Analytical concentrations at the effluent for the SRT system analysis.

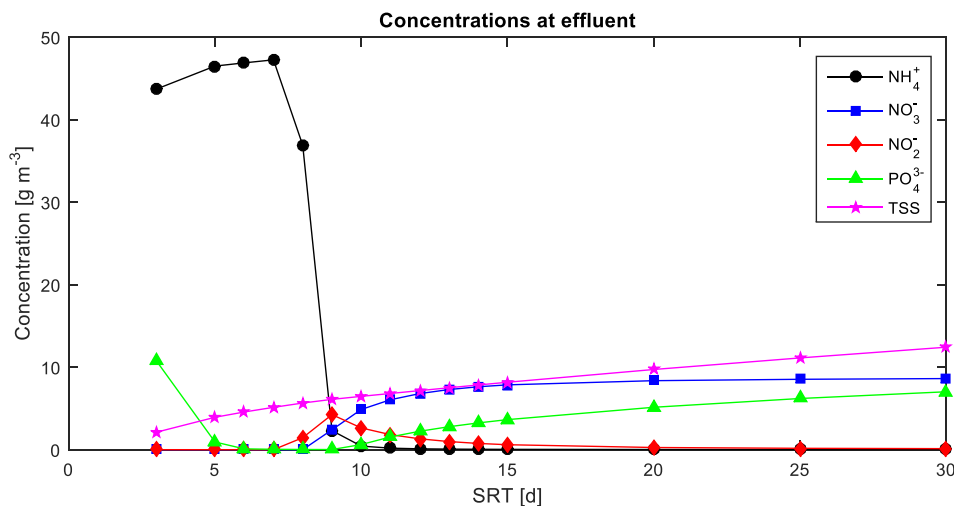


Figure A3.4. Concentrations at the effluent for the SRT system analysis.

Figure A3.2c shows the results of the GHG emissions. The minimum value of GHG emissions obtained are at SRT below 8 days ( $2.1 \text{ kg CO}_{2\text{eq}} \text{ m}^{-3}$ ), since the BNR is not achieved (Figure A3.4) and, therefore, the total GHG emissions do not include  $\text{N}_2\text{O}$ . At SRT of 9 days, there is a sharp increase in the GHG emissions because BNR is achieved via nitrite and during SRTs from 9 to 30 days the emissions decrease. The obtained peak of GHG emissions at SRT of 9 days is mostly due to the  $\text{N}_2\text{O}$  emissions (Figure A3.5). The emitted  $\text{N}_2\text{O}$  at different SRTs shows the same trend as the total GHG emissions. The maximum values at SRT of 9 days are  $0.052 \text{ kg N-N}_2\text{O kg TN}_{\text{in}}^{-1}$  and  $3.35 \text{ kg CO}_{2\text{eq}} \text{ m}^{-3}$ , respectively. The reason is that at SRT of 9 days nitrogen is mostly removed via nitrite. Nitrite is a precursor of  $\text{N}_2\text{O}$  and its presence triggers off its emissions. The total GHG emissions and the  $\text{N}_2\text{O}$  emissions decrease when the SRT increases because the nitrification and denitrification processes are via nitrate (Figure A3.4). The model allows also the calculation of the rates for all the biological  $\text{N}_2\text{O}$  production pathways, and



demonstrates in this case that Nitrifier Denitrification (ND) pathway of the AOBs is the major contributor to the production of  $N_2O$ , since in the presence of  $NO_2^-$  (the substrate of the ND pathway) emissions are higher than in the absence of it.

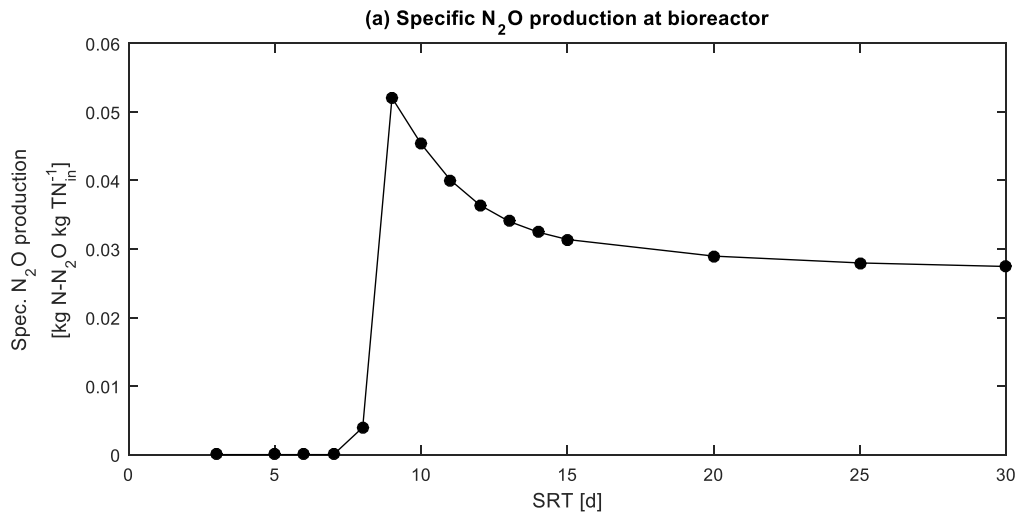


Figure A3.5. Specific  $N_2O$  emissions in the WWTP for the SRT system analysis.

Figure A3.6 shows the energy recovered from the biogas combustion per cubic meter of treated wastewater. An increase of SRT causes a decrease of the energy obtained from the biogas combustion. This fact is because less biogas is produced, since less sludge is diverted to the anaerobic digester (i.e. the WAS flow decreases as SRT increases). The energy recovered from biogas decreases from 0.21 to 0.14  $kWh\ m^{-3}$ , at SRT of 3 and 30 days, respectively. The energy recovery ratio (i.e. the energy recovered from biogas combustion with respect to the total energy consumption) decreases from 85% at SRT = 3 d to 37% at SRT = 30 d.

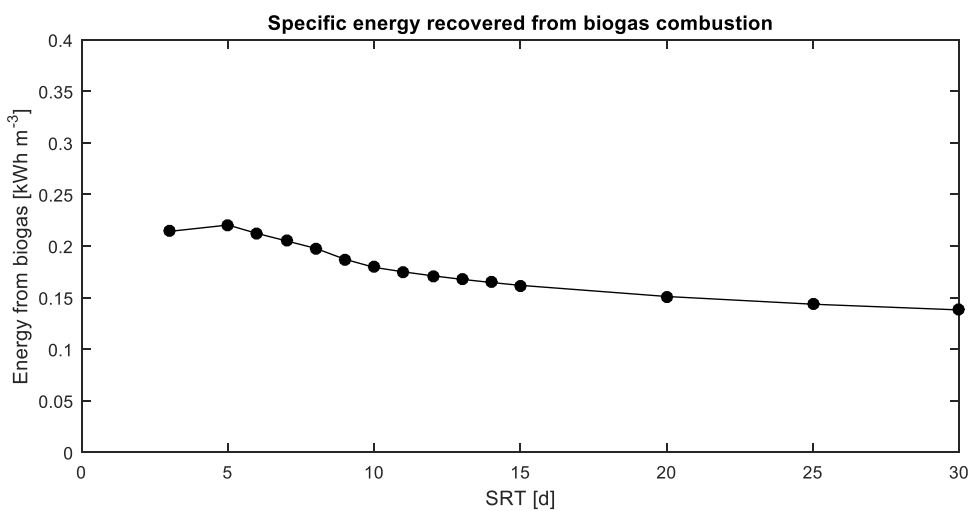


Figure A3.6. Specific energy recovered from biogas combustion for the SRT system analysis.

### A3.3.1.2. Dissolved Oxygen

Figure A3.7 shows the results of the performance indices when the DO set-point for the aerobic reactors is modified: the specific EQI (Figure A3.7a), the specific energy consumption (Figure A3.7b) and the specific total GHG emissions (Figure A3.7c). For DO below  $1.4 \text{ g O}_2 \text{ m}^{-3}$ , the EQI obtained is approximately constant at its maximum value ( $1.5 \text{ kg pollution unit m}^{-3}$ , Figure A3.7a). This is because BNR is not achieved (Figure A3.8 and Figure A3.9), despite EBPR occurs at DO concentrations above  $0.75 \text{ g O}_2 \text{ m}^{-3}$  since the TP concentration at the effluent is below  $1 \text{ g P m}^{-3}$ .

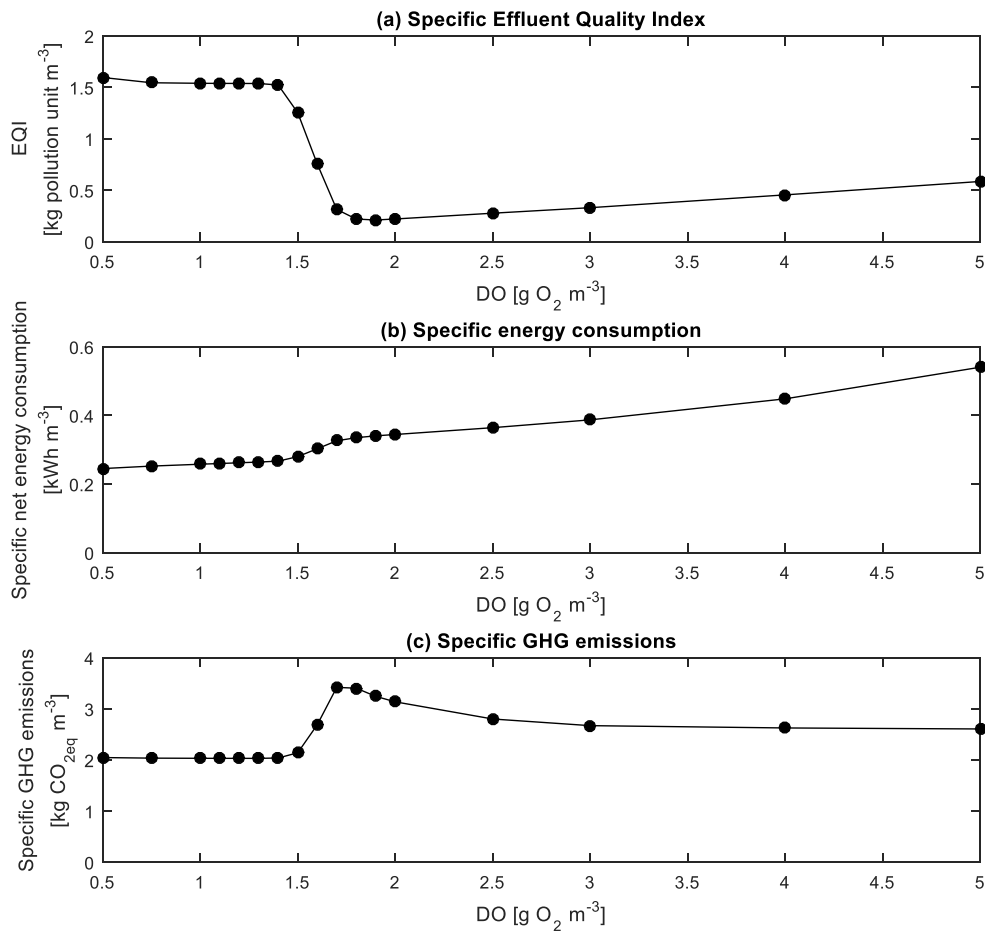


Figure A3.7. Performance indices for the DO system analysis. Effluent Quality Index (a), total energy consumption (b) and total GHG emissions (c).

From a DO setpoint of  $1.5 \text{ g O}_2 \text{ m}^{-3}$  onwards, BNR is achieved and the EQI decreases considerably: all the ammonium is oxidised at a DO of  $2 \text{ g O}_2 \text{ m}^{-3}$ . The minimum EQI obtained is  $0.21 \text{ kg pollution unit m}^{-3}$  with a DO of  $1.9 \text{ g O}_2 \text{ m}^{-3}$ . EQI increases to a value of  $0.59 \text{ kg pollution unit m}^{-3}$  at DO of  $5.0 \text{ g O}_2 \text{ m}^{-3}$  since TP and TN effluent concentrations increase (Figure A3.8). The reason is that the oxygen input to the anoxic reactor increases

due to the increased DO concentration in the last aerobic reactor, which finally affects the anoxic reactor via the internal recycle. Then, the anoxic reactor loses part of its denitrification capacity since part of the organic matter is consumed aerobically with the oxygen recycled from the aerobic reactor. The fact that the effluent TP concentration increases as well is because, with the increase of the DO set point, more nitrate is recirculated to the anaerobic reactor via the external recycle. This causes that part of the anaerobic reactor volume behaves as an anoxic reactor and therefore, the EBPR activity is negatively affected (Figure A3.9).

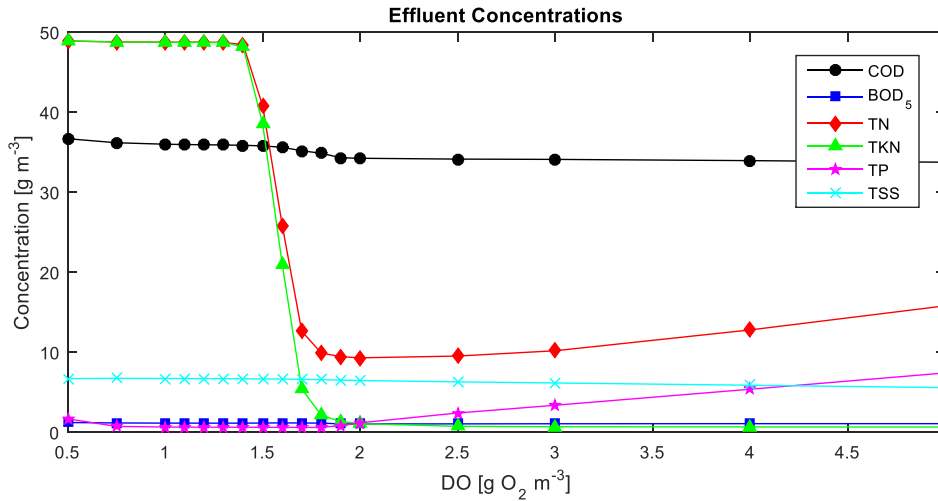


Figure A3.8. Analytical concentrations at the effluent for the DO system analysis.

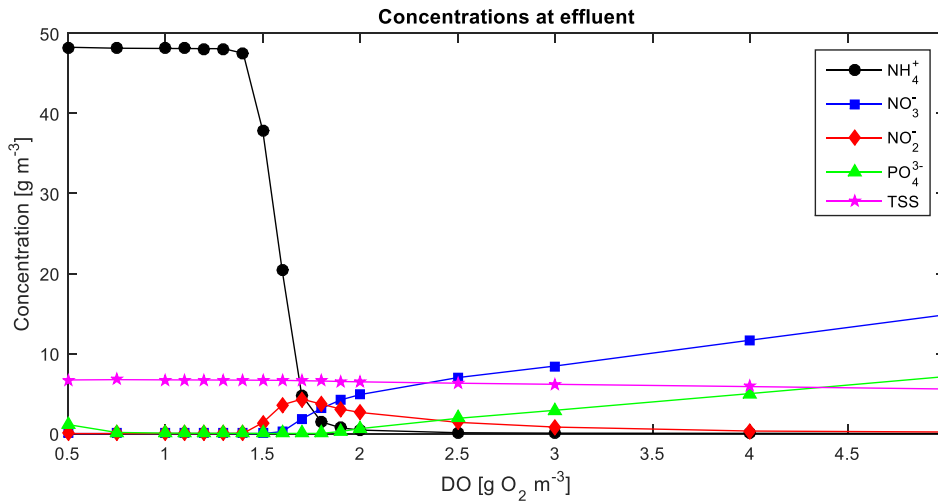


Figure A3.9. Concentrations at the effluent for the DO system analysis.

Figure A3.7c shows the total GHG emissions per cubic meter of treated wastewater for each DO concentration in the aerobic zones. The total GHG emissions remain constant at 2 kg CO<sub>2eq</sub> m<sup>-3</sup> in the DO range of 0.5 to 1.4 g O<sub>2</sub> m<sup>-3</sup>. This is because BNR is not achieved (Figure A3.8) and, therefore, there is no contribution of N<sub>2</sub>O to GHG emissions. From DO values between 1.5 and 1.8 g O<sub>2</sub> m<sup>-3</sup>, there is a sharp increase of the GHG emissions

( $3.4 \text{ kg CO}_{2\text{eq}} \text{ m}^{-3}$ ), and from DO  $1.9 \text{ g O}_2 \text{ m}^{-3}$  forward, the GHG emissions decreases until  $2.6 \text{ kg CO}_{2\text{eq}} \text{ m}^{-3}$  at DO of  $5.0 \text{ g O}_2 \text{ m}^{-3}$ . The increase of the GHG emissions is related to the BNR, since  $\text{N}_2\text{O}$  is being emitted (Figure A3.10). The maximum emissions found, for DO between  $1.5$  and  $1.8 \text{ g O}_2 \text{ m}^{-3}$ , are directly related to nitrite presence. When short-cut BNR is occurring, there is the maximum nitrite concentration at the effluent and this favours  $\text{N}_2\text{O}$  emissions. The major biological pathway for  $\text{N}_2\text{O}$  production when nitrite accumulates is the ND pathway, as nitrite is the substrate of the reaction. An accumulation of nitrite (Figure A3.9) is directly related to an increase of GHG emissions and  $\text{N}_2\text{O}$  emissions (Figure A3.7c and Figure A3.10). For DO higher than  $1.9 \text{ g O}_2 \text{ m}^{-3}$  forward, the GHG and the  $\text{N}_2\text{O}$  emissions decrease because of the decrease of the nitrite concentration in the aerobic reactors (Figure A3.9).

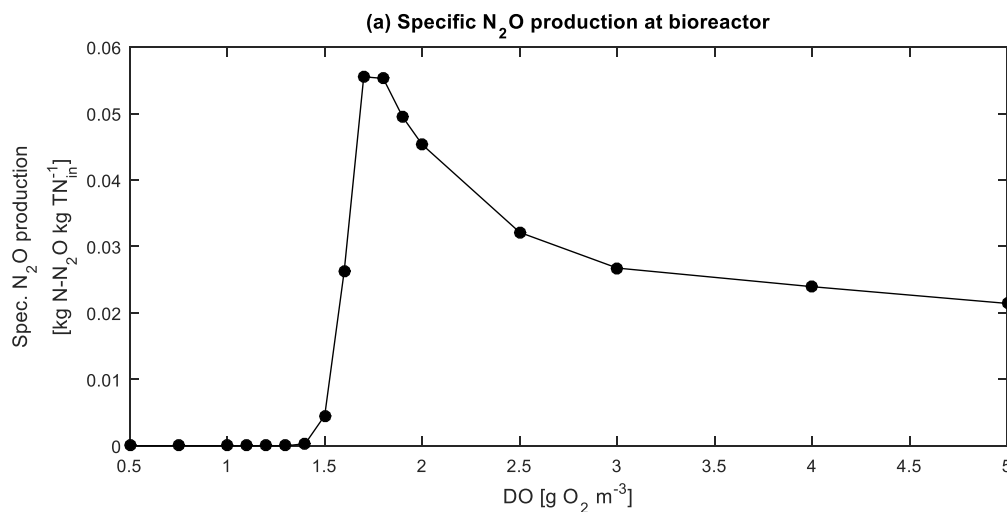


Figure A3.10. Specific  $\text{N}_2\text{O}$  emissions in the WWTP for the DO system analysis.

Regarding the total energy consumption (Figure A3.7b), this value increases with the increase of the DO set points in the aerobic reactors, because the aeration demand increases. There is a sharp increase in the energy consumption between DO set points of  $1.5$  and  $2 \text{ g O}_2 \text{ m}^{-3}$ , because nitrification is achieved and the oxygen consumption of the nitrifying organisms increases. From DO of  $2 \text{ g O}_2 \text{ m}^{-3}$  onwards, the increase of the energy consumption is directly related to the increase of the aeration energy consumption. Figure A3.11 shows the energy recovered from biogas combustion. It shows that the energy recovered slightly decreases with the increase of the DO setpoint in aerobic reactors (from  $0.19 \text{ kWh m}^{-3}$  at DO  $0.5 \text{ g O}_2 \text{ m}^{-3}$  to  $0.17 \text{ kWh m}^{-3}$  at DO  $5.0 \text{ g O}_2 \text{ m}^{-3}$ ). The SRT for all the DO scenarios is the same (10 d) and hence, the mass of sewage sludge being removed from the activated sludge system is almost constant (i.e. the minor variations observed are to compensate the higher biomass growth at higher DO). Then the energy recovery ratio goes from 79% at DO of  $0.5 \text{ g O}_2 \text{ m}^{-3}$  to 32% at DO of  $5.0 \text{ g O}_2 \text{ m}^{-3}$ .

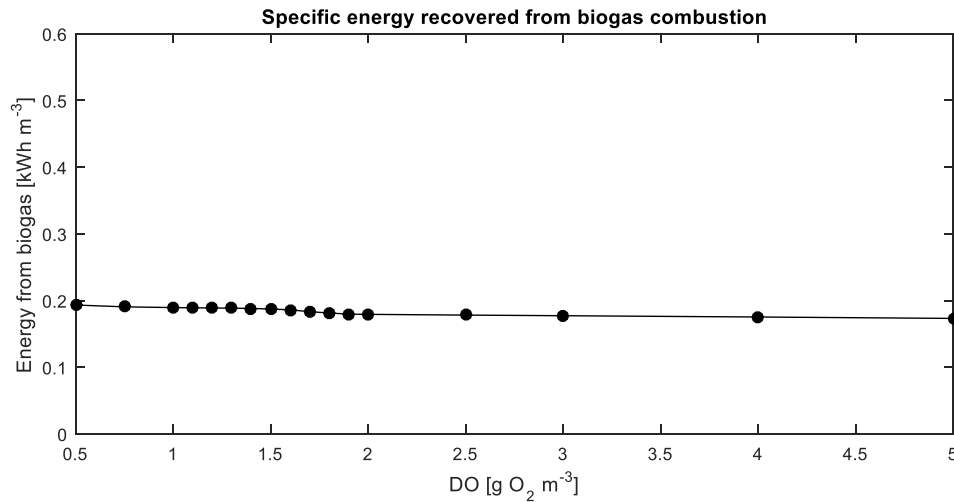


Figure A3.11. Specific energy recovered from biogas combustion for the DO system analysis.

### A3.3.1.3. Primary Clarifier solids removal efficiency

Figure A3.12 shows the results of the performance indices for the PC solids removal efficiency system analysis: the specific EQI (Figure A3.12a), the specific energy consumption (Figure A3.12b) and the total GHG emissions (Figure A3.12c). The EQI obtained increases with the increase of the PC solids removal efficiency from 0.22 to 0.71 kg pollution unit m<sup>-3</sup> at PC solids removal efficiencies of 40 and 90%, respectively. This EQI increase is due to the increase of the effluent TN and TP concentrations (Figure A3.13). The increase of the PC solids removal efficiency implies an increase of the particulate COD removal, which causes a decrease on the denitrification capacity in the anoxic reactor. When the influent carbon to nitrogen ratio (C/N) decreases, there might be a lack of COD available to denitrify the oxidized nitrogen species (NO<sub>x</sub>, i.e. nitrate and nitrite). Then, more NO<sub>x</sub> is recirculated to the anaerobic reactor (via the external recirculation), which in turn causes a loss of the EBPR capacity and an increase of the TP effluent concentration (Figure A3.13 and Figure A3.14).

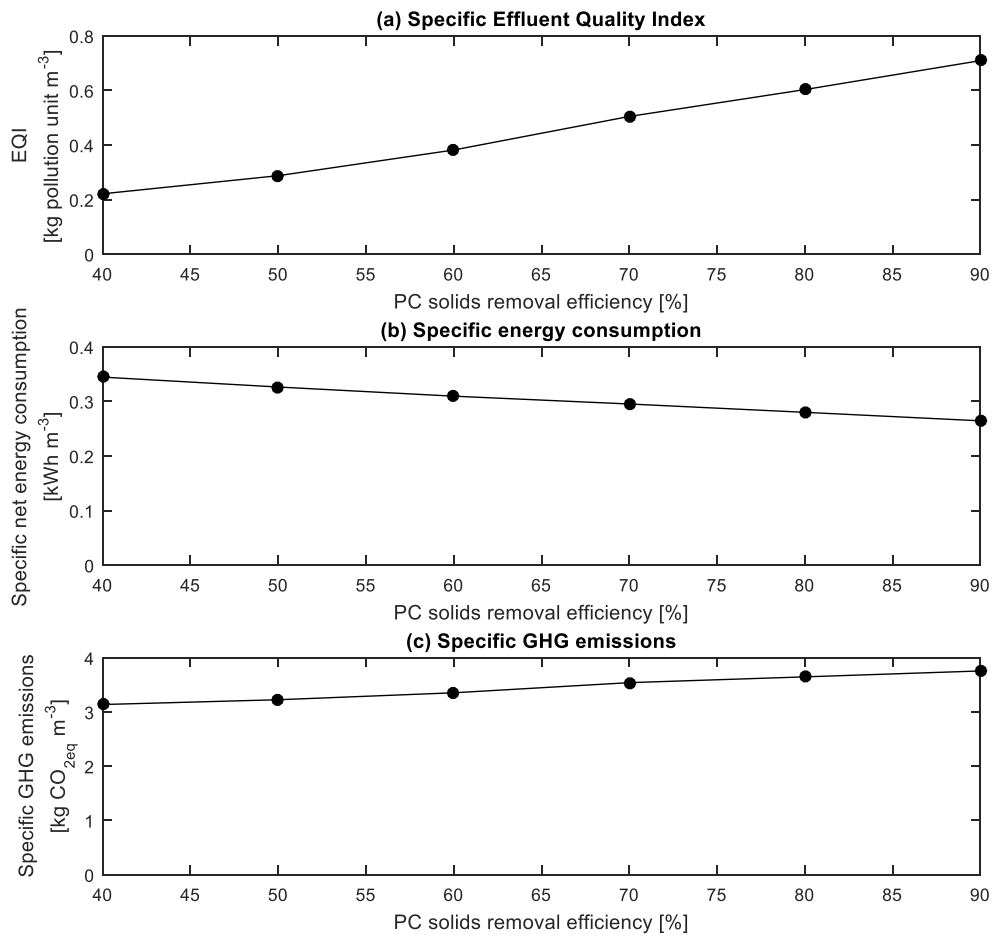


Figure A3.12. Performance indices for the PC solids removal efficiency system analysis. Effluent Quality Index (a), total energy consumption (b) and total GHG emissions (c).

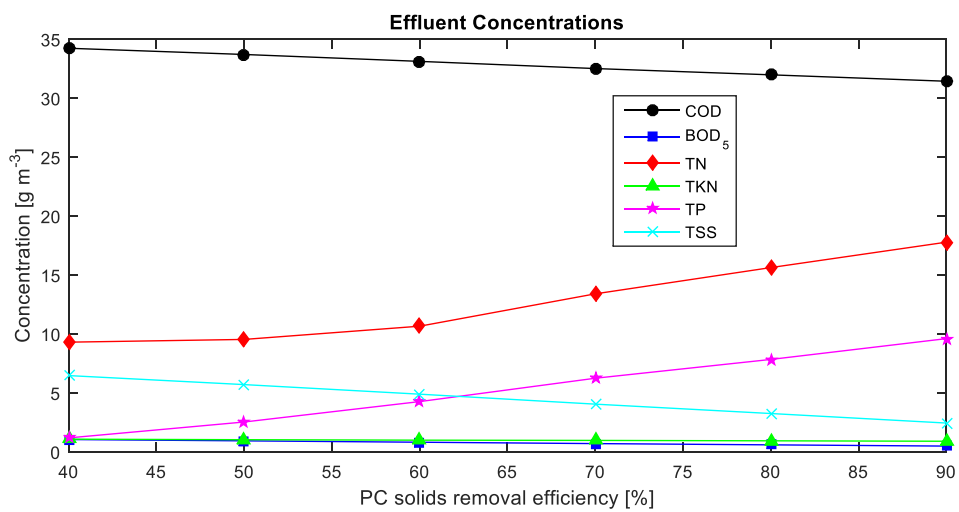


Figure A3.13. Analytical concentrations at the effluent for the PC solids removal efficiency system analysis.

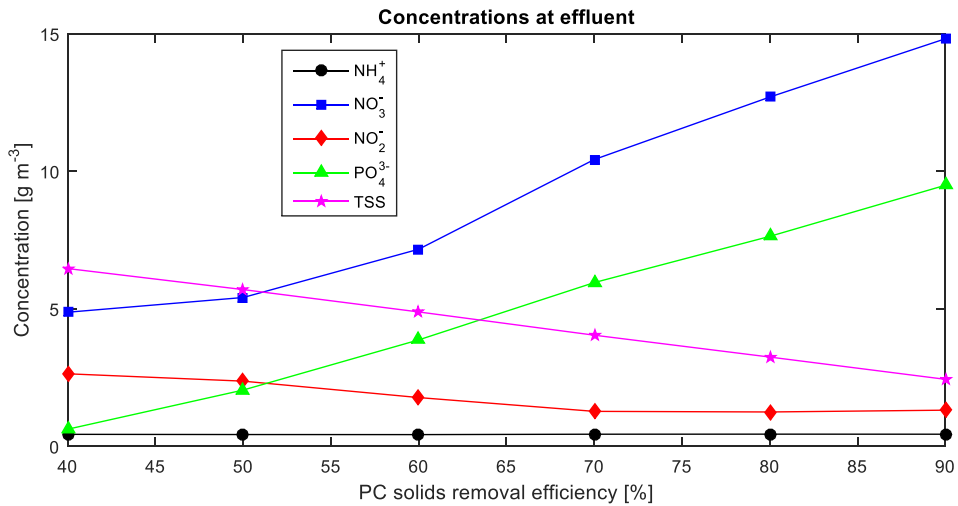


Figure A3.14. Concentrations at the effluent for the PC solids removal efficiency system analysis.

Regarding the total energy consumption, the results show that an increase of the PC solids removal efficiency causes a decrease on the total energy consumption of the WWTP, from 0.34 kWh m<sup>-3</sup> with a PC solids removal efficiency of 40% to 0.26 kWh m<sup>-3</sup> with a PC solids removal efficiency of 90% (Figure A3.12b). When influent particulate COD decreases, less biomass is produced and, therefore, less oxygen is consumed. This causes a reduction in the aeration needs. Figure A3.15 shows the energy obtained from the biogas combustion at the cogeneration unit. The energy obtained from biogas increases linearly with the increase of the PC solid removal efficiency, from 0.18 to 0.27 kWh m<sup>-3</sup> with PC solids removal efficiency of 40 and 90%, respectively. The increase of the PC solids removal efficiency results in a primary sludge with higher COD content and, therefore, the COD load entering to the anaerobic digester and the biogas production are higher.

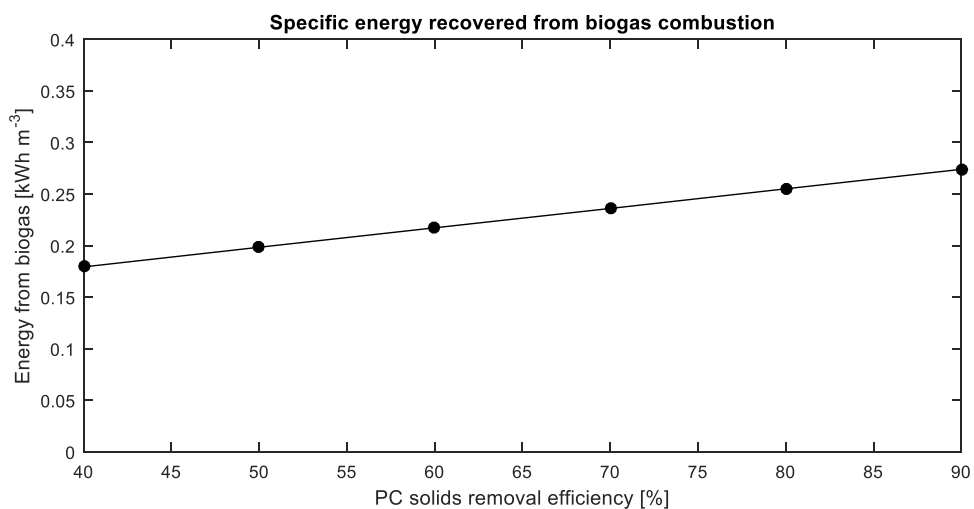


Figure A3.15. Specific energy recovered from biogas combustion for the PC solids removal efficiency system analysis.

Figure A3.12c shows the total GHG emissions per cubic meter of wastewater treated obtained per each PC solids removal efficiency. The GHG emissions increase with the increase of the PC solids removal efficiency, from 3.1 to 7.5 kg CO<sub>2eq</sub> m<sup>-3</sup> with PC solids removal efficiency of 40 and 90%, respectively. This increase is related to the increase of the N<sub>2</sub>O emissions (Figure A3.16), which is caused by the loss of the denitrification capacity associated to lower influent particulate COD. As shown in Figure A3.17, the increase of the PC solids removal efficiency causes an accumulation of N-NO<sub>2</sub><sup>-</sup> in the anoxic reactor as there is no COD available for the biomass to denitrify the NO<sub>x</sub>. This causes NO<sub>2</sub><sup>-</sup> accumulation and an increase of the N<sub>2</sub>O emissions. However, higher NO<sub>2</sub><sup>-</sup> in the anoxic reactor causes a decrease of the N-NO<sub>2</sub><sup>-</sup> concentration in the two last aerated reactors and a decrease of the N<sub>2</sub>O emissions in these reactors (Figure A3.17). In any case, the total N<sub>2</sub>O emissions and the total GHG emissions increase with the increase of NO<sub>2</sub><sup>-</sup> in the anoxic reactor (Figure A3.12 and Figure A3.14).

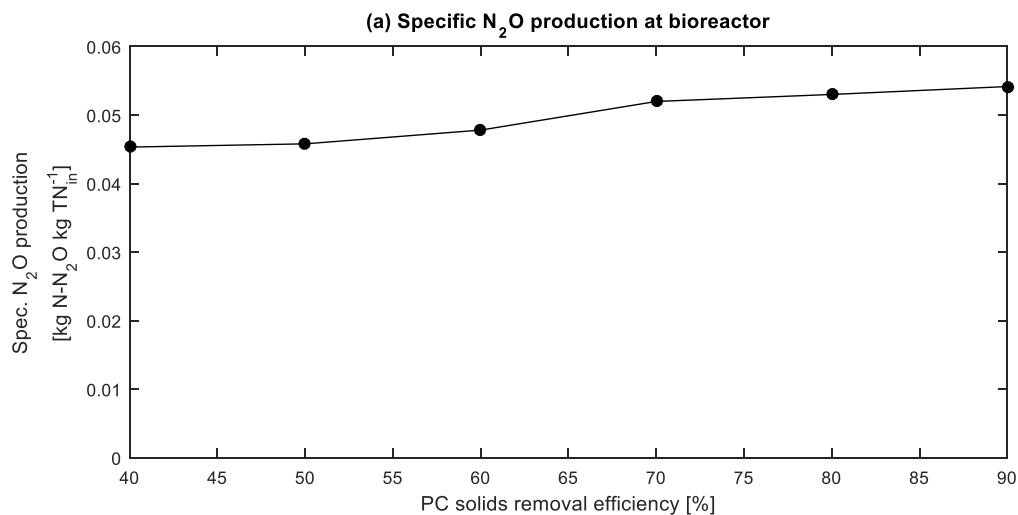


Figure A3.16. Specific N<sub>2</sub>O emissions in the WWTP for the PC solids removal efficiency system analysis.



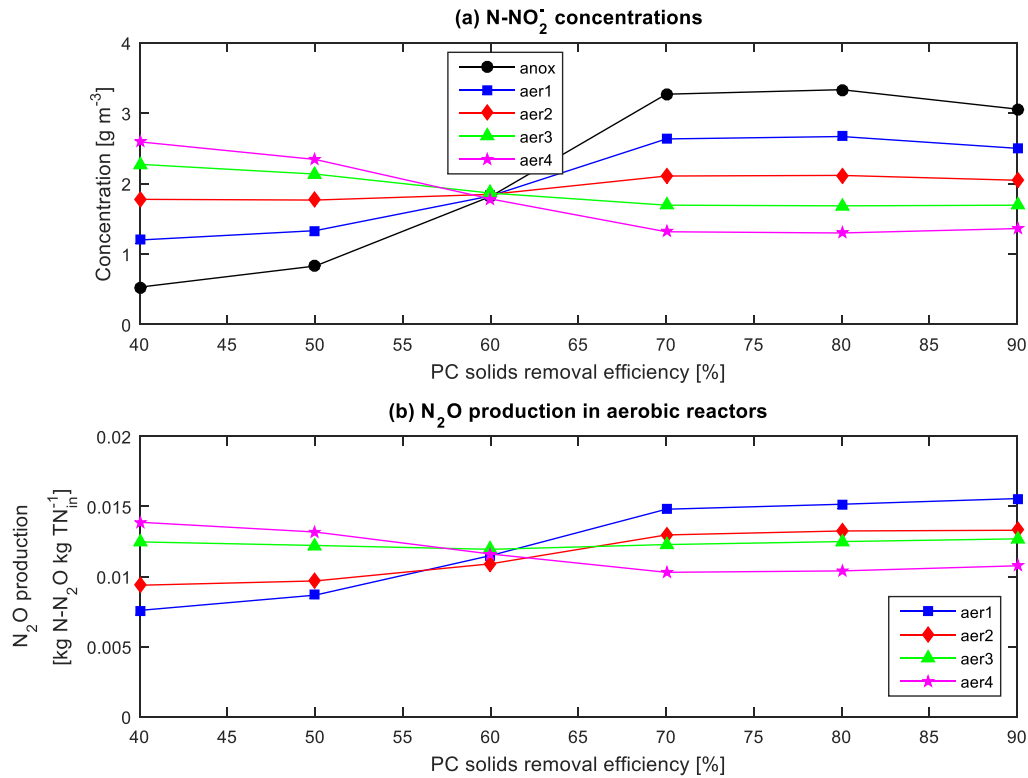


Figure A3.17. Nitrite (N-NO<sub>2</sub><sup>-</sup>) concentrations in anoxic and aerobic reactors (a) and N<sub>2</sub>O emission in each aerobic reactor (b) for the PC solids removal efficiency system analysis.

### A3.3.2. Scenarios

#### A3.3.2.1. Scenario 1: Low influent N-NH<sub>4</sub><sup>+</sup> step increase

The results for the scenario 1, i.e. an increase of the influent N-NH<sub>4</sub><sup>+</sup> of 5 g N m<sup>-3</sup> (Figure A3.18) are summarized in the following figures. The SRT and the PC solids removal efficiency for all the results were maintained at 10 days and 40%, respectively.

Figure A3.18 shows the increase of the ammonium influent concentration from 40 to 45 g N-NH<sub>4</sub> m<sup>-3</sup> at time 10 days, which represents an increase of 12.5% of the ammonium load, from 2480 to 2790 kg N-NH<sub>4</sub> d<sup>-1</sup>. The effluent N-NH<sub>4</sub><sup>+</sup> concentration increases for all control strategies followed by a decrease below 1 g N-NH<sub>4</sub> m<sup>-3</sup>. There is a peak for control strategies CL0 and CL2. The maximum effluent N-NH<sub>4</sub><sup>+</sup> peak found was for the control strategy CL2 (2.8 g N-NH<sub>4</sub> m<sup>-3</sup>), the second maximum peak found was for the default control strategy (CL0, 1.8 N-NH<sub>4</sub> m<sup>-3</sup>), while for the CL1 and CL3 control strategies, the maximum effluent NH<sub>4</sub><sup>+</sup> concentration was 0.22 g N-NH<sub>4</sub> m<sup>-3</sup>.

Figure A3.19 and Figure A3.20 show the total GHG emissions and the N<sub>2</sub>O emissions from the bioreactor, respectively. For CL0, the total GHG emissions increase by 6.7% due to the ammonium influent increase, from 3.13 to 3.34 kg CO<sub>2eq</sub> m<sup>-3</sup> (Figure A3.19). The control strategy CL1 is the control strategy that shows the highest GHG mitigation.

The total GHG emissions are reduced at the steady state conditions by 13.5% when compared to CL0. The CL3 control strategy reduces the total GHG emissions by 2.4% and the CL2 control strategy is not able to reduce the total GHG emissions. In fact, GHG emissions increase by 13.7%. However, all the control strategies are able to reduce N<sub>2</sub>O emissions when compared with the default control strategy (Figure A3.20), except for the control strategy CL2 that obtains the same N<sub>2</sub>O emissions in the bioreactor at the new steady state conditions. CL2 and CL3 are based on the addition of methanol in the anoxic reactor and, even though the N<sub>2</sub>O emissions decrease, the total GHG emissions increase due to the fact that this organic matter source causes indirect emissions for the production of methanol (1.54 kg CO<sub>2eq</sub> per kg methanol) and the biomass produces direct CO<sub>2</sub> emissions by the respiration of this added organic matter. With the default control strategy CL0, the steady state N<sub>2</sub>O emissions from the bioreactor increase from 272.5 to 321.0 kg N<sub>2</sub>O d<sup>-1</sup> (18%). The CL3 control strategy is the control strategy that most mitigates these N<sub>2</sub>O emissions, obtaining a decrease of 49.7% compared with the emissions obtained with CL0, followed by the CL1 control strategy, which obtains a reduction of 34%.

Figure A3.21 shows the results of the energy consumption for all the control strategies implemented for scenario 1. It shows how the default control strategy CL0 increases the energy consumption only by 2.1%, since more oxygen is consumed due to the increase of the influent N-NH<sub>4</sub><sup>+</sup>. The control strategy CL3 is the control strategy that increases most the energy consumption since i) the DO setpoint increases from 2 to 3 g O<sub>2</sub> m<sup>-3</sup> and therefore the aeration energy increases and ii) methanol addition causes an increase of the biomass production in the system and hence an increase on the aeration demand of this biomass. The CL3 control strategy increases the energy consumption by 42.3% comparing with the CL0. The CL2 control strategy presents the second maximum increase of the energy consumption, with an increase of 20.9% with respect to CL0. Finally, the CL1 control strategy increases the energy consumption by 13.5% compared to CL0.

Finally, Figure A3.22 shows the specific EQI for scenario 1. The control strategies CL0, CL1 and CL2 show a peak on the EQI after the N-NH<sub>4</sub><sup>+</sup> influent increase due to the increased N-NH<sub>4</sub><sup>+</sup> concentration in the effluent (Figure A3.18). The control actions decrease the effluent N-NH<sub>4</sub><sup>+</sup> concentration and the EQI. The control strategy CL0 increases the EQI from 0.22 to 0.28 kg pollution unit m<sup>-3</sup> (26.7%). The control strategy CL1 is the control strategy that most increases the EQI: it is increased by 102.2% with respect to before the N-NH<sub>4</sub><sup>+</sup> influent increase (from 0.22 to 0.44 kg pollution unit m<sup>-3</sup>). This sharp increase on the EQI with CL1 is due to the fact that the DO SP is increased from 2 to 3 g O<sub>2</sub> m<sup>-3</sup> and this deteriorates the EBPR activity in the anaerobic reactor, since the external recycle contains more oxygen. The EQI obtained in steady state conditions for control strategies CL2 and CL3 is 0.21 kg pollution unit m<sup>-3</sup>, slightly lower than the

EQI prior to the  $\text{NH}_4^+$  influent increase, resulting in a reduction of the EQI of 5.4% for both control strategies.

The best control strategy implemented is CL1 (increase in the DO SP with the increase of the N influent load) if the objective of the implementation of the control strategies is the mitigation of the GHG emissions. This is the control strategy that greatly reduces the total GHG emissions. However, this control strategy increases drastically the EQI when EBPR is performed in the WWTP.

Considering the three criteria and the objective of GHG emissions mitigation maintaining a high effluent quality, the best control strategy studied is CL3 (increase in the DO SP with the increase of the N influent concentration and addition of methanol to promote denitrification in the anoxic reactor). This is because the total GHG emissions are reduced and the effluent quality is high (low value of EQI). Moreover, CL3 is the control strategy that mostly reduces the emission of  $\text{N}_2\text{O}$  in the bioreactor. However, the energy consumption is increased for the two control strategies discussed, resulting in an increase of the operational costs of the WWTP.

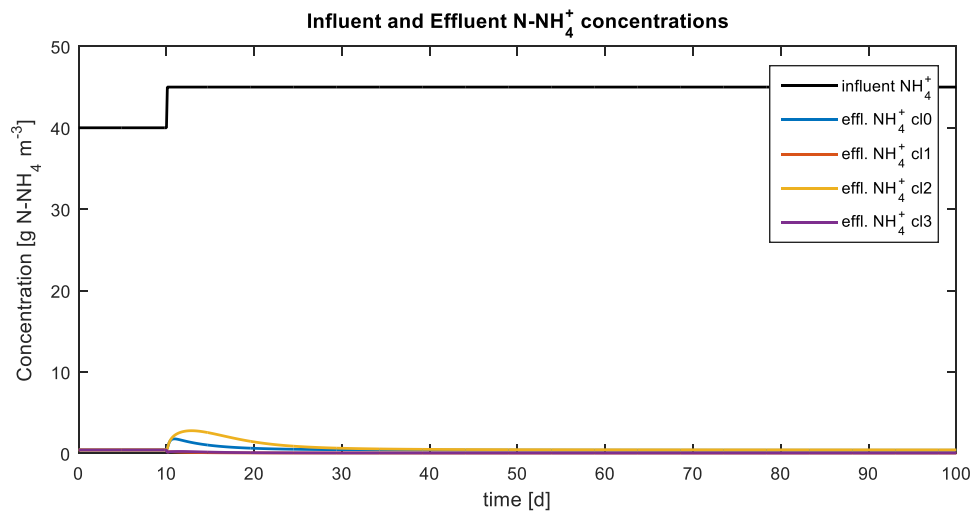


Figure A3.18. Influent  $\text{NH}_4^+$  concentration for the scenario 1 and effluent concentrations for each control strategy implemented.

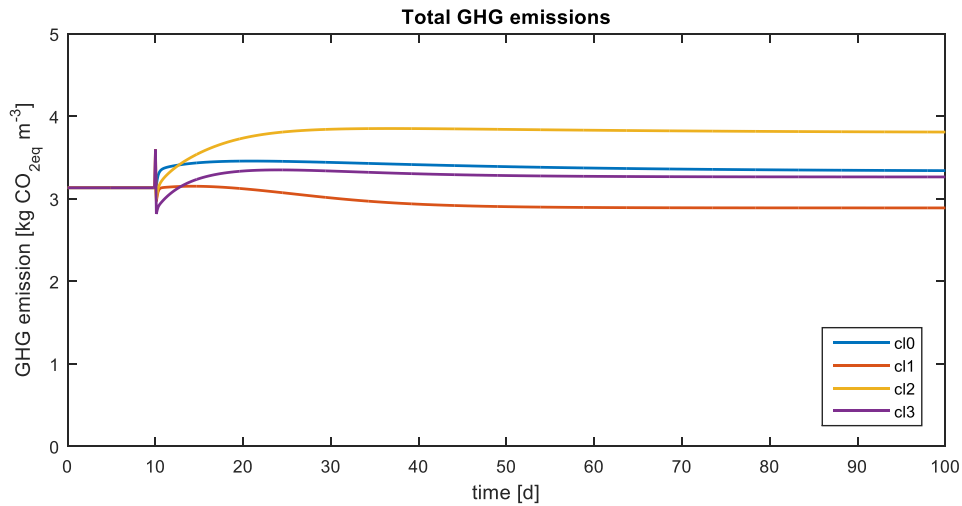


Figure A3.19. Total GHG emissions for each control strategy for the scenario 1.

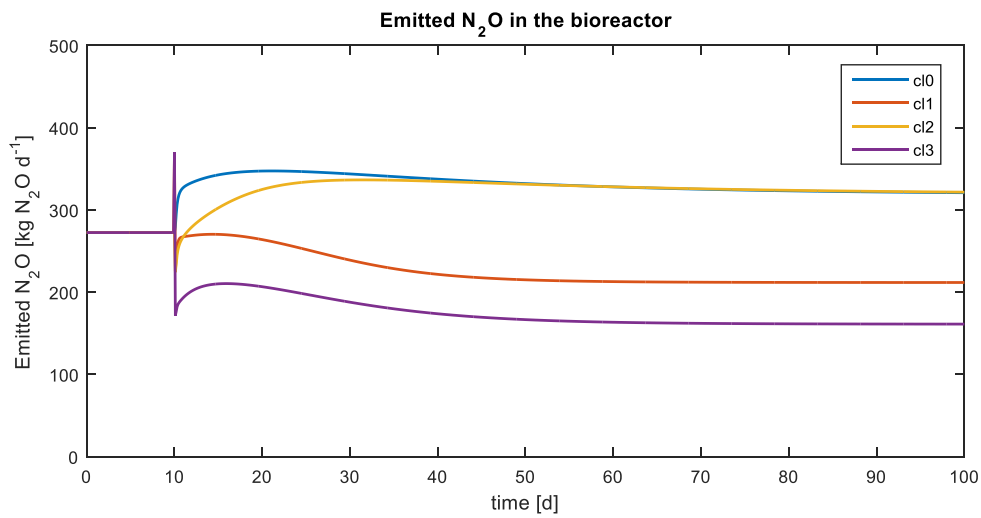


Figure A3.20. Emitted N<sub>2</sub>O in the bioreactor for each control strategy for the scenario 1.

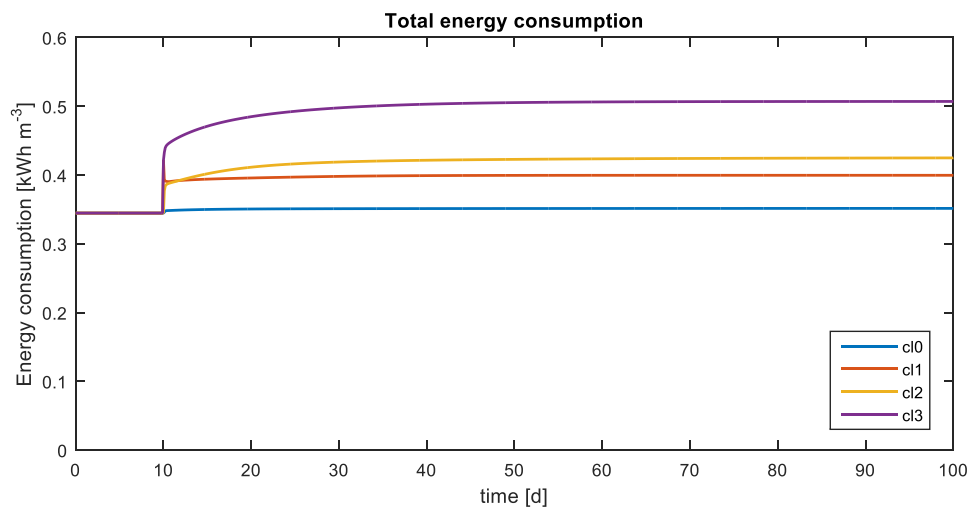


Figure A3.21. Total energy consumption for each control strategy for the scenario 1.

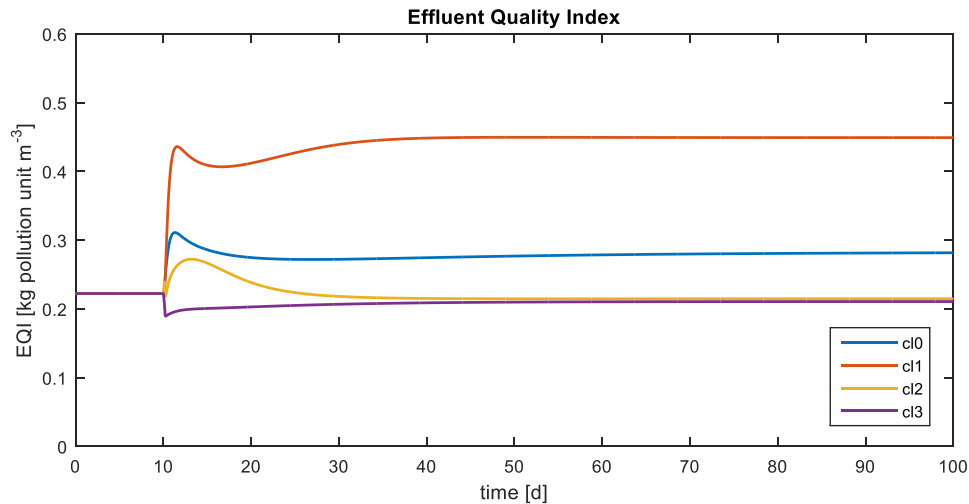


Figure A3.22. Dynamic EQI for each control strategy for the scenario 1.

#### A3.3.2.2. Scenario 2: High influent $N-NH_4^+$ step increase

The results for the scenario 2, i.e. an increase of the influent  $N-NH_4^+$  of  $10 \text{ g N m}^{-3}$  (Figure A3.23), are summarized in the following figures. The SRT and the PC solids removal efficiency for all the results are maintained at 10 days and 40%, respectively.

Figure A3.23 shows the increase of the ammonium influent concentration from  $40$  to  $50 \text{ g N-NH}_4 \text{ m}^{-3}$  on day 10, which represents an increase of 25% of the ammonium load, from  $2480$  to  $3100 \text{ kg N-NH}_4 \text{ d}^{-1}$ . Following the influent ammonia nitrogen increase, the effluent  $N-NH_4^+$  concentration increases as well for all the control strategies. Then, the concentration decreases below  $1 \text{ g N-NH}_4 \text{ m}^{-3}$ . The maximum effluent  $N-NH_4^+$  peak found was recorded for the control strategy CL2 ( $6.4 \text{ g N-NH}_4 \text{ m}^{-3}$ ), the second maximum peak was observed for the default control strategy (CL0,  $4.8 \text{ g N-NH}_4 \text{ m}^{-3}$ ), while for the CL1 and CL3 control strategies, the maximum effluent  $N-NH_4^+$  concentration was  $0.8 \text{ g N-NH}_4 \text{ m}^{-3}$ .

Figure A3.24 and Figure A3.25 show the total GHG emissions and the  $N_2O$  emissions from the bioreactor, respectively. For the default control strategy CL0, the total GHG emissions increased 15% due to the ammonium influent increase, from  $3.13$  to  $3.61 \text{ kg CO}_{2\text{eq}} \text{ m}^{-3}$  (Figure A3.24). The control strategy CL1 is the control strategy that shows less GHG emissions, reducing the total GHG emissions at the steady state conditions by 14% comparing to those obtained with CL0. The CL3 control strategy reduces the total GHG emissions by 6% comparing to those obtained with CL0, and the CL2 control strategy is not able to reduce the total GHG emissions, since the emissions increase by 12.8%. However, all the control strategies are able to reduce  $N_2O$  emissions compared with the default control strategy (Figure A3.25). The CL2 and CL3 control strategies are based on methanol dosage in the anoxic reactor. Even though the  $N_2O$  emissions decrease, the total GHG emissions increase due to the indirect emissions due to methanol dosage ( $1.54 \text{ kg}$

CO<sub>2eq</sub> kg methanol). Besides that, the biomass produces direct CO<sub>2</sub> emissions by the respiration of this added organic matter. With the default control strategy, the steady state N<sub>2</sub>O emissions from the bioreactor increase from 272.5 to 384.5 kg N<sub>2</sub>O d<sup>-1</sup> (41%). The CL3 control strategy is the control strategy that most mitigate these emissions, obtaining a decrease of 53% compared with the emissions obtained with CL0, followed by the CL1 control strategy, which obtains a reduction of 32% and last the CL2 control strategy, obtaining a 5% of reduction compared with those obtained with CL0.

Figure A3.26 shows the results of the energy consumption for all the control strategies implemented for scenario 2. It shows how the default control strategy only increases the energy consumption by 4.4%. This increase is linked to the fact that more oxygen is needed due to the increase of the influent N-NH<sub>4</sub><sup>+</sup>. The control strategy CL3 is the control strategy that most increases the energy consumption since the DO setpoint is increased from 2 to 3 g O<sub>2</sub> m<sup>-3</sup> and therefore both the aeration energy and methanol dosage increase. This causes an increase of the biomass production and of the aeration demand. The CL3 control strategy increases the energy consumption by 46.6% when compared to the CL0. The CL2 control strategy presents the second maximum increase of the energy consumption, with an increase of 22.8% with respect to CL0 and last, the CL1 control strategy increases the energy consumption by 14.8% compared to CL0.

Finally, Figure A3.27 shows the specific EQI for each time step and for each control strategy implemented for scenario 2. It shows that a peak on the EQI is found just after the N-NH<sub>4</sub><sup>+</sup> influent increase for control strategies CL0, CL1 and CL2. This is due to the NH<sub>4</sub><sup>+</sup> observed in the effluent (Figure A3.23). Later, the effluent NH<sub>4</sub><sup>+</sup> decreases to those values obtained before the step and the EQI decreases. The control strategy CL0 increases the EQI from 0.22 to 0.37 kg pollution unit m<sup>-3</sup> (66.7%). The control strategy CL1 is the control strategy that most increases the EQI, more than the CL0, increased by 156.7% with respect to before the N-NH<sub>4</sub><sup>+</sup> influent increase. This sharp increase on the EQI with CL1 is due to the fact that the DO SP is increased from 2 to 3 g O<sub>2</sub> m<sup>-3</sup> and this deteriorates the EBPR activity in the anaerobic reactor, since the external recycle presents more DO concentration. The EQI obtained in steady state conditions for control strategies CL2 and CL3 is the same to prior the N-NH<sub>4</sub><sup>+</sup> influent increase, resulting in the same effluent quality with higher influent load.

The best control strategy in view of GHG mitigation is CL1 (increase in the DO SP with the increase of the N influent load). Nevertheless, this control strategy increases drastically the EQI when EBPR is performed in the WWTP. Therefore, considering the three studied criteria, the best control strategy is CL3 (increase in the DO SP with the increase of the N influent load and addition of methanol to promote denitrification in the anoxic reactor). The objective of the control strategies is GHG emissions mitigation but without compromising effluent quality, i.e. maintaining a low value of EQI. Moreover,

the control strategy CL3 is the control strategy that mostly reduce the  $N_2O$  emissions in the bioreactor. However, the energy consumption is increased for the control strategies discussed, resulting in an increase on the operational costs of the WWTP.

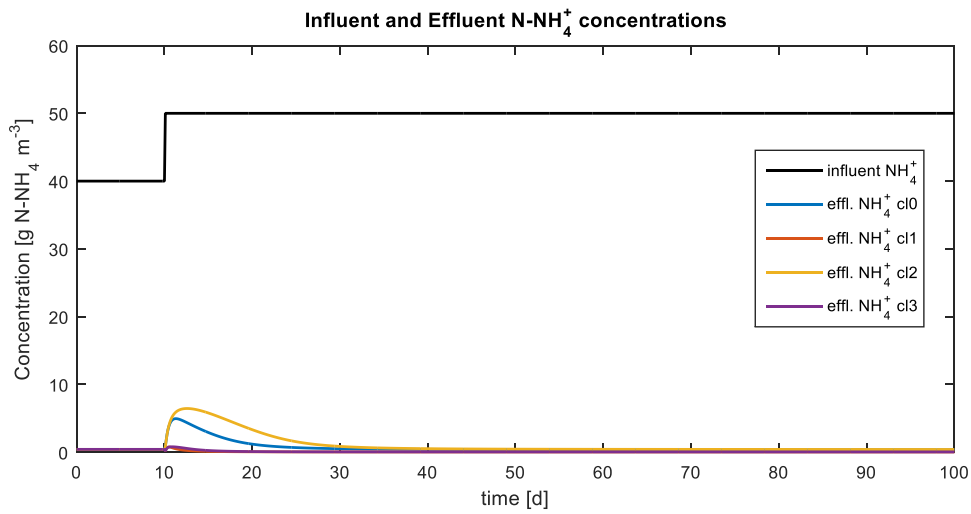


Figure A3.23. Influent  $NH_4^+$  concentration for the scenario 2 and effluent concentrations for each control strategy implemented.

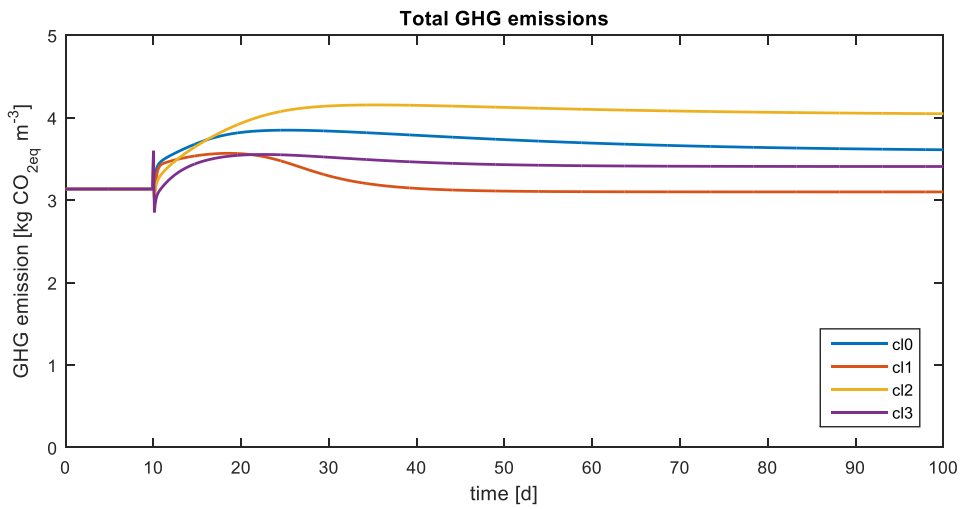


Figure A3.24. Total GHG emissions for each control strategy for the scenario 2.

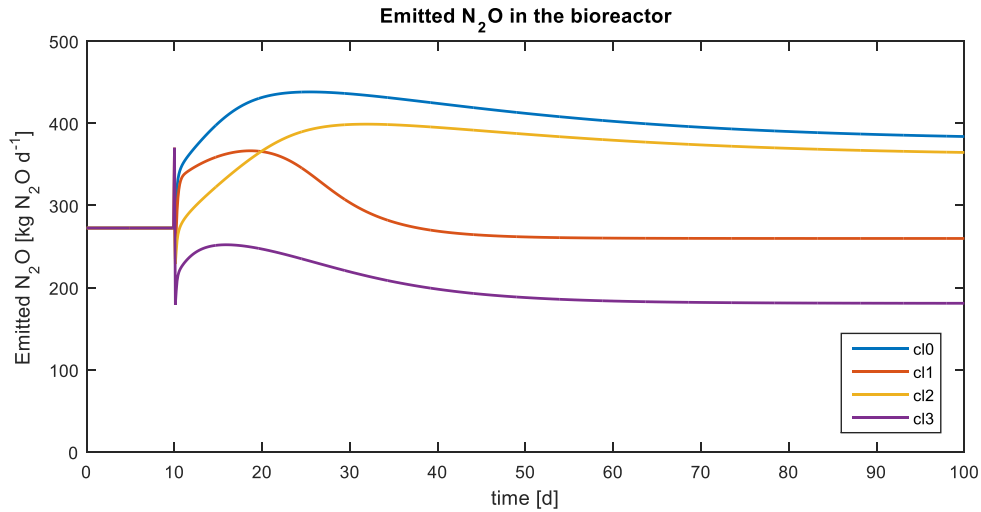


Figure A3.25. Emitted N<sub>2</sub>O in the bioreactor for each control strategy for the scenario 2.

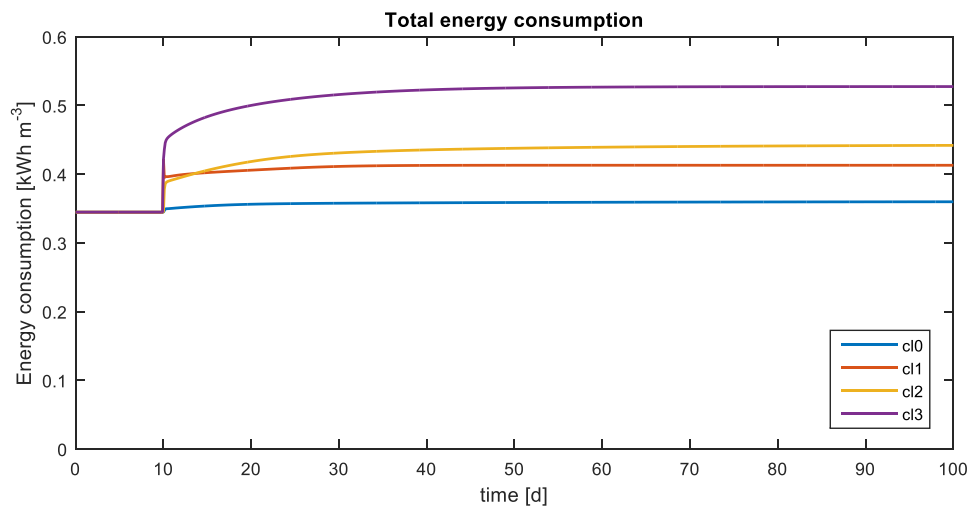


Figure A3.26. Total energy consumption for each control strategy for the scenario 2.

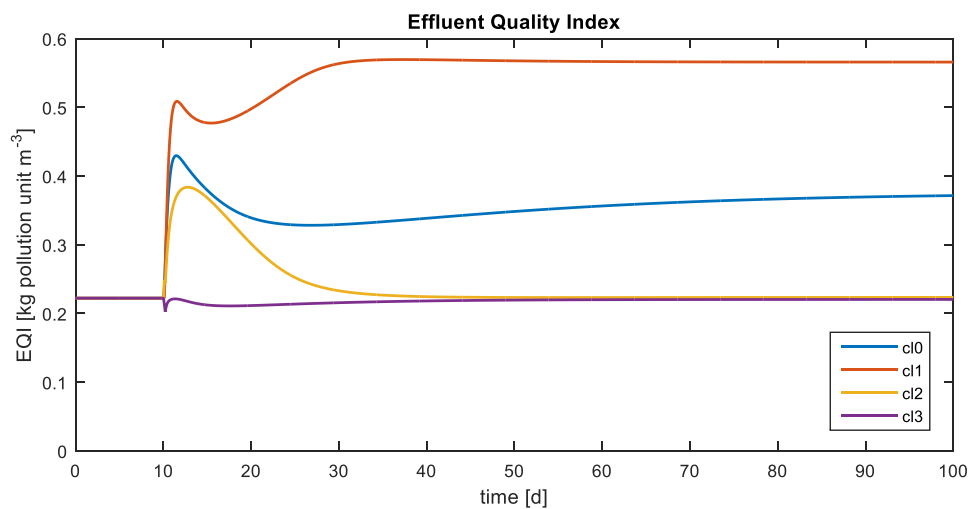


Figure A3.27. Dynamic EQI for each control strategy for the scenario 2.



### A3.4. Conclusions

Different control strategies have been proposed and tested by modelling tools to mitigate the GHG emissions of the studied WWTP in view of reducing energy consumption and obtaining a proper effluent quality.

The results for the scenarios proposed of high/low increase of the ammonium influent load show that the best control strategy to mitigate the total GHG emissions is CL1, i.e. increase the DO SP in the aerobic compartments as a function of the ammonium influent concentration. This control strategy reduces the total GHG emissions of the plant by 13.5 and 14% for high and low influent N-NH<sub>4</sub><sup>+</sup> load increase, respectively, compared to the total GHG emissions obtained with the default CL0 control strategy of the WWTP. However, this control strategy increases the EQI by 102 and 156%, for high and low influent N-NH<sub>4</sub><sup>+</sup> load increase, respectively, compared to the EQI prior to the ammonium influent load increase.

Therefore, the best control strategy tested is CL3, i.e. increasing the DO SP in the aerobic compartments as a function of the ammonium influent concentration, as well as methanol dosage in the anoxic compartment for complete denitrification. This control strategy reduces the total GHG emissions by 2.4 and 6% and the N<sub>2</sub>O emissions from the bioreactor by 50 and 53%, for high and low influent N-NH<sub>4</sub><sup>+</sup> load increase, respectively, compared to the default control strategy of the WWTP. CL3 also presents the same EQI prior to the ammonium influent concentration increase. However, it must be taken into account that both control strategies increase the energy consumption of the plant, resulting in a higher operational cost.

### A3.5. References

- Deliverable 3.1: Development of the carbon footprint model, 2016, viewed, 10 July 2021, <<https://ec.europa.eu/research/participants/documents/downloadPublic?documentIds=080166e5ac61383c&appId=PPGMS>>
- Deliverable 7.1: Development of the methodology followed to assess the mitigation of GHG emissions, 2019, viewed 10 July 2021, <<https://ec.europa.eu/research/participants/documents/downloadPublic?documentIds=080166e5c431da8f&appId=PPGMS>>
- Deliverable 7.2: Development of mitigation strategies to reduce GHG emissions, 2019, viewed 10 July 2021, <<https://ec.europa.eu/research/participants/documents/downloadPublic?documentIds=080166e5c431d283&appId=PPGMS>>